IDO-16668

REACTOR PHYSICS STUDIES FOR THE FINAL CONCEPTUAL DESIGN OF THE ADVANCED TEST REACTOR

R. S. Marsden et al

March 24, 1961

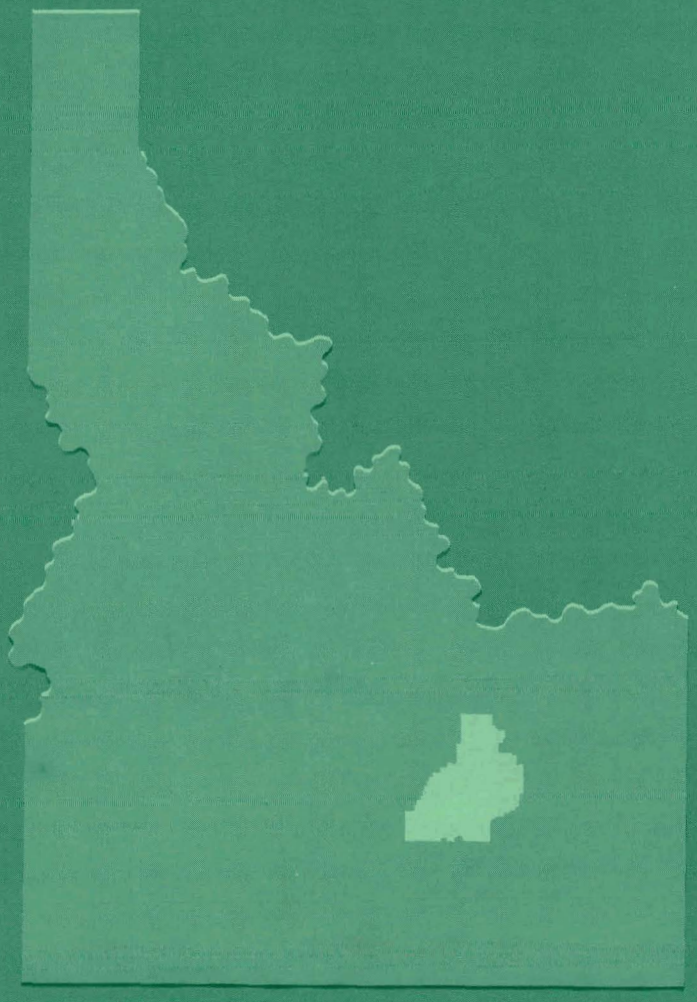

PHILLIPS PETROLEUM COMPANY

ATOMIC ENERGY DIVISION

NATIONAL REACTOR TESTING STATION

US ATOMIC ENERGY COMMISSION

DISCLAIMER

PRICE $2.75

Available from the
Office of Technical Services
U. S. Department of Commerce
Washington 25, D. C.

Printed in USA

IDO-16668
AEC Research and Development Report
Physics
TID-4500 (16th Ed.)
Issued: March 24, 1961

REACTOR PHYSICS STUDIES FOR THE FINAL CONCEPTUAL DESIGN OF THE ADVANCED TEST REACTOR

Edited by: R. S. Marsden

Work done by:

A. W. Brown
R. W. Goin
R. S. Marsden
D. R. Metcalf
J. M. Waage
O. J. Elgert*
T. L. Francis*
B. H. Leonard, Jr.*
E. E. Mason*
R. J. Neuhold*
D. G. Ott*
G. E. Putnam*

*Internuclear Company

PHILLIPS
PETROLEUM
COMPANY

Atomic Energy Division
Contract AT(10-1)-205
Idaho Operations Office
U. S. ATOMIC ENERGY COMMISSION

*Internuclear Company (Clayton, Missouri)
Contributions to this report were made under
Subcontract No. C-222
to
Phillips Petroleum Company

REACTOR PHYSICS STUDIES FOR THE FINAL CONCEPTUAL DESIGN OF THE ADVANCED TEST REACTOR

S U M M A R Y

This report presents a detailed account of the reactor physics studies for the final conceptual design of the Advanced Test Reactor which is described in IDO-16667[1]. It is not the purpose of the present report to draw conclusions as these are discussed in the report on the final conceptual design.

The diffusion theory methods used for calculations of flux distributions and reactivity effects are described and compared with measurements and with higher order approximations to transport theory. These comparisons show diffusion theory to be adequate for the ATR conceptual design.

Two-dimensional flux distributions for a number of shim control conditions and experimental loadings are determined by PDQ-3 and TRANSAC-PDQ. The worths and effects on flux distributions of chemical and of blade type mechanical shim controls are compared. The effects of heavy water and of beryllium reflectors on reactivity and flux pattern are calculated.

The time-dependent behavior of the reactor is investigated by use of TURBO and CANDLE. The changes in shim control poison and test and core flux distributions with fuel burnup are calculated and the full-power cycle time estimated. An investigation is made of the xenon transient after a full-power shutdown and recovery. Results of one- and two-dimensional fuel depletion studies are compared.

The results of a number of time independent one-dimensional calculations and parametric studies are presented. Some comparisons are made of the results for one-dimensional and two-dimensional models of the ATR.

The void coefficient of reactivity is found for the core, reflector, experiment and flux trap regions of the reactor. Calculations of the temperature coefficient for the entire reactor and for individual regions are determined for one- and two-dimensional models.

Xenon instability is studied for oscillations around one lobe, between lobes and along the vertical axis. TURBO and CANDLE calculations are used to determine the effects of perturbations on the axial stability. An analytic method for determining axial stability is derived and applied to a single lobe model of the ATR.

---

1. D. R. deBoisblanc et al., "The Advanced Test Reactor - ATR Final Conceptual Design," Phillips Petroleum Company, Idaho Falls, Idaho IDO-16667, November 1, 1960.

A perturbation technique is used to find the effects of reflector type and poisoning on the average core neutron lifetime. Calculations of the approximate lifetime of the delayed group from the reflector are made for a number of reflector conditions.

Plots and tables of the gamma heat distribution in the ATR as determined by an IBM-704 program are presented.

REACTOR PHYSICS STUDIES FOR THE FINAL CONCEPTUAL DESIGN OF THE ADVANCED TEST REACTOR

Table of Contents

Table of Contents (Continued)

1.0 INTRODUCTION

The Advanced Test Reactor, ATR, has a unique design with a very high power density in the core and with provisions for a considerable degree of adjustment of the flux levels in the individual test facilities. This report contains the reactor physics studies made to establish the feasibility of the final conceptual design. Two previous reports describe the conceptual design and the work leading to its selection.[1,2] To provide the necessary information the work has covered the following general areas:

1. Establishment of the control requirements.

2. Determination of the feasibility of control throughout an operating cycle.

3. Evaluation of alternate systems of reactivity control and of neutron reflectors.

4. Calculation of flux and power distributions throughout a cycle.

5. Study of instability problems including xenon oscillations.

6. Determination of temperature and void coefficients of reactivity.

7. Investigation of the effects of reflector conditions upon neutron lifetime.

A schematic layout of the ATR core, reflector and control regions is shown for orientation in Figure 1.0-1. The characteristics of the conceptual design are summarized in Table 1.0-A. Detailed drawings are included in the previously mentioned conceptual design reports. It should be noted that although the ATR core can be described as having a four-lobe arrangement it is best represented for reactor physics purposes as having five fuel regions, one around each of the experimental facilities interior to the core. The center fuel region is sometimes referred to as the center lobe and to prevent confusion the other fuel regions are designated the outer core lobes or the outer lobes. The test or experimental regions located outside of the core are labeled exterior. The reflector shim control is sometimes called the inner reflector when a chemical control system is used.

---

1. D. R. deBoisblanc et al., "Proposal for an Advanced Engineering Test Reactor - ETR II," Phillips Petroleum Company, Idaho Falls, Idaho IDO-16666, March 17, 1960.

2. D. R. deBoisblanc et al., "The Advanced Test Reactor - ATR Final Conceptual Design," Phillips Petroleum Company, Idaho Falls, Idaho, IDO-16667, November 1, 1960.

TABLE 1.0-A

ATR SPECIFICATIONS

Core height	48 in.
Core thickness	2.5 in.
Core volume	262 liters
Core metal-to-water ratio (volume)	0.8
Core structural material and cladding	Aluminum
Fuel	93% enriched U-235
Fuel loading	33 kg U-235
Burnable poison in core	128 g natural boron
A-5 experiment fast flux - avg midplane value	1.0×10^{15} n/cm^2 sec
A-5 experiment thermal flux - avg midplane value	0.32×10^{15} n/cm^2 sec
A-3 experiment fast flux - avg midplane value	1.5×10^{15} n/cm^2 sec
A-3 experiment thermal flux - avg midplane value	0.48×10^{15} n/cm^2 sec
Control requirements	
Safety blades	10.0% $\Delta k/k$
Neck shims	2.9% $\Delta k/k$
Reflector shims	6.5% $\Delta k/k$
Burnable poison	4.8% $\Delta k/k$
Core power	250 Mw
Maximum power density	2.5 Mw/liter
Vertical maximum-to-average power ratio	1.4 or less
Cycle time at full power	17 days

The flux plots and power distributions for the ATR have in general been obtained by two-neutron-group diffusion theory calculations using the PDQ-3 program for the IBM-704 computer. The calculational methods have been compared with measurements and with higher order approximations to diffusion theory and found to be satisfactory for purposes of a conceptual design. The behavior with burnup during operation has been found by use of the CANDLE-2 and TURBO depletion programs. Calculations of axial flux patterns have been made in (r, z) geometry with the PDQ-2 program. Supplementary and parametric studies have been made on one-dimensional models and the results compared with two-dimensional calculations.

Most of the calculations have been for a reactor with a D_2O outer reflector, three-inch thick poisoned D_2O annuli adjacent to the core for reflector shim control and poisoned H_2O regions for neck shim control. In the final conceptual design the poisoned D_2O annuli were replaced with one-half inch poisoned H_2O annuli as being essentially equal for control purposes while easing processing problems. Solid reflectors and blade type controls were investigated as alternates to the liquid reflector and chemical controls of the conceptual design.

It is not possible to predict all of the requirements that will be imposed upon the ATR during its operating history. Therefore, the experimental loadings assumed for the calculations have been selected to be typical of those now anticipated while requiring test fluxes and core power distributions that demand rather full utilization of the reactors capabilities. These flux requirements and the various types of experiments and facilities are described in Appendix 12.3.

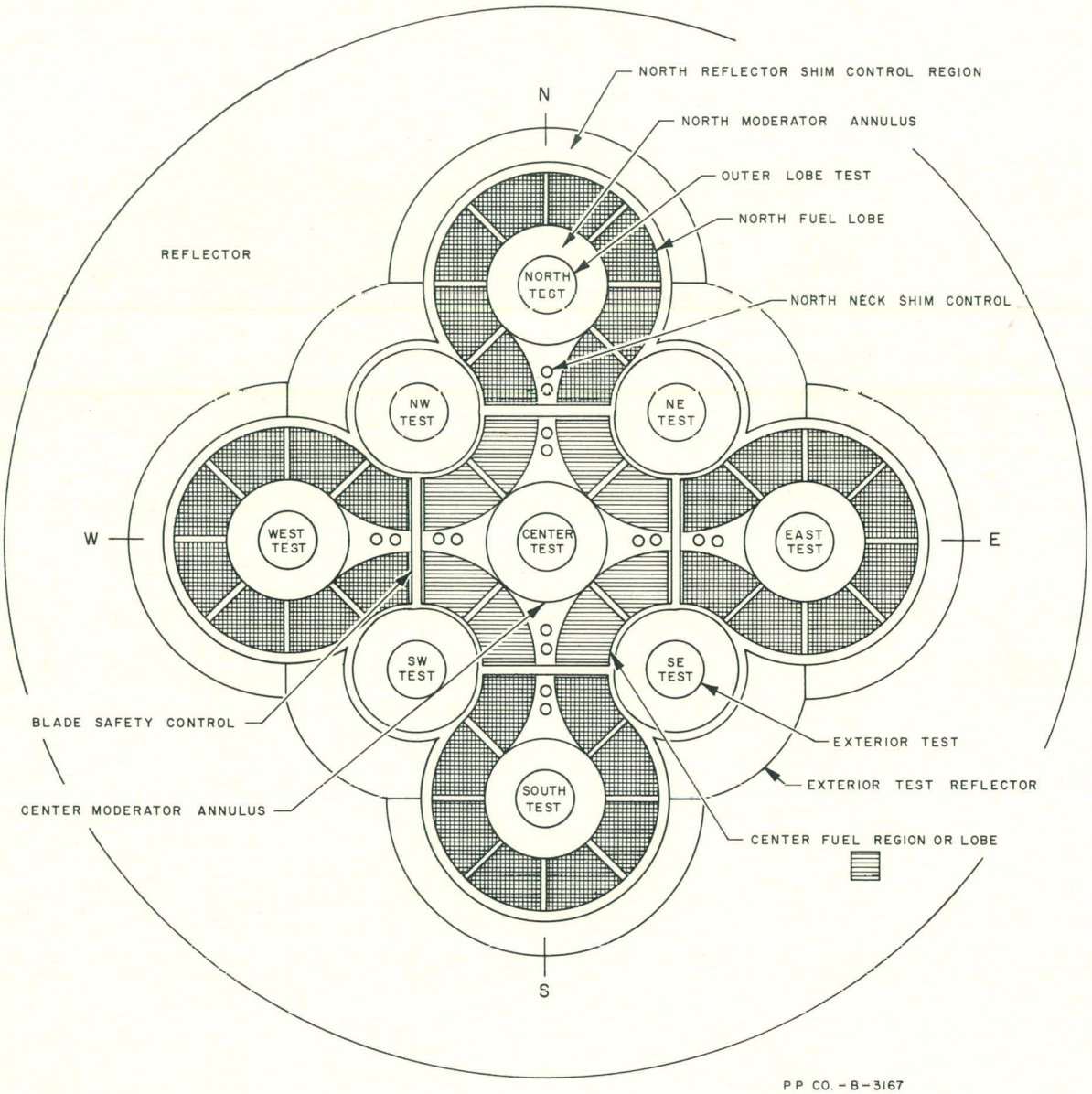

FIG. 1.0-1
SCHEMATIC LAYOUT OF ATR

2.0 CALCULATIONAL METHODS

2.1 Computational Programs

The majority of the calculations of reactivity and flux distributions for this study have relied on two-group diffusion theory. Four-group diffusion theory and higher order approximations to transport theory have been used to check the validity of the two-group calculations.

Machine methods have been used to obtain all the necessary constants. In particular the thermal constants have been obtained by averaging over a Maxwellian energy spectrum with an IBM-650 program. The Maxwellian temperature for the machine calculation of the thermal constants is 217°F with the atom densities computed for 200°F except for the experiments. The experiments are considered as having an average Maxwellian temperature of 400°F, with the atom densities computed for 600°F to make the cross sections consistent with the neutron sources from regions of two different temperatures. The two-dimensional temperature coefficient studies used the same Maxwellian temperature as the temperature being considered for that particular region. The thermal cross section data are the same as used in the IBM-704 SOFOCATE[1] code. The fast constants have been obtained by utilizing the MUFT-4[2] program using the self-consistent B-1 approximation on the IBM-704. The MUFT-4 program used has input data for nonhydrogenous moderators which refine the slowing down calculation over what can be obtained with MUFT-3. This Goertzel-Grueling[3] approximation to nonhydrogenous slowing down processes has been found to give a significant improvement in the calculation of fast group constants. The MUFT buckling is B = 0.01 in all cases. An extensive listing of fast and thermal group constants for the ATR is shown in Section 12.4 of the Appendix.

The two-dimensional calculations of the ATR in (x,y) geometry have been made with the PDQ-3[4] program on the IBM-704 except for one calculation to check the effect of mesh spacing which uses the TRANSAC PDQ. The three-dimensional ATR geometry is reduced to two dimensions by adding an appropriate reflector saving in the axial direction and thus making an equivalent bare reactor in this direction. Axial flux distortions caused by solid reflector

---

1. Harvey Amster, "Cross Sections in the SOFOCATE Code: Second Deck," WAPD-TM-67, June 1957.
2. H. Boyl, Jr., E. M. Gelbard, G. H. Ryan, "MUFT-IV Fast Neutron Spectrum Code for the IBM-704," WAPD-TM-72, July 1957.
3. F. Clark, E. Grueling, G. Goertzel, "A Multigroup Approximation to the Boltzmann Equation for Critical Reactors," NDA-10-96, 1953.
4. W. R. Cadwell et al., "PDQ-3 - A Program for the Solution of the Neutron-Diffusion Equations in Two-Dimensions on the IBM-704," WAPD-TM-179, March 1960.

shim control are studied by using the PDQ-2[1] code in (r, z) geometry. This code is used in lieu of PDQ-3 because PDQ-3 does not handle (r, z) geometry.

One-dimensional few group reactor calculations use the DMM[2] code on the IBM-650 and the WANDA[3] code on the IBM-704. One-dimensional studies have been utilized whenever information has been needed to guide the direction that the two-dimensional studies should take. Also when fine convergence has been required on the fission eigenvalue such as for lifetime studies, the one-dimensional program has been used. Higher order approximations to transport theory use Carlson's S_n program as modified and extended by NDA[4]. A detailed discussion of S_n versus diffusion theory comparison is given in Appendix 12.1.

The effect of mesh coarseness and the test region homogenization on reaction rates and fluxes on both a one-dimensional and a two-dimensional basis is described in Appendix 12.2. Both the S_n studies and mesh coarseness studies verify the adequacy of using diffusion theory in studies of this type.

2.2 Comparison of Two- and Four-Group PDQ Calculations

Two PDQ calculations (Problems 1017 and 1034) have been run to evaluate the difference between two-group and four-group calculations. These calculations had 36 kg U-235 in the core and A-1 experiments in all outer lobes.

The results from these problems are given in Table 2.0-A and Figures 2.0-1 through 2.0-3. These data show that within the fuel (core) regions the two- and four-group problems yield essentially the same results for power densities and thermal neutron flux values. However within the experiment region the four-group problem gives values 3 to 6% higher than the two-group problem, and in the moderator regions peak thermal flux values are obtained which are 8 to 15% higher in the four-group problem than in the two-group problem. The absolute difference in k_{eff} between the four-group and two-group problems is 0.009 with the two-group problem yielding the higher value.

---

1. G. G. Bilodeau et al., "PDQ - An IBM-704 Code to Solve the Two-Dimensional Few-Group Neutron-Diffusion Equations," WAPD-TM-70, August 1957.
2. J. Franklin and E. J. Leshan, "A Multigroup, Multiregion, One-Space Dimensional Program Using Neutron Diffusion Theory," ASAE-4, December 1956.
3. O. J. Marlowe et al., "WANDA - A One-Dimensional Few Group Diffusion Equation Code for the IBM-704," WAPD-TM-28, November 1956.
4. B. H. Duane, "Neutron and Photon Transport Plane-Cylinder - Sphere GE-ANPD Program S Variational Optimum Formulation," XDC-59-9-118 January 9, 1959.

TABLE 2.0-A

COMPARISON OF TWO-GROUP AND FOUR-GROUP PDQ PROBLEMS

Four-Group (Prob. 1017) $k_{eff} = 1.3368$

Two-Group (Prob. 1034) $k_{eff} = 1.3459$

	Power (Mw)		Average Midplane Thermal Neutron Flux (n/cm^2 sec x 10^{-14})		Maximum-to-Average Midplane Thermal Neutron Flux (n/cm^2 sec x 10^{-14})	
	4 Group	2 Group	4 Group	2 Group	4 Group	2 Group
E-W lobe fuel	97.55	97.86	2.45	2.45	2.772	2.722
Center lobe fuel	53.62	54.64	2.62	2.67	2.713	2.685
N-S lobe fuel	98.83	97.50	2.48	2.44	2.770	2.724
E-W lobe A-1 exp.	0.683	0.646	5.54	5.23		
N-S lobe A-1 exp.	0.694	0.643	5.63	5.20		
Center lobe A-3 exp.	0.710	0.688	5.15	5.00		
Outer lobe A-5 exp.	3.033	2.844	3.98	3.73		

NOTE:

Energy groups	Range	
1 of 3 fast	0.821 mev $\leq E \leq$ 10 mev	
2 of 3 fast	5.53 kev $\leq E \leq$ 0.821 mev	For four-group calculations
3 of 3 fast	0.625 ev $\leq E \leq$ 5.53 kev	
1 of 1 fast	0.625 ev $\leq E \leq$ 10 mev	For two-group calculations
Thermal	$0 < E \leq$ 0.625 ev	

It must be emphasized here that the more accurate four-group calculations give calculated thermal fluxes that are about 5% higher than the two-group thermal fluxes in the experiments.

Reactor burnout studies use the one-dimensional burnout code CANDLE[1]. These problems study the variation of k_{eff} with time and the effects of burnable poison in the fuel. The two-dimensional burnout code TURBO[2] is used in studies of the actual reactor behavior as required flux levels are maintained in experiments by appropriate reflector and neck shim poisoning. The TURBO studies confirm the expected versatility of the ATR reactor.

2.3 Reflector Savings

For most diffusion theory type calculations the axial buckling has been calculated for an equivalent core reactor with a height equal to the actual core height plus 30 cm. For a core height of 4 ft or 121.92 cm this gives an equivalent height of 151.92 cm. The axial buckling B_z^2 is determined from the equation below to have a value of 0.00043 cm^{-2}.

$$B_z^2 = \frac{\pi^2}{L^2} = \frac{9.8696}{23,080} = 0.00043 \text{ cm}^{-2}$$

$L = H + 2\delta$

L is the actual core height.

δ is the reflector savings.

2δ is the total reflector savings.

The value of 15 cm for the axial reflector savings, or 30 cm for the total axial reflector savings represents a somewhat arbitrary selection. Internuclear Company in studies on D_2O moderated or reflected reactors has used a value of 23 cm for the reflector savings.[3,4] For H_2O moderated

---

1. O. J. Marlowe, P. A. Ombrellaro, "CANDLE - A One-Dimensional Few-Group Depletion Code for the IBM-704," WAPD-TM-53, May 1957.
2. J. B. Callaghan et al., "TURBO - A Two-Dimensional Few-Group Depletion Code for the IBM-704," WAPD-TM-95, November 1957.
3. O. J. Elgert, C. F. Leyse, D. G. Ott, "Preliminary Investigations for an Advanced Engineering Test Reactor," AECU-3427, February 22, 1957
4. C. F. Leyse et al., "An Advanced Engineering Test Reactor," AECU-3775, March 1958.

reactors such as the MTR, a reflector savings of about 8.5 cm has been measured.[1]

The ATR with a D_2O reflector is considered intermediate between these two systems and on this basis 15 cm reflector savings is selected. With a 4 ft core height for most purposes the results are not significantly influenced by any reasonable choice of reflector savings. Calculations to determine axial stability are an exception as the occurrence of xenon oscillations is strongly dependent on the equivalent core height.

For an actual core height of 4 ft the use of 30 cm total reflector savings and the assumption of a sinusoidal flux pattern over the length of the core plus reflector savings gives an axial maximum-to-average flux ratio over the core of 1.33. This agrees quite well with the value of 1.35 obtained from a PDQ-2 calculation of the axial flux distribution in the core. This agreement confirms the selection of 15 cm for the reflector savings.

A few PDQ-3 cases have been run where the entire reflector is beryllium plus water and for these cases a reflector savings of 7.5 cm is used. This gives a total of 15 cm reflector savings which is close to the MTR. A $B_z^2 = 0.00053$ is calculated from this reflector savings for a 4 ft core height.

---

1. M. L. Batt, J. W. Webster, H. L. McMurry, "Reflector Savings Due to the MTR Water Blanket," IDO-16075, 1953.

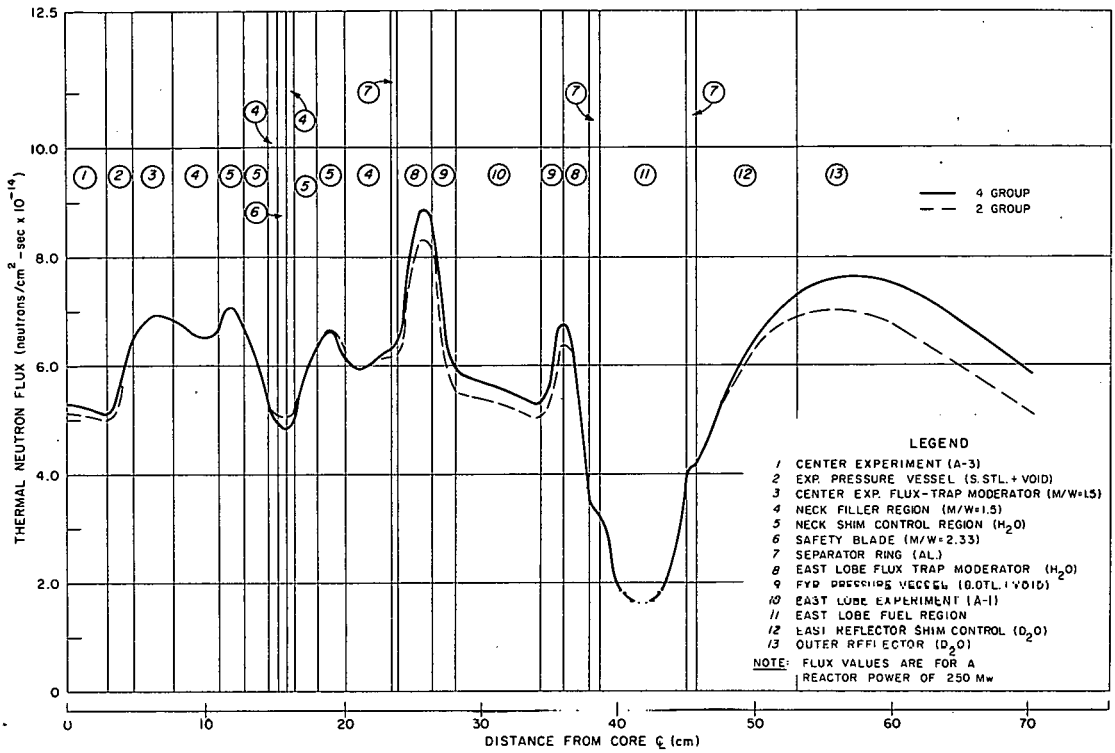

FIG. 2.0-1
EAST TRAVERSE - COMPARISON OF THERMAL NEUTRON FLUX FROM 2 GROUP AND 4 GROUP PDQ CALCULATIONS

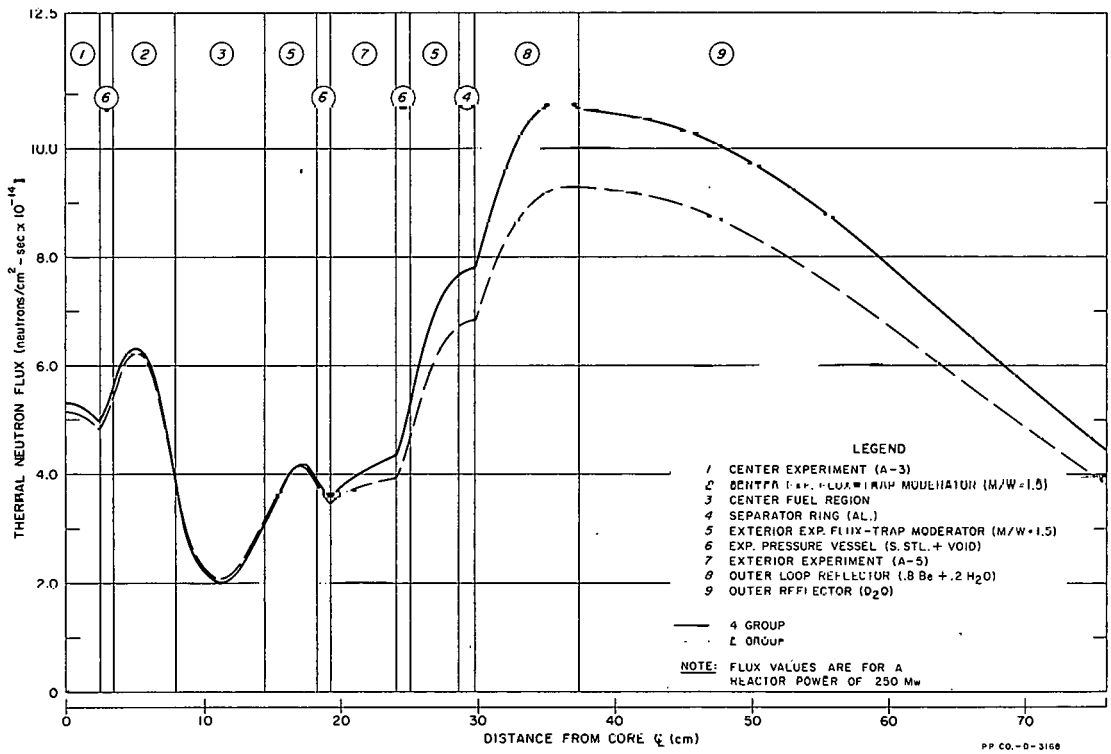

FIG. 2.0-2
DIAGONAL TRAVERSE - COMPARISON OF THERMAL NEUTRON FLUX FROM 2 GROUP AND 4 GROUP PDQ CALCULATIONS

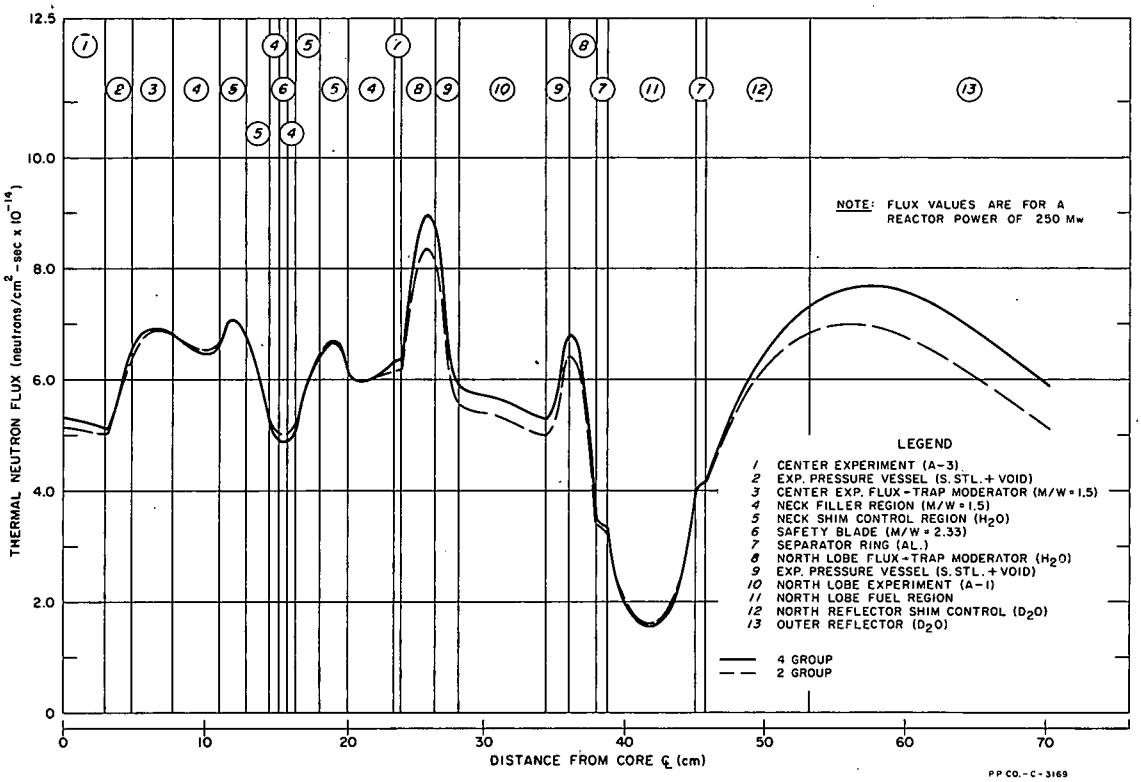

FIG. 2.0-3
NORTH TRAVERSE - COMPARISON OF THERMAL NEUTRON FLUX FROM 2 GROUP AND 4 GROUP PDQ CALCULATIONS

3.0 ETR CRITICAL FACILITY MOCKUP OF THE ATR

The unusual geometry of the ATR with its thin core annulus and with its many boundaries between highly and lightly absorbing regions makes it desirable to have some experimental justification for the calculational methods. It was recognized that the ETRC, Engineering Test Reactor Critical Facility, could be used to approximate the geometry of the ATR with a 3 in. core thickness and a beryllium reflector. The mockup of the ATR consisted of four 6 in. x 6 in. experimental spaces, surrounded with ETR fuel elements or control rods placed in the corners of the ETRC core and coupled with eight more fuel elements, making a fifth 6 in. x 6 in. experimental space. After preliminary reactivity measurements in the ETRC showed that an approximate loading could be made critical with two additional fuel elements, it was decided that critical experiments would be performed. These critical experiments were then used to evaluate the ATR calculational procedures and results against actual measured values.

Because the program being carried out in support of ETR by the ETRC is quite pressing, only one week of ETRC time was allotted for the measurements reported herein. Therefore, it was not possible to make all the studies desired. Also, because time was limited, no modifications were made to the ETRC. With the exception of two experiment mockups, all materials used, e.g., fuel elements and control rods, were standard ETR or ETRC components.

3.1 Description of the Facility and Components

The ETRC is a low power, highly enriched, water-cooled and moderated, beryllium-beryllium oxide reflected reactor. It is a full-scale nuclear mockup of the core and reflector of its parent reactor, the ETR. In fact it is more than just a mockup because most of the in-pile components (fuel elements and control rods) are identical to those in the parent reactor. For reasons of economy there are, however, slight modifications in the reflector. Over a period of several years, experiments have displaced enough 3 in. square beryllium pieces from the MTR to provide a complete reflector for the ETRC. These, however, make up only a 3 in. reflector as compared to 4-1/2 in. in the ETR. The remaining 1-1/2 in. are made up of canned beryllium oxide. Around the beryllium-beryllium oxide reflector is an aluminum reflector. The arrangement of the standard ETRC core and reflector is shown in Figure 3.0-1. A perspective drawing of the core, its support structure, control bridge, etc., is shown in Figure 3.0-2. A more detailed description of the facility can be found in IDO-16332[1].

With the exception of the experiment mockup, the core components (fuel elements, control rod fuel sections and guide tubes, and aluminum filler pieces) are standard ETR or ETRC components. The ETRC filler pieces are made of aluminum and have machined slots. These slots simulate

---

1. D. R. deBoisblanc et al., "The Engineering Test Reactor Critical Facility Hazards Summary Report," IDO-16332, March 27, 1957.

the coolant passages in ETR filler pieces. The water volume associated with these pieces is 20% of the total volume (metal-to-water ratio = 4). In all loadings studied an aluminum filler piece was also desired in grid position I-9 where a control rod guide tube is located. Aluminum plates were inserted in this guide tube to displace enough water to duplicate the metal-to-water ratio of the standard filler pieces.

The fuel elements which were used in these measurements contained 320 g U-235 and on the average 1.7 g natural boron. In addition, six elements with the same U-235 content but which contained no boron were used to shim the reactor by loading them with boron impregnated polyethylene tapes. The control rod fuel sections used contained 130 g U-235 and on the average 0.68 g natural boron. Drawings of the fuel element, and control rod fuel section and its guide tube are shown in Figures 3.0-3 and 3.0-4.

The experiment mockups were made from stock aluminum rod (2.5 in. diameter) and schedule 40 stainless steel pipe (3.068 in. i.d. and 3.5 in. o.d).

3.2 Loading Configurations for ATR Mockups

Inasmuch as no control rods are currently planned in the fuel region for the ATR it would have been desirable to mockup the core of the ATR completely with fuel elements in the arrangement shown in Figure 3.0-5 (Core 1). This was impossible in these critical experiments however because the safety rods were necessary for shutdown and because time did not permit removing the control rod guide tubes to permit insertion of fuel elements in those control rod positions which did not contain safety rods. The fuel arrangement desired, intersected ten control rod positions. Fortunately, all four safety rod positions (H-7, K-9, G-11, M-11) and a driven shim (gray) rod position (H-13) were located in fueled regions. The remaining five positions contained fixed control rod fuel sections. As was mentioned previously, the other six guide tubes remained in the core but were water filled. These six tubes are not shown in the figures.

Because of these considerations, plus the boron built into the ETR elements, it was not possible to achieve criticality with the desired loading configuration as shown in Figure 3.0-5 (Core 1). As a result, two extra elements had to be added. Because adding these elements produces flux distributions different from those in the desired loading, two loadings in which the two elements were placed in different locations were studied to determine the effects of these elements. In one loading the elements were located in the center experimental space so that almost symmetrical neutron flux distributions would be produced. In the second, the elements were located in the experimental space in diametrically opposite lobes. These loading arrangements are shown as Core 2 and Core 3 respectively in Figure 3.0-5. The effects on the calculated neutron flux of different PDQ mesh descriptions were studied for Core 4 of Figure 3.0-5.

3.3 Experimental Procedures and Treatment of Data

Thermal neutron flux distributions were measured to determine 1) the flux gradients that could be expected from narrow fueled regions, and 2) the effects of the reflector on the flux in an experiment located within a lobe. Most of the detailed measurements were made in and around the NE quadrant, or lobe, which contained no control rod fuel sections. In those fuel elements where detailed measurements were not made, the one measurement was made at the midplane in the center of the element. As is seen in the detailed flux plots, this is approximately the minimum flux within the element at the horizontal midplane.

The thermal neutron flux distributions were determined from the activity of irradiated gold foils, and bare and cadmium covered gold wires. The foils were 5/32 in. diameter by 0.005 in. thick. The cadmium ratios were determined from 0.040 in. diameter gold wires 3 in. long, the centers of which were covered with a cadmium sleeve (0.020 in. wall and 1 in. long). After irradiation the wires were cut into 1/4 in. sections and the average activity of the bare and covered sections was used to calculate the cadmium ratios. The cadmium ratios from sleeves were normalized against standard cadmium covered foils.

The foils and wires, with cadmium sleeves, were taped with plastic electricians tape to either lucite strips, aluminum strips, or directly on an experiment. The lucite strips were used where measurements were made within a fuel element. These strips were inserted in the fuel element coolant channels and were designed to position the neutron detectors within $\pm$ 0.03 in. of the desired location. The aluminum strips were used where measurements were desired in a water space. These strips, containing the detectors, were taped on some object, usually a fuel element, such that they protruded into the desired region.

The activity of all the foils was converted to relative thermal flux by use of the cadmium ratios. A more complete discussion of the experimental measurements can be found in IDO-16667[2].

3.4 PDQ Calculations

Two dimensional calculations were made for the three experimental loadings (Cores 2, 3, and 4) using the IBM-704 code PDQ-3 and utilizing almost the entire number of mesh points allowed in the PDQ code. All three loadings went critical with the shim rod in position H-13 partially inserted and all other rods fully withdrawn. However, for the two-dimensional calculations, the rod in position H-13 was assumed to be fully withdrawn and the position filled with the 130 g shim fuel section.

A two-group problem was run for each core using a "standard" mesh overlay. A four-group problem was run for Core 3 using this standard mesh and a two-group problem was run for Core 4 using a

---

1. D. R. deBoisblanc et al., "The Advanced Test Reactor - ATR Final Conceptual Design," IDO-16667, November 1, 1960.

"special" mesh wherein the experiment in the NE lobe was better represented than in the standard mesh.

The fuel elements in the standard mesh and in the NE quadrant of the special mesh were divided into five regions as shown in Figure 3.0-6. Region 1 is the fuel zone with narrow channel spacing (0.105 in.), regions 2 are the fuel zones with the wide channel spacing, and regions 3 are the side plate zones which include the nonfuel bearing edges of the fuel plates and associated water channels. All material within each region was assumed to be homogenized uniformly throughout the region.

Because the number of mesh points in PDQ is limited, it was necessary to use the same size of regions to homogenize the shim rods and shim rod guide tubes (positions J-5, J-7, E-9, G-9, and M-9) as was used for the fuel elements. Thus, the fuel of each shim rod was homogenized into region 1 (Figure 3.0-6) by keeping the metal-to-water ratio in this region the same as in the fueled portion of the actual shim rod. All remaining metal and water was homogenized uniformly into regions 2 and 3. The guide tubes were homogenized by putting pure water in region 1 and uniformly homogenizing the guide tube and the necessary amount of water into regions 2 and 3.

The experiments in the standard mesh were each homogenized into two regions as shown in Figure 3.0-7. The area of the inner region is equal to that of the aluminum rod. The stainless steel tube and water in the annulus are homogenized into the outer region.

In the special mesh, the fuel elements, shim rods, and guide tubes in all but the northeast quadrant were homogenized uniformly over their respective 3.04 in. square cells.

The aluminum, stainless steel and water of the experiment in the SW lobe of the special mesh were homogenized over the entire 3.1018 in. square cell. The mesh lines that were made available by this "coarse" homogenization were then utilized in the NE lobe to obtain a better representation of the experiment. The representation of the experiment in this special mesh is shown in Figure 3.0-8. The stainless steel pipe, the water annulus and the aluminum rod are each represented separately.

The fast group constants for these problems were obtained from the MUFT-4 program and the thermal constants are Maxwellian averaged. All constants were obtained from the same cross section data and by the same methods as discussed in Section 2.0.

3.5 Results

The measured relative thermal flux values were normalized to the PDQ values of thermal flux. This was done by summing the thermal flux values at the center of each fuel element and then multiplying the measured values by the ratio of the PDQ sum to the measured sum.

The following measurements were made in addition to the flux measurements at the fuel element center. In Core 2, flux measurements were made in the N-S direction through the center of position L-8, and in the E-W direction through the center of positions I-10, J-10 and K-10. In Core 3, thermal flux measurements were made in the E-W direction, completely across the core, along the center of the 8 row. In Core 4, thermal flux measurements were made in the NE lobe in the E-W direction in channel 18 of the 6 row, and at the center of the 8 row. Thermal flux measurements were also made circumferentially around the experiment in the NE lobe in Core 4. These measured traverses normalized to the PDQ values, are shown in Figures 3.0-9 through 3.0-14 along with the calculated values. Figure 3.0-15 shows the comparison over the core of the PDQ and measured values of thermal flux at the center of each fuel element for Core 2. As can be seen, there is in general good agreement between the measured and calculated thermal flux values. The error in H-14 is believed to result from the partial withdrawal of the rod in H-13 for criticality. Table 3.0-A gives a comparison of calculated and measured fuel element maximum-to-average thermal flux ratios in the E-W direction of the 8 row of load 3. This table also brings out the good agreement between measured and calculated distributions within a fuel element.

TABLE 3.0-A

MAXIMUM-TO-AVERAGE THERMAL FLUX VALUES

ALONG THE CENTER OF ROW 8 OF ATR MOCKUP - CORE 3

Position	2-Group	4-Group	Measured
E-8	1.34	1.40	1.22
F-8	1.19	1.19	1.18
G-8	1.20	1.17	1.19
H-8	1.14	1.14	1.18
I-8	1.28	1.26	1.28
J-8	1.27	1.28	1.31
K-8	1.26	1.25	1.30
L-8	1.31	1.32	1.42
M-8	1.32	1.34	1.33
N-8	1.34	1.46	1.31

NOTE: Values apply to fuel containing region only, i.e., to region 1 of Figure 3.0-6.

The two-group and four-group thermal flux distributions along the 8 row of Core 3 are shown in Figure 3.0-16. In this figure, the four-group flux was power normalized over the core to the two-group flux.

The flux obtained from the special mesh PDQ problem (Core 4) was power normalized over the NE lobe to the standard mesh flux. Since each fuel element was homogenized into one region in three lobes of this special mesh case there is no thermal flux peaking between fuel elements in these three lobes. This effect may be seen in Figure 3.0-13 where the special mesh flux is plotted with the standard meshflux along row 8. On the right half of this figure the traverse is through the NE lobe and the two flux distributions are nearly the same. The greater peaking in the special mesh case between elements L-8 and M-8 is due to the proximity of the experiment in the NE lobe and the better representation of the experiment in the special mesh. The shape of the circumferential flux around the experiment (Figure 3.0-14) is given quite well by the special mesh PDQ case. However, the measured values are about 10% higher than the PDQ values.

Table 3.0-B lists the measured and the calculated values of k_{eff} for the 3 cores. The two-group standard mesh PDQ values are all about 5-1/2% high, the four-group value is about 3% high, and the special mesh value is 7% high.

Thus, the use of the PDQ program with Maxwellian averaged thermal constants gives good agreement to the measured thermal flux values but the calculated values of k_{eff} are in rather poor agreement with the measured values. The four-group problem yields better agreement in the value of k_{eff} and a somewhat different (but no better) flux distribution from the two-group problem. In the special mesh problem the flux distribution in the homogenized elements follows the general trend of the standard mesh flux distribution but does not give the thermal flux peaking between fuel elements.

TABLE 3.0-B

MEASURED k_{eff} AND PDQ EIGENVALUES

FOR THREE ATR MOCKUP CORES

Core	Measured k_{eff}	PDQ Eigenvalues		
		2-Group Standard Mesh	4-Group	Special Mesh
2	1.0016	1.058	-	-
3	1.0017	1.052	1.034	-
4	1.0022	1.058	-	1.070

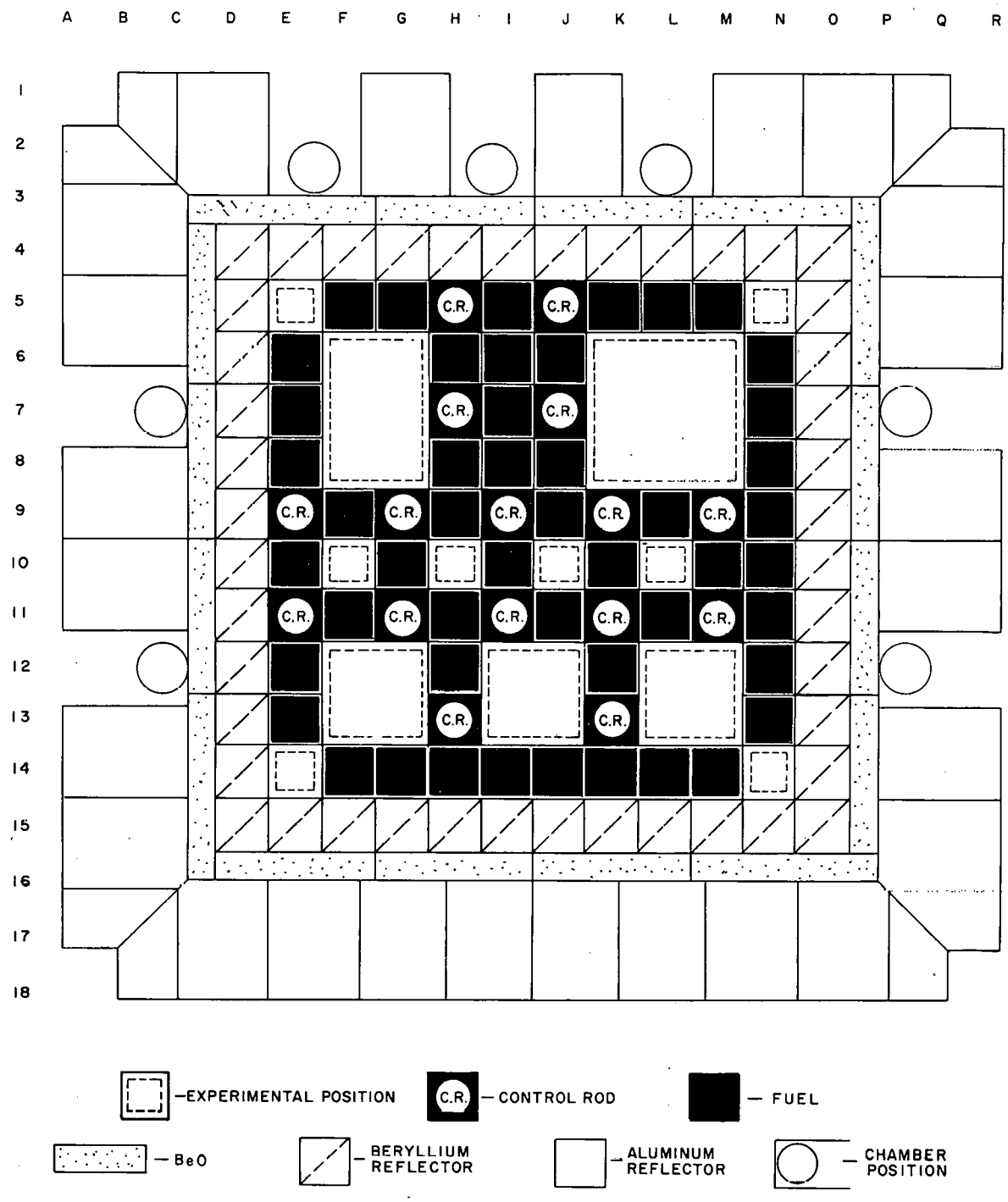

FIG. 3.0-1

ETRC CORE DIAGRAM

PP CO-C-2751

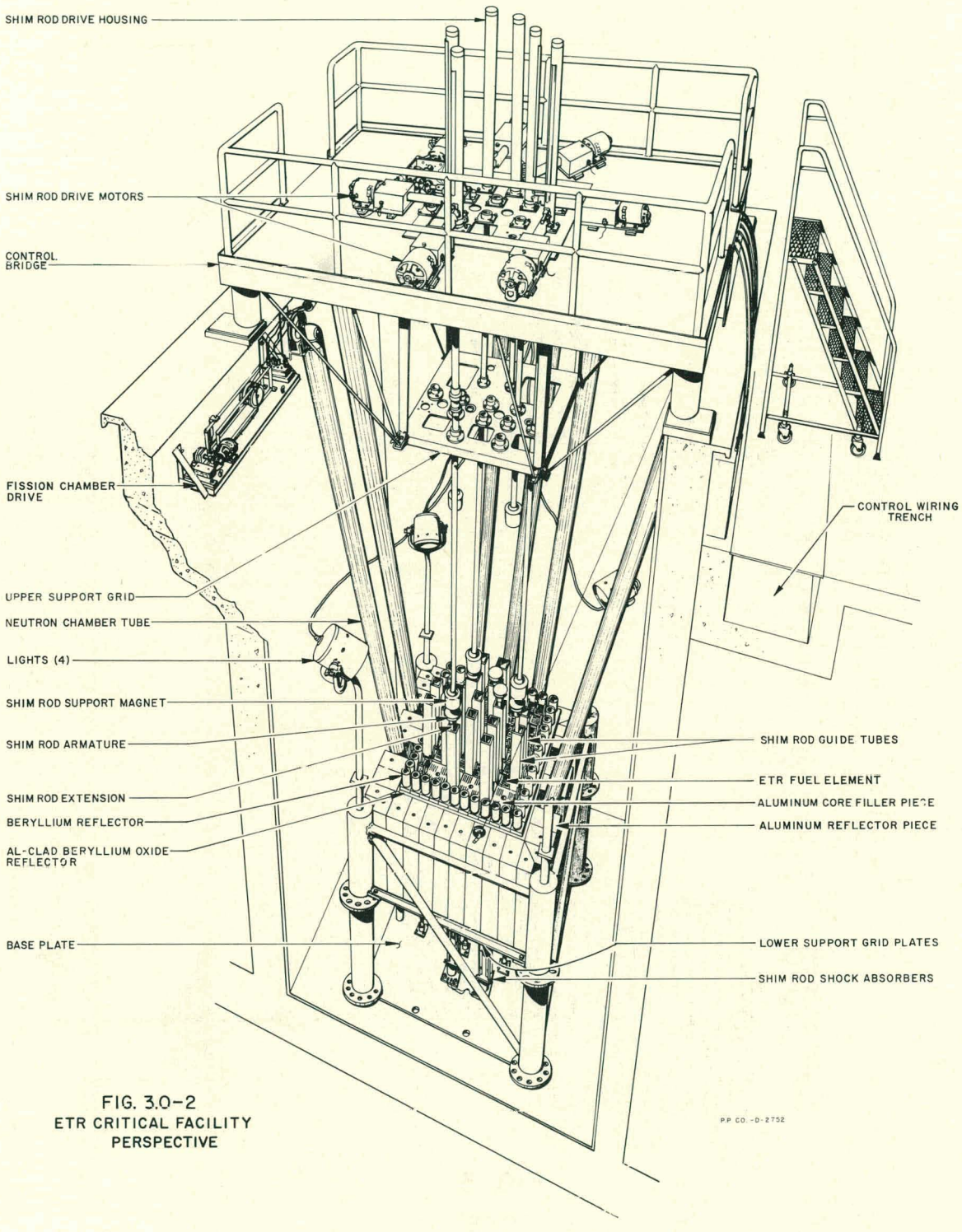

FIG. 3.0-2
ETR CRITICAL FACILITY
PERSPECTIVE

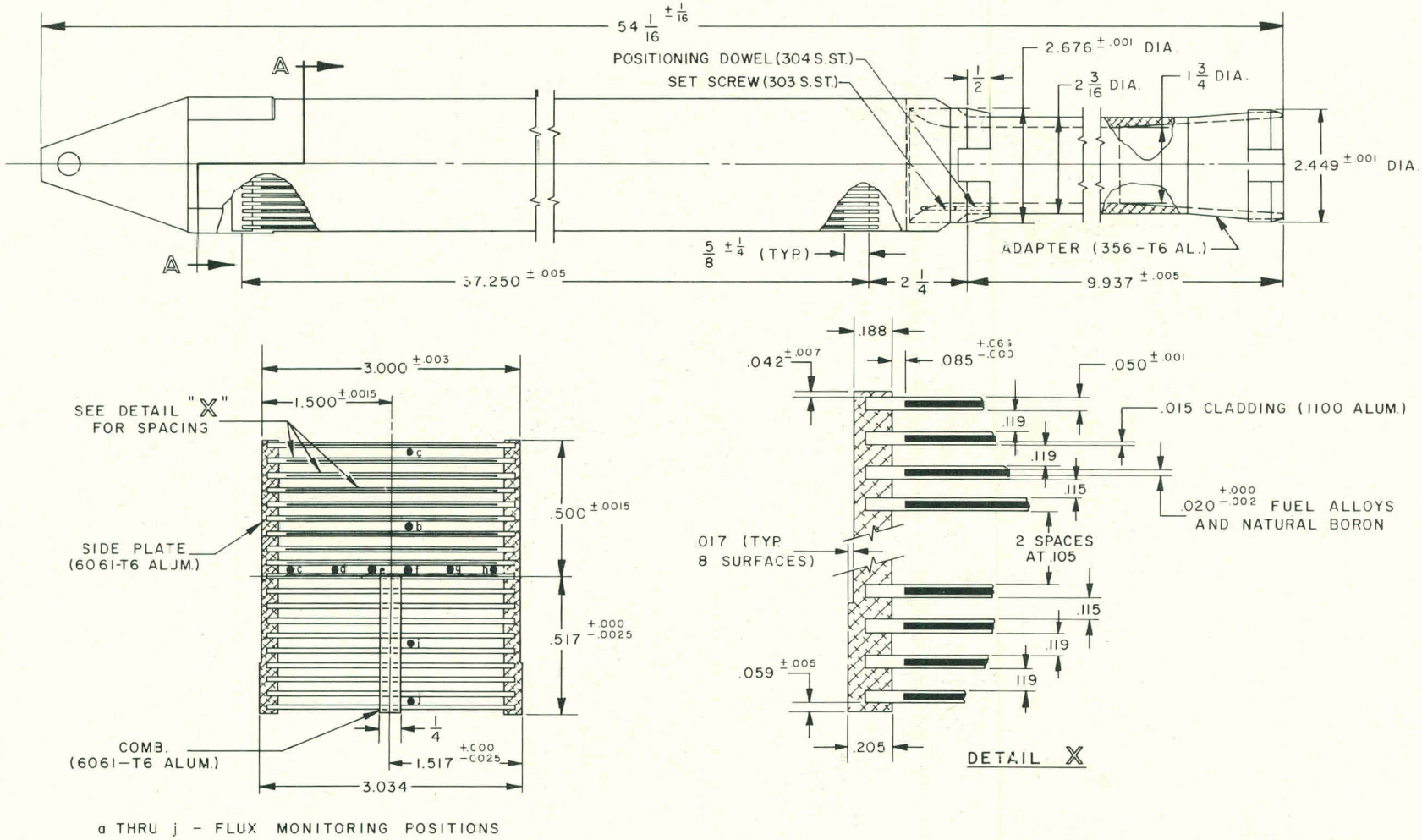

FIG. 3.0-3

ETR AND ETRC FUEL ASSEMELY

PP CO.-C-2884

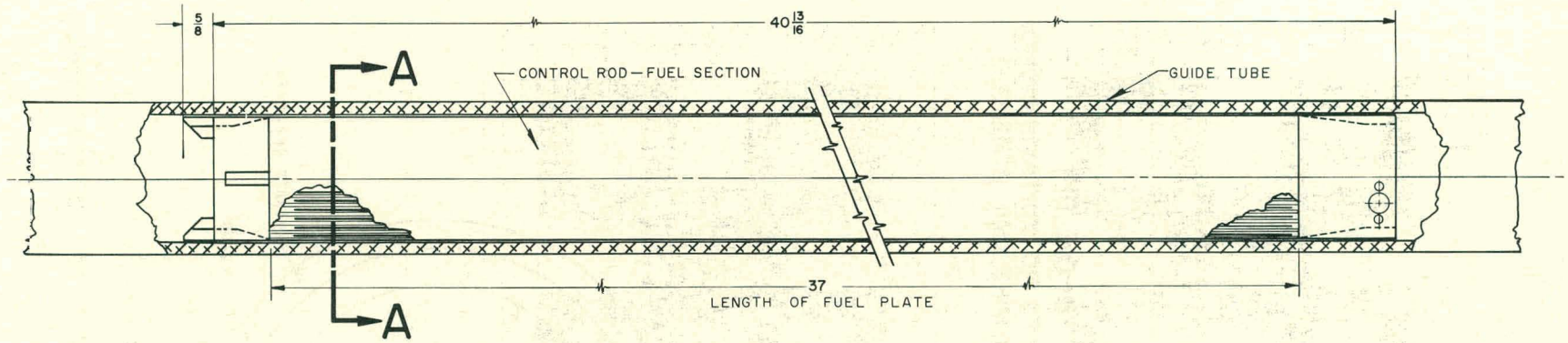

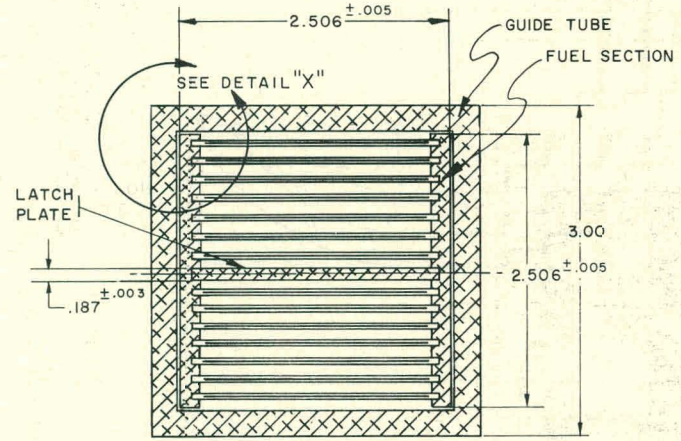

SECTION A-A

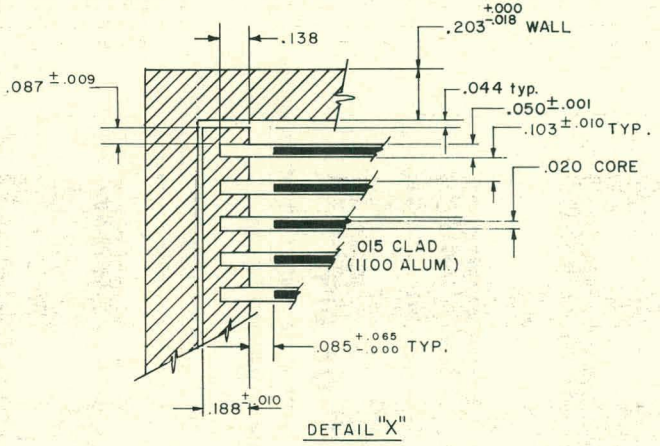

DETAIL "X"

FIG. 3.0-4

P.P.CO.-C-2754

ETR AND ETRC CONTROL ROD
FUEL SECTION AND GUIDE TUBE

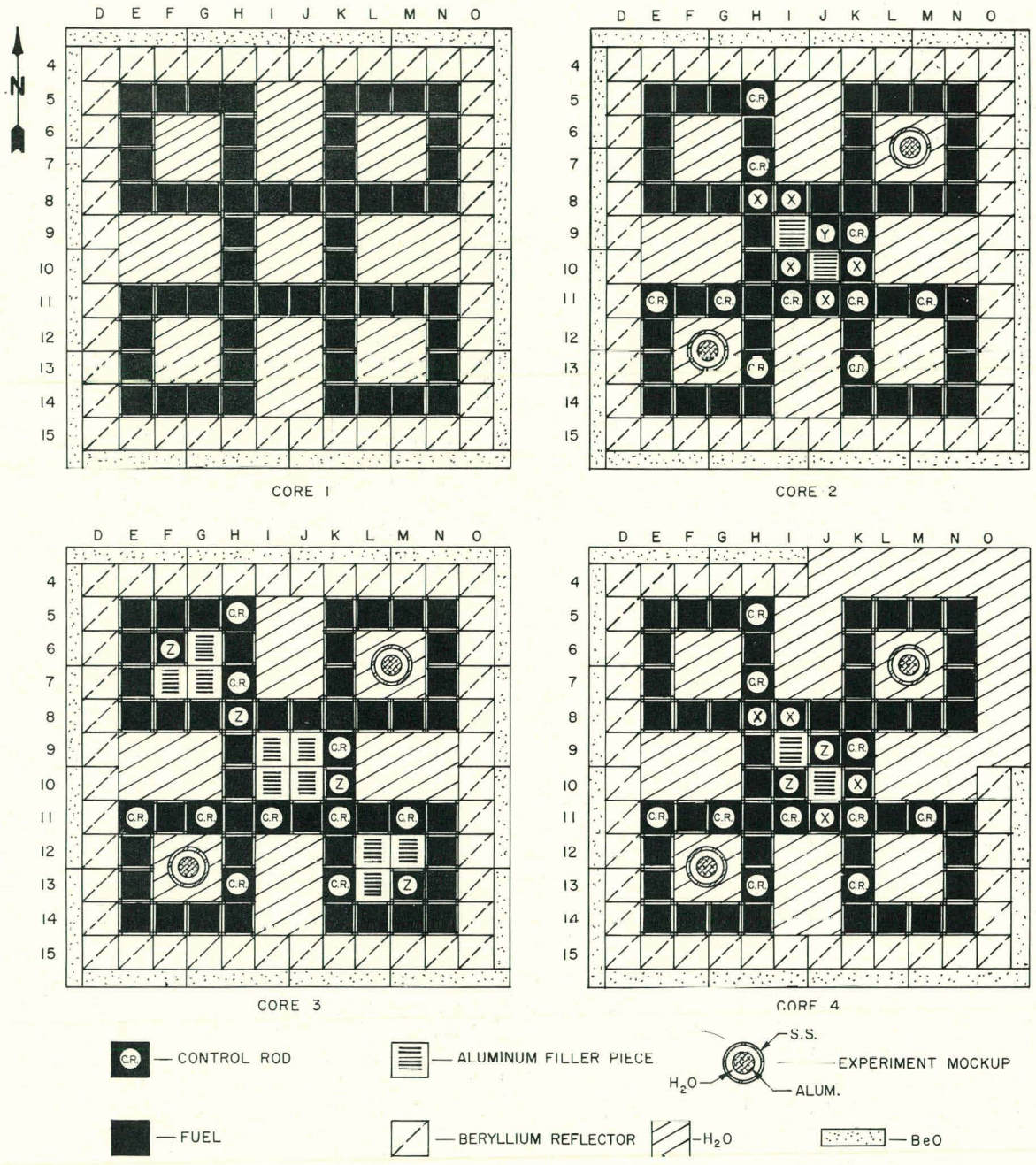

P.P. CO.-C-3170

FIG. 3.0-5
ATR MOCKUP LOADING IN THE ETRC

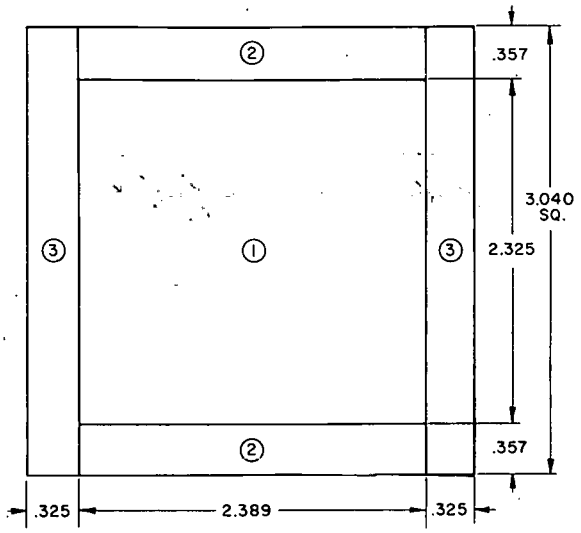

FIG. 3.0-6
HOMOGENIZATION OF ETRC FUEL ELEMENTS AND SHIM RODS

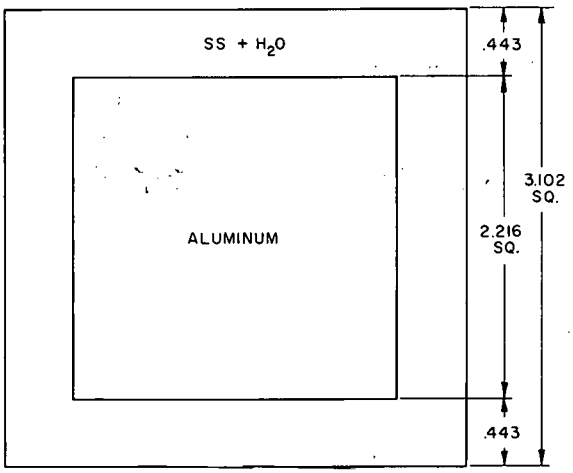

FIG. 3.0-7
HOMOGENIZATION OF ETRC EXPERIMENT IN STANDARD MESH

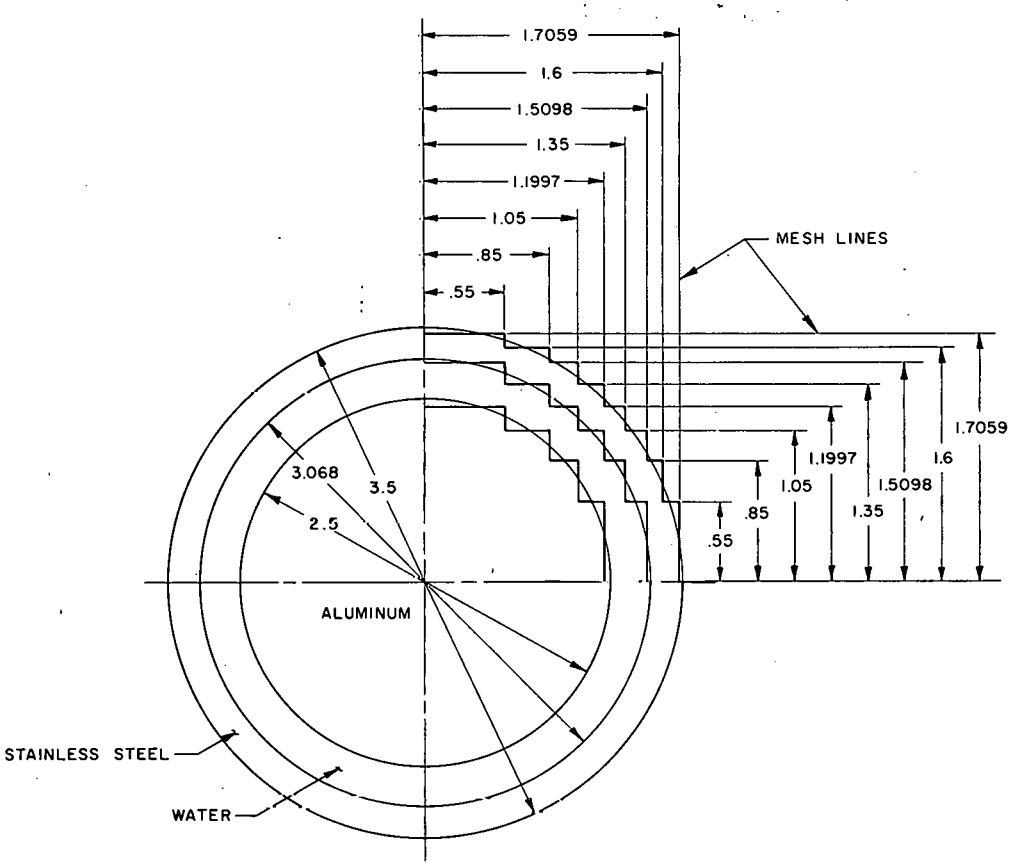

PP CO.-C-3171

FIG. 3.0-8
REPRESENTATION OF ETRC EXPERIMENT IN NORTHEAST LOBE OF SPECIAL MESH

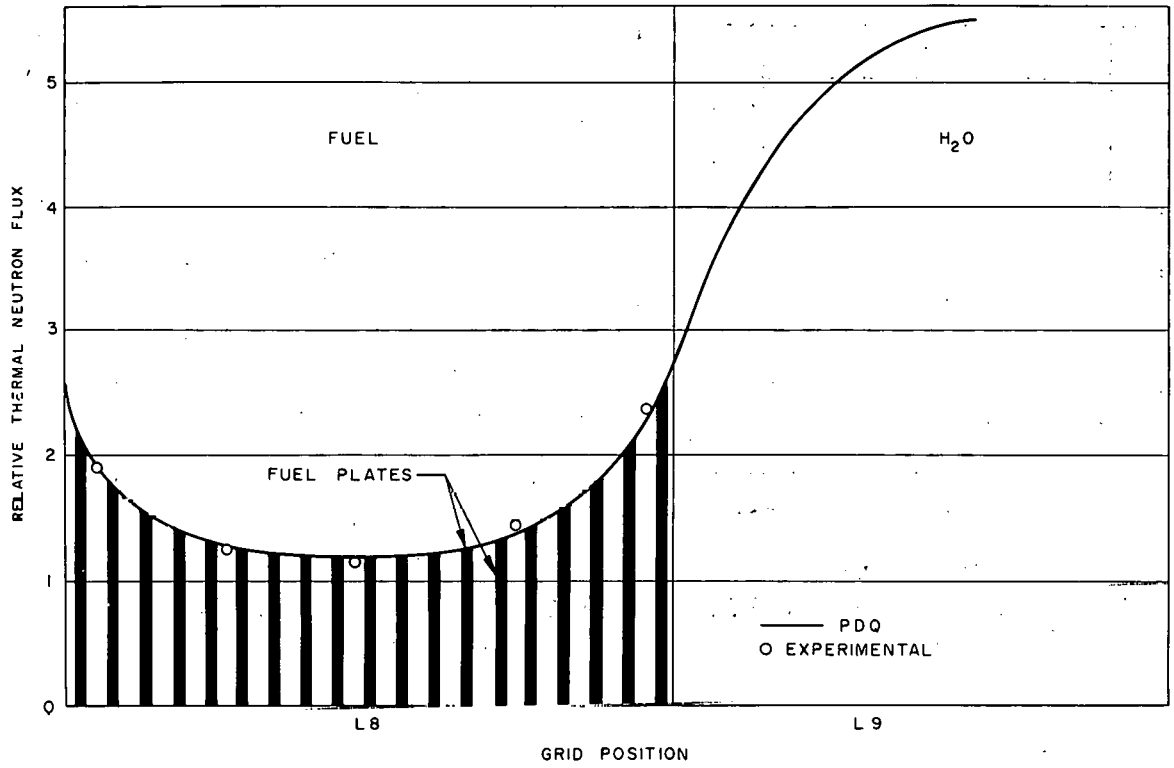

FIG. 3.0-9 PP CO.-B-3172

THERMAL FLUX IN POSITION L8 (N-S TRAVERSE) OF ATR MOCKUP-CORE 2

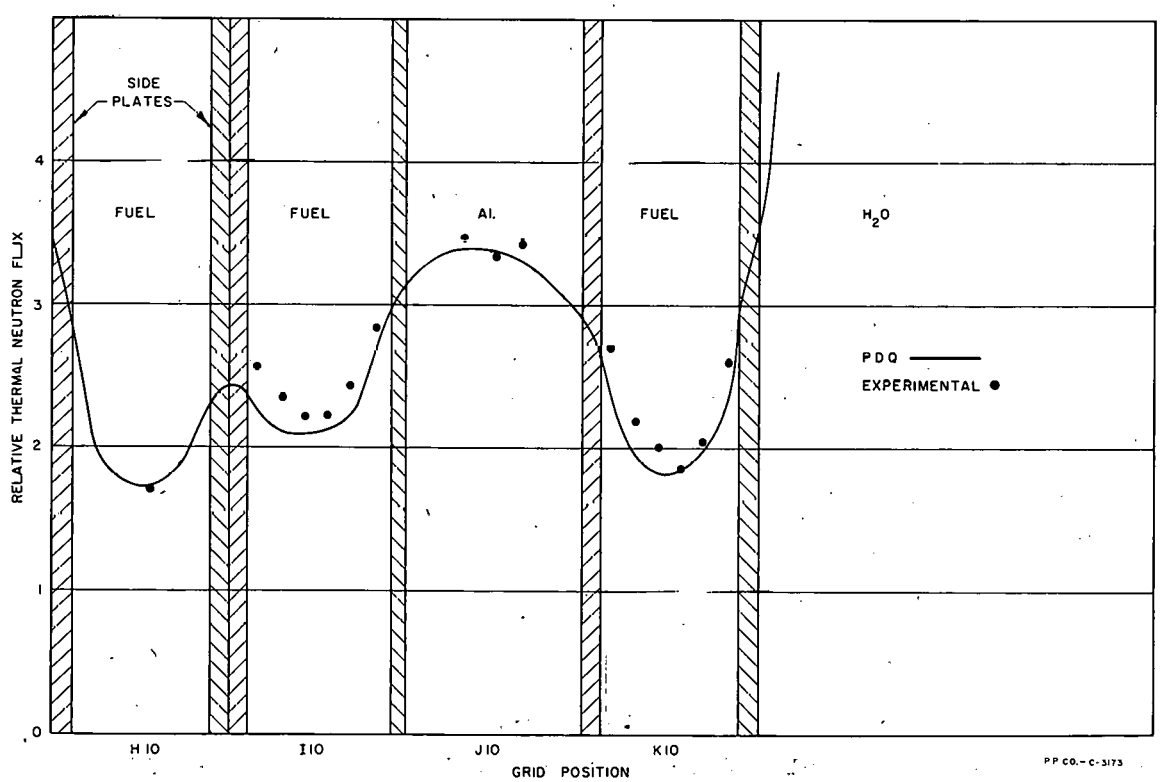

FIG. 3.0-10

THERMAL FLUX IN ROW 10 OF ATR MOCKUP-CORE 2

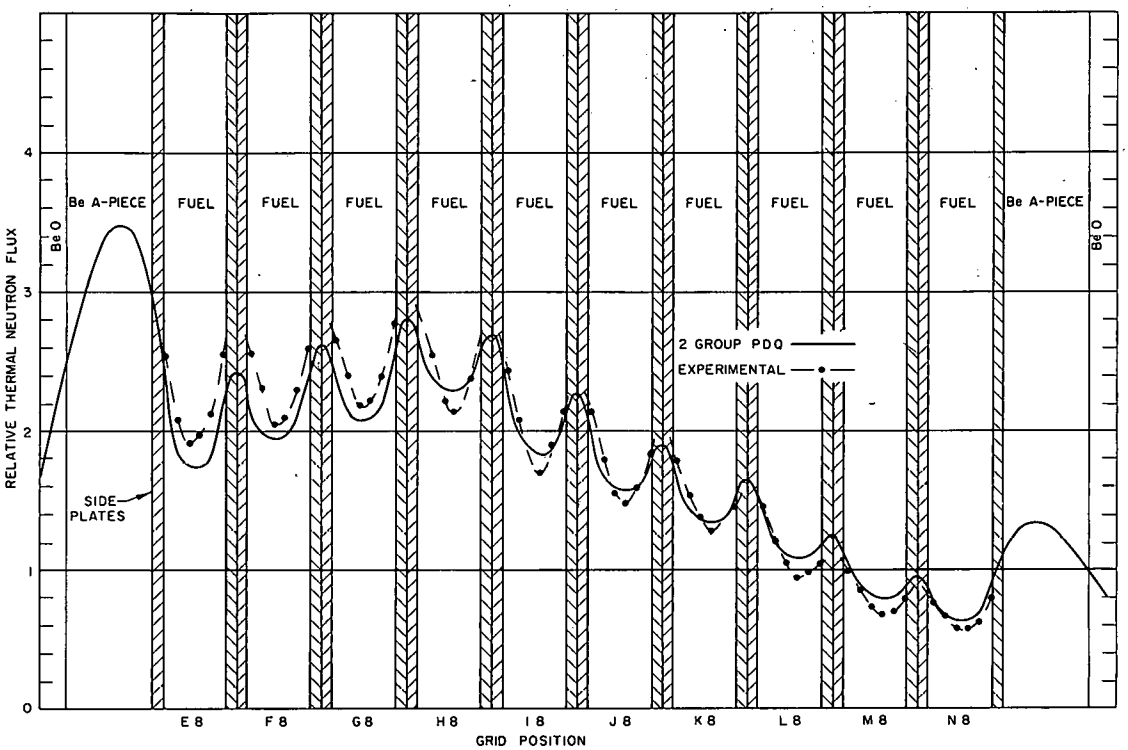

FIG. 3.0-11
THERMAL FLUX IN ROW 8 OF ATR MOCKUP-CORE 3

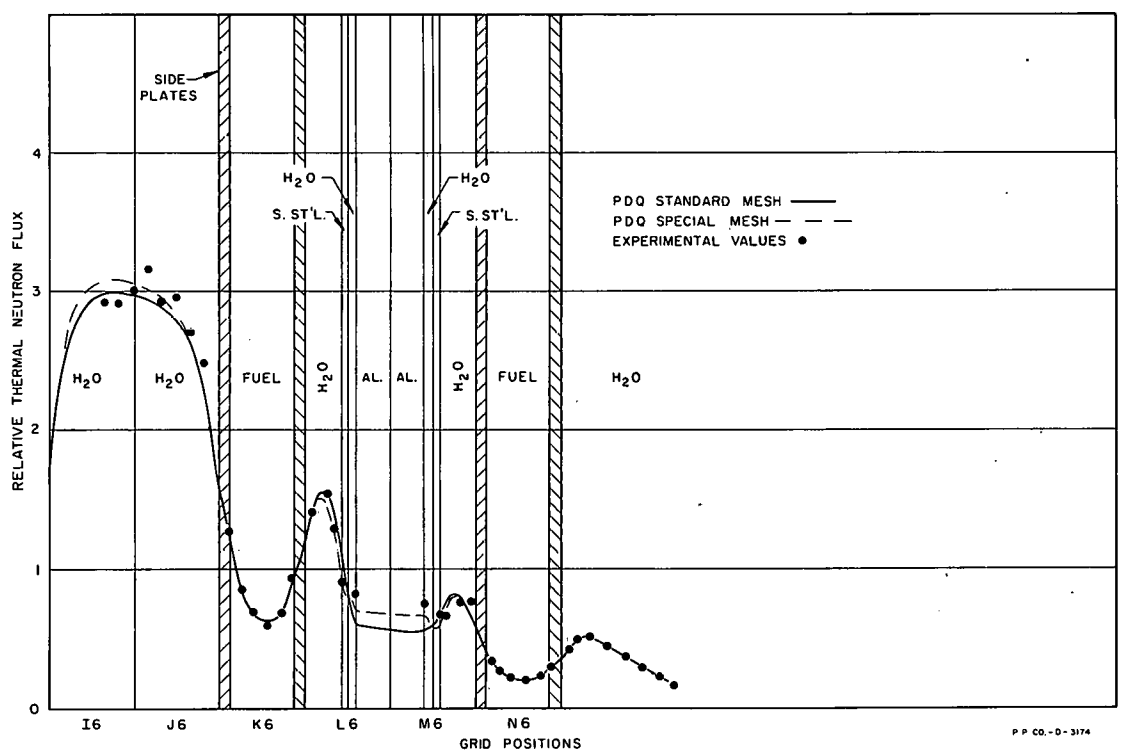

FIG. 3.0-12
THERMAL FLUX IN ROW 6 OF ATR MOCKUP-CORE 4

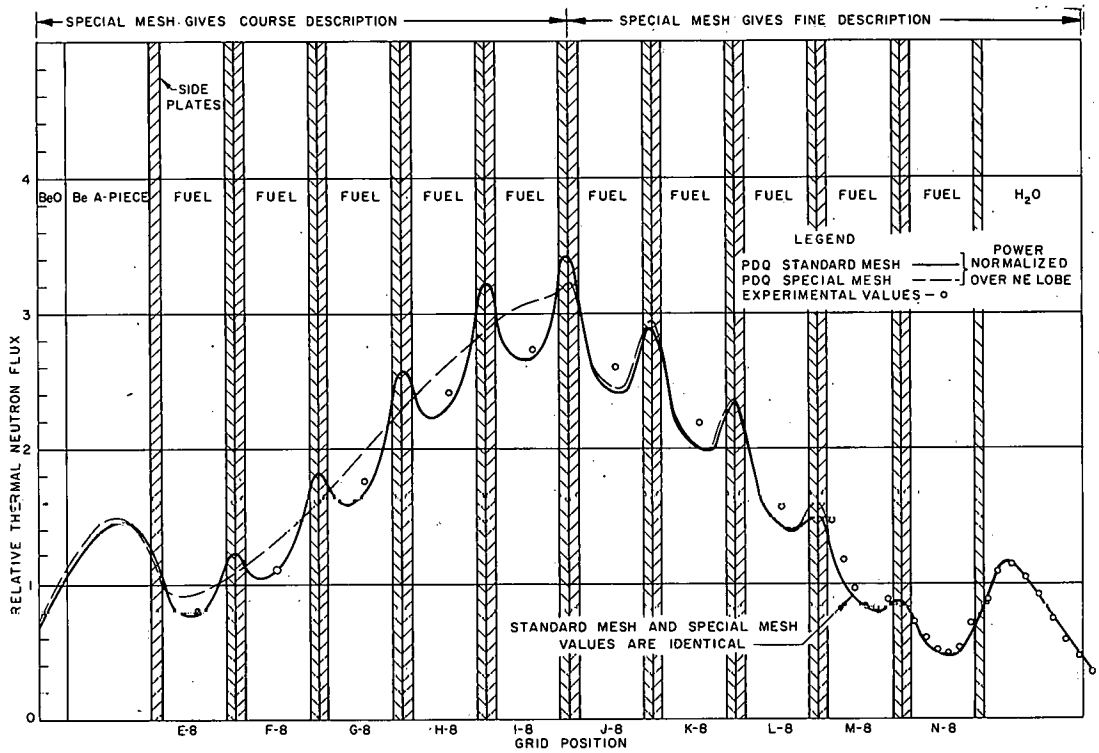

FIG. 3.0-13
THERMAL FLUX IN ROW 8 OF ATR MOCKUP-CORE 4

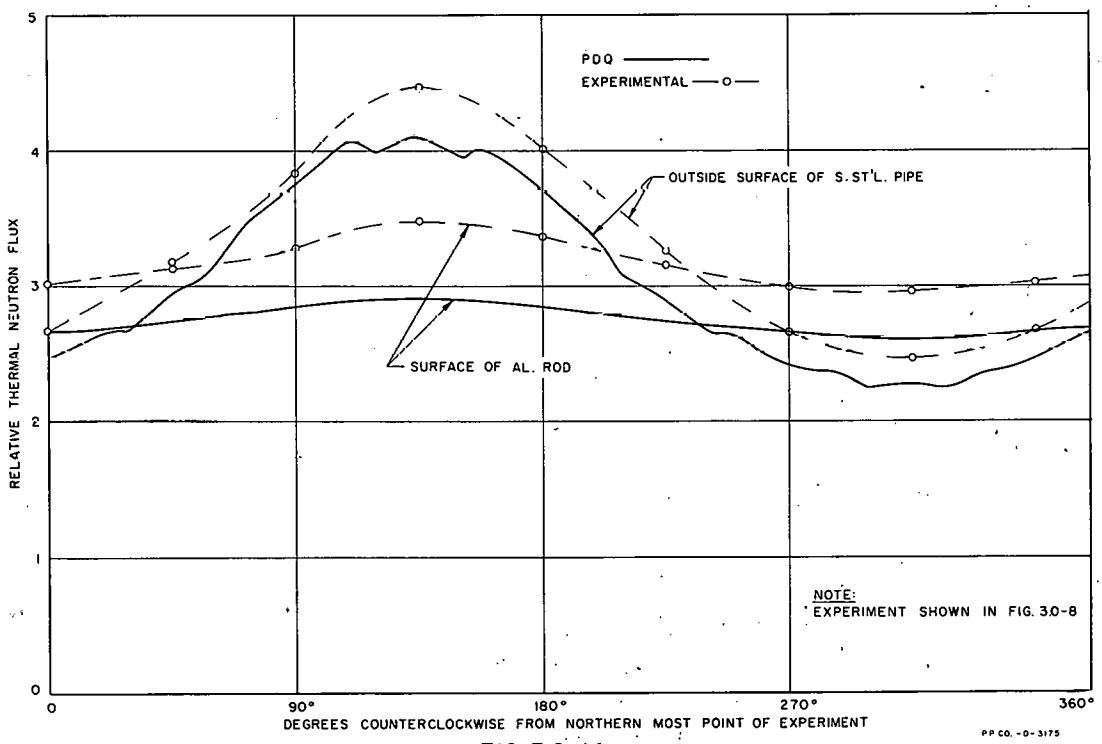

FIG. 3.0-14
THERMAL FLUX IN NORTHEAST EXPERIMENTAL FACILITY OF ATR MOCKUP-CORE 4

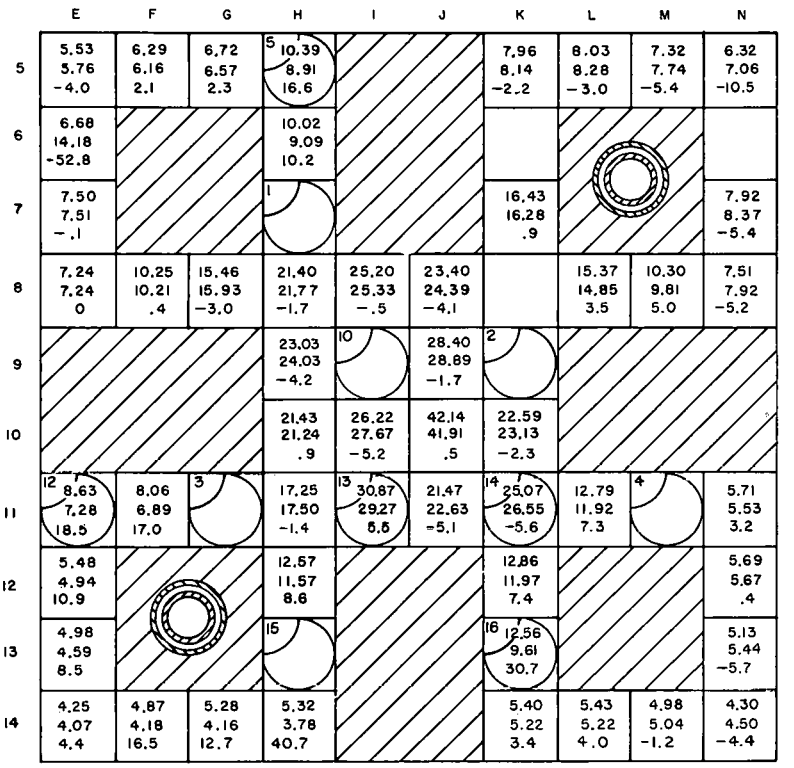

1. PDQ VALUE
2. MEASURED VALUE
3. PERCENT ERROR = $\frac{\text{PDQ} - \text{MEAS.}}{\text{MEAS.}} \times 100$

PP CO.-B-3176

FIG. 3.0-15

MIDPLANE THERMAL FLUX IN ATR MOCKUP-CORE 2

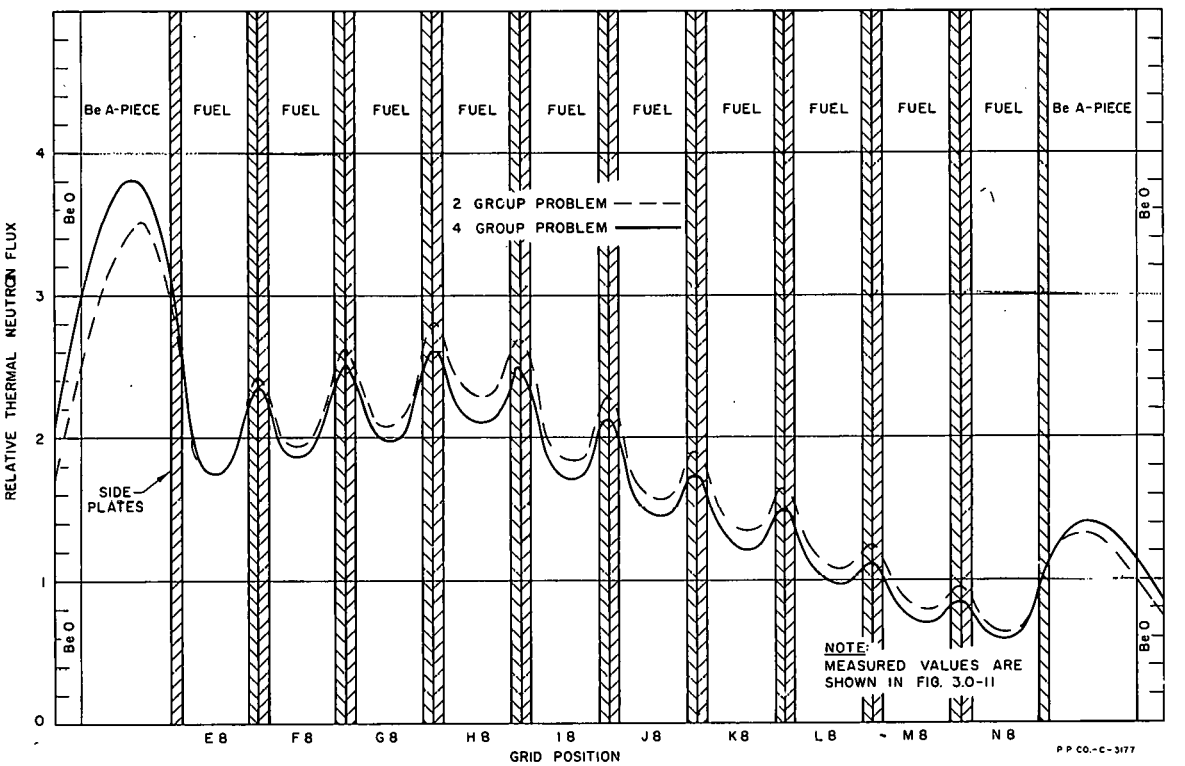

FIG. 3.0-16

THERMAL FLUX FROM 2 GROUP AND 4 GROUP CALCULATIONS FOR ROW 8 OF ATR MOCKUP-CORE 3

4.0 TWO-DIMENSIONAL CALCULATIONS

The flux and power distributions and effective multiplication factors or eigenvalues for two-dimensional models of the ATR as determined by PDQ-3 calculations are presented in this section. Burnup effects and time dependent behavior are presented in Section 6.0. Each PDQ problem has been assigned a case number to facilitate reference to the original data. The case numbers are grouped into series for problems on similar models of the reactor.

4.1 PDQ-3 Problem Summary

Each of the 1000 series problems has a 3 in. D_2O reflector shim control region and an explicit representation of the pressure tubes separate from the experiment. This series uses a quarter core fine mesh representation for all problems as shown in Figure 4.0-1. As the 1000 series problems progressed changes in metal-to-water ratio, fuel densities, and reflector and neck shim poisoning were made as seemed appropriate to be more realistic toward the final selected design.

The 3000 series problems also have a 3 in. D_2O reflector shim control region but the pressure tubes are homogenized into the experiments and there are no aluminum separator rings. These problems were principally to examine the power shifting from various combinations of neck and reflector shim control poisoning and also the effects produced by adding an absorber to the fueled region. The PDQ temperature coefficient studies are a part of this series. The quarter core coarse mesh with 1764 mesh points shown in Figure 4.0-2 gives considerable savings in machine time as well as good results for the purposes for which it is used.

The 4000 series problems are of the coarse mesh type similar to the 3000 series mesh and are also described by Figure 4.0-2. These problems differ from 3000 series problems in that they have a half core description instead of a quarter core as the 1000 and 3000 series have. The half core description enables poisoning of one lobe or one neck region and observing the power shifting effect produced by this perturbation. Also, lobe fuel and center fueled regions can be poisoned further or the burnable poison removed to observe the power shifting effect.

The 5000 series problems use the fine mesh description of Figure 4.0-3 which differs from the 1000 series problems in that a solid reflector shim control region is described. Various combinations of reflector blades in and out and neck poisoned with safety blades in and out are studied. The principal purpose here is to get the total control worth (both shutdown and shim) and power shifting effects of this type of control.

The 6000 series problems are similar to the 5000 series problems in having a fine mesh description but this series has a 1/2 in. light or heavy water reflector shim control region rather than the 1/4 in. solid blade control as shown in Figure 4.0-4. Various combinations of light or heavy water poisoning and outer reflector materials have been used to evaluate this type of system.

A representative sample of each series is shown in Table 4.0-A. The 2000 series problems are concerned with the PDQ calculations on the ETRC and are not included in the table. The effects of the mesh description on the calculations and the results from a TRANSAC problem using 20,000 mesh points are discussed in Appendix 12.2.

4.2 Results of Two-Dimensional Calculations

The conditions existing at the start of the cycle for a typical experimental loading in the reactor with reflector shim control by poisoning of D_2O regions are summarized in Table 4.0-B. The same data are given for a system with poisoned H_2O reflector shim control but with a somewhat different array of experiments in Table 4.0-C. If the two shim control systems are adjusted to produce the same core power distribution the effects on the reactor are essentially equivalent. The power distribution of Table 4.0-B is adjusted to be near optimum for meeting or exceeding the flux requirements given in that table. The power division of Table 4.0-C represents a typical amount of power shifting but produces different fluxes in the same type experiment and no requirements are stated.

Tables 4.0-B and 4.0-C show that the A-3 and A-5 test flux requirements can be substantially exceeded at a reactor power of 250 Mw and a peak power density in the core of 2.5 Mw/liter. No requirements have been set for the experimental facilities exterior to the core but the flux levels there are quite satisfactory. However, it should be recognized that these fluxes cannot be controlled independently of those in the core. It is difficult to meet the thermal flux specification of 1.0×10^{15} n/cm^2 sec for an A-1 experiment when a stainless steel pressure tube is used. In this case, it is necessary to place the experiment in the center facility and use some power flattening technique to keep the maximum power density from being excessive. Replacement of the stainless with a material having the properties of zirconium increases the thermal flux by a factor of about two so that there is no problem in meeting the thermal flux requirements.

Detailed thermal flux plots along the north, east, and diagonal directions for the three mesh descriptions discussed in Appendix 12.2 are shown in Figures 4.0-5, 4.0-6 and 4.0-7, respectively. Corresponding fast fluxes are shown in Figures 4.0-8 and 4.0-9 for the east and diagonal directions. Combined fast and thermal flux plots for a fine mesh representation are shown in Figures 4.0-10, 4.0-11 and 4.0-12. These plots are typical for the ATR with the exception that a zirconium tube is used instead of stainless steel for the A-1 tests and therefore the fluxes in these tests are too high.

TABLE 4.0-A

TYPICAL PDQ-3 PROBLEMS

Problem #	1035	3C01	4008△	50C2△	6007△
Mesh	84 x 84 (7056)	42 x 42 (1764)	43 x 86 (3698)	87 x 87 (7569)	87 x 87 (7569)
k_{eff}	1.C96	1.2265	1.2075	1.1449	1.1636
Composition Number and Description	(1) Outer reflector (D_2O)	D_2O	-- **	(1) Outer reflector(D_2O)	D_2O
	(2) E. refl. shim control	—	--	(2) E. inner refl.(Be+10% H_2O)	D_2O
	D_2O +3.8 g/liter D_3BO_3	D_2O	D_2O + 3 g/liter D_3BO_3	(3) Outer loop refl(Be+10%H_2O)	D_2O
	(3) Outer loop reflector	--	--	(6) East lobe fuel	--
	Be + 10% H_2O	--	--	(8) E. lobe flux trap mod.	--
	(4) N. refl. shim control	--	--	40% H_2O + Al	--
	D_2O + 4.9 g/liter D_3BO_3	D_2O	D_2O	(9) Exp. pressure vessel	--
	(5) Separation ring (Al)	None	None	SS + void	--
	(6) E. lobe fuel region*	--	--	(10) E. lobe exper. (A-5)	--
	(7) E. lobe sep. ring (Al)	None	(7) W. refl.shim con.(D_2O)	(11) Ext. exp. flux trap mod.	--
	(8) E. lobe flux trap mod.(H_2O)	--	(8) E.&W. lobe flux tr.mod.	40% H_2O + Al	--
	(9) Exper. press. ves.(SS & void	--	40% H_2O + Al	(12) Ext. Exper. (A-5)	--
	(10) E. lobe exper. (A-1)	A-1, Zr, void homog.	(10) A-5, SS, void homog.	(16) Neck filler(20%H_2O+Al)	--
	(11) Ext.Exp.flux trap mod.	--	--	(17) Center Exper. (A-3)	--
	40% H_2O + Al	--	--	(18) E. lobe safety	--
	(12) Ext. Exper. (A-5)	A-5, SS, void homog.	(12) N.E.ext. exp(A-5,SS)	30% H_2O + Al	--
	(13) N. lobe sep. ring	None	(13) W. lobe fuel	(19) E lobe neck shim(H_2O)	--
	40% H_2O + Al	None	(14) N. lobe flux trap mod.	(26) Center lobe fuel	--
	(14) N. lobe flux trap mod.	--	40% H_2O + Al	(30) Safety blade guide reg.	--
	40% H_2O + Al	--	(15) N. lobe exper.	50% H_2O + Al	--
	(15) N. lobe exper.(A-5)	A-5, SS, void homog.	A-5, SS, void homog.	(31) E. refl. control blades	None
	(16) Neck filler(20% H_2O+Al)	--	(16) Neck fill.(20%H_2O+Al)	30% H_2O + Al	None
	(17) Center Exper. (A-3)	A-3, SS, void homog.	(17) Center Experiment	(33) E. lobe sep. ring (Zr)	(34) E. refl. liq. shim con.
	(18) E. lobe safety(30%H_2O+Al)	--	A-3, SS, void homog.		H_2O
	(19) E.lobe neck shim control	None	(18) E.&W. safety(30%H_2O+Al)		

(more)

TABLE 4.0-A (Cont.)

TYPICAL PDQ-3 PROBLEMS

Problem #	1035	3001	4008△	5002△	6007△
Composition Number and Description	(20) N.lobe safety(30%H_2O+Al)	--	(21) N.lobe neck shim(H_2O)		
	(21) N.lobe neck shim control	--	(22) Center Exp.flux trap mod.		
	H_2O+25 g/liter H_3BO_3	H_2O	20% H_2O + Al		
	(22) Center Exp.flux trap mod.	--	(23) E.lobe neck shim(H_2O)		
	20% H_2O + Al	--	(24) W. lobe exper.		
	(23) E.lobe neck shim control	--	A-5, SS, void homog.		
	H_2O+25 g/liter H_3BO_3	H_2O	(26) Center lobe fuel		
	(24) N.lobe neck shim control	None	(27) N. lobe fuel		
	H_2O+25 g/liter H_3BO_3	None	(29) N.W. Ext. Experiment		
	(25) Outer reflector(D_2O)	None	A-5,SS, void homog.		
	(26)	--	(30) W.lobe neck shim(H_2O)		
	(27) N. lobe fuel region*	--	/		
	(28) None	None			
	(29) E.exper.pres.ves.(Zr+void)	None			

* 25 kg of U-235 in core
** A dash (--) indicates same as previous column
△ Run with diagonal symmetry
/ Composition numbers omitted are not used in calculation

TABLE 4.0-B

TYPICAL START OF CYCLE CONDITIONS
FOR REACTOR WITH POISONED D_2O REFLECTOR SHIM CONTROL

PDQ Case	1035
Mesh Description	Figure 4.0-1
Core Fuel Content	25.2 Kg U-235
Core Burnable Poison Content	128 g natural boron

Reflector Control Region	Grams D_3BO_3/liter of D_2O
East	3.8
West	3.8
North	4.9
South	4.9

Neck Control Region	Grams H_3BO_3/liter of H_2O
East	25
West	25
North	25
South	25

Core Region	Fraction of Core Power
Center	25.4
East	20.1
West	20.1
North	17.2
South	17.2

Reactor Power	250 Mw
Peak Power Density	2.56 Mw/liter

Experiment			Fast Flux(n/cm^2 sec)		Ther.Flux(n/cm^2 sec)	
Location	Type	Loop	Calc.	Required	Calc.	Required
Center	A-3	SS	2.1×10^{15}	1.5	0.61×10^{15}	0.48
East Lobe	A-1	Zr	1.3×10^{15}	1.0	1.4×10^{15}	1.0
West Lobe	A-1	Zr	1.3×10^{15}	1.0	1.4×10^{15}	1.0
North Lobe	A-5	SS	1.3×10^{15}	1.0	0.45×10^{15}	0.32
South Lobe	A-5	SS	1.3×10^{15}	1.0	0.45×10^{15}	0.32
Exterior	A-5	SS	1.6×10^{15}	-	0.55×10^{15}	-
East Lobe*	A-1	SS	1.3×10^{15}	1.0	0.66×10^{15}	1.0
West Lobe*	A-1	SS	1.3×10^{15}	1.0	0.66×10^{15}	1.0

Safety Blades**	Eigenvalue
Withdrawn	1.096
Inserted	1.015 (Case 1037, flux and power distributions not applicable for comparison with other calculations)

* Flux values adjusted
** Narrow type blades. See Figure 4.0-1

TABLE 4.0-C

TYPICAL START OF CYCLE CONDITIONS
FOR REACTOR WITH POISONED H_2O REFLECTOR SHIM CONTROL

PDQ Case	6014
Mesh Description	Figure 4.0-4
Core Fuel Content	
For PDQ Calculations	25.2 Kg U-235
After Adjustment for Structural Mat'l in Refl.	33 Kg U-235
Core Burnable Poison Content	128 g natural boron
Eigenvalue	1.086

Reflector Control Region	Grams H_3BO_3/liter of H_2O
East	22.8
West	22.8
North	29.4
South	29.4

Neck Control Region	Grams H_3BO_3/liter of H_2O
East	25
West	25
North	25
South	25

Core Region	Fraction of Core Power
Center	27.8
East	19.1
West	19.1
North	17.0
South	17.0

Reactor Power	250 Mw
Peak Power Density	2.51 Mw/liter

Experiment			Fast Flux	Thermal Flux
Location	Type	Loop	n/cm^2 sec	n/cm^2 sec
Center	A-3	SS	2.1×10^{15}	0.55×10^{15}
East Lobe	A-5	SS	1.4×10^{15}	0.76×10^{15}
West Lobe	A-5	SS	1.4×10^{15}	0.76×10^{15}
North Lobe	A-5	SS	1.2×10^{15}	0.39×10^{15}
South Lobe	A-5	SS	1.2×10^{15}	0.39×10^{15}
Exterior	A-5	SS	1.3×10^{15}	0.56×10^{15}

A number of reactivity effects as found by two-dimensional calculations are tabulated in Tables 4.0-D to 4.0-J. One-dimensional results are discussed in Section 7.0.

The maximum power density depends upon the experimental loading, the core power distribution, the composition in the flux traps and the detailed design of the core and adjacent regions. Therefore, the results are given for situations expected to be typical in operation of the ATR but not necessarily representing the extreme conditions that may be desired. The maximum power densities as given in Tables 4.0-B and 4.0-C are for uniform distribution of fuel and burnable poison in the core and can be reduced if necessary by appropriate power flattening measures. Calculation of the peak power density is subject to a number of uncertainties and the following procedure has been used to provide a consistent approach. The maximum value of the pointwise flux as calculated by PDQ for the homogenized core region is found and the maximum-to-average thermal flux ratio determined for the PDQ plane and multiplied by 1.4, the axial maximum-to-average ratio. The average power density is then multiplied by this ratio and several corrections applied as described below to obtain the estimate of the peak power density. The fast flux is flatter than the thermal flux and from examination of a number of cases a correction factor which reduces the peak by 8% has been determined. The homogenization of the core eliminates the peaking along the core annulus near the sideplates of the elements. Supplementary one-dimensional WANDA and S_n calculations show that this effect increases the peaking by about 10 to 15%. The actual value will depend on the design of the element and can be reduced if necessary by inclusion of some of the burnable poison in the sideplates. It is necessary to represent the core as homogenized into rectangular regions for the PDQ calculations. As a result the core is described as having corners jutting out into the adjacent reflector or flux trap moderator and this produces a calculated flux peaking somewhat greater than if the boundary is a smooth curve. In addition, this representation makes it difficult to assign the point at which the fuel should be considered as ending in the homogenized core region which extends somewhat beyond this point. From examination of several two-dimensional flux maps a correction which decreases the peaking by 15% is estimated for these two effects. Taking all corrections into account the maximum-to-average ratio as determined for the thermal flux at the highest point in the core region and at the midpoint from top to bottom of the core is multiplied by 0.9 before it is applied to the average power density to obtain the peak when a fine mesh description of the core is used. When a coarse mesh is used an additional correction is made as described in Appendix 12.2 Calculations have been made using two different widths of blades for the followers for the safety controls as shown in Figures 4.0-1 and 4.0-4. The results shown in Table 4.0-B are for the wide blade and those of Table 4.0-C for the narrow blade and for these two cases, the blade width does not seem to be important. However, direct comparison shows that in some instances going from the narrow to the wide blade can increase the peak power density by 30%.

The effect probably depends on the core power distribution and as considerable adjustment of this distribution must be available, care must be taken to keep the safety rod structure from increasing the flux peaking.

In evaluating reactivity calculations, it is necessary to decide what calculated eigenvalue corresponds to a k_{eff} of unity for the actual system. The comparisons of measurements and calculations in Section 3.0 indicate that a beryllium reflected reactor is just critical when the calculated eigenvalue is approximately 1.06. It is assumed that the same difference exists with a D_2O reflector. In the calculations it was convenient to use a square reflector to permit use of diagonal symmetry when desired. This further increases the discrepancy. In addition, engineering details of structural materials in the core and reflector were not available for the calculations. As a result of these factors it is estimated that the system would be just critical with a calculated eigenvalue of 1.09. The PDQ convergence procedure causes the test fluxes to be low with respect to the core fluxes when the eigenvalue is above unity and so the procedure is conservative in this respect. The fuel loadings may be somewhat high and should be re-evaluated when a more accurate description is available.

The loose coupling between lobes in ATR introduces the property that a perturbation in the operating conditions of one lobe can cause a shift of power from lobe to lobe. The control system must be capable of holding deviations from the desired lobe power levels within acceptable limits. In addition, the control system must be capable of producing the initial power unbalance among the core lobes to give the desired test fluxes. The effects on the core power distribution of changes in the absorption cross section of individual core lobes and of the controls individually and in groups are listed in Table 4.0-K.

The addition of 0.02 cm^{-1} poison in the east lobe fueled region causes a power reduction in the east lobe of approximately 66%. In order to restore this power to its value before the addition of the poison it is necessary to pull poison out of the east reflector. If, originally, there were 3 g/liter of boric acid in the east reflector and this is pulled out, the power in the east fueled region will be restored to or slightly above what it was before the introduction of the 0.02 cm^{-1} poison in the fueled region.

Poison in a single neck region has a minor effect on power shifting when compared to the poisoning in a reflector region.

Conclusions are that the combination of reflector and neck poison certainly gives adequate control for power restoration from disturbances while operating.

Under more realistic operating conditions, poison will be found in all necks and reflectors. As can be seen a great deal of power shifting can be accomplished by a combination of removing poison from one reflector and adding it to another.

TABLE 4.0-D

SHUTDOWN CAPABILITY OF SAFETY BLADES

PDQ No.	Blade Type	Blade Position	Control Condition		Eigenvalue
			Reflector	Neck	
1031	Narrow	Withdrawn	Clean	Clean	1.215
1036	Narrow	Inserted	Clean	Clean	1.142
1004	Narrow	Withdrawn		200 g/l	1.298*
1025	Narrow	Inserted		200 g/l	1.254*
1035	Narrow	Withdrawn	(Startup conditions)		1.096
			(See Table 4.0-D)		1.015
5004	Wide	Withdrawn		Clean	1.149
5008	Wide	Inserted		Clean	1.072
5005	Wide	Withdrawn		200 g/l	1.095
5006	Wide	Inserted		200 g/l	1.057

* Contains 36 Kg of U-235, all other cases contain 25.2 Kg of U-235.

Notes: Blades are black when inserted, and 70% Al-30% H_2O when withdrawn. Epithermal constants for 20 mil cadmium are described in WAPD-170, "Experimental and Theoretical Study of Critical Slabs - Effect of Absorbing Membranes of Cadmium, Gold, and Boron," A. D. Voorhis et al

Narrow blades - see Figure 4.0-1

Wide blades - see Figure 4.0-4

TABLE 4.0-E

REACTIVITY EFFECT OF POISON

IN THREE-INCH THICK D_2O REFLECTOR SHIM CONTROLS

PDQ No.	Grams D_3BO_3/liter of D_2O	Eigenvalue
3002	Clean	1.225
3012	3	1.151
3005	10	1.119
3006	22	1.108

Note: Mesh is described by Figure 4.0-2.

TABLE 4.0-F

REACTIVITY EFFECT OF POISON
IN ONE-HALF INCH THICK H_2O REFLECTOR SHIM CONTROLS

PDQ No.	Grams H_3BO_3/liter of H_2O	Exterior Loop Reflector Region	Eigenvalue
6007	Clean	D_2O	1.164
6008	50	D_2O	1.093
6009	Clean	90% Be - 10% H_2O	1.151
6010	50	90% Be - 10% H_2O	1.090

Note: Mesh is described by Figure 4.0-4.

TABLE 4.0-G

REACTIVITY EFFECT OF POISON IN NECK SHIM CONTROLS

PDQ No.	Grams H_3BO_3/liter of H_2O	Eigenvalue
3002	Clean	1.225
3007	10	1.208
3008	50	1.180
3009	200	1.169

Note: Mesh is described by Figure 4.0-2.

TABLE 4.0-H

REACTIVITY EFFECT OF BLADE REFLECTOR SHIM CONTROL

PDQ No.	Blade Type	Blade Position	Outer Reflector	Eigenvalue
5002	Black	Withdrawn	90% Be - 10% H_2O	1.145
5001	Black	Inserted	90% Be - 10% H_2O	1.052
5004	Black	Withdrawn	D_2O	1.149
5003	Black	Inserted	D_2O	1.051
5004	Gray	Withdrawn	D_2O	1.149
5007	Gray	Inserted	D_2O	1.072

Notes: Mesh is described by Figure 4.0-3.

Black blades are 30% H_2O - 70% Al when withdrawn and equivalent to box of 20 mil cadmium when inserted, constants are consistent with WAPD-170.

Gray blades $\Sigma_{2a} = 0.244$.

TABLE 4.0-I

REACTIVITY EFFECT OF FUEL LOADING

PDQ No.	Fuel Content	Eigenvalue
1022	45 kg U-235	1.400
1019	36 kg U-235	1.357
1009	27 kg U-235	1.302*

* Corrected for mesh error

Notes: Mesh described by Figure 4.0-1.

Core contains no burnable poison.

TABLE 4.0-J

REACTIVITY EFFECT OF BURNABLE POISON IN CORE

PDQ No.	Contribution of Poison (Σ_{2p}) to Σ_{2a}(cm^{-1})	Region to Which Poison is Added	Eigenvalue
3003	0	Entire Core	1.335
3002	0.015	Entire Core	1.225
3004	0.035	Entire Core	1.105
3010	0	Center Fuel Region	1.252*
3002	0.015	Center Fuel Region	1.225*
3010	0.035	Center Fuel Region	1.200*
4001	0	East Core Lobe	1.254*
4007	0.015	East Core Lobe	1.224*
4002	0.035	East Core Lobe	1.207*

* Σ_{2p} = 0.015 in all other core regions.

Note: Meshes are described by Figure 4.0-2.

TABLE 4.0-K

EFFECTS OF CONTROLS AND CORE POISONING ON ATR POWER DISTRIBUTION

Half Core Cases		k_{eff}	Power - Mw				% Shift (+ increase) (- decrease)			
PDQ No.	Core Lobe		E	W	N & S	C	E	W	N & S	C
4007	Reference Case Σ^p = .015 all lobes	1.224	50.6	49.9	50.2	49.1	---	---	---	---
4001	Σ^p = 0 in east lobe	1.254	75.6	38.1	45.0	46.4	+49.4	-23.6	-10.4	-5.5
4002	Σ^p = .035 in east lobe	1.207	33.2	58.4	53.9	50.7	-34.4	+17.0	+ 7.4	+3.3
4008	3 g/liter boric acid in east reflector shim	1.208	32.5	58.3	53.5	52.3	-35.8	+16.8	+ 6.6	+6.5
4005	10 g/liter boric acid in east reflector shim	1.202	24.9	62.6	54.6	53.4	-50.8	+25.5	+ 8.8	+8.8
4006	22 g/liter boric acid in east reflector shim	1.200	22.4	64.1	54.9	53.7	-55.7	+28.5	+ 9.4	+9.4
4003	10 g/liter boric acid in east neck shim	1.220	49.5	50.5	50.8	48.5	- 2.2	+ 1.2	+ 1.2	-1.2
4004	50 g/liter boric acid in east neck shim	1.213	46.1	53.1	52.0	46.9	- 8.9	+ 6.4	+ 3.6	-4.5
Quarter Core Cases				Same as E	Same as E			Same as E	Same as E	
3002	Reference Case Σ^p = .015 all lobes	1.225	50.2			49.2	---	---	---	---
3010	Σ^p = 0 in center lobe	1.252	48.2			57.2	- 4.0			+16.3
3011	Σ^p = .035 in center lobe	1.200	52.1			41.5	- 3.8			+15.7
3012	3 g/liter boric acid in all reflector shims	1.151	45.8			66.9	- 8.8			+36.0
3005	10 g/liter boric acid in all reflector shims	1.119	43.1			77.7	-14.1			+57.9
3006	22 g/liter boric acid in all reflector shims	1.108	41.9			82.3	-15.5			+67.3
3007	10 g/liter boric acid in all neck shims	1.208	51.0			46.2	+ 1.6			- 6.1
3008	50 g/liter boric acid in all neck shims	1.180	52.6			39.8	+ 4.8			-19.1
3009	200 g/liter boric acid in all neck shims	1.169	53.5			35.9	+ 6.6			-27.0

Note: g/liter boric acid = grams of boric acid containing natural boron per liter

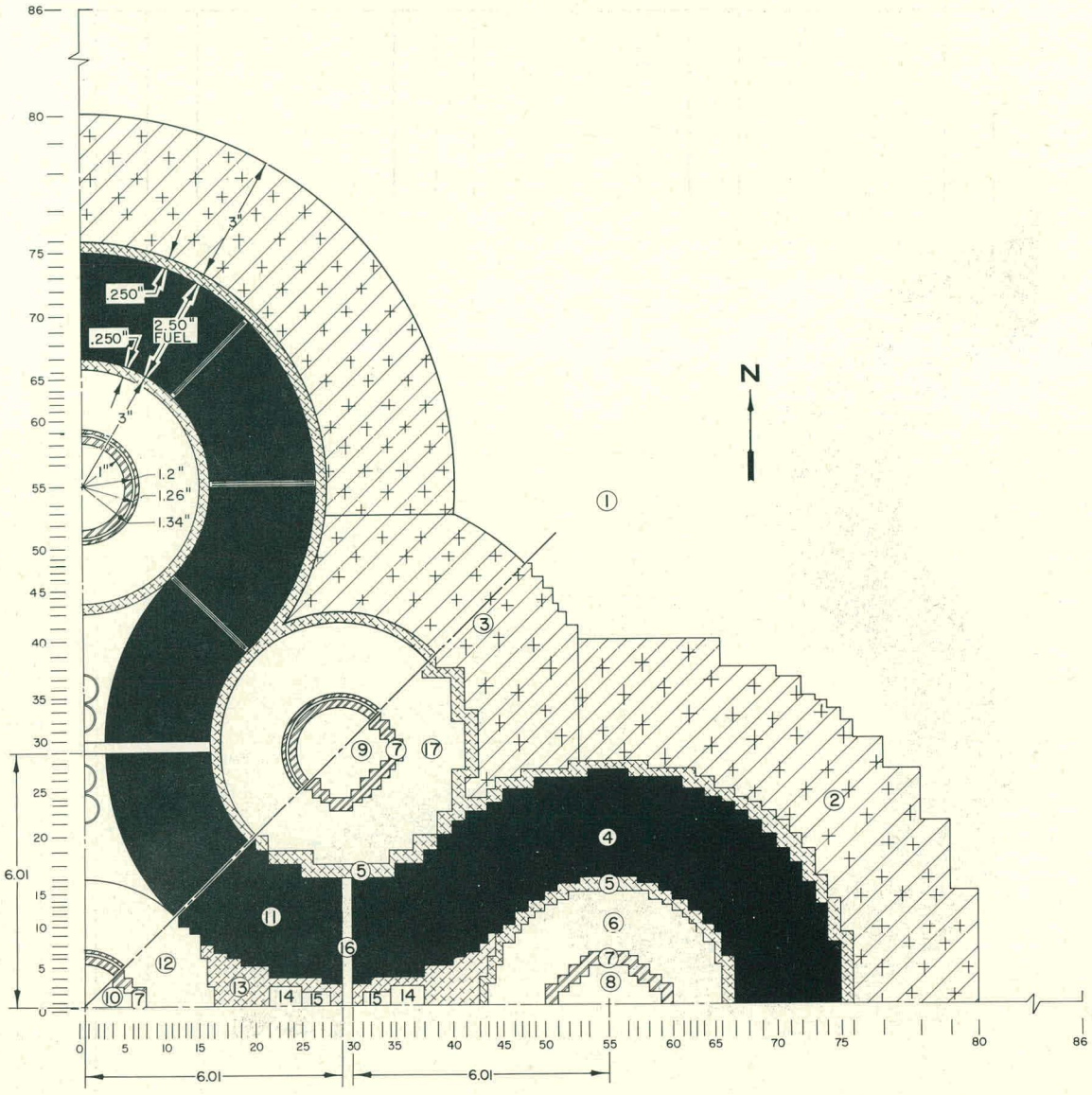

1. OUTER REFLECTOR
2. INNER REFLECTOR (REFLECTOR SHIM CONTROL)
3. OUTER LOOP REFLECTOR
4. LOBE FUEL REGION
5. SEPARATOR RING
6. LOBE FLUX-TRAP MODERATOR
7. EXPERIMENT PRESSURE VESSEL
8. LOBE EXPERIMENT
9. EXTERIOR EXPERIMENT
10. CENTER EXPERIMENT
11. CENTER FUEL REGION
12. CENTER EXPERIMENT FLUX-TRAP MODERATOR
13. NECK FILLER REGION
14. NECK SHIM CONTROL REGION
15. NECK SHIM CONTROL REGION
16. SAFETY BLADE
17. EXTERIOR EXPERIMENT FLUX-TRAP MODERATOR

NOTES: THIS MESH IS USED IN 1000 SERIES PROBLEMS WITH 7225 INTERIOR MESH POINTS IN ONE QUADRANT
ADDITIONAL COMPOSITIONS ARE USED AS REQUIRED WHEN CONTENTS OF SIMILAR REGIONS DIFFER

PPCo-E-3013

FIG. 4.0-1

FINE MESH PDQ MODEL OF ATR WITH THREE INCH REFLECTOR SHIM CONTROL

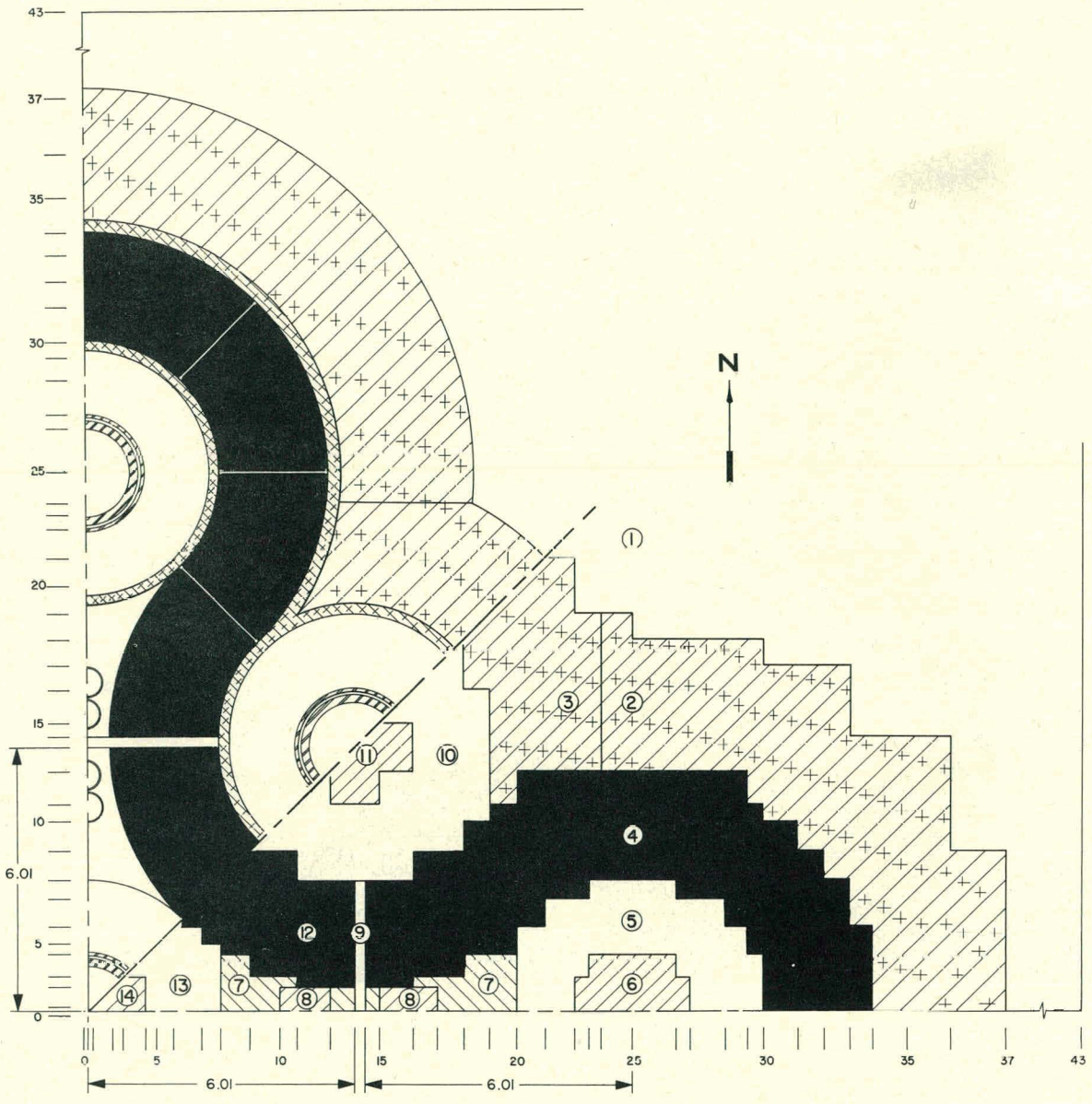

1	OUTER REFLECTOR	8	EAST NECK SHIM CONTROL REGION
2	INNER REFLECTOR (SHIM CONTROL)	9	SAFETY BLADE
3	OUTER LOOP REFLECTOR	10	EXTERIOR EXPERIMENT FLUX TRAP MODERATOR
4	LOBE FUEL	11	EXTERIOR EXPERIMENT
5	LOBE FLUX TRAP MODERATOR	12	CENTER FUEL REGION
6	LOBE EXPERIMENT AND PRESSURE VESSEL	13	CENTER EXPERIMENT FLUX TRAP MODERATOR
7	NECK FILLER REGION	14	CENTER EXPERIMENT

NOTES: THIS MESH IS USED FOR 3000 SERIES PROBLEMS WITH 1764 INTERIOR MESH POINTS IN ONE QUADRANT, AND FOR 4000 SERIES PROBLEMS WITH 3570 INTERIOR MESH POINTS IN TWO QUADRANTS.

ADDITIONAL COMPOSITIONS ARE USED AS REQUIRED WHEN CONTENTS OF SIMILAR REGIONS DIFFER

PP Co.-E-3178

FIG. 4.0-2

COARSE MESH PDQ MODEL OF ATR WITH THREE INCH REFLECTOR SHIM CONTROL

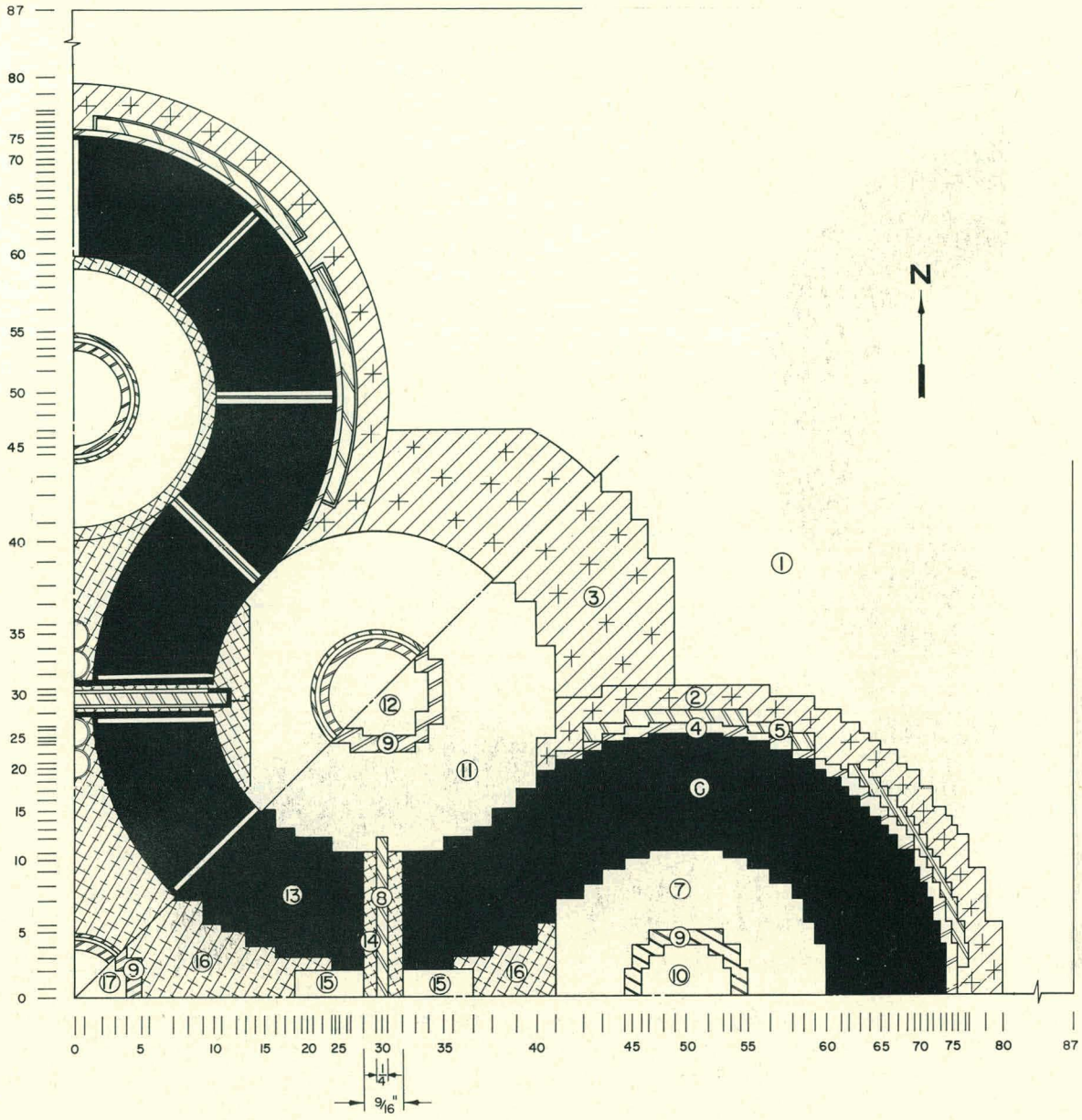

1. OUTER REFLECTOR
2. LOBE INNER REFLECTOR
3. OUTER LOOP REFLECTOR
4. ZIRCONIUM LINER FOR LOBE FUEL
5. REFLECTOR CONTROL BLADE
6. LOBE FUEL
7. LOBE FLUX TRAP MODERATOR
8. SAFETY BLADE
9. EXPERIMENT PRESSURE VESSEL
10. LOBE EXPERIMENT
11. EXTERIOR EXPERIMENT FLUX TRAP MODERATOR
12. EXTERIOR EXPERIMENT
13. CENTER FUEL REGION
14. SAFETY BLADE GUIDE SECTION
15. NECK SHIM CONTROL REGION
16. NECK FILLER REGION
17. CENTER EXPERIMENT

NOTES: THIS MESH IS USED IN 5000 SERIES PROBLEMS WITH 7396 INTERIOR MESH POINTS IN ONE QUADRANT
ADDITIONAL COMPOSITIONS ARE USED AS REQUIRED WHEN CONTENTS OF SIMILAR REGIONS DIFFER

FIG. 4.0-3

PP Co.-E-3179

PDQ MODEL OF ATR WITH BLADE REFLECTOR SHIM CONTROL

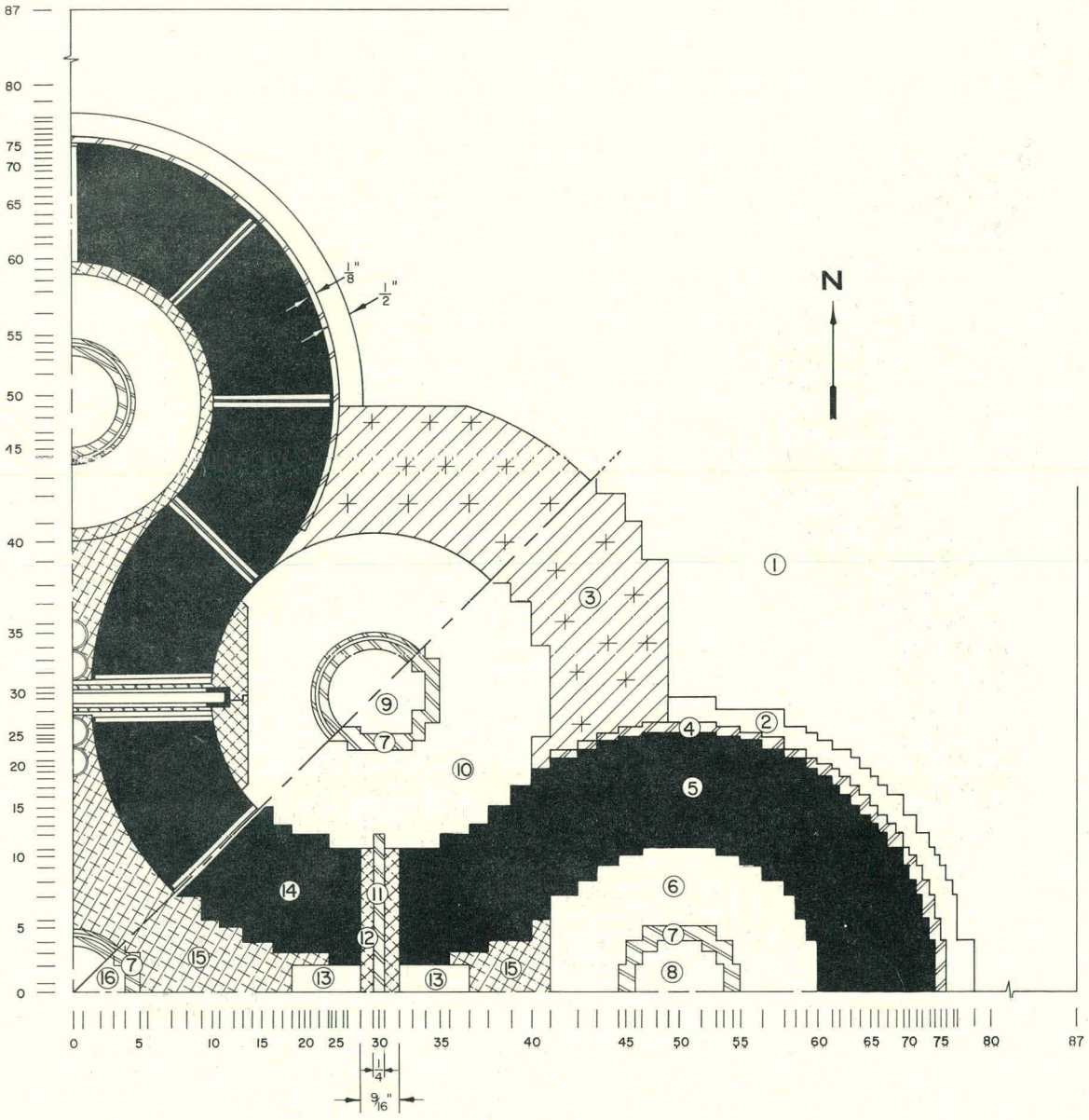

1. OUTER REFLECTOR
2. INNER REFLECTOR (SHIM CONTROL)
3. OUTER LOOP REFLECTOR
4. ZIRCONIUM LINER FOR LOBE FUEL
5. LOBE FUEL
6. LOBE FLUX TRAP MODERATOR
7. EXPERIMENT PRESSURE TUBE
8. LOBE EXPERIMENT
9. EXTERIOR EXPERIMENT
10. EXTERIOR EXPERIMENT FLUX TRAP MODERATOR
11. SAFETY BLADE
12. SAFETY BLADE GUIDE SECTION
13. NECK SHIM CONTROL REGION
14. CENTER FUEL REGION
15. NECK FILLER REGION
16. CENTER EXPERIMENT

NOTES: THIS MESH IS USED FOR 6000 SERIES PROBLEMS WITH 7396 INTERIOR MESH POINTS IN ONE QUADRANT
ADDITIONAL COMPOSITIONS ARE USED AS REQUIRED WHEN CONTENTS OF SIMILAR REGIONS DIFFER

FIG. 4.0-4

PP CO.-E-3180

PDQ MODEL OF ATR WITH ONE-HALF INCH REFLECTOR SHIM CONTROL

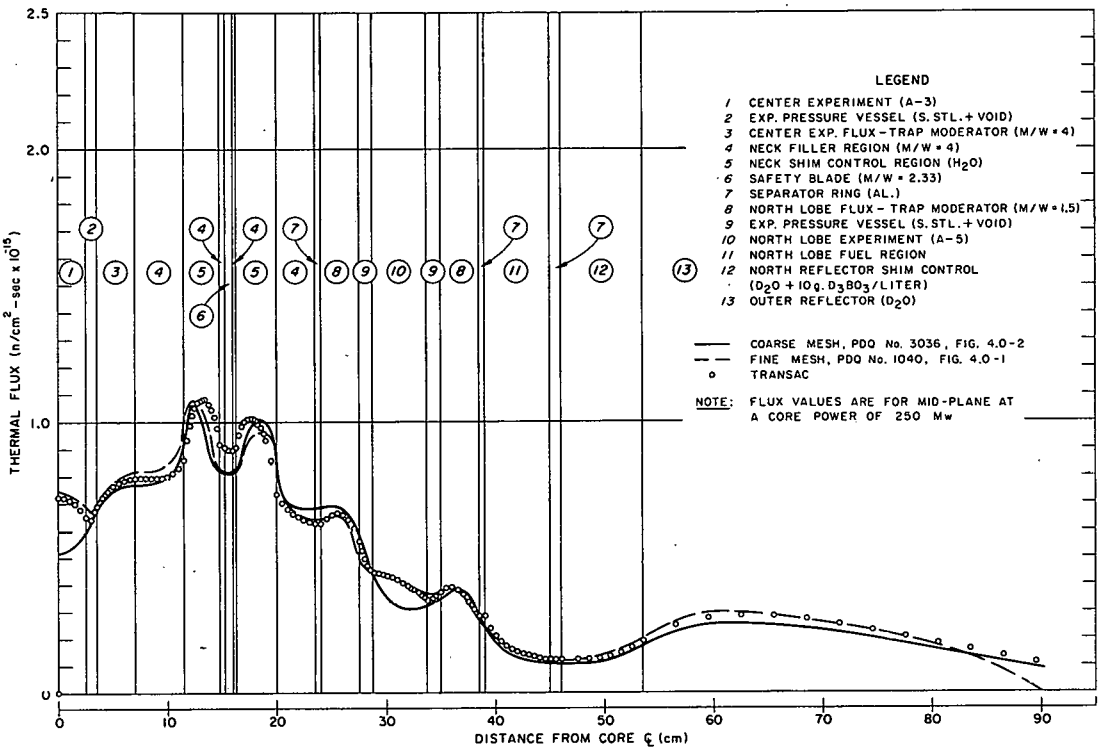

FIG. 4.0-5
ATR THERMAL FLUX PLOTS - NORTH TRAVERSE

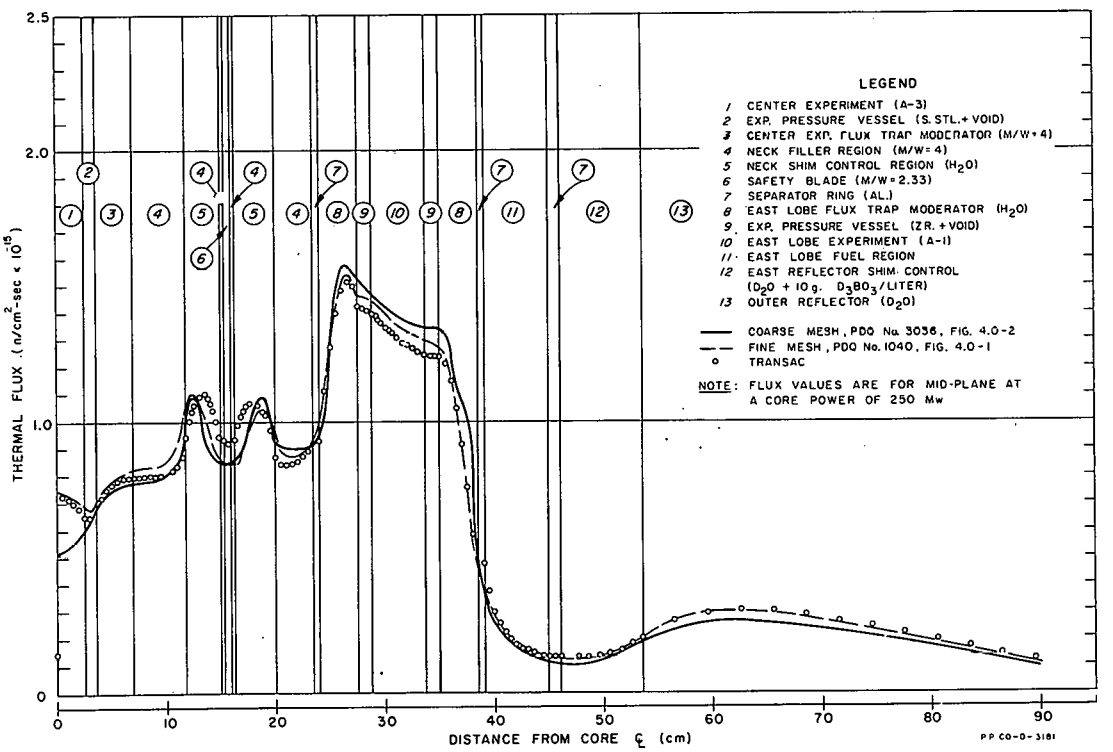

FIG. 4.0-6
ATR THERMAL FLUX PLOTS - EAST TRAVERSE

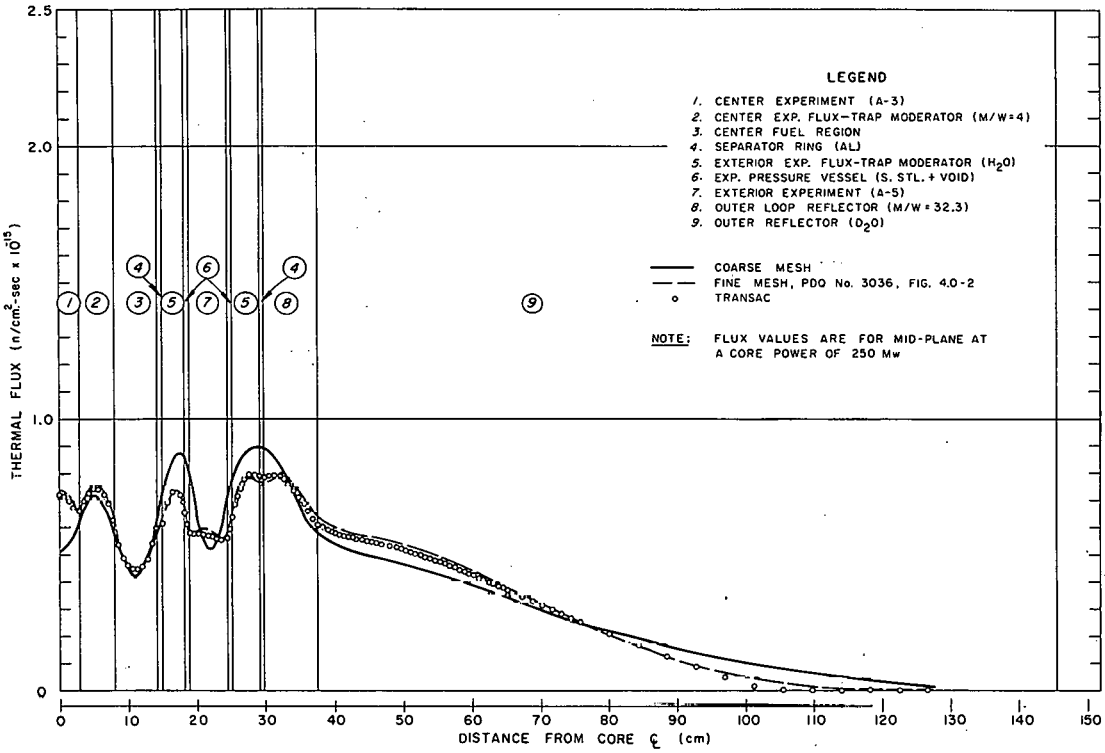

FIG. 4.0-7

ATR THERMAL FLUX PLOTS - NORTH EAST DIAGONAL TRAVERSE

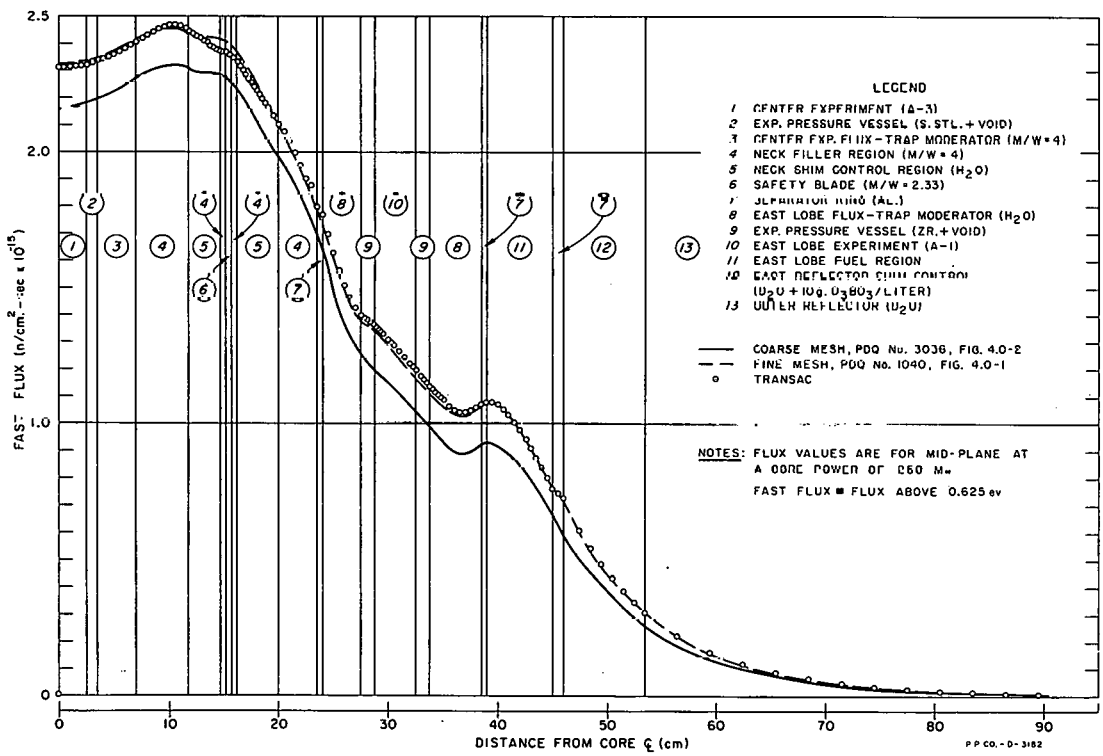

FIG. 4.0-8

ATR FAST FLUX PLOTS - EAST TRAVERSE

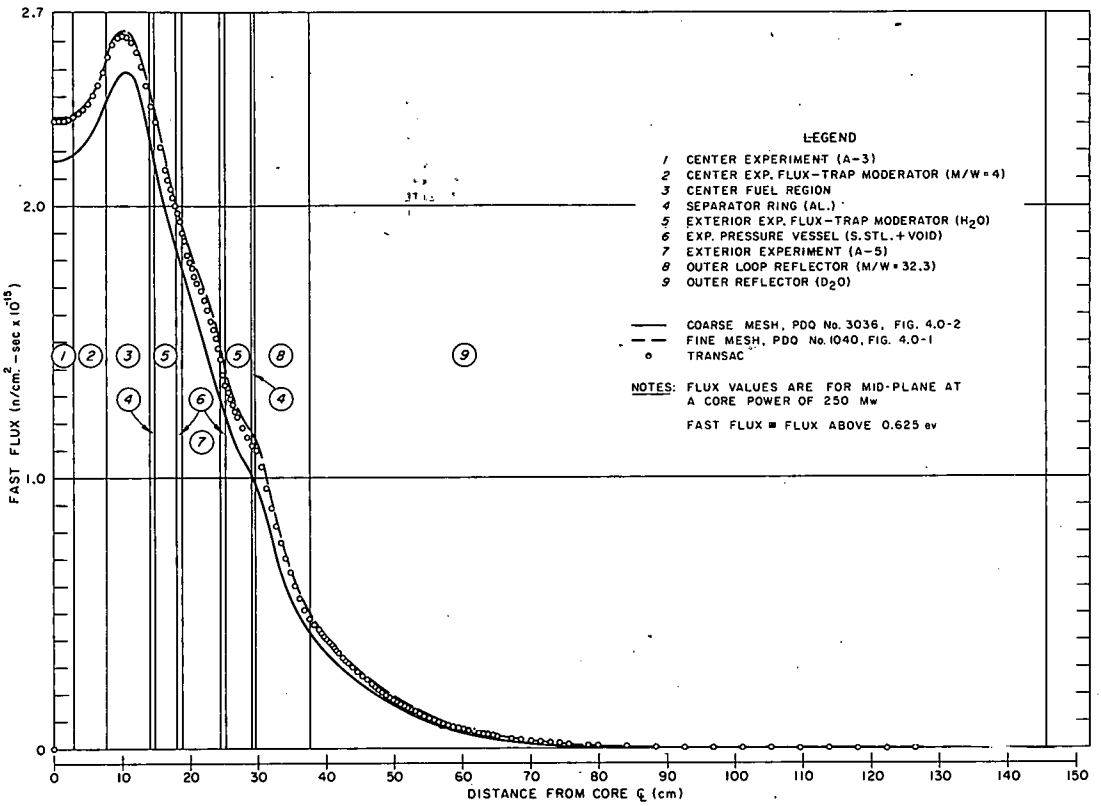

FIG. 4.0-9

ATR FAST FLUX PLOTS - NORTH-EAST DIAGONAL TRAVERSE

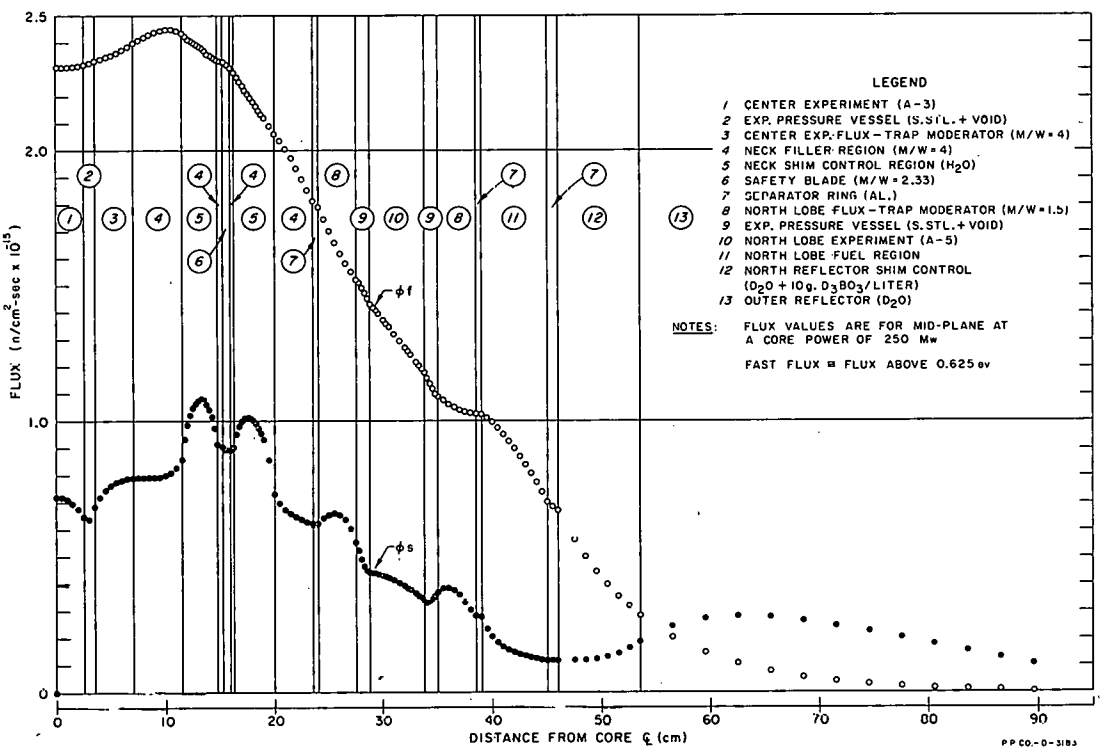

FIG. 4.0-10

TRANSAC PDQ FLUX PLOTS ALONG NORTH TRAVERSE OF ATR

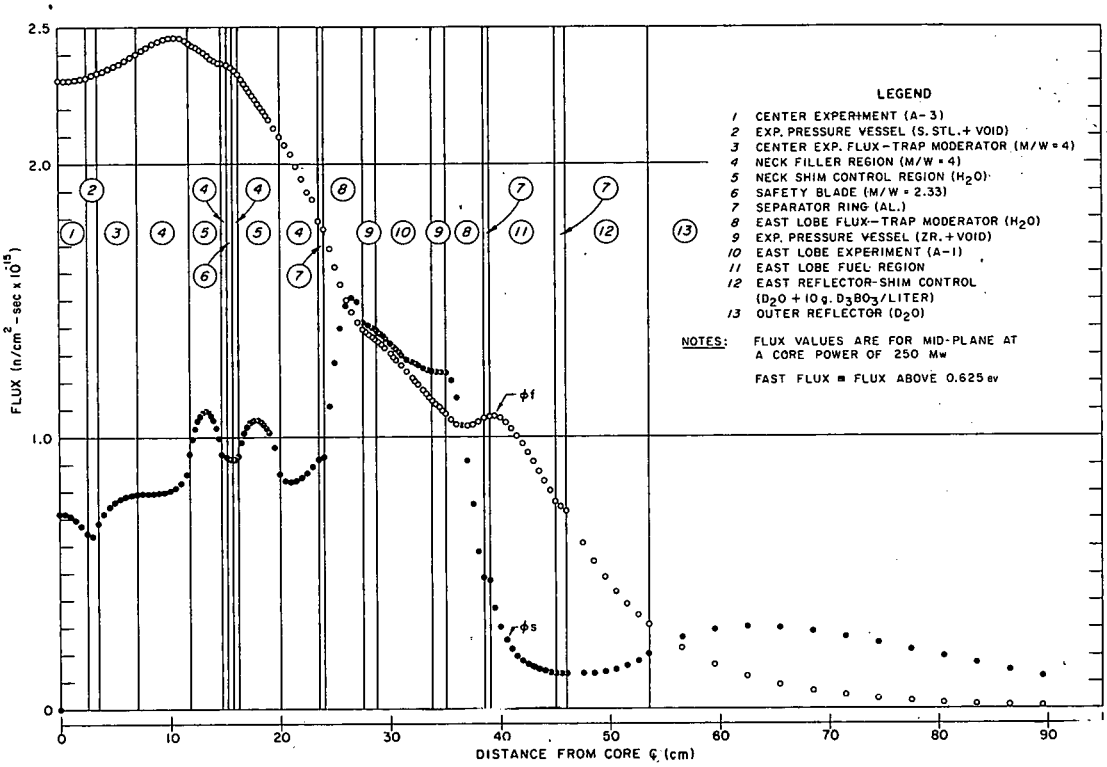

FIG. 4.0-11

TRANSAC PDQ FLUX PLOTS ALONG EAST TRAVERSE OF ATR

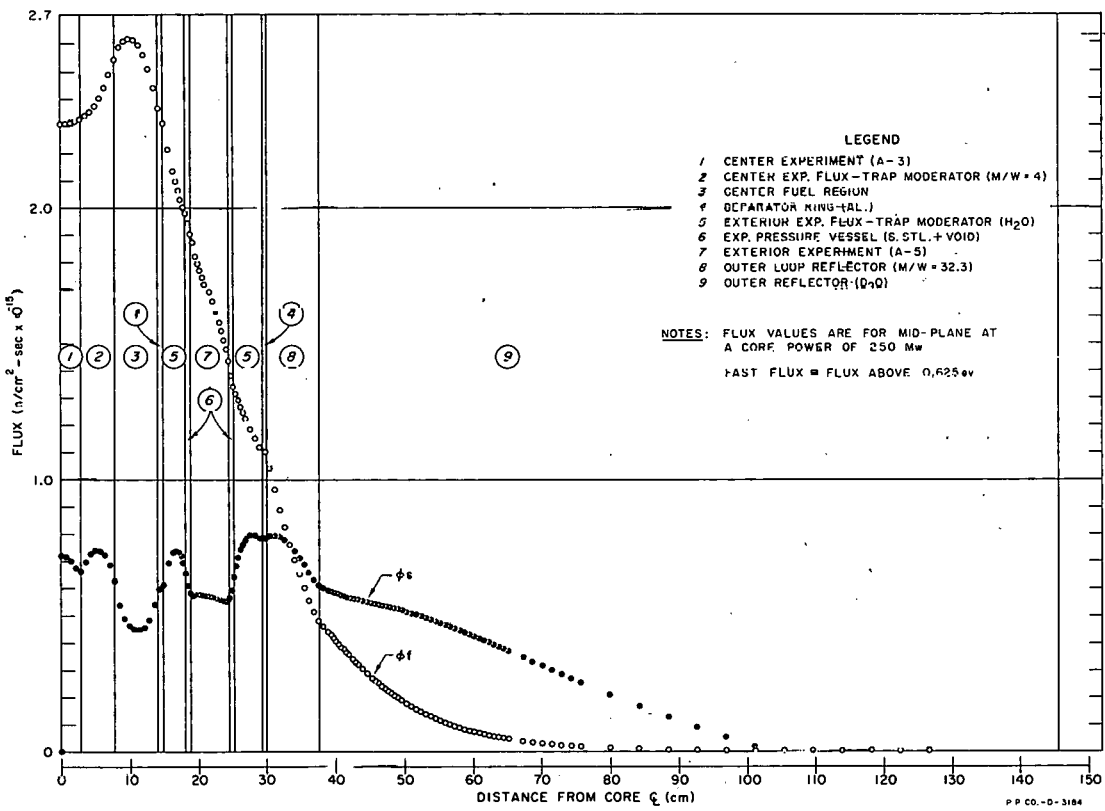

FIG. 4.0-12

TRANSAC PDQ FLUX PLOTS ALONG NORTH-EAST DIAGONAL TRAVERSE OF ATR

5.0 EFFECTS OF SHIM CONTROL BLADES ON AXIAL FLUX AND POWER DISTRIBUTIONS

In considering possible shim control schemes for the ATR, it is recognized that one of the principal problems introduced by a conventional mechanical blade-type control is the shift in axial power and thermal flux distributions caused by blade withdrawal or insertion during the course of the operating cycle. The magnitude of the axial perturbations due to shim blade movement is dependent on the control requirements. As the amount of burnable poison is increased in the reactor to handle fuel burnup, the shim control requirements are correspondingly decreased. In the ATR, the minimum control requirements are established by the amount of interlobe power balancing needed.

In order to obtain some information about the axial perturbations caused by shim blades, two-dimensional calculations in (r, z) geometry were performed on a one-lobe model of the ATR with PDQ-2. The experiment described was an A-5 type with a 40% H_2O - 60% Al flux trap moderator annulus surrounding it. Four problems were run-- one with no control blade, one with a black control blade inserted 50%, one with a black control blade inserted 75%, and one with a gray control blade inserted 50%.

In utilizing the results of these calculations, it is assumed that the axial perturbations caused by a shim blade (of given blackness) surrounding the outer portion of one lobe of the ATR are approximately equivalent to the effects of the blade surrounding completely the one-lobe model. This assumption is considered reasonable in considering the maximum local axial distortions in the fueled core, and to a lesser extent, in the experiment.

The thermal and fast group neutron fluxes along the experimental axis are shown in Figures 5.0-1 and 5.0-2, respectively, for each of the four cases calculated. The axial power distribution along the experimental axis, the inside edge of the core, the middle of the core, and the outside edge of the core, is shown in Figures 5.0-3, 5.0-4, 5.0-5 and 5.0-6 for each of the cases. The average and maximum-to-average radial power as a function of core height are shown in Figures 5.0-7, 5.0-8, 5.0-9 and 5.0-10. Figures 5.0-11 and 5.0-12 relate the eigenvalue and maximum-to-average axial core power density to rod position for the four cases.

The nonuniformity, which is the percentage by which the maximum (or minimum) power varies from the numerical average of the maximum and minimum power density over a certain length of the experiment, is presented in Table 5.0-A for two section lengths-- 3 ft and 4 ft.

In order to estimate the approximate rod position (or blackness) required for the ATR, the following assumptions and data are utilized:

1. The case considered is consistent with the TURBO burnout study. From this study, the initial excess k, excluding that controlled

by burnable poison, is approximately 12%, of which 8.6% must be achieved in the reflector for power balancing.

2. The proportionality between reflector control worths for the one and multi-lobe situations is given in Table 5.0-B.

3. These values were obtained from comparisons of DMM and PDQ-3 calculations. Using the average value of (one-dimensional worth)/(two-dimensional worth) of 3.35 gives a one-dimensional equivalence of 29% that must be achieved for power balancing in the reflector.

TABLE 5.0-A

NONUNIFORMITY OF POWER DISTRIBUTION

IN 3 AND 4 FT LONG EXPERIMENTAL SECTIONS

Case	Nonuniformity, %	
	3 ft long Section	4 ft long Section
No rod	34.8	59
Black rod inserted 50%	99.5	99.9
Black rod inserted 75%	82.1	91.3
Gray rod inserted 50%	81.3	92.2

NOTE: $$\text{Nonuniformity} = 100 \left\{ \frac{(P_{\max \text{ or } \min}) - \left|\frac{P_{\max} - P_{\min}}{2}\right|}{\left|\frac{P_{\max} - P_{\min}}{2}\right|} \right\} \text{ per cent}$$

TABLE 5.0-B

COMPARISON OF CONTROL WORTH FROM

ONE- AND TWO-DIMENSIONAL CALCULATIONS

Case	Code	k_{eff} Clean	k_{eff} Poisoned*	Δk	$\frac{\Delta k \text{ One-Dimensional}}{\Delta k \text{ Two-Dimensional}}$
1/2 in. H_2O	DMM	1.0417	0.7858	0.2559	-
Annulus	PDQ	1.1616	1.0902	0.0714	3.59
3 in. D_2O	DMM	1.1170	0.7524	0.3646	-
Annulus	PDQ	1.2129	1.0953	0.1176	3.11

*50 g/liter of boric acid, $\bar{\Sigma}_{a2} = 0.28756$

From Figure 5.0-11 it is estimated that about 85% insertion of the black rod or 95% insertion of the gray rod is required initially for control. Using Figure 5.0-12 it is also estimated that the maximum-to-average axial power density is increased from a "no rod" value of 1.35 to approximately 2.1 to 2.5 for the above insertions. During the initial ten hours of operation the rods must be withdrawn a considerable amount to compensate for the buildup of xenon. Therefore, it is somewhat difficult to estimate the axial maximum-to-average power density at the beginning of the cycle. For 50% black rod insertion, the maximum-to-average axial power density is reduced from 2.5 to 2.3. As the cycle progresses, however, the burnup effects will tend to decrease the maximum-to-average power density, as shown in the TURBO burnout studies.

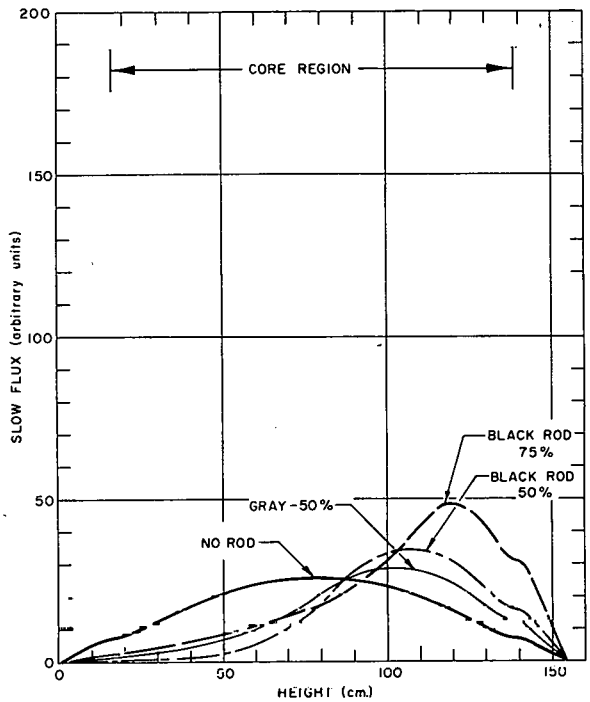

FIG. 5.0 – 1
SLOW GROUP FLUXES ALONG EXPERIMENTAL AXIS

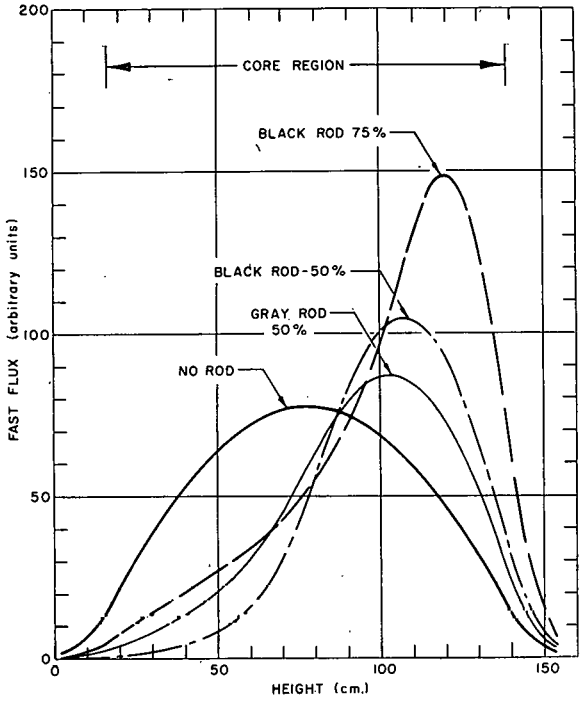

FIG. 5.0 – 2
FAST GROUP FLUXES ALONG EXPERIMENTAL AXIS

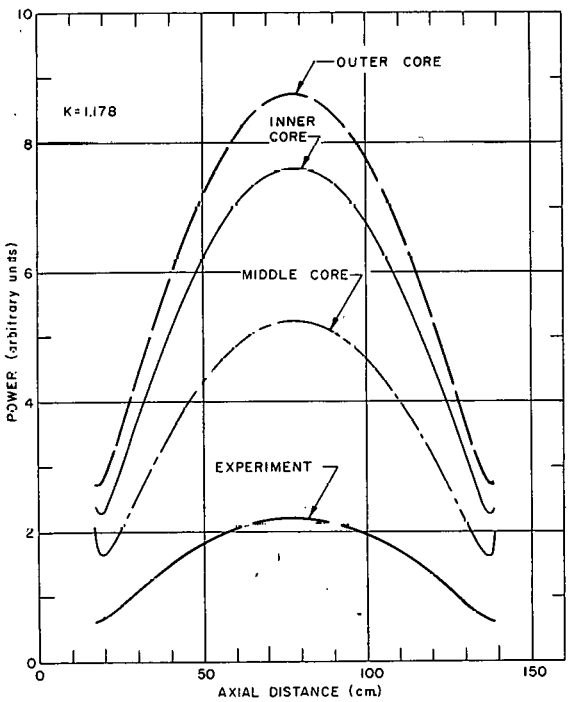

FIG. 5.0 – 3
AXIAL POWER DISTRIBUTION – NO ROD

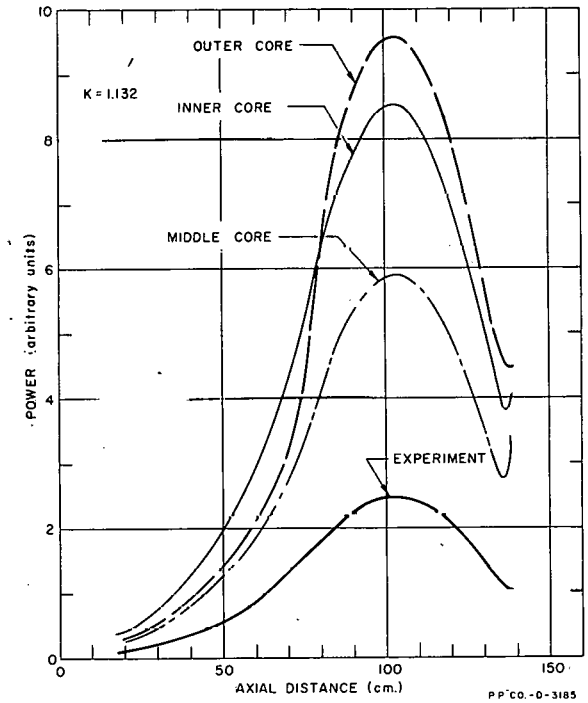

FIG. 5.0 – 4
AXIAL POWER DISTRIBUTION
GRAY ROD INSERTED 50%

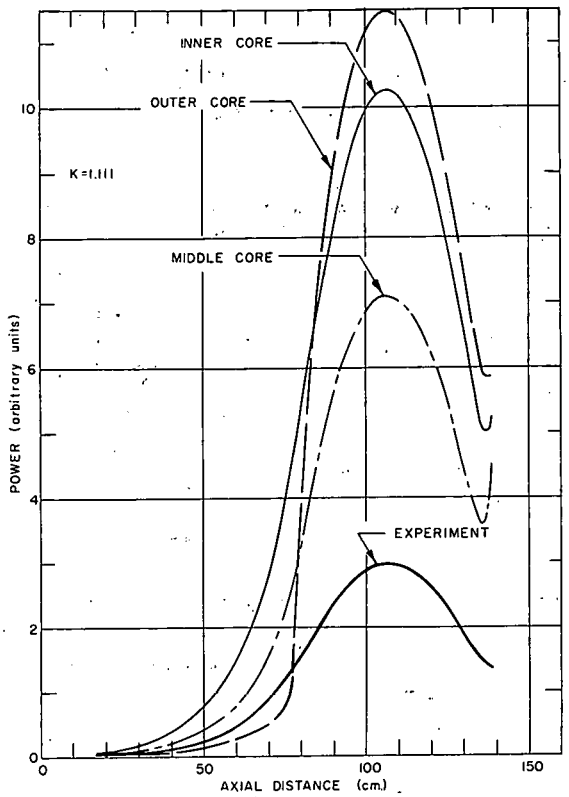

FIG. 5.0 – 5
AXIAL POWER DISTRIBUTION
BLACK ROD INSERTED 50%

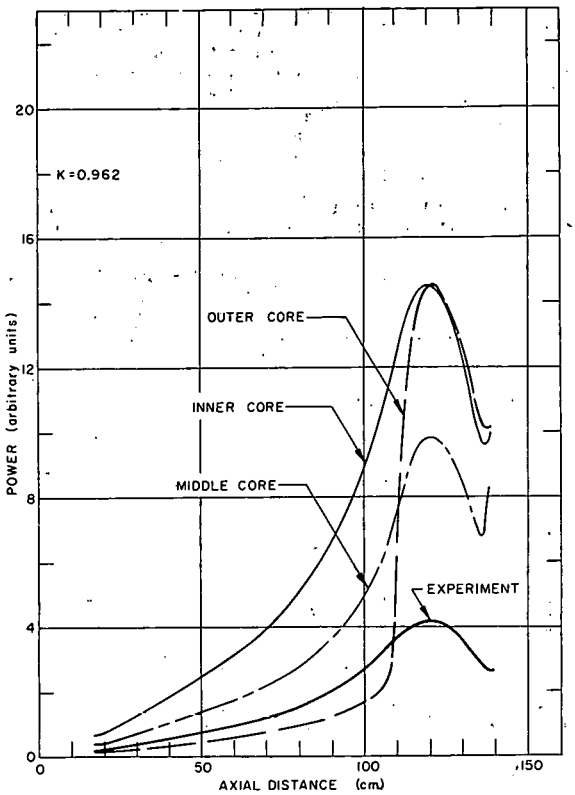

FIG. 5.0 – 6
AXIAL POWER DISTRIBUTION
BLACK ROD INSERTED 75%

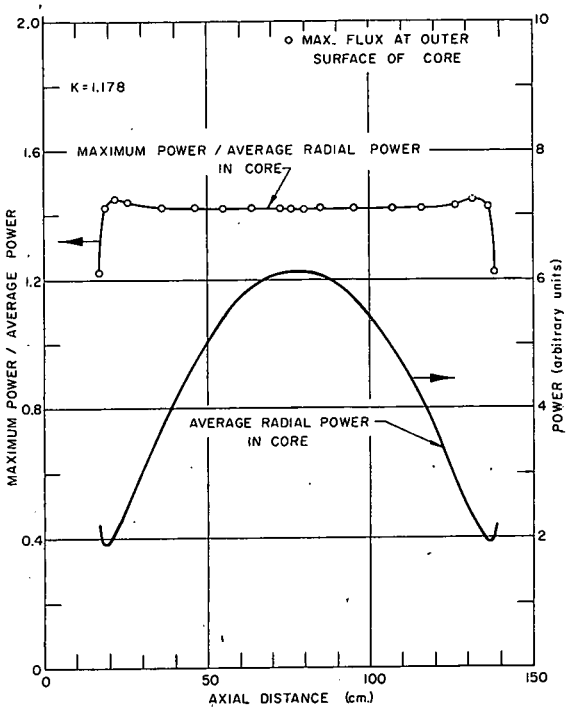

FIG. 5.0 – 7
AXIAL POWER AND POWER RATIO DISTRIBUTIONS
NO ROD

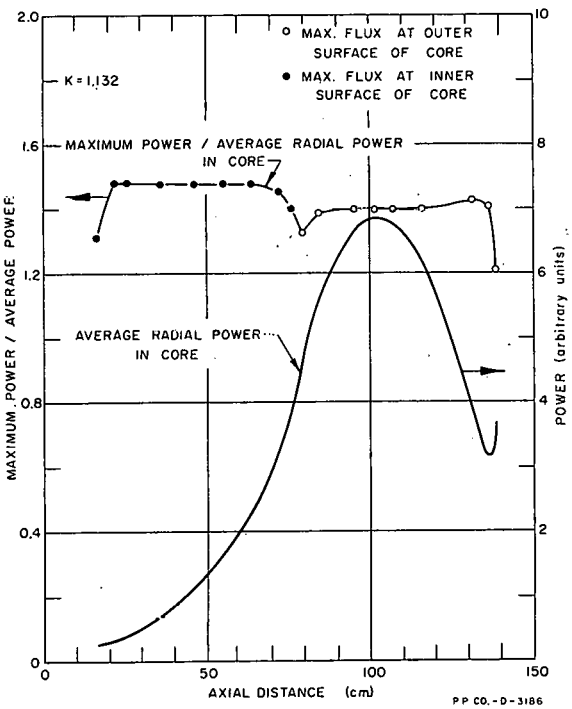

FIG. 5.0 – 8
AXIAL POWER AND POWER RATIO DISTRIBUTIONS
GRAY ROD INSERTED 50%

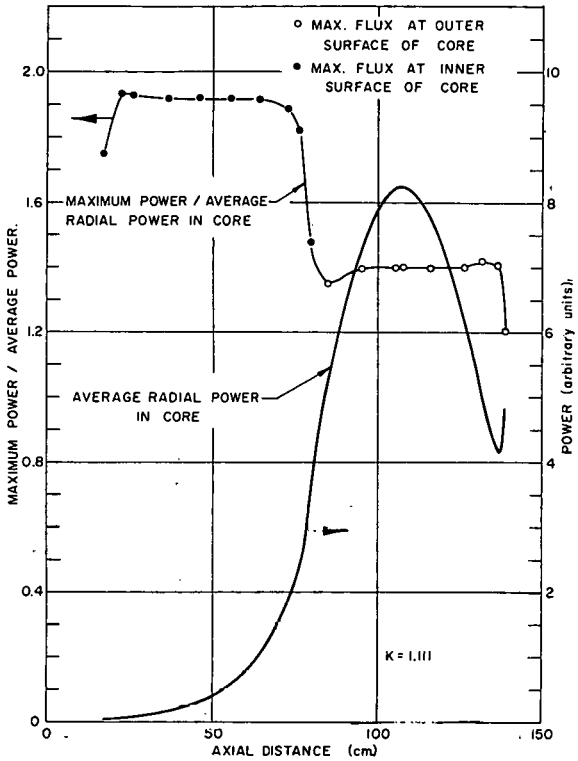

FIG. 5.0 – 9
AXIAL POWER AND POWER RATIO DISTRIBUTIONS
BLACK ROD INSERTED 50%

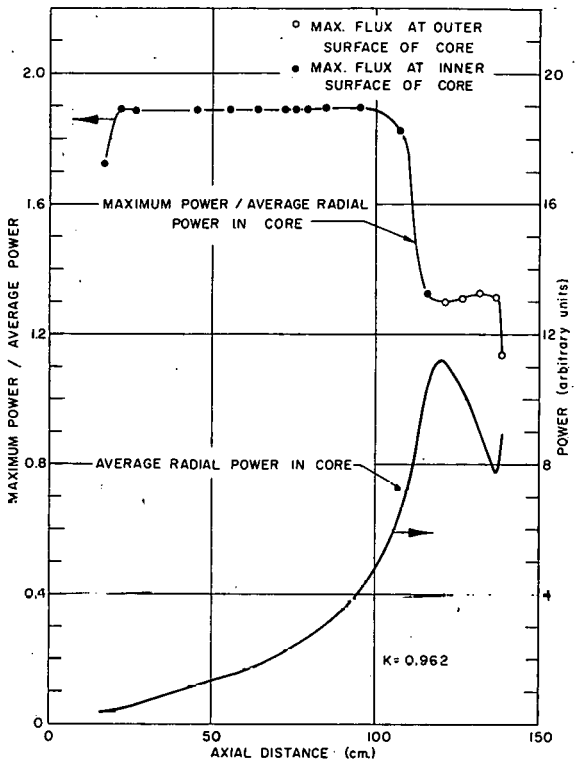

FIG. 5.0 – 10
AXIAL POWER AND POWER RATIO DISTRIBUTIONS
BLACK ROD INSERTED 75%

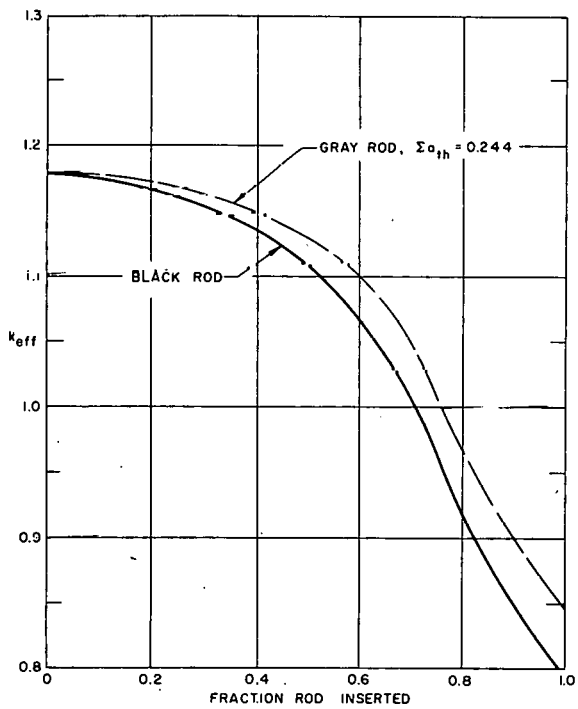

FIG. 5.0 – 11
k_{eff} VERSUS ROD INSERTION

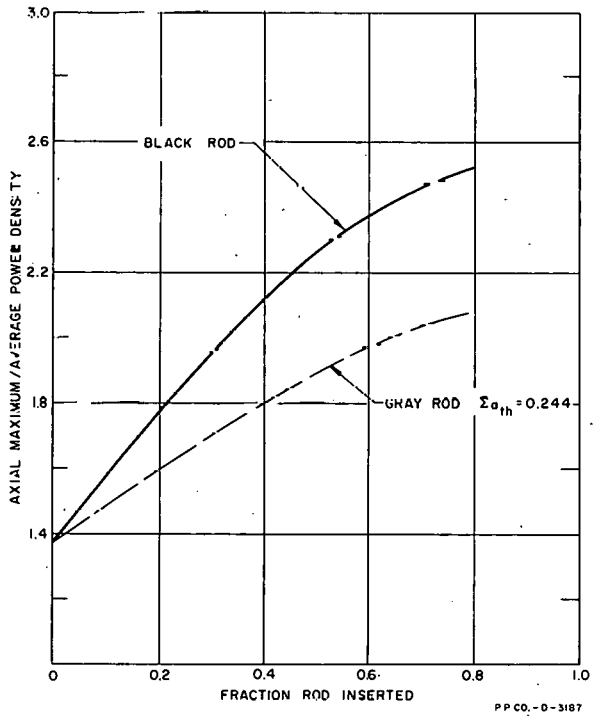

FIG. 5.0 – 12
AXIAL MAXIMUM / AVERAGE POWER DENSITY
VERSUS ROD INSERTION

6.0 REACTOR BEHAVIOR DURING OPERATION

Several studies were made to determine the reactor behavior during operation and to establish the feasibility of maintaining the desired test fluxes throughout an operating cycle. A two-dimensional TURBO problem was run to investigate the cycle time and behavior of the reactor during burnup or depletion of fuel and a second TURBO problem was run to investigate the reactor behavior after a midcycle shutdown and subsequent return to full power operation. Previous to the TURBO problems, several one-dimensional CANDLE problems were run to obtain estimates of the control requirements for the TURBO problems. CANDLE problems were also used to investigate the effects during burnup of having burnable poison in the core and to investigate the core behavior as a function of power level.

6.1 TURBO Calculations

The two TURBO problems, the burnup TURBO and the midcycle shutdown and recovery TURBO, were calculated in x,y geometry using quarter core symmetry. The experimental loading consisted of an A-1 experiment in the east lobe, an A-5 experiment in the north lobe, an A-3 experiment in the center lobe, and an A-5 experiment in the northeast outer experiment position. The A-1 experiment had zirconium pressure tubes and all other experiments had stainless steel pressure tubes. The configuration used in these TURBO problems is similar to that used in PDQ problem 3001 listed in Table 4.0-A.

At each time step in the problems the eigenvalue and core power distribution were adjusted by regulating the poison in the various controls. The required core power distribution given in Table 6.0-A was chosen so that the approximate flux requirements in the experiments would be obtained, and a calculated eigenvalue of 1.09 was assumed to represent a just critical reactor to allow for the variations in eigenvalue due to the various computational expedients which were used. To save computing time the calculations were made with the coarse mesh description of the ATR shown in Figure 4.0-2. The TURBO results were then assumed to show the changes in reactor behavior during the cycle and were corrected to those which would have been obtained with the fine mesh description by means of the PDQ cases comparing the fine mesh and coarse mesh descriptions. After the TURBO problems were completed a final adjustment was made on the control poison at each time step. This final adjustment was made to correct to the required values, the power distribution and eigenvalue obtained by TURBO.

6.11 Burnup TURBO

The power distribution in the ATR core can be adjusted to very nearly the required values by varying the neck control poison as a whole and the reflector control poison as a whole. Therefore this method, as outlined in Appendix 12.61, was used in the burnout TURBO problem in order to eliminate the computer time necessary to obtain the fine adjustment of power level among the outer lobes.

TABLE 6.0-A

REQUIRED CORE POWER DISTRIBUTION FOR TURBO PROBLEMS

Core Lobe	Fraction of Total Core Power
North	0.17
South	0.17
East	0.21
West	0.21
Center	0.24

The pertinent results as determined by the burnup TURBO problems are given in Table 6.0-B. The final adjusted values are shown in Figures 6.0-1 through 6.0-8. The eigenvalue which would have resulted at each time step if all control poisons were removed was estimated as shown in Section 6.2. Figure 6.0-9 of eigenvalue versus time was then made after subtracting 0.09 from the values given in Table 6.0-G of Section 6.2. The results show the feasibility of adequately controlling the core power distribution for 17 days of operation.

At this time all of the neck control had been used and the power distribution in the outer lobes was regulated such that the fractional error in power from that desired was identical in all outer lobes. At about 26 days all control in the east-west reflector system had been used and only the eigenvalue could be adjusted by means of the control left in the north-south reflector system. All control was finally used up at about 31 days of operation.

The model used for the TURBO calculations has considerable excess reactivity remaining after 17 days when control of the core power distribution is lost. By modification of the shim control designs the initial excess reactivity required for a 17 day full power cycle can be reduced somewhat below the value of 1.12 used in these computations.

TABLE 6.0-B

RESULTS FROM BURNUP TURBO-CALCULATION

Time Step	Time (days)	Eigen-value λ	Fraction of Total Core Power Generated in Lobe		
			Center	North	East
0	0	1.0885	0.24145	0.17546	0.20382
1	0.417	1.0883	0.23728	0.17732	0.20404
2	2.5	1.0887	0.24177	0.17692	0.20218
3	8.33	1.0937	0.24060	0.17842	0.20128
4	16.713	1.0939	0.23185	0.18332	0.20076
5	25.0	1.0908	0.19598	0.19542	0.20660
6	33.33	1.0766	0.16758	0.20636	0.20986

Time Step	Average Neutron Flux Within Experiments at a Core Power of 250 Mw (n/cm^2 sec x 10^{-15})					
	Fast			Thermal		
	Center	North	East	Center	North	East
0	1.3348	0.8977	0.8350	0.3521	0.2831	1.0724
1	1.3183	0.8994	0.8291	0.3491	0.2821	1.0619
2	1.3382	0.8971	0.8170	0.3617	0.2831	1.0594
3	1.3268	0.8964	0.7951	0.3767	0.2910	1.0736
4	1.2855	0.9126	0.7737	0.3924	0.3090	1.0997
5	1.1160	0.9526	0.7718	0.3631	0.3353	1.1445
6	0.9909	1.0021	0.7742	0.3420	0.3680	1.1929

Time Step	Poison in Necks Σ_p (cm^{-1})	Poison in Reflectors Σ_p (cm^{-1})
0	0.1565	0.0258
1	0.095	0.018
2	0.0462	0.0163
3	0.0235	0.0138
4	0	0.0100
5	0	0.0035
6	0	0

6.12 Midcycle Recovery TURBO

The operation of the ATR with the core power distribution determined by the shim controls introduces the problem of maintaining this power distribution, after recovery from a power reduction, in spite of the transient xenon effects. The behavior following recovery to full power from a shutdown lasting one-half hour after attainment of equilibrium xenon was investigated by a TURBO calculation.

The power distribution and subsequent xenon concentration in this shutdown and recovery TURBO problem is of more importance than in the burnout TURBO problem; therefore, for the shutdown and recovery problem, after the eigenvalue and center power adjustments were made, the power distribution in the outer lobes was adjusted by varying the amount of poison in the individual reflector control regions. The pertinent results from this TURBO problem are listed in Table 6.0-C and the final adjusted values are shown in Figures 6.0-10 through 6.0-14. The eigenvalue which would have resulted at each time step if all control poisons were removed was estimated as shown in Section 6.2. Figure 6.0-15 of eigenvalue versus time was then made after subtracting 0.09 from the values given in Table 6.0-H.

The difference in the power densities of the lobes causes the loss of reactivity from nonequilibrium xenon formation after shutdown and subsequent return to full power to tend to decrease the power in the lobe where the highest power is desired (the center lobe) and to increase it where the lower powers are wanted. Thus after return to full power it is necessary to exert all available shim control in the reflector in order to shift the power as far as possible from the outer lobes into the center lobe. Then, as the burnup of the nonequilibrium xenon proceeds, more control becomes available and it again becomes possible to obtain the desired power balance between lobes by use of all control regions. The desired power balance is obtained within one-half hour after return to full power. Immediately after startup the worst power deviation occurs with the center lobe power being 14% lower than desired and each of the outer lobe powers being 4% higher than desired. After burnup of the nonequilibrium xenon is complete, the xenon concentration will be at a lower value than when the reactor was shut down and more excess reactivity is available than at shutdown until equilibrium is again reached.

6.13 Constants and Procedure

The reactor constants used in the TURBO code can be determined by two general methods: 1) the constants are read in region-wise and then not varied throughout the calculation (however an additional thermal Σ_p with specified epithermal fraction can be read in at each time step for each region), or 2) the constants are determined for each mesh rectangle within specified regions by means of the isotopic densities within those regions. The first method is used for those regions whose constants are unaffected (time independent constants) by neutron irradiation and the second method is used for the regions that have fuel or poison burnup

TABLE 6.0-C

RESULTS FROM MIDCYCLE RECOVERY TURBO CALCULATION

Time Step	Time (hours)	Eigen-value (λ)	Fraction of Total Core Power Generated in Lobe		
			Center	North	East
0	0	1.0889	0.24069	0.17042	0.20923
1	200	1.0934	0.24012	0.17256	0.20738
2	200.5	1.0899	0.20689	0.18034	0.21622
3	200.67	1.0902	0.22605	0.17405	0.21292
4	201	1.0887	0.24371	0.16830	0.20984
5	201.5	1.0894	0.24089	0.17080	0.20874
6	203	1.0918	0.23677	0.17528	0.20634
7	402.22	1.0896	0.23682	0.17102	0.21058

Time Step	Core Power (Mw)	Average Neutron Flux within Experiments (n/cm^2 sec x 10^{-15})					
		Fast			Thermal		
		Center	North	East	Center	North	East
0	250	1.3300	0.8756	0.8535	0.3509	0.2761	1.0963
1	2.5	0.013247	0.008730	0.008145	0.003752	0.002831	0.011013
2	250	1.1695	0.8939	0.8279	0.3264	0.2850	1.0851
3	250	1.2612	0.8742	0.8277	0.3554	0.2809	1.1104
4	250	1.3459	0.8585	0.8280	0.3818	0.2778	1.1192
5	250	1.3318	0.8702	0.8225	0.3766	0.2818	1.1124
6	250	1.3104	0.8832	0.8124	0.3701	0.2864	1.0994
7	250	1.3123	0.8677	0.8099	0.3995	0.2936	1.1535

Time Step	Poison in Necks Σ_p (cm^{-1})	Poison in North Reflector Σ_p (cm^{-1})	Poison in East Reflector Σ_p (cm^{-1})
0	0.1565	0.029	0.02283
1	0.0235	0.0165	0.0116
2	0	0.0067	0.0022
3	0	0.0115	0.00617
4	0.011	0.01885	0.01155
5	0.034	0.0183	0.0122
6	0.041	0.0152	0.0126
7	0	0.0162	0.0084

or formation (time dependent constants) during irradiation. The time independent constants are in general the same as those used in the PDQ studies and are included in Appendix 12.4. However, for the reflector and neck control regions the constants for pure D_2O and pure H_2O were used as input and then a thermal Σ_p was added to these regions at each time step to adjust the eigenvalue and to regulate the power distribution.

The input for the time dependent constants consists in the initial atom densities for each region and, if desired, the four-group microscopic cross sections for each element (if not specified as input, the code uses built-in four-group microscopic cross sections). The code then computes the reactor constants for each mesh rectangle within the time dependent regions as specified in the TURBO manual.[1] The input atom densities and four-group microscopic cross sections along with the resulting two-group reactor constants as calculated by the TURBO code at time step zero, are given in Appendix 12.5.

For the purpose of the TURBO calculations, it was assumed that the just critical core should yield a calculated eigenvalue of 1.09, as discussed in Section 4.2. The amount of poison in the neck and reflector control regions was adjusted at each time step to achieve the eigenvalue of 1.09 ± 0.005 and the approximate required core power distribution. The required core power distribution given in Table 6.0-A was calculated from previously completed PDQ problems by assuming the flux in the experiment in each lobe to be directly proportional to the power generated in the lobe and then finding the power distribution which would satisfy the experimental requirements.

After the TURBO problems had been run, it was realized that the results of some of the PDQ problems could have been used more effectively to adjust the eigenvalue and power distribution at each time step. Therefore, when the test flux values as obtained from the TURBO results were adjusted by the coarse to fine mesh corrections given in Table 6.0-D, additional corrections were also applied. Thus the neck and reflector poison concentrations were adjusted such that an eigenvalue of 1.090 and the power levels given in Table 6.0-A would have been obtained as long as sufficient neck and reflector control remained. The test flux values were then corrected for the resulting lobe power level changes by assuming the flux to be directly proportional to the power in the surrounding lobe. The method of making this poison adjustment is shown in Appendix 12.62.

---

1. J. E. Callaghan et al., "TURBO - A Two-Dimensional Few-Group Depletion Code for the IBM-704," WAPD-TM-95, November 1957.

TABLE 6.0-D

CORRECTION FACTORS TO ADJUST THE

COARSE MESH EXPERIMENT FLUXES TO THE FINE MESH

Fast Flux Factors			Thermal Flux Factors		
Center	North	East	Center	North	East
1.130	1.062	1.097	1.238	1.139	0.9444

6.2 Comparison of CANDLE and TURBO Calculations of k_{eff}

Several CANDLE[1] studies were made to more effectively estimate the control requirements for the TURBO problems.

The ATR may be considered to consist of two A-1, one A-3, and two A-5 one-dimensional configurations. CANDLE calculations were therefore made with each of the three loop types at its respective local power level. The estimated values of k_{eff} for a synthesized two-dimensional model were then determined by weighting the A-1, A-3, and A-5 values by factors of 2/5, 1/5, and 2/5, respectively. Table 6.0-E lists these values for comparison with the burnout TURBO problem and Table 6.0-F lists them for comparison with the midcycle shutdown and recovery TURBO problem.

In running the TURBO problems the k_{eff} was adjusted to approximately 1.09 by manipulation of the neck and reflector control poison and the no-control k_{eff} was not determined explicitly. A close estimate was made, however, by adding to the calculated k_{eff}, the Δk_{eff} associated with the neck, the north-south reflector, and the east-west reflector systems. This information is taken from curves obtained from the PDQ studies. Table 6.0-G contains the tabulation of this estimated k_{eff} from the burnup TURBO problem and Table 6.0-H contains this information from the midcycle shutdown and recovery TURBO problem. Because of the different poison levels in the two reflector systems of the midcycle shutdown and recovery TURBO problem it was necessary to compute in two steps the Δk_{eff} due to reflector poison. Thus, first the Δk_{eff} due to poison in all reflectors was found for the poison concentration in the east-west reflector system (since these reflectors had the lower poison concentration) then the Δk_{eff} due to

1. O. J. Marlowe, P. A. Ombrellaro et al., "CANDLE - A One-Dimensional Few Group Depletion Code for the IBM-704," WAPD-PM-53, May 1957.

TABLE 6.0-E

BEHAVIOR OF ONE-DIMENSIONAL AND SYNTHESIZED

TWO-DIMENSIONAL REACTOR MODELS FOR COMPARISON WITH BURNUP TURBO

Time Step	Time		CANDLE k_{eff}			Estimate of k_{eff} for Synthesized Two-Dimensional Model (Compare with Results From Burnup TURBO)
			A-1	A-3	A-5	
	Hours	Days	Power = 52.5 Mw	Power = 60 Mw	Power = 42.5 Mw	
0	0	0	1.1323	1.1101	1.1134	1.1203
1	10	.42	1.1046	1.0831	1.0867	1.0931
2	60	2.5	1.0883	1.0676	1.0710	1.0772
3	200	8.33	1.0821	1.0601	1.0667	1.0715
4	400	16.67	1.0645	1.0355	1.0564	1.0555
5	600	25	1.0319	0.9914	1.0359	1.0254
6	800	33.33	0.9836	-	1.0047	-

TABLE 6.0-F

BEHAVIOR OF ONE-DIMENSIONAL AND

SYNTHESIZED TWO-DIMENSIONAL REACTOR MODELS

FOR COMPARISON WITH MIDCYCLE RECOVERY TURBO

Time Step	Time Hours	CANDLE k_{eff} A-1 Power = 52.5 Mw	CANDLE k_{eff} A-3 Power = 60 Mw	CANDLE k_{eff} A-5 Power = 42.5 Mw	Estimate of k_{eff} For Synthesized Two-Dimensional Model (Compare with Results From Recovery TURBO)
0	0	1.1323	1.1101	1.1134	1.1203
1	10	1.1046	1.0831	1.0867	1.0931
2	60	1.0883	1.0676	1.0710	1.0772
3	200	1.0821	1.0601	1.0667	1.0715
4	200.5	1.0328	1.0058	1.0291	1.0259
5	200.67	1.0546	1.0324	1.0429	1.0455
6	200.83	1.0673	1.0467	1.0520	1.0571
7	201	1.0749	1.0546	1.0580	1.0641
8	203	1.0865	1.0648	1.0703	1.0757
9	400	1.0646	1.0357	1.0565	1.0556
10	600	1.0320	0.9915	1.0360	1.0255
11	800	0.9837	-	1.0048	-

TABLE 6.0-G

k_{eff} VERSUS TIME FROM THE BURNUP TURBO PROBLEM

Time Step	Time		Poison in Necks Σ_p (cm^{-1})	Poison in Reflectors Σ_p (cm^{-1})
	Hours	Days		
0	0	0	0.1565	0.0258
1	10	.42	0.095	0.0180
2	60	2.5	0.0462	0.0163
3	200	8.33	0.0235	0.0138
4	401.11	16.71	0	0.0100
5	600	25.00	0	0.0035
6	800	33.33	0	0

Time Step	Calculated k_{eff}	Δk_{eff}		No-Control k_{eff}	k_{eff} - 0.0964
		Due to Neck Poison	Due to Reflector Poison		
0	1.0885	0.0339	0.0862	1.2086	1.1122
1	1.0883	0.0247	0.0755	1.1885	1.0921
2	1.0887	0.0139	0.0720	1.1745	1.0781
3	1.0937	0.0077	0.0665	1.1679	1.0715
4	1.0939	0	0.0558	1.1497	1.0533
5	1.0908	0	0.0283	1.1191	1.0227
6	1.0766	0	0	1.0766	0.9802

TABLE 6.0-H

k_{eff} VERSUS TIME FROM THE MIDCYCLE RECOVERY TURBO PROBLEM

Time Step	Time Hours	Calculated k_{eff}	Poison in Necks Σ_p (cm^{-1})	Poison in E-W Reflectors Σ_p (cm^{-1})	Poison in N-S Reflectors Σ_p (cm^{-1})
0	0	1.0889	0.1565	0.02283	0.029
1	200	1.0934	0.0235	0.0116	0.0165
2	200.5	1.0899	0	0.0022	0.0067
3	200.67	1.0902	0	0.00617	0.0115
4	201.0	1.0887	0.011	0.01155	0.01885
5	201.5	1.0894	0.034	0.0122	0.0183
6	203	1.0918	0.041	0.0126	0.0152
7	402.22	1.0896	0	0.0084	0.0162

Time Step	Δk_{eff}			No-Control k_{eff}	k_{eff} - 0.0962
	Due to Neck Poison	Due to poison Level of E-W Reflectors	Due to Additional Poison in N-S Reflectors		
0	0.0339	0.0826	0.0037	1.2091	1.1129
1	0.00765	0.0605	0.0061	1.1677	1.0715
2	0	0.0200	0.0131	1.1230	1.0268
3	0	0.0415	0.0095	1.1412	1.0450
4	0.0038	0.0605	0.0087	1.1617	1.0655
5	0.01065	0.0623	0.0072	1.1696	1.0734
6	0.01255	0.0634	0.0033	1.1711	1.0749
7	0	0.0505	0.0111	1.1512	1.0550

the additional poison in the north-south reflector system was added on. A comparison of the TURBO results with the predicted effects from the CANDLE problems is made by subtracting a constant from the TURBO k_{eff} to make k_{eff} = 1.0715 at 200 hours for both the TURBO and for the CANDLE cases. Figures 6.0-16 and 6.0-17 show these comparisons for the two problems.

6.3 CANDLE Problems to Investigate the Effects of Burnable Poison and Core Power Level

Several one-dimensional CANDLE problems were run to examine the burnup or depletion of fuel in a one-lobe model of the ATR. Using the problem identification numbers these cases were as follows: cases numbered 3,4,5, and 6 were run to investigate the effects of uniformly distributed poison, cases 3,7,8, and 9 were used to investigate the effects of burnable poison placed in the inside two and outside two fuel places (case 3 was the reference case with no burnable poison), and cases 2,10,11,12,13, and 14 to investigate the behavior as a function of power level and after a midcycle power reduction. Problem 15 determined the effect on calculated values of using large time steps. The input parameters for these CANDLE problems are summarized in Table 6.0-I and the results summarized in Table 6.0-J.

In each of the CANDLE problems with burnable poison in the core, the reactor was maintained critical by automatic regulation of the poison content in the 3 in. reflector control region. The other CANDLE problems were run with no reflector control, i.e., with an unpoisoned reflector. The values of k_{eff}, given in Table 6.0-J and on Figures 6.0-18, 16.0-19 and 6.0-20 are the values which would have been obtained at each time step if the reflector control poison had been removed at that time step. Figure 6.0-18 is a plot of k_{eff} versus operating time for the core with no burnable poison and shows the effect of reflector control on k_{eff}. The values of k_{eff} obtained from problem 15 are also plotted on Figure 6.0-18. This figure shows 1) that the change in burnup distribution due to reflector poison has little effect on k_{eff} and 2) that large time steps may be used to good advantage in some types of problems.

The effect of core power on k_{eff} is shown in Figure 6.0-21. In this figure a separate scale for the operating time was used for each of the CANDLE problems so that the curves could be compared at equal values of burnup. This figure indicates that for a change of a factor of two in core power the variation in k_{eff} at equal amounts of total burnup is negligible.

Plots of k_{eff} versus operating time for various amounts of burnable poison in the core are given in Figures 6.0-19 and 6.0-20, and the variation of k_{eff} produced by xenon formation after a midcycle power reduction is shown in Figure 6.0-22.

The neutron leakage into the reflector of the one-lobe model of the ATR is greater than into the reflector of the full core model, therefore the reflector control scheme used in the CANDLE problems cannot be compared to that of the full core ATR on the basis of

TABLE 6.0-I

SUMMARY OF INPUT PARAMETERS FOR "CANDLE" PROBLEMS

Problem	B^{10} Concentration (atoms/cm^3 x 10^{-24})	Core Power (Mw)	Reactivity Initially Controlled by Burnable Poison	U^{235} Concentration (atoms/cm^3 x 10^{-24})	Ratio N^{10}/N^{25}
2+	0	65	0	0.00035136	0
3	0	65	0	0.00035136	0
4	0.00000339	65	0.0530	0.00035136	0.00965
5	0.00000678	65	0.1013	0.00035136	0.01930
6	0.00001017	65	0.1457	0.00035136	0.02895
7	0.000014426*	65	0.0693	0.00035136	0.04106*
8	0.000028852*	65	0.1292	0.00035136	0.08212*
9	0.000043278*	65	0.1815	0.00035136	0.12319*
10+	0	32.5	0	0.00035136	0
11+	0	0.65	0	0.00035136	0
12+	0	0.325	0	0.00035136	0
13+	0	48.75	0	0.00035136	0
14+	0	24.375	0	0.00035136	0
15+	0	65	0	0.00035136	0

* B^{10} in inner two and outer two fuel plates only.

+ No reflector control used in these problems.

TABLE 6.0-J

RESULTS OF "CANDLE" PROBLEMS

Problem	Time Step	Operating Time (Hours)	k_{eff}	Control Poison (cm^{-1})	Inside Power*	Outside Power*
2	0	0	1.2197	0	1.591	1.901
	1	3.5	1.2028	0		
	2	10	1.1839	0	1.604	1.916
	3	20	1.1701	0		
	4	60	1.1545	0	1.588	1.887
	5	120	1.1422	0		
	6	200	1.1283	0	1.512	1.762
	7	300	1.1120	0		
	8	400	1.0954	0	1.400	1.583
	9	500	1.0776	0		
	10	600	1.0583	0	1.290	1.408
	11	700	1.0375	0		
	12	800	1.0147	0	1.183	1.240
	13	900	0.9899	0		
	14	1000	0.9625	0	1.087	1.130
3	0	0	1.2197	0.02047	2.008	1.254
	1	3.5	1.2025	0.01806		
	2	10	1.1833	0.01567	1.953	1.370
	3	20	1.1694	0.01400		
	4	60	1.1538	0.01219	1.865	1.450
	5	120	1.1418	0.01080		
	6	200	1.1283	0.00934	1.700	1.466
	7	300	1.1125	0.00777		
	8	400	1.0963	0.00632	1.489	1.447
	9	500	1.0790	0.00492		
	10	600	1.0602	0.00354	1.296	1.408
	11	700	1.0397	0.00221		
	12	800	1.0172	0.00091	1.120	1.352
	13	900	0.9924	0		
4	0	0	1.1667	0.01368	1.941	1.432
	1	10	1.1346	0.01040	1.893	1.538
	2	60	1.1121	0.00819	1.817	1.592
	3	200	1.0980	0.00675	1.674	1.554
	4	400	1.0775	0.00491	1.483	1.484
	5	600	1.0499	0.00292	1.302	1.413
	6	800	1.0133	0.00074	1.131	1.339

* The power is relative to the average radial core power.

TABLE 6.0-J (Cont.)

Problem	Time Step	Operating Time (Hours)	k_{eff}	Control Poison (cm^{-1})	Inside Power*	Outside Power*
5	0	0	1.1184	0.00877	1.879	1.605
	1	10	1.0900	0.00637	1.836	1.703
	2	60	1.0736	0.00500	1.771	1.730
	3	200	1.0701	0.00457	1.649	1.635
	4	400	1.0599	0.00371	1.476	1.509
	5	600	1.0391	0.00219	1.303	1.408
	6	800	1.0068	0.00039	1.139	1.312
6	0	0	1.0740	0.00580	1.821	1.775
	1	10	1.0489	0.00321	1.783	1.864
	2	60	1.0379	0.00241	1.728	1.865
	3	200	1.0437	0.00273	1.623	1.713
	4	400	1.0428	0.00254	1.467	1.537
	5	600	1.0283	0.00158	1.305	1.400
	6	800	1.0002	0	1.144	1.288
7	0	0	1.1504	0.01260	1.877	1.430
	1	10	1.1194	0.00950	1.836	1.534
	2	60	1.1009	0.00756	1.775	1.584
	3	200	1.0945	0.00667	1.658	1.535
	4	400	1.0795	0.00517	1.485	1.464
	5	600	1.0535	0.00318	1.309	1.401
	6	800	1.0167	0.00093	1.140	1.336
8	0	0	1.0905	0.00715	1.768	1.592
	1	10	1.0639	0.00478	1.732	1.695
	2	60	1.0542	0.00387	1.692	1.713
	3	200	1.0644	0.00444	1.616	1.597
	4	400	1.0643	0.00407	1.476	1.475
	5	600	1.0465	0.00274	1.318	1.384
	6	800	1.0136	0.00075	1.156	1.307
9	0	0	1.0382	0.00285	1.671	1.754
	1	10	1.0152	0.00109	1.642	1.852
	2	60	1.0127	0.00085	1.615	1.841
	3	200	1.0368	0.00245	1.571	1.661
	4	400	1.0500	0.00313	1.465	1.484
	5	600	1.0397	0.00228	1.324	1.369
	6	800	1.0106	0.00058	1.170	1.280

TABLE 6.0-J (Cont.)

Problem	Time Step	Operating Time (Hours)	k_{eff}	Control Poison (cm^{-1})	Inside Power*	Outside Power*
10	0	0	1.2197	0	1.591	1.901
	1	3.5	1.2053	0		
	2	10	1.1867	0	1.606	1.919
	3	20	1.1737	0		
	4	60	1.1617	0	1.603	1.912
	5	120	1.1537	0		
	6	200	1.1454	0	1.567	1.852
	7	300	1.1370	0		
	8	400	1.1293	0	1.511	1.760
	9	500	1.1216	0		
	10	600	1.1136	0	1.454	1.669
	11	700	1.1054	0		
	12	800	1.0968	0	1.398	1.579
	13	900	1.0879	0		
	14	1000	1.0786	0	1.342	1.491
11	0	120	1.1422	0	1.556	1.834
	1	122	0.9902	0	1.645	1.913
	2	124	0.9158	0	1.698	1.964
	3	126	0.8792	0	1.727	1.993
	4	128	0.8637	0	1.741	2.008
	5	130	0.8612	0	1.743	2.013
	6	132	0.8672	0	1.739	2.010
12	0	120	1.1537	0	1.588	1.887
	1	122	1.0736	0	1.633	1.925
	2	124	1.0286	0	1.661	1.950
	3	126	1.0042	0	1.676	1.964
	4	128	0.9929	0	1.684	1.971
	5	130	0.9902	0	1.686	1.973
	6	132	0.9935	0	1.684	1.971
13	0	120	1.1422	0	1.556	1.834
	1	121	1.1322	0	1.561	1.840
	2	122	1.1314	0	1.561	1.840
	3	123	1.1320	0	1.560	1.839
	4	124	1.1327	0	1.559	1.838
	5	125	1.1335	0	1.558	1.836
	6	126	1.1341	0	1.557	1.835
14	0	120	1.1537	0	1.588	1.887
	1	121	1.1463	0	1.592	1.890
	2	122	1.1443	0	1.593	1.892
	3	123	1.1440	0	1.593	1.892
	4	124	1.1444	0	1.592	1.892
	5	125	1.1451	0	1.592	1.891
	6	126	1.1457	0	1.591	1.890

TABLE 6.0-J (Cont.)

Problem	Time Step	Operating Time (Hours)	k_{eff}	Control Poison (cm^{-1})	Inside Power*	Outside Power*
15	0	0	1.2197	0.02047	2.008	1.254
	1	200	1.1276	0.00929	1.692	1.494
	2	600	1.0620	0.00365	1.293	1.460

* The power is relative to the average radial core power.

absolute poison concentration. Therefore to obtain a meaningful appraisal of the power flattening effects of the burnable poison, the shifting effects of the reflector control poison must be factored out. However, the power peaking at the edges of the core is a function of both the poison in the reflector control and the burnout distribution, and from the information available in these CANDLE problems, these two effects cannot be satisfactorily separated. Therefore, problem to problem comparison of the peak power values given in Table 6.0-J cannot be made.

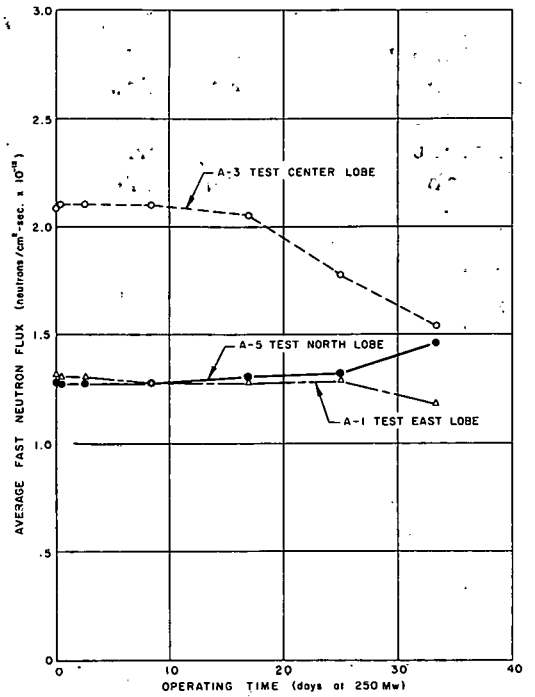

FIG. 6.0-1
MIDPLANE FAST NEUTRON FLUX IN ATR TESTS VERSUS OPERATING TIME

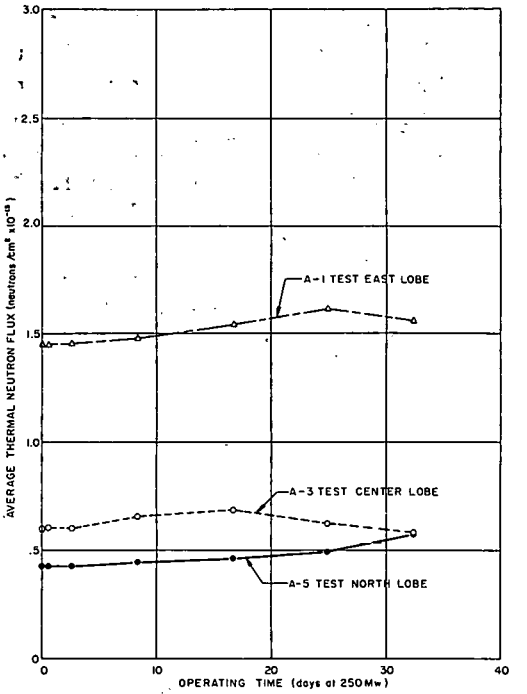

FIG. 6.0-2
MIDPLANE THERMAL NEUTRON FLUX IN ATR TESTS VERSUS OPERATING TIME

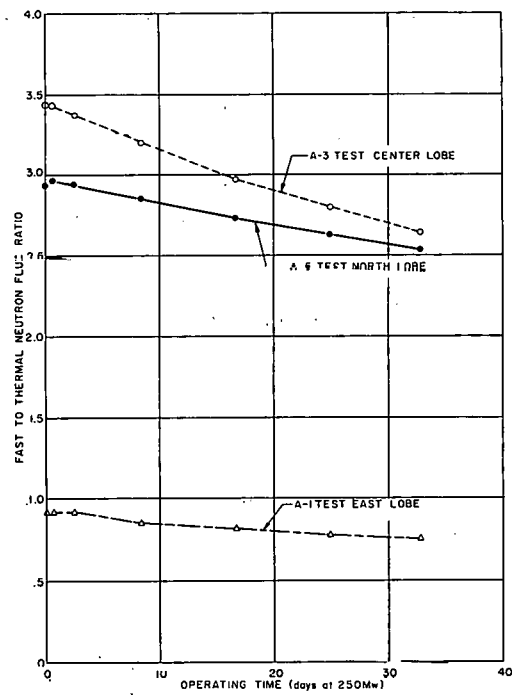

FIG. 6.0-3
FAST-TO-THERMAL NEUTRON FLUX RATIO IN ATR TESTS VERSUS OPERATING TIME

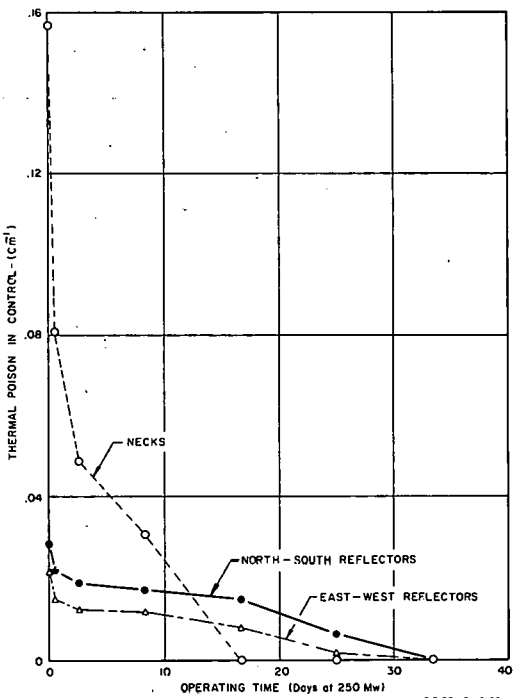

FIG. 6.0-4
POISON IN ATR CONTROL REGIONS VERSUS OPERATING TIME

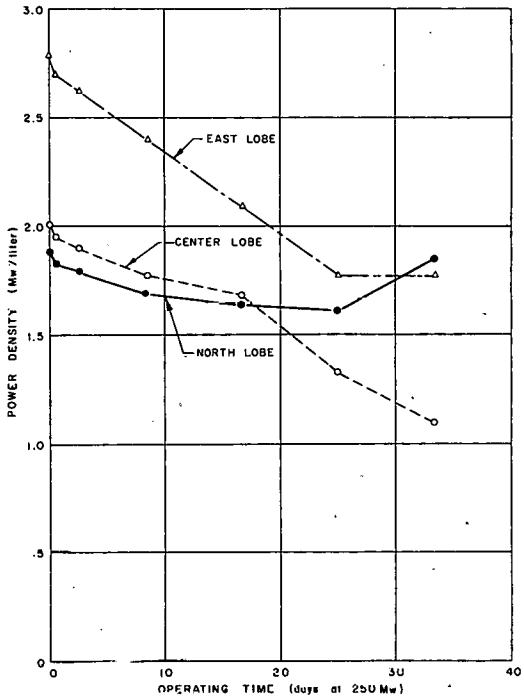

FIG. 6.0-5
MAXIMUM POWER DENSITY IN ATR CORE LOBES VERSUS OPERATING TIME

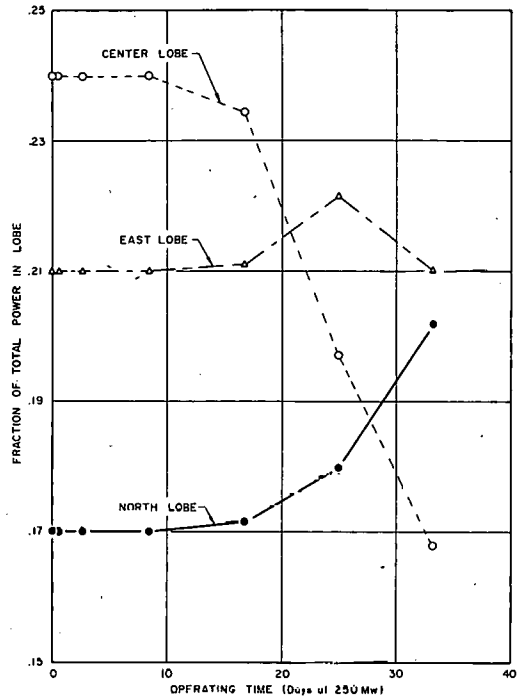

FIG. 6.0-6
POWER DISTRIBUTION IN ATR CORE VERSUS OPERATING TIME

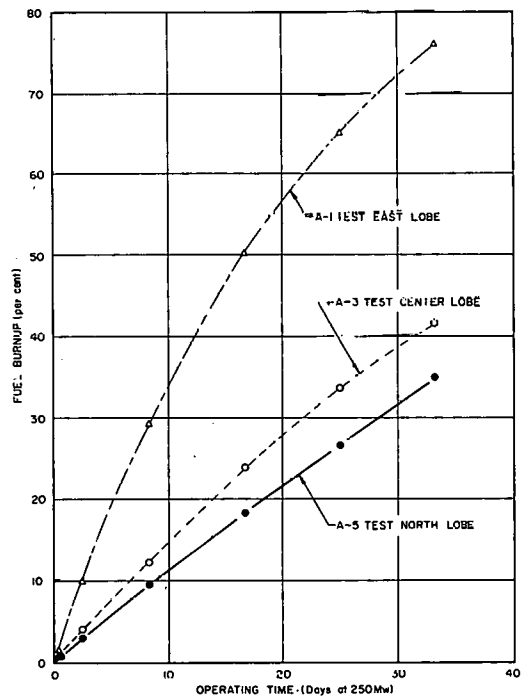

FIG. 6.0-7
BURNUP OF FUEL IN ATR EXPERIMENTS VERSUS OPERATING TIME

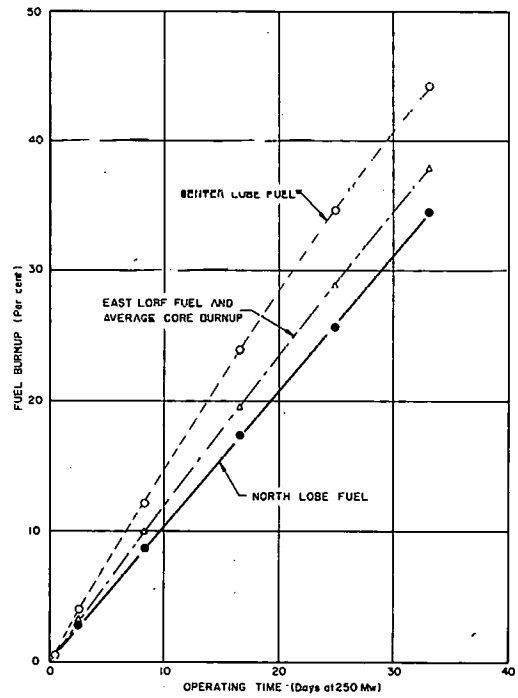

FIG. 6.0-8
PER-CENT FUEL BURNUP IN ATR CORE LOBES VERSUS OPERATING TIME

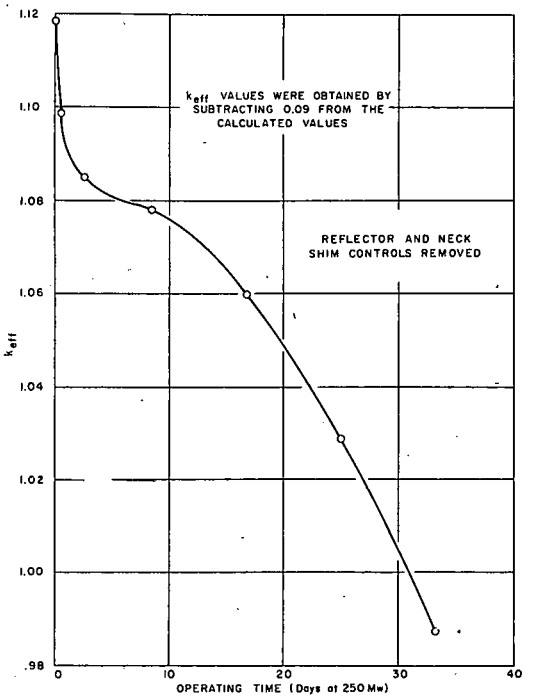

FIG. 6.0-9
k_{eff} VERSUS OPERATING TIME

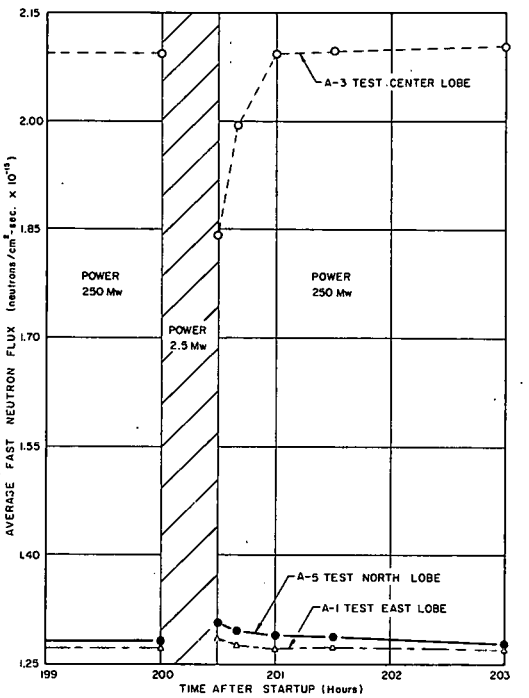

FIG. 6.0-10
MIDPLANE FAST NEUTRON FLUX IN ATR TEST
MIDCYCLE SHUTDOWN AND RECOVERY

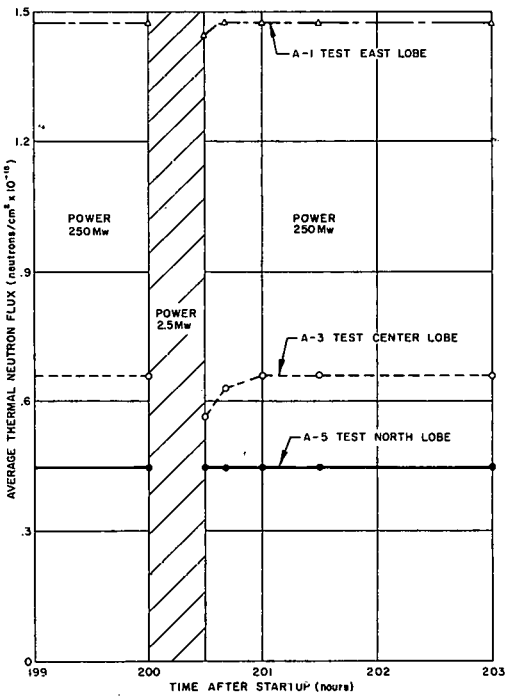

FIG. 6.0-11
MIDPLANE THERMAL NEUTRON FLUX IN ATR TESTS
MIDCYCLE SHUTDOWN AND RECOVERY

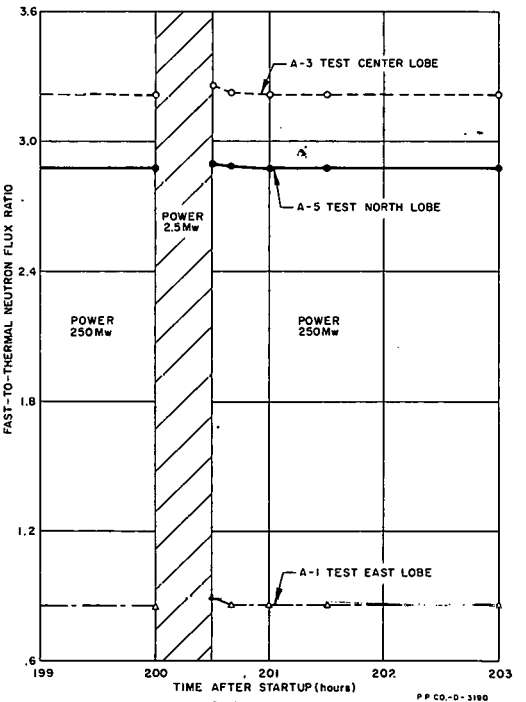

FIG. 6.0-12
FAST-TO-THERMAL FLUX RATIO IN ATR TESTS
MIDCYCLE SHUTDOWN AND RECOVERY

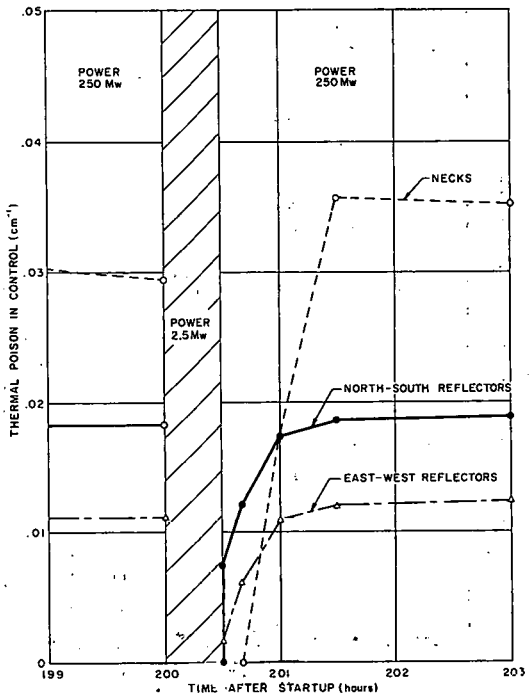

FIG. 6.0-13
POISON IN ATR CONTROL REGIONS
MIDCYCLE SHUTDOWN AND RECOVERY

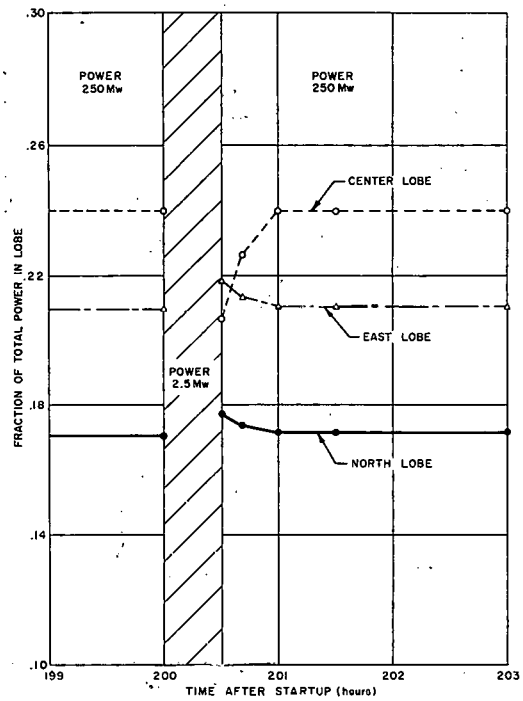

FIG. 6.0-14
ATR CORE POWER DISTRIBUTION
MIDCYCLE SHUTDOWR AND RECOVERY

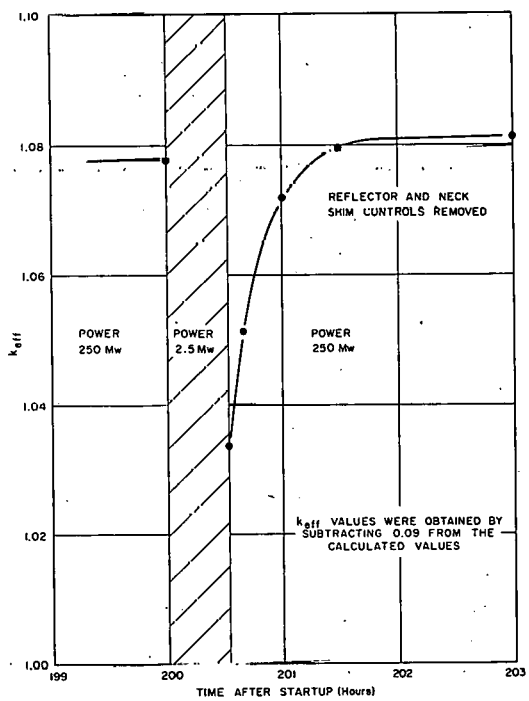

FIG. 6.0-15
k_{eff} MIDCYCLE SHUTDOWN AND RECOVERY

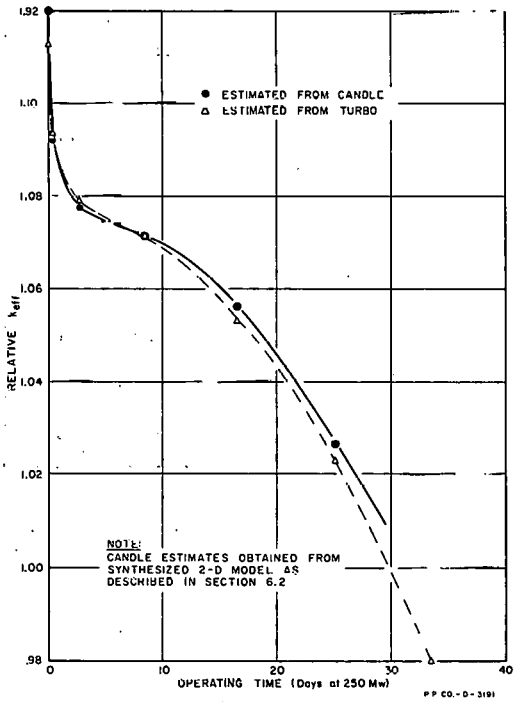

FIG. 6.0-16
COMPARISON OF CANDLE AND TURBO
k_{eff} VALUES BURNUP CALCULATIONS

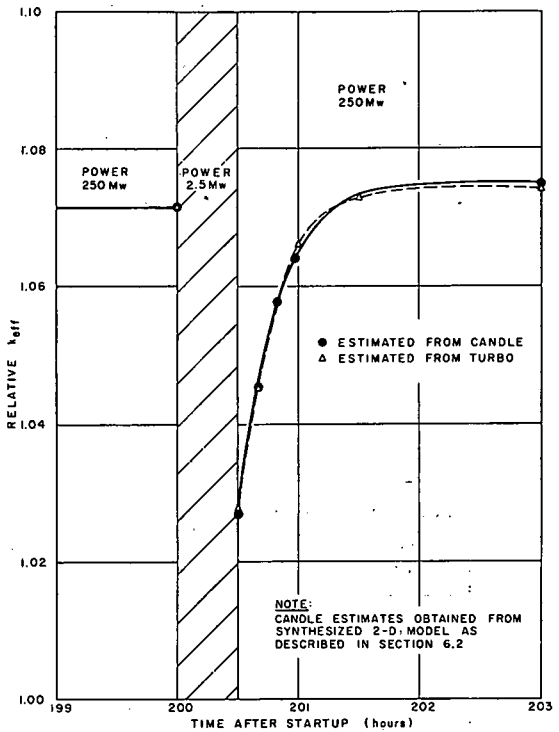

FIG. 6.0-17

COMPARISON OF CANDLE AND TURBO k_{eff} VALUES MIDCYCLE RECOVERY CALCULATIONS

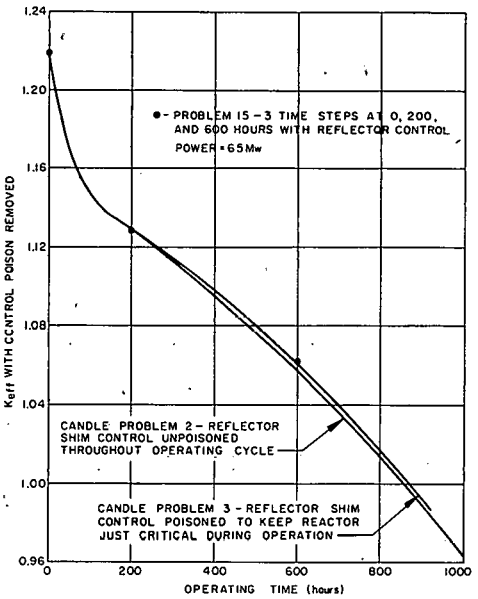

FIG. 6.0-18

EFFECT OF CONTROL POISON AND OF TIME STEP INTERVAL ON k_{eff} (SINGLE-LOBE MODEL OF ATR)

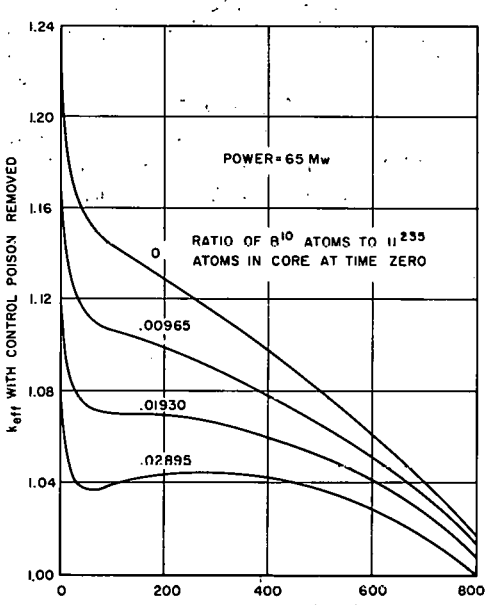

FIG. 6.0-19

EFFECT OF HOMOGENEOUS B^{10} IN CORE ON k_{eff} VERSUS OPERATION (SINGLE-LOBE MODEL OF ATR)

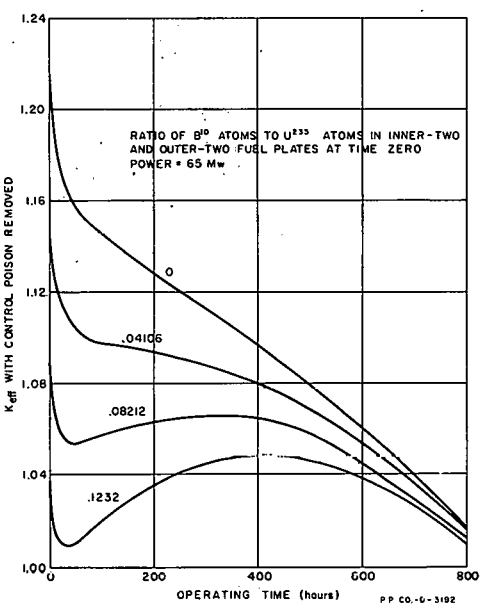

FIG. 6.0-20

EFFECT OF B^{10} IN INNER-TWO AND OUTER-TWO FUEL PLATES ON k_{eff} VERSUS OPERATING TIME (SINGLE-LOBE MODEL OF ATR)

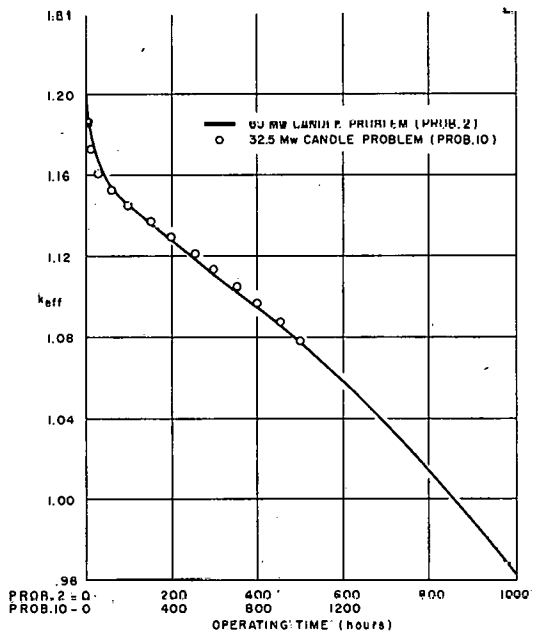

FIG. 6.0-21
VARIATION OF k_{eff} WITH BURNUP FOR
65 Mw CORE POWER AND 32.5 Mw CORE POWER
(SINGLE-LOBE MODEL OF ATR)

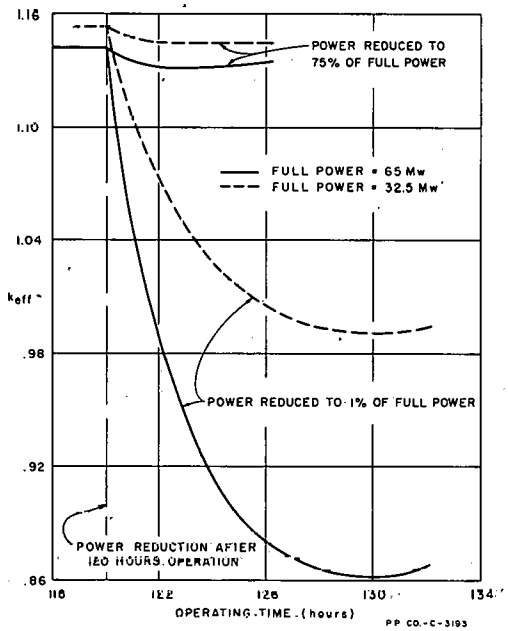

FIG. 6.0-22
EFFECT OF XENON FORMATION ON k_{eff}
AFTER A MIDCYCLE POWER REDUCTION
(SINGLE-LOBE MODEL OF ATR)

7.0 ONE-DIMENSIONAL CALCULATIONS

A number of one-dimensional calculations were made to provide initial estimates for the two-dimensional calculations. In addition, parametric studies and supplementary calculations were made with one-space dimension to reduce computational time. These results are interpreted by comparison with appropriate two-dimensional cases.

The one-dimensional diffusion theory problems were run with the IBM-650 DMM, a multiregion, multigroup diffusion theory code; and with a similar code, WANDA for the IBM-704. The output of these codes consists of the eigenvalue for the problem and, if requested, the pointwise flux for each energy group. Most of the problems made use of a cylindrical model, and in general, two neutron energy groups were used. In addition to those in this section, one-dimensional studies are also described in other appropriate sections.

7.1 Comparison of Various Methods of Reflector Control

Several different reflector control systems were studied in one-dimensional cylindrical geometry to compare reactivity worths using various compositions. The DMM models used in this study are shown in Figure 7.0-1. The compositions of Models A and D are fully described in Table 7.0-A; and, referring to Figure 7.0-1, Models B and C are identical to Model A with the exception of the geometrical description of the inner reflector. Model A was used to compare the control worth of various homogenized beryllium-water-boric acid control systems with the D_2O-D_3BO_3 system. The beryllium systems studied contained either 10% or 20% water, and the poison in the inner reflector was given in grams of boric acid per liter of water. Inner reflector thicknesses of 3 in., 4.5 in. and 6 in. were used in the beryllium plus 10% water study to see how much more control worth could be obtained by going to a larger control region.

In an actual system a beryllium-water reflector is not homogeneous. The water flows through small holes bored through a beryllium block. Models B and C were set up to try to see what effect this nonhomogeneity would have on the control worth of a beryllium-water-boric acid system. Model B was set up with a single coolant annulus halfway through the inner reflector having a volume equal to 10% of the total inner reflector volume. Model C was set up with two coolant annuli, one one-third the way through the inner reflector and the other two-thirds through. The two annuli had equal volume and the sum of their volumes was 10% of the total inner reflector volume. Both Model B and Model C were run with an inner reflector composition (excluding the coolant annulus) of pure beryllium and of beryllium plus 10% water. The results of the studies made using Models A, B and C are shown in Table 7.0-B.

TABLE 7.0-A

DMM CORE DESCRIPTIONS OF SINGLE-LOBE ATR MODELS

Region	Model A		Model D	
	Composition	Outer Radius	Composition	Outer Radius
1	A-1 Exp.	2.54	A-5 Exp.	2.54
2	Zr	3.41376	ss + Void	3.4036
3	Void	3.56616	40% H_2O, 60% Al	7.60
4	Zr	3.9116	0.096 g/cc fuel + 0.015 poison	14.00
5	H_2O	7.5997	Al tank wall	14.3175
6	0.137 g/cc fuel	14.000	Inner Refl.	15.5875
7	Inner Refl.	Variable	Outer Refl.	100.00
8	D_2O	100.00	-	-

TABLE 7.0-B

EFFECT OF REFLECTOR ON k_{eff}, MODELS A, B and C

Grams Boric Acid per Liter \ Inner Refl. Composition	Model A					Model B		Model C	
	3 in. D_2O	3 in. Be plus 10% H_2O	4.5 in. Be plus 10% H_2O	6 in. Be plus 10% H_2O	3 in. Be plus 20% H_2O	3 in. Pure Be	3 in. Be plus 10% H_2O	3 in. Pure Be	3 in. Be plus 10% H_2O
0	1.2877	1.2265	-	-	-	1.2416	1.1866	-	-
1	1.1901	-	-	-	-	-	-	-	-
3	1.0917	1.2137	-	-	-	-	1.1657	-	-
10	0.9872	1.1787	-	-	-	-	1.1306	-	-
15	0.9629	-	-	-	-	-	-	-	-
50	0.9213	1.0761	1.0699	1.0692	-	1.0865	1.0540	-	-
200	-	1.0031	-	1.0058	0.9491	1.0365	1.0092	1.0366	1.0072

NOTE: Models are described in Table 7.0-A and Figure 7.0-1.

If we define the reactivity change introduced by adding poison to the inner reflector as

$$\Delta \rho \ \frac{k_{clean} - k_{pois}}{(k_{clean})\ (k_{pois})}$$

then the 3 in. D_2O-D_3BO_3 system would have a 31% change in reactivity in going from clean D_2O to 50 g boric acid per liter, whereas the 3 in. beryllium plus 10% water system (homogenized) would only have an 18% change in reactivity going from clean to 200 g of boric acid per liter of water.

It can be seen also from the studies using Models B and C that the heterogeneity of the beryllium-water system would result in even less reactivity worth.

It should be remembered here that the one-dimensional case exaggerates the control worth because only one lobe of the reactor is considered, and in the actual ATR, the leakage into the inner reflector is much smaller than predicted by the one-dimensional model. An example of the difference is the reactivity change in going from 0 to 50 g boric acid per liter. In the two-dimensional case $\Delta\rho \approx$ 9% whereas the one-dimensional case indicates 31%. It may be concluded from this study that Be + 10% H_2O or even Be + 20% H_2O chemical control cannot provide adequate control of reactivity.

Using the same problem setup as in Model A, five more problems were run to see the effect of poisoning both the outer and inner reflectors. Table 7.0-C shows the results of this study. It can be seen that the total reactivity change in going from 0 to 50 g of H_3BO_3 per liter is very nearly the same as only poisoning the 3 in. inner reflector, i.e., about 30%. These results are shown graphically in Figure 7.0-2.

Table 7.0-D gives the results of Model D, in which various combinations of inner reflector widths and composition were studied. These results are shown in Figure 7.0-3. The eigenvalues obtained here cannot be compared directly with those using Model A; however, it may be noted that in the case with 1/2 in. H_2O+H_3BO_3 inner reflector, D_2O outer reflector, the reactivity change going from 0 - 50 grams H_3BO_3 per liter is:

$$\Delta\rho\ (0 - 50) = 31\%$$

7.2 Effect of H_2O Contamination of a D_2O Reflector

Several problems were run to determine the effect of varying the H_2O contaminant in D_2O on the reactivity and on neutron lifetime. The procedure for computing neutron lifetime is discussed in Section 10.0. In these cases, Σ_{2p} = 0.0001 and Σ_{1p} = 0.000002. The DMM model used was Model D discussed in 7.1, with an A-3 experiment. The results of this study are given in Table 7.0-E.

TABLE 7.0-C

K_{eff} VS. H_3BO_3 CONCENTRATION IN BOTH INNER AND OUTER REFLECTOR

Grams/Liter H_3BO_3	K_{eff}
0	1.2877
1	1.1003
3	1.0284
10	0.9677
15	0.9522
50	0.9189

NOTE: Calculations are for Model A of Table 7.0-A and Figure 7.0-1.

TABLE 7.0-D

EFFECT OF REFLECTOR ON K_{eff}, MODEL D

Inner Reflector		Outer Reflector		Inner Reflector Thickness			
Composition	Poison Concentration g/liter H_3BO_3	Composition	Poison Concentration g/liter H_3BO_3	1/2 in.	1-1/2 in.	3 in.	6 in.
H_2O	0	D_2O	0	1.0417	0.9324	0.8625	-
H_2O	1	D_2O	0	1.0267	0.9028	-	-
H_2O	3	D_2O	0	1.0001	0.8594	-	-
H_2O	10	D_2O	0	0.9308	0.7825	0.7355	-
H_2O	50	D_2O	0	0.7858	0.6950	-	-
H_2O	200	D_2O	0	0.7106	0.6567	-	-
H_2O	0	H_2O	0	-	-	0.8414	-
D_2O	0	D_2O	0	-	-	1.1170	-
D_2O	50	D_2O	0	-	-	0.7524	-
Be + 10% H_2O	0	H_2O	0	-	-	-	1.0479
Be + 10% H_2O	50	H_2O	0	-	-	-	0.9005
H_2O	50	D_2O	50	0.7367	-	-	-
H_2O	50	D_2O	200	0.7239	-	-	-

NOTE: Model is described in Table 7.0-A and Figure 7.0-1.

TABLE 7.0-E

EFFECTS OF H_2O CONTAMINATION OF D_2O

Inner Reflector		Percent H_2O in D_2O Outer Reflector	λ Clean	λ Poison	ρ	Lifetime (μ sec)
Composition	Poison Concentration g/liter H_3BO_3					
H_2O	0	.25%	1.04204	1.03303	0.00872	317
H_2O	0	1%	1.03512	1.02694	0.00797	290
H_2O	0	3%	1.01933	1.01279	0.00646	235
H_2O	0	5%	1.00674	1.00128	0.00545	198
H_2O	25	.25%	0.84851	0.84542	0.00365	133
H_2O	25	1%	0.84530	0.84245	0.00338	123
H_2O	25	3%	0.83754	0.83515	0.00286	104
H_2O	25	5%	0.83094	0.82887	0.00256	91

This study indicates that even in the one-dimensional model, the effect of increasing H_2O contamination in the D_2O does not have a large effect on either the neutron lifetime or the reactivity. In the actual case the effect would be much smaller because the leakage into the reflector is smaller in the actual case than in the one-dimensional model.

7.3 Separating Tank Thickness

Since most of the PDQ problems were run without a separate region to describe the tank wall separating the inner reflector from the outer reflector, a one-dimensional study was set up to determine the effect of putting an aluminum tank in. These problems were run using the same reflector setup as Model D described in 7.1.

Table 7.0-F shows that $\Delta\rho$ (due to the addition of 25 g/liter H_3BO_3) could go down by as much as 20% due to a 1 in. aluminum tank wall separating the inner reflector from the outer reflector; or about 10% due to a 1/2 in. aluminum tank wall.

It should be remembered here that these results are for the one-dimensional case. The effect of a 1/2 in. aluminum tank wall on $\Delta\rho$ due to the addition of 25 g/liter H_3BO_3 to the inner reflector would be about half that indicated in the one-dimensional study.

TABLE 7.0-F

EFFECT OF INNER REFLECTOR TANK WALL ON REACTIVITY

Thickness of Tank Wall	Inner Reflector		K_{eff}	$\Delta\rho$
	Composition	Poison Concentration g/liter H_3BO_3		
0	H_2O	0	1.0420	0.219
0	H_2O	25	0.8485	
1/4 in.	H_2O	0	1.0235	0.206
1/4 in.	H_2O	25	0.8450	
1/2 in.	H_2O	0	1.0076	0.196
1/2 in.	H_2O	25	0.8417	
3/4 in.	H_2O	0	0.9932	0.185
3/4 in.	H_2O	25	0.8387	
1 in.	H_2O	0	0.9803	0.176
1 in.	H_2O	25	0.8358	

7.4 Determination of Be-H_2O Reflector Thickness

A series of thirty-five problems on a model of one lobe of the ATR was run to determine the thickness of the beryllium reflector for two-dimensional calculations. It is somewhat difficult to properly account for the neutrons produced by the (n, 2n) reaction in beryllium so comparisons were made of two and four neutron group calculations and several schemes tried for representing the (n, 2n) neutrons in order to provide a basis for comparison with two-group two-dimensional calculations.

The calculations are made for varying thickness of beryllium plus H_2O as coolant around a cylindrical fuel annulus with 0.137 g U-235 per cc. The experimental facility interior to the core contained an A-1 experiment in a stainless steel pressure tube. In all cases the inner beryllium reflector was surrounded by an essentially infinite light water outer reflector.

Table 7.0-G shows the problem description with the corresponding eigenvalue. These results are plotted in Figure 7.0-4. From these studies, the Be-H_2O inner reflector thickness was chosen to be 6 in. with a H_2O volume fraction of 10% which is as low as heat transfer

TABLE 7.0-G

ONE-DIMENSIONAL STUDIES OF BERYLLIUM REFLECTORS

Problem No.	Materials		No. of Groups	Thickness Region 5	λ
	Region 5	Region 6			
1	D_2O	D_2O	4	-	1.238
2	Be	Be	4	-	1.304
3	Be + 5% H_2O	Be + 5% H_2O	4	-	1.260
4	Be + 10% H_2O	Be + 10% H_2O	4	-	1.225
5	Be + 20% H_2O	Be + 20% H_2O	4	-	1.172
6	H_2O	H_2O	4	-	0.905
7	Be + 20% H_2O	H_2O	4	2 in.	1.054
8	Be + 20% H_2O	H_2O	4	3 in.	1.099
9	Be + 20% H_2O	H_2O	4	4 in.	1.128
10	Be + 20% H_2O	H_2O	4	5 in.	1.146
11	Be + 20% H_2O	H_2O	4	6 in.	1.156
12	Be + 20% H_2O	H_2O	4	7 in.	1.162
13	Be + 20% H_2O	H_2O	4	8 in.	1.166
14	Be + 20% H_2O	H_2O	2	2 in.	1.134
15	Be + 20% H_2O	H_2O	2	3 in.	1.175
19	Be + 20% H_2O	H_2O	2	7 in.	1.235
20	Be + 20% H_2O	H_2O	2	8 in.	1.238
21	D_2O	D_2O	2	-	1.259
22	Be + 10% H_2O	H_2O	4	2 in.	1.070
23	Be + 10% H_2O	H_2O	4	3 in.	1.130
24	Be + 10% H_2O	H_2O	4	4 in.	1.156
25	Be + 10% H_2O	H_2O	4	5 in.	1.180
26	Be + 10% H_2O	H_2O	4	6 in.	1.196
27	Be + 10% H_2O	H_2O	4	7 in.	1.207
28	Be + 10% H_2O	H_2O	4	8 in.	1.213
29	Be + 5% H_2O	H_2O	4	2 in.	1.076
30	Be + 5% H_2O	H_2O	4	3 in.	1.128
31	Be + 5% H_2O	H_2O	4	4 in.	1.167
32	Be + 5% H_2O	H_2O	4	5 in.	1.195
33	Be + 5% H_2O	H_2O	4	6 in.	1.215
34	Be + 5% H_2O	H_2O	4	7 in.	1.229
35	Be + 5% H_2O	H_2O	4	8 in.	1.238
36	Be + 20% H_2O	H_2O	2 ($\nu\Sigma_f$ for R_c = 0)	2 in.	1.073
37	Be + 20% H_2O	H_2O	2 (Σ_R in & $\nu\Sigma_f$ = 0)	2 in.	1.106
38	Be + 20% H_2O	H_2O	2 (Σ_R in & $\nu\Sigma_f$ in)	2 in.	1.095

NOTE: Models are described in Table 7.0-A and Figure 7.0-1.

would permit. It was decided that the proper way to take the (n, 2n) reaction into account in the four-group scheme was to subtract the value of $\nu\Sigma_{1f}$ (calculated by MUFT) from the absorption cross section for the first fast group, and add it to the removal cross section for that group.[1] To determine the best way to handle beryllium in two-group problems, three different methods were tried in problems 36, 37 and 38 to compare with problem 7 (Table 7.0-G). From this comparison it was decided that it was best simply to ignore the value of $\nu\Sigma_{1f}$ calculated by the MUFT program and use the D, Σ_{1a}, Σ_{1r} just as they come from MUFT.

7.5 One-Dimensional Calculations of Fluxes in Experiments

7.51 Effect of Reflector Composition on Experiment Fluxes

Two models, described in Table 7.0-A, with different reflector compositions but with roughly the same eigenvalue were used to observe the effect of the reflector on the test fluxes. The first case had a 3 in. thick inner D_2O reflector with 3 g of boric acid per liter and an eigenvalue of 1.0917, and the second case had a 90% Be + 10% H_2O reflector with 50 g of boric acid per liter of H_2O and an eigenvalue of 1.0761. Table 7.0-H gives the results of this comparison, where the fluxes are normalized to the same core power in both cases.

TABLE 7.0-H

EXPERIMENT FLUXES VS. REFLECTOR COMPOSITION

	D_2O + 3 g/liter	Be + H_2O + 50 g/liter
ϕ_1	1.803	1.782
ϕ_2	2.194	2.290
ϕ_1/ϕ_2	0.822	0.778

The change in both the fast and thermal fluxes is small and there is about a 5% change in the fast-to-thermal flux ratio in going from D_2O to beryllium in the reflectors. It should be noted that the experiment is in the center of the core and thus the effect should be even more than in the actual case.

7.52 Effect of Moderator Composition on Fast-to-Thermal Flux Ratio in Experiment

A series of problems was run using the same problem setup as listed in Table 7.0-A, Model A with region 5 varied from pure H_2O

1. Personal communication with Glen E. Putnam of Internuclear Company.

to 10% H_2O, 90% Al. Both inner and outer reflector regions contained pure D_2O (0.25% H_2O). The results of this study are given in Table 7.0-I. This information was used to help determine an optimum metal-to-water ratio to use in the two-dimensional cases to obtain a ϕ_f/ϕ_s ratio of one in the A-1 experiment with the zirconium tube.

TABLE 7.0-I

EFFECT OF H_2O CONTENT OF MODERATOR ANNULUS

ON FAST-TO-THERMAL FLUX RATIO IN EXPERIMENT

% H_2O in Aluminum-Water Moderator Annulus	ϕ_f/ϕ_s Experiment
10	3.8195
20	2.8298
70	1.1260
90	0.8962
100	0.8145

Figure 7.0-5 shows the curves of the fast-to-thermal flux ratio versus the percent water in the moderator annulus for A-1 experiment with stainless steel pressure tube, A-1 experiment with zirconium pressure tube, and A-3 experiment with stainless steel pressure tube.

Also, several problems with different setups were run to determine how to get a desired fast flux or the fast-to-thermal flux ratio in an experiment. These problems were run prior to any two-dimensional studies and were exploratory in nature. Table 7.0-J gives a description of each problem and the results are listed in Table 7.0-K.

7.6 Flux Peaking Due to Safety Blade

A one-dimensional problem was set up to obtain a flux plot across a fuel element located next to a safety blade of one proposed design. This problem was run in slab geometry as a cell problem, with x = o located at the center of the safety blade (poison section withdrawn) and the outer boundary located approximately in the center of the fuel element. Figure 7.0-6 shows the results of this study along with the dimensions and composition of each region. This study shows that the maximum-to-average thermal flux due only to the safety blade follower is about 1.25. Therefore, the final detailed design should be such that most of this peaking is eliminated.

TABLE 7.0-J

PROBLEM DESCRIPTION FOR ONE-DIMENSIONAL FLUX CALCULATIONS

Problem No.	Region 1 Experiment	Region 2 Metal	Region 3 Void	Region 4 Metal	Region 5 Moderator	Region 6 Fuel In.	Region 7 Inner Reflector	Region 8 Outer Reflector
1001	A-1	ss	Void	ss	H_2O	2-1/2	H_2O	H_2O
1002	A-1	Zr	"	Zr	H_2O	2-1/2	H_2O	H_2O
1003	A-1	Zr	"	Zr	Be+10% H_2O	2-1/2	H_2O	H_2O
1004	A-3	ss	"	ss	60% Al, 40% H_2O	2-1/2	H_2O	H_2O
1005	A-3	ss	"	ss	"	2	H_2O	H_2O
1006	A-1	ss	"	ss	H_2O	2	H_2O	H_2O
1007	A-3	ss	"	ss	60% Al, 40% H_2O	2-1/2	H_2O+3 g/l H_3BO_3	H_2O
1008	A-3	ss	"	ss	"	2	"	H_2O
1009	A-1	ss	"	ss	H_2O	2	"	H_2O

TABLE 7.0-K

EXPERIMENT FLUXES IN ONE-DIMENSIONAL MODELS

Problem No.	k_{eff}	Experiment Fluxes in Arbitrary Units			Average Experiment Flux Normalized to 100 Mw Core Power n/cm^2 sec		k_{eff} x Average Flux		Maximum to Average Core Flux
		ϕ_f	ϕ_s	ϕ_f/ϕ_s	$\phi_f \times 10^{-15}$	$\phi_s \times 10^{-15}$	$\phi_f \times k_{eff} \times 10^{-15}$	$\phi_s \times k_{eff} \times 10^{-15}$	
1001	1.241	711.0	451.5	1.575	1.164	0.739	1.445	0.917	2.23
1002	1.280	757.1	1027.3	0.737	1.215	1.649	1.555	2.111	2.17
1003	1.328	936.0	574.0	1.631	1.426	0.874	1.894	1.161	2.32
1004	1.276	939.7	306.9	3.062	1.489	0.486	1.900	0.620	2.36
1005	1.215	1087.2	356.1	3.053	1.832	0.800	2.226	0.729	2.15
1006	1.182	815.4	518.0	1.574	1.421	0.903	1.680	1.067	2.00
1007	1.033	1013.1	328.1	3.088	2.054	0.665	2.122	0.687	1.71
1008	0.952	1158.4	374.6	3.092	2.575	0.833	2.451	0.793	1.59
1009	0.943	868.8	546.8	1.589	1.957	1.232	1.845	1.162	2.08

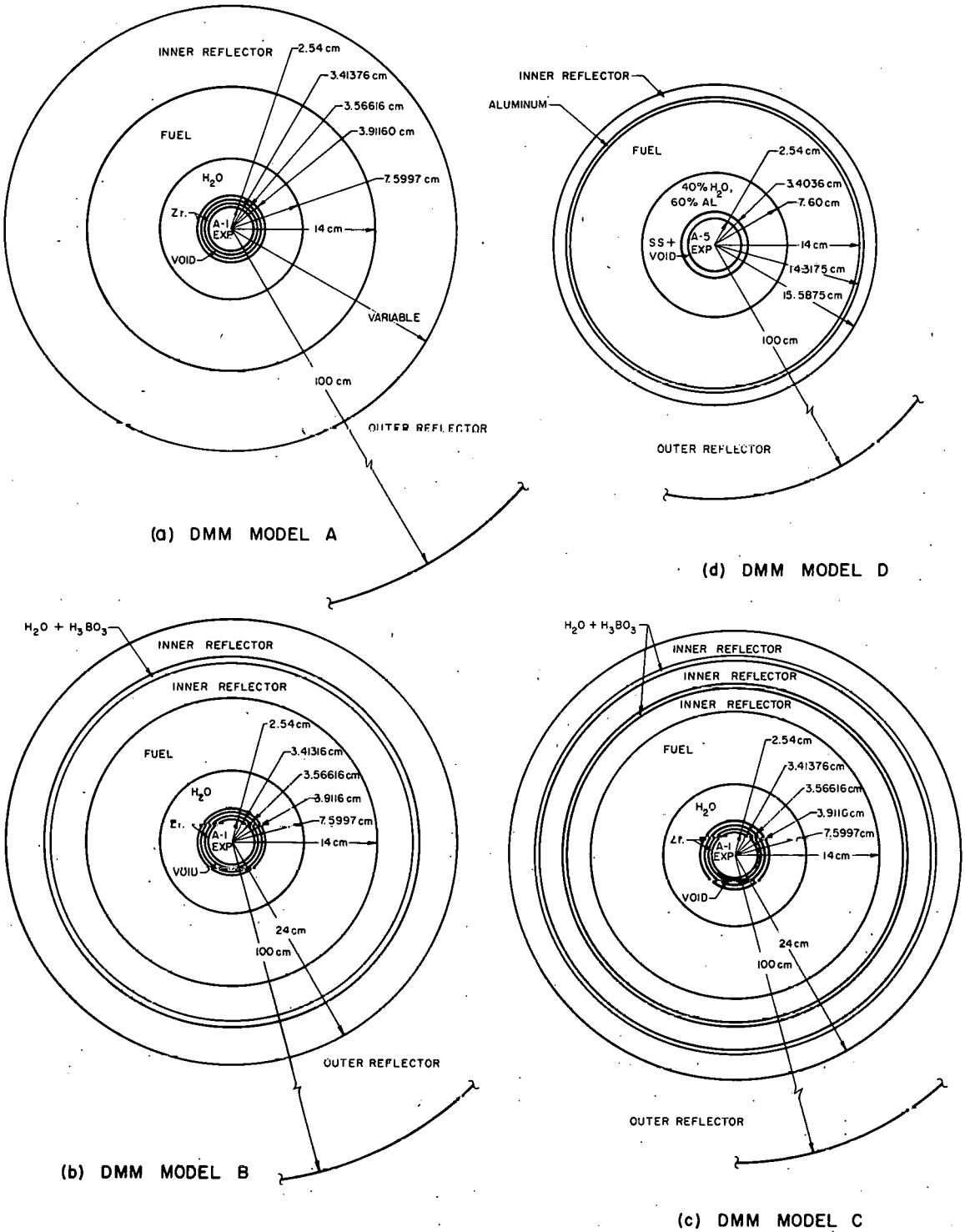

FIG. 7.0 – 1

PP CO.-C-3194

CYLINDRICAL MODELS FOR ONE – DIMENSIONAL CALCULATIONS

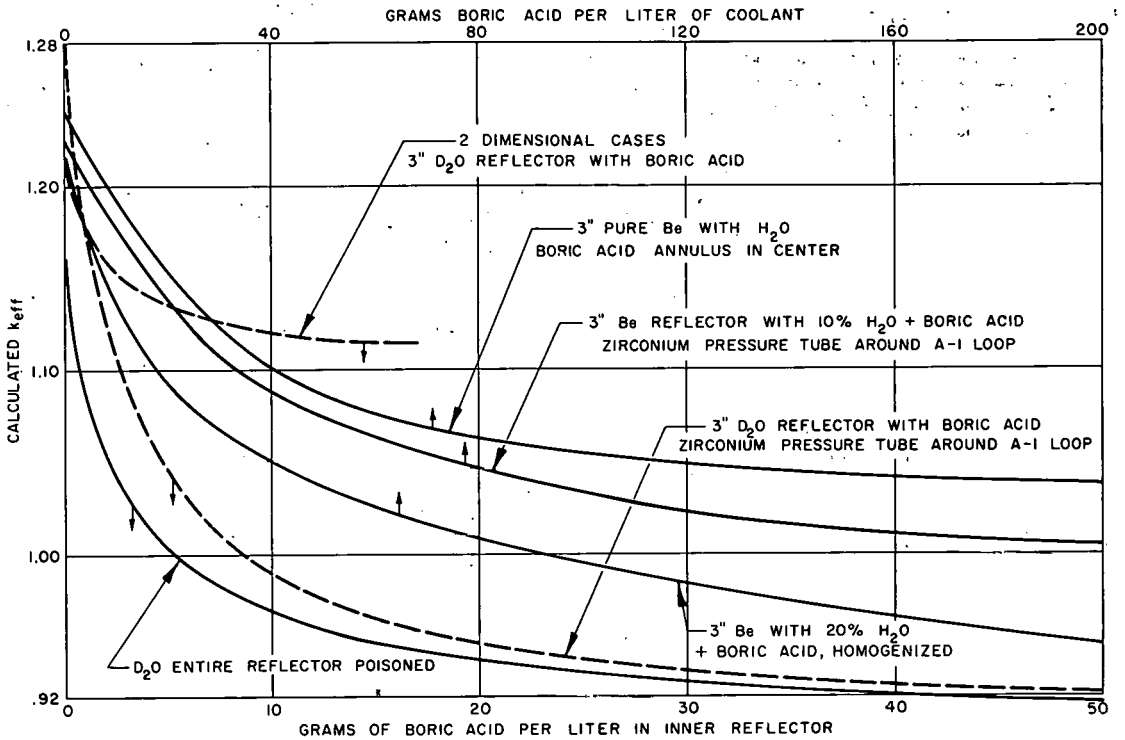

FIG. 7.0 – 2

EFFECT OF REFLECTOR CONDITIONS ON k_{eff} USING MODEL A

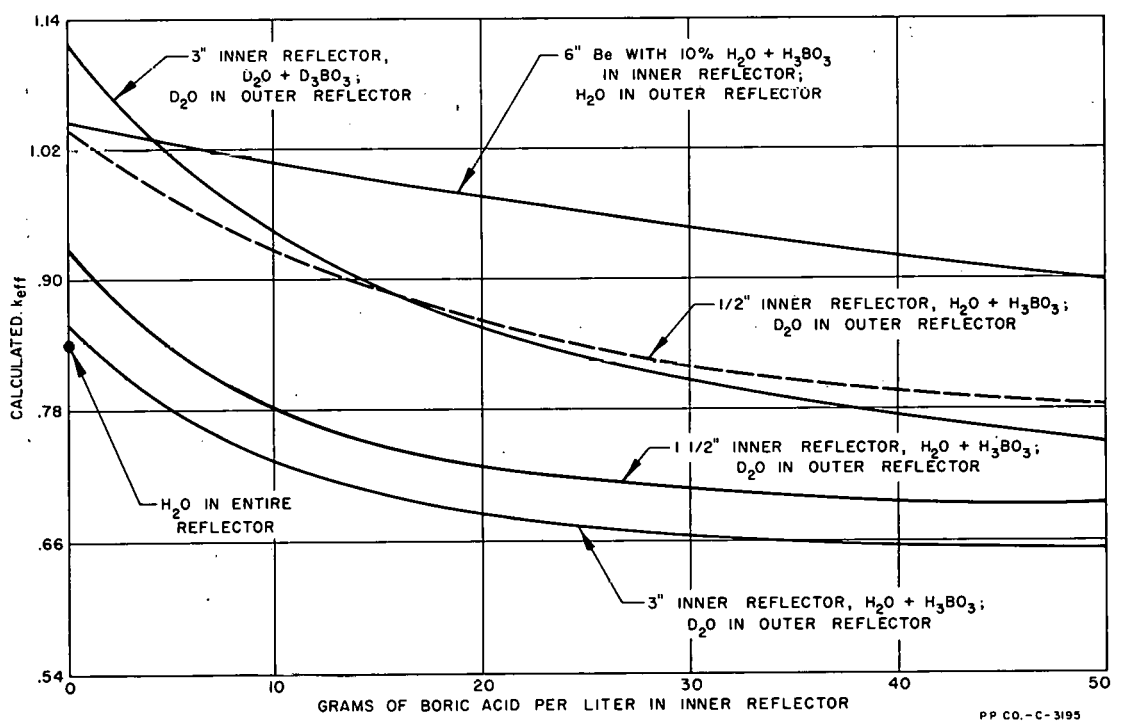

FIG. 7.0 – 3

VARIATION OF k_{eff} WITH POISON IN REFLECTOR USING MODEL D

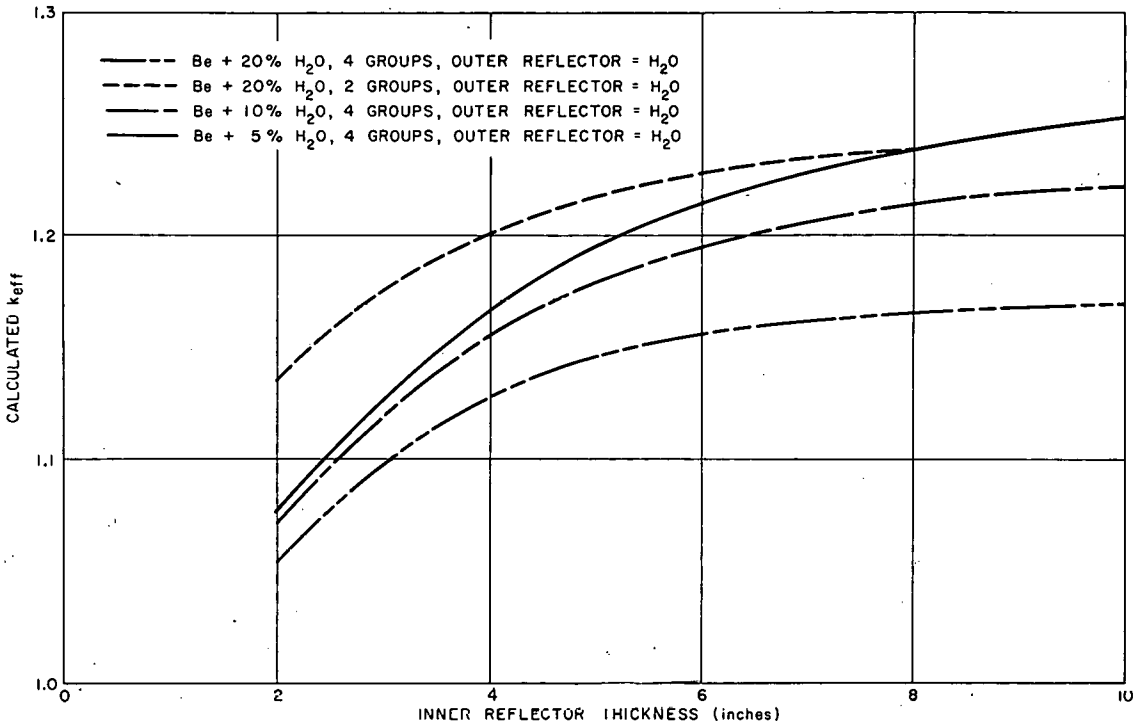

FIG. 7.0-4

k_{eff} VERSUS BERYLLIUM - WATER INNER REFLECTOR THICKNESS

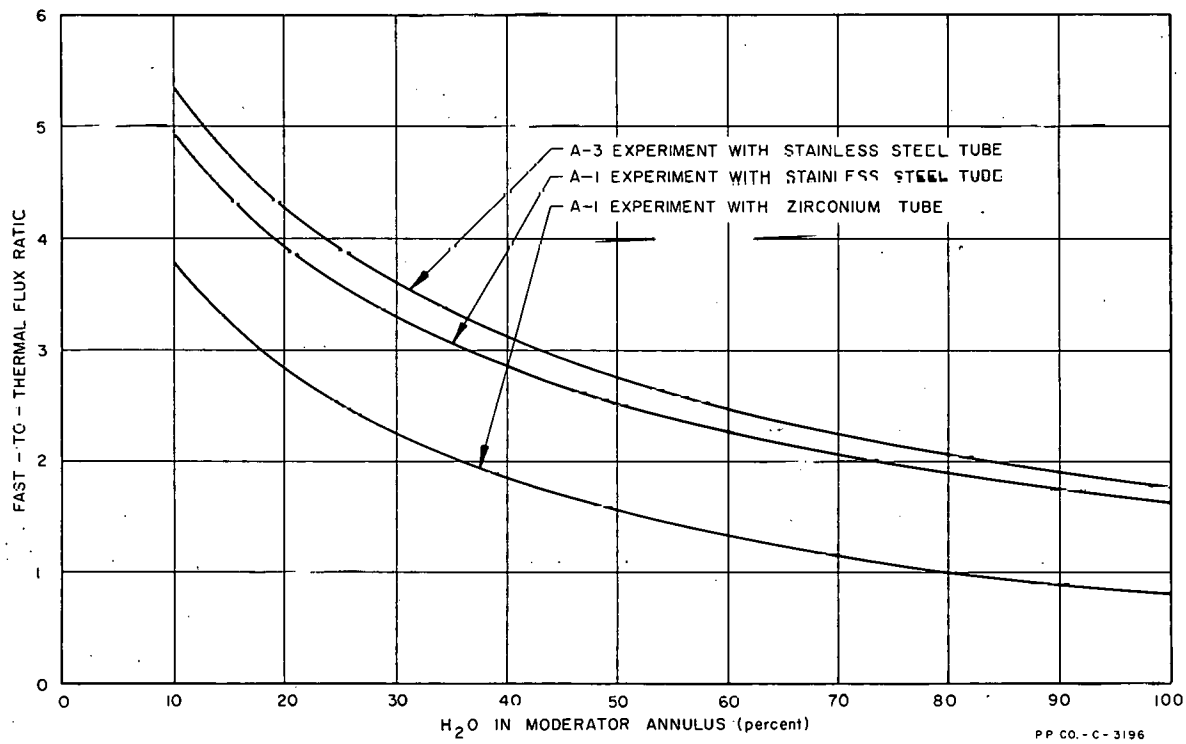

FIG. 7.0-5

FAST - TO - THERMAL FLUX RATIO IN EXPERIMENT VERSUS PER CENT H_2O IN MODERATOR ANNULUS

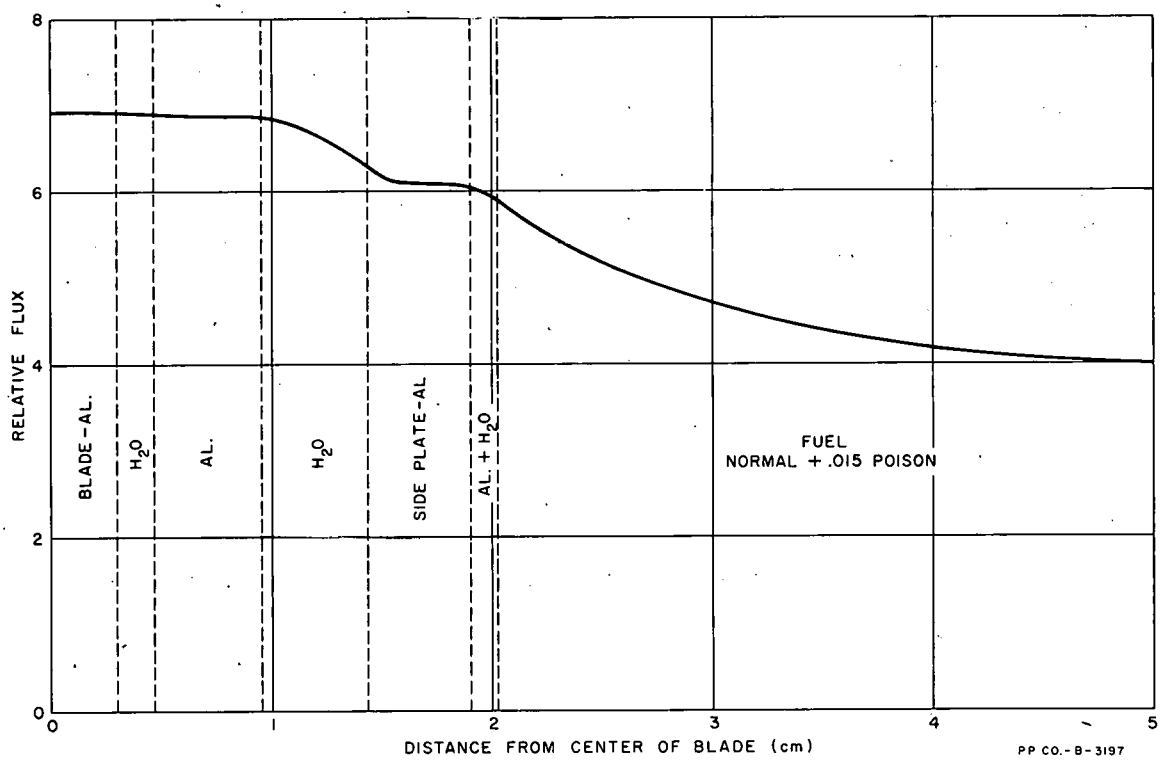

FIG. 7.0 – 6

PLOT OF SLOW FLUX FROM CENTER OF BLADE
TO CENTER OF FUEL ASSEMBLY

8.0 VOID AND TEMPERATURE COEFFICIENTS OF REACTIVITY

8.1 Void Coefficients

The temperature coefficient of reactivity is determined by the net balance of a number of positive and negative effects but in ATR is primarily due to changes in the density of the coolant and moderator fluids in the reactor, i.e., by the void coefficient.

Moreover, the possibility of boiling at various locations and the introduction of cooler and more dense water into the different regions of the reactor place additional emphasis on a knowledge of the void coefficient of reactivity. The variation of the void coefficient of reactivity with position (mainly radial position) allows the further possibility that the reactivity change can be different in sign as well as magnitude if boiling in a region takes place uniformly rather than near some hot spot near the surface of the region.

The void coefficient as a function of radial position in single lobe models of ATR has been determined with a series of one-dimensional diffusion theory studies performed using the WANDA-4 code. Two models, as described in Table 8.0-A, have been considered; the first has an A-1 test with a zirconium pressure tube and the second has an A-5 test with a stainless steel pressure tube. The studies are based on the simplifying assumption that initial study of void coefficients in a single detached lobe can be directly related to those of the complete reactor by the effect of reactivity change in one lobe upon net reactivity of the complete reactor. The reactivity changes for the single lobe model as listed in Tables 8.0-B and 8.0-C are about three times the corresponding values for ATR.

All void coefficients were calculated from the difference in the k value (calculated by the WANDA-4 code) of the "reference" reactor and the reactor with a small-finite change in the H_2O and D_2O density in some radial annulus. In the test region, the filler and the core, the change in reactivity (k) was observed for a change in the density throughout the region, in only the inner 1/4 in. of the region, and in only the outer 1/4 in. of the region. A complete list of all of the cases run is given in Tables 8.0-B and 8.0-C, together with the Δk values which resulted. Also listed in these tables are the values $\Delta k/\Delta V$ and $\Delta k/v$ for each case.

The void coefficient of reactivity is assumed to be simply $\Delta k/\Delta V$, where Δk is the observed difference in k equal to $k-k_o$ (k_o is the k of the reference case), and ΔV is the effective void which results from the change in H_2O or D_2O density. For example, if the Δk results from changing the H_2O density in a region from ρ_o to $0.75\ \rho_o$, the ΔV is simply 0.25. Hence, ΔV is the fraction of the H_2O which is replaced by void.

In order to obtain a meaningful measure of the radial position dependence of the void coefficient, a set of numbers termed $\Delta k/v$ was also computed. These numbers represent the change in k produced by adding one cm^3 of void per cm of reactor length at each of the respective positions. Hence $\Delta k/v = \Delta k/(\Delta V \times \text{Volume of region perturbed})$.

Whether the lobe contains the A-1 or the A-5 test, the positive void coefficient in the test is reassuringly small and relatively constant with radial position. Cases 14 and 35, respectively, refer to the entirely dry test region for the A-1 and A-5; and in both of these cases the Δk is less than that needed for prompt neutron reactivity. The A-1 test has the higher void coefficient by about a factor of 3.5 as compared with the A-5 test, but when even the A-1 is dry the reactivity increase is more than a factor of 3.0 away from that needed for prompt criticality of the single lobe model.

In the 40 per cent H_2O-60 per cent aluminum filler which is used with the A-5 test, the void coefficient is small and it is positive only at the extreme inside boundary (near the test). The void coefficient for voids distributed uniformly is negative and it apparently becomes more and more negative toward the core. However, in the 100 per cent H_2O filler used with the A-1 test the void coefficient is rather large and positive throughout the region with the highest value at the boundary near the test.

The indication is that a uniform distribution of about 16 per cent void in the A-1 filler region represents enough Δk to meet the usual criterion for prompt criticality (about .72 per cent $\Delta k/k$) in a single lobe model. There is considerable reassurance, however, in the fact that such a reactivity rise would have to occur relatively rapidly and in all lobes simultaneously in order to be hazardous and considerable bulk boiling would have to occur in order to attain this void fraction. In addition, the possibility of nucleate boiling in the region adjacent to the core or the test does not appear to represent a hazard even should it occur, for the results indicate that about a 100 per cent void fraction is necessary in the 1/4 in. layer near the core or near the test in all lobes at the same time in order to meet the usual conditions for prompt criticality.

Two kinds of dependence are indicated for the void coefficient in the core. First, the coefficient becomes much more negative in the center of the core annulus than at the edges; and, second, the coefficient becomes more negative as poison is added to the control region outside the core. The void coefficient for uniform distribution of voids in the core is over twice as large as the value near the edges, and the average core void coefficient with 8 g/liter of H_3BO_3 in the control region is about twice as large as the value obtained with the control region clean.

In the control region, the void coefficient near the core is negative whether or not the reflector control is poisoned and it is only

slightly more negative when it is unpoisoned. In the unpoisoned case, the void coefficient remains negative throughout the control region, but it becomes positive enough in the poisoned case to cause the void coefficient for uniform control region void to be a small positive value. It is evident that decreasing the density of poisoned reflector control (uniformly) causes as large an increase in neutron leakage losses as a decrease in thermal neutron absorption.

In assessing the results of Tables 8.0-B and 8.0-C it should be kept in mind that they apply to a single annulus model. The change of reactivity for the same change in void in one annulus of ATR is roughly one-third that of the corresponding value in these tables. The delayed group of neutrons from the reflector makes reactivity insertion for prompt criticality considerably greater than the usual value of .72 per cent $\Delta k/k$.

TABLE 8.0-B

VOID COEFFICIENTS FOR SINGLE-LOBE MODEL
WITH A-1 TEST AND ZIRCONIUM LOOP

Case No.	Perturbed Region	Perturbation, ΔV =Void Fraction of H_2O	Water Fraction	Volume of Region (cm^3/cm)	K	$\Delta K \times 10^2$	$\frac{\Delta K}{\Delta V} \times 10^2$	$\frac{\Delta K}{V_{H_2O}} \times 10^4$
0	Reference Case				.91573148			
1	Inner 1/4" of Test	0.25	0.515	1.2668	.91578024	+.004876	.019504	+2.9897
2	Entire test	0.25	0.515	20.2683	.91653108	+.079960	.31984	+3.0641
3	Outer 1/4" of test	0.25	0.515	8.8674	.9160965	+.036502	.14601	+3.1973
4	Inner 1/4" of filler	0.10	1.0	14.2527	.9165406	+.080907	.80907	+56.766
5	Entire Filler	0.10	1.0	105.46	.92034215	+.461067	4.61067	+43.720
6	Outer 1/4" of Filler	0.10	1.0	26.6021	.91667063	+.093915	.93915	+35.304
7	Inner 1/4" of Core	0.10	0.556	31.6692	.91519423	-.053724	-.53724	-3.0510
8	Entire Core	0.10	0.556	430.7012	.89145217	-.2427931	-24.2793	-10.1388
9	Outer 1/4" of Core	0.10	0.556	54.4710	.91432276	-.140872	-1.40872	-4.6514
10	Inner 1/4" of Control Region	0.10	1.0	59.5381	.91523149	-.05000	-.5000	-.83978
11	Entire Control Region	0.10	1.0	881.6705	.91597369	+.024221	+.24221	+.02747
12	D_2O Reflector	0.10	1.0	31,693.	.91218641	-.354507	-3.54507	-.01119
13	Control Region and D_2O Reflector	0.10	1.0	32,575.	.91164447	-.408701	-4.08701	-.01255
14	Entire Test	1.00	0.515	20.2683	.9179775	+.22460	+.22460	+2.1517
15	Middle 2" of Core	0.10	0.556	344.5610	.89354987	-2.218161	-22.18161	-11.5784
*16	Reference Case				1.2201704			
17	Middle 2" of Core	0.10	0.556	344.5610	1.2091922	-1.09782	-10.9782	-5.7304
18	Entire Core	0.10	0.556	430.701	1.2104614	-.9709	-9.709	-4.0543
19	Inner 1/4" of Control Region	0.10	1.0	59.5381	1.2193461	-.08242	-.8243	-1.3845
20	Entire Control Region	0.10	1.0	881.6705	1.2106277	-.95427	-9.5427	-1.0823
21	D_2O Reflector	0.10	1.0	31,693.	1.1981379	-2.20325	-22.0325	-.069518
22	Control Region and D_2O Reflector	0.10	1.0	32,575.	1.1877533	-3.24171	-32.4171	-.099515

* In cases 0 through 15, there are 8 grams of H_3BO_3/liter in the control region.
In cases 16 through 22 there is no H_3BO_3 in the control region.
V_{H_2O} = ΔV x Water Fraction

TABLE 8.0-C

VOID COEFFICIENTS FOR SINGLE-LOBE MODEL
WITH A-5 TEST AND STAINLESS LOOP

Case No.	Perturbed Region	Perturbation, ΔV = Void Fraction of H_2O	Water Fraction	Volume of Region (cm^3/cm)	K	$\Delta K \times 10^2$	$\frac{\Delta K}{\Delta V} \times 10^2$	$\frac{\Delta K}{V_{H_2O}} \times 10^4$
23	Reference Case				.8732584			
24	Inner 1/4" of Test	0.25	0.515	1.26677	.8732615	.00031	.00124	.1903
25	Entire Test	0.25	0.515	20.2683	.8734875	.02291	.09162	.8777
26	Outer 1/4" of Test	0.25	0.515	8.8674	.8734006	.014217	.05687	1.2452
27	Inner 1/4" of Filler	0.3575	1.0	25.6779	.8732750	.001655	.004629	.01803
28	Entire Filler	0.3575	1.0	116.8853	.8729031	-.035537	-.09940	-.08504
29	Outer 1/4" of Filler	0.3575	1.0	26.6021	.8731346	-.012384	-.034641	-.1302
30	Inner 1/4" of Core	0.10	0.556	31.6692	.8718496	-.14088	-1.4088	-8.0011
31	Entire Core	0.10	0.556	430.7012	.8443828	-2.88756	-28.8756	-12.0581
32	Outer 1/4" of Core	0.10	0.556	54.5710	.8716190	-.16395	-1.6395	-5.4133
33	Inner 1/4" of Control Region	0.10	1.0	59.5381	.8727535	-.05050	-.5050	-.84813
34	Entire Control Region	0.10	1.0	881.6705	.8738043	.05459	.5459	.06191
35	Entire Test	1.0	0.515	20.2683	.8738670	.060857	.060857	.5830

Note: In cases 23 through 35 (inclusive) there are 8 grams of H_3BO_3/liter in control region.

V_{H_2O} = ΔV x Water Fraction.

TABLE 8.0-A
SINGLE-LOBE MODELS FOR THE VOID COEFFICIENT CALCULATIONS

Region No.	A-1 Test and Zirconium Loop		A-5 Test and Stainless Steel Loop	
	Outer Radius (in)	Composition	Outer Radius (in)	Composition
1	1.0	A-1 Test	1.0	A-5 Test
2	1.536	Zircalloy 2 (+ homogenized void)	1.34	Stainless steel (+ homogenized void)
3	2.75	Filler of H_2O	2.75	Filler of 40% H_2O and 60% Al
4	3.00	Aluminum	3.00	Aluminum
5	5.50	Core	5.50	Core
6	5.75	Aluminum	5.75	Aluminum
7	8.75	D_2O Control region	8.75	D_2O Control region
8	40.50	D_2O Reflector	40.50	D_2O Reflector
9	43.50	Stainless Steel	43.50	Stainless Steel

8.2 The Components of the Temperature Coefficient

Estimates of the major components of the temperature coefficient in the core of one lobe of the ATR have been made. The results, together with the calculated or assumed constants, are shown in Table 8.0-D. The lobe contains the A-1 test, zircalloy pressure tubing, the normal fuel loading, and 3 grams/liter of D_3BO_3 in the 3 in. D_2O control region. K_{eff} of this reactor is 1.0127; the model is similar to that of Table 8.0-A.

TABLE 8.0-D

MAJOR COMPONENTS OF THE TEMPERATURE COEFFICIENT

(in the Core of a Single-Lobe Model of the ATR)

Effect	$\frac{\Delta K}{\Delta T} \times 10^4 (\frac{\Delta K}{\Delta F})$	Formula for $\frac{\Delta K}{\Delta T}$
Thermal		
U-235 Abs.	+ 4.324 } -0.874	$(\frac{\Delta K}{\Delta \Sigma_a})(N_{25})(\frac{\Delta \sigma_{a25}}{\Delta T})$
U-235 Fiss.	- 5.198 }	$(\frac{\Delta K}{\Delta \Sigma_f})(N_{25})(\frac{\Delta \sigma_{f25}}{\Delta T})$
U-238 Abs.	+ 0.011	$(\frac{\Delta K}{\Delta \Sigma_a})(N_{28})(\frac{\Delta \sigma_{a28}}{\Delta T})$
H_2O Abs.	+ 0.277	$(\frac{\Delta K}{\Delta \Sigma_a})(N_H)(\frac{\Delta \sigma_{aH}}{\Delta T})$
Al Abs.	+ 0.139	$(\frac{\Delta K}{\Delta \Sigma_a})(N_{Al})(\frac{\Delta \sigma_{aAl}}{\Delta T})$
Boron Abs. (Σ_a .015)	+ 0.349	$(\frac{\Delta K}{\Delta \Sigma_a})(\Sigma_a)(\frac{\Delta \sigma \text{ unit } 1/v}{\Delta T})$
Xe-135 Abs.	+ 0.164 } +0.147	$(\frac{\Delta K}{\Delta \Sigma_a})(N_{xe})(\frac{\Delta \sigma_{a\ xe}}{\Delta T})$
Sm-149 Abs.	- 0.017 }	$(\frac{\Delta K}{\Delta \Sigma_a})(N_{sm})(\frac{\Delta \sigma_{a\ sm}}{\Delta T})$

(more)

Table 8.0-D (Cont.)

Effect	$\frac{\Delta K}{\Delta T} \times 10^4 (\frac{\Delta K}{\Delta F})$	Formula for $\frac{\Delta K}{\Delta T}$
Resonance:		
U-235 Abs.	- 0.255	$(\frac{\Delta K}{\Delta \Sigma_a})_3 (N_{25})(\sigma_{a25})(\frac{1}{\sigma_a} \frac{\partial \sigma_a}{\partial T})$
U-235 Fiss.	+ 0.309 (+0.054)	$(\frac{\Delta K}{\Delta \Sigma_f})_3 (N_{25})(\sigma_{f25})_3(\frac{1}{\sigma_a} \frac{\partial \sigma_a}{\partial T})$
U-238 Abs.	- 0.010	$(\frac{\Delta K}{\Delta \Sigma_a})_3 (N_{28})(\sigma_{a28})_3(\frac{1}{\sigma_a} \frac{\partial \sigma_a}{\partial T})$
Aluminum Expansion	- 0.165	$(-\frac{2}{3}^*)(\frac{\Delta K}{\Delta \rho_{Al}})(\frac{\partial \rho_{Al}}{\partial T})$
H_2O Expansion	- 0.752	$^*(\frac{\Delta K}{\Delta \rho_{H_2O}})(\frac{\partial \rho_{H_2O}}{\partial T})$
Total Thermal	+ 0.049	
Total Resonance	+ 0.044	
Total Expansion	- 0.917	
GRAND TOTAL	- 0.824	

* $\frac{\Delta K}{\Delta \rho_{H_2O}} = (\frac{\Delta K}{\Delta_{Void}})(\frac{1}{\rho_{H_2O}})$, where $\frac{\Delta K}{\Delta_{Void}}$ is the void coefficient, and

$\rho_{H_2O} = 0.9633.$

The total temperature coefficient of -0.824×10^{-4} $\Delta K/^{o}F$ includes the effect (0.349×10^{-4} $\Delta K/^{o}F$) of an amount of burnable poison (boron) in the core such that Σ_{a4} of boron equals 0.015 cm^{-1}. Otherwise, the temperature coefficient excluding Al and H_2O expansion effects would be negative.

It is to be noted that the expansion effect is the most significant part of the temperature coefficient and that the results of previous studies show that this part of the coefficient can vary from about one-half the present value (when that is no D_3BO_3 in the control region) to about twice the present value (when the control region is fully poisoned).

8.2.1 Methods and Assumptions

To obtain the "thermal" and "resonance" effects; i.e., the effect of changes in microscopic cross sections due to temperature, four WANDA-4 cases were run in which Σ_{a4}, $\nu\Sigma_{f4}$, Σ_{a3}, and $\nu\Sigma_{f3}$ were changed, one by one, and compared with the case in which no change occured. The results are tabulated in Table 8.0-E. Also, in this table is the result of a WANDA-4 case in which the H_2O density was reduced to 9/10 of the usual value; the resulting void coefficient is the basis of the "expansion" components of the temperature coefficient.

TABLE 8.0-E

WANDA-4 PERTURBATION RESULTS

FOR TEMPERATURE COEFFICIENT CALCULATIONS

Case No.	Perturbation	K	ΔK	$\frac{\Delta K}{\Delta}$ or $\frac{\Delta K}{\Delta_{void}}$
140	None	1.01273	--	--
141	$.9\,\rho_{H_2O}$ in core	0.99419	-0.01854	- 0.1854 (void coeff.)
142	$\Delta\Sigma_{a4} = -0.01437$	1.09822	+0.08549	- 5.9492
143	$\Delta\Sigma_{f4} = -0.01101$	0.92219	-0.090539	+ 8.222
144	$\Delta\Sigma_{a3} = -0.001271$	1.02006	+0.007334	- 5.771
145	$\Delta\Sigma_{f3} = -0.000714$	1.00503	-0.007696	+10.778

It is assumed that all changes in diffusion constants are small compared with those which result from the expansion of H_2O, hence, all leakage effects are neglected except those which are directly related to the void coefficient. The 2/3 factor in the aluminum expansion component derives from the fact that expansion of aluminum in the axial direction causes no H_2O displacement, so that 1/3 of the expansion coefficient of aluminum is omitted.

Alteration of the neutron leakage due to axial core expansion is neglected because the core is too long for the effect to be significant (τB^2 is about 0.03 and $\frac{1}{\ell}\frac{d\ell}{dt}$ for aluminum is $4.3 \times 10^{-5}/^{\circ}F^{-1}$). The B^2 change might represent about $+0.03 \times 10^{-4}$ $\Delta k/^{\circ}F$.

The Doppler coefficient used is $\frac{1}{\sigma}\frac{\partial\sigma}{\partial T} = +4.0 \times 10^{-4}/^{\circ}F$, and is the upper limit (in absolute value) of the measured volume absorption values for U-238 metal. This value represents, therefore, only a conservative guess in an attempt to obtain an "order of magnitude" upper limit for this effect in the present core. The values of σ_{a3} and σ_{f3} for U-235 and U-238 were taken from MUFT-IV data. The values are: σ_{a3}(U-235) = 44.9 barns, σ_{f3}(U-235) = 29.2 barns, and σ_{a2}(U-238) = 25.0 barns.

The changes in microscopic absorption and fission cross sections with regard to temperature were derived from WAPD-185 data (SOFOCATE results) and for each element $\Delta\sigma/\Delta T$ is simply the observed change in σ for a change from 68°F to 260°F divided by 260 - 68 = 192°F.

Table 8.0-F lists the basic data (and computed values of $\Delta\sigma/\Delta T$) from WAPD-185 and opposite each element is the atomic density used in the formula for $\Delta K/\Delta T$.

TABLE 8.0-F

DATA FOR COMPUTING $\Delta\Sigma/\Delta T$ (THERMAL)

($\Delta T = 192^{\circ}F$, Values for $N_{25}/N_H = 0.005$)

Element Cross Section	Value at 68°F (b)	Value at 260°F(b)	$\Delta\sigma$ (b)	$\frac{\Delta\sigma(b)}{\Delta T\,^{\circ}F}$	$10^{-24}N$ (atoms/cm^3)
σ_{a25}	481.8	424.9	-56.9	-0.2954	0.000246
σ_{f25}	411.5	362.0	044.5	-0.2570	0.0010177
σ_{a28}	Values computed from data of unit 1/v absorption cross section			-0.001084	0.0000177
σ_{aH}				-0.00013	0.03577
σ_{aAl}				-0.00009	0.026
Σ_a boron				$\frac{\Delta\Sigma}{\Delta T} = 5.87\times10^{-7}$	--
σ_a xe	2.289×10^{6}	2.144×10^{6}	-0.145×10^{6}	-752.9	3.67×10^{-9}
σ_a Sm	65,510.0	67,910.0	2,400.0	12.46	2.29×10^{-8}
σ_a(unit 1/v)	0.7365	0.6611	-0.0754	-0.00003415	--

N_{xe} was computed from $\dfrac{(Y_{xe}+Y_I)(\Sigma_{f4}\Phi_{th})(1.16)}{(\lambda_{xe}+\sigma_{xe}\Phi_{th})}$

with: $Y_{xe} + Y_I = .069$, $\Sigma_{f4} = 0.108$, $\lambda_{xe} = 2.9 \times 10^{-5}$, and $\sigma_{xe} = 2.2 \times 10^{-10}$ cm^2. Φ_{th} was computed from $\dfrac{(50\ MW)/(3.2\times10^{17}\ MW/fiss)}{(1.16)(\Sigma_{f4})(V_{core})}$

with $V_{core} = 5.25 \times 10^{6}$ cm^3; hence, $\Phi_{th} = 2.37 \times 10^{14}$ n/cm^2-sec.

N_{Sm} was computed from $\dfrac{Y_{sm}\Sigma_{f4}\Phi_{th}(1.16)}{\sigma_{sm}}$ with $Y_{sm} = 0.014$ and σ_{sm} $= 6.6 \times 10^{-20}$ cm^2.

8.3 Two-Dimensional Calculations of Temperature Coefficients in the ATR

The temperature coefficient of reactivity was studied using the PDQ-3 code with a quarter-core model of the ATR. This study was made to supplement and confirm the one-dimensional studies of the void coefficient of reactivity as well as the temperature coefficient calculation by the component technique. By using a coarse mesh description and symmetry about the diagonal, it was found that convergence could be obtained in a reasonable length of time even with the small convergence criteria required. In addition to an overall temperature variation in the entire reactor, the temperature was varied in selected regions so as to get the position dependence of the temperature coefficient.

Two-group constants were determined for each region for 100°F, 160°F, and 200°F. The MUFT-IV code was used to determine fast group constants by using the atom densities appropriate to each temperature. All solid material atom densities were assumed not to change with temperature. Average Maxwellian constants were determined for the thermal group by averaging over the appropriate spectrum. The outer reflector control region had 5 grams per liter of D_3BO_3. The other regions were all clean except the core which had some burnable poison.

The PDQ model selected for this study is the same as in Figure 4.0-2. A-5 Experiments with stainless steel were considered to be in the north and east lobes, an A-5 experiment in the outer lobe and an A-3 experiment in the center. The fuel density was the same as in the one-dimensional model with a total U-235 mass of 25.2 kg. The reference temperature was taken as 160°F because this was thought to be near the operating temperature of the ATR. When selected regions were studied all other regions were held at 160°F except the region being perturbed.

These studies give an overall overall negative temperature coefficient in going from 100°F to 200°F of $-.34 \times 10^{-4}$ $\Delta k/°F$. Case 3023 had the reflector shim control region and the entire outer reflector perturbed by increasing the temperature to 200°F giving a Δk of $.063 \times 10^{-2}$ while, when the temperature of the reflector shim control region alone was increased as in Case 3031, the Δk increased to $.081 \times 10^{-2}$. This means that the reflector shim control region has a positive temperature coefficient while the outer reflector has a negative temperature coefficient. This same result was found in the one-dimensional void coefficient study. The fueled region had a negative temperature coefficient while the flux traps and neck regions had a positive temperature coefficient.

The atom density change of hydrogen and oxygen in going from 160°F to 200°F corresponds to a ΔV of .0144 or this is the fraction of the H_2O that would be replaced by void if the temperature effect was considered as only reducing the water density. Now, if we compute V which is the total volume of void in each region and divide this into Δk, we get the change in k produced by adding one cm^3 of void per cm of reactor length at each of the respective positions. In Table 8.0-G we have three computed values for three different regions. The problem in which the

TABLE 8.0-G

TWO-DIMENSIONAL TEMPERATURE COEFFICIENT CALCULATIONS

Case No.	Perturbed Region	Temp. °F	K	$\Delta K \times 10^2$	$\Delta F \times 10^2/\Delta T$	$\Delta K \times 10^4/v$	Area of H_2O in Region cm^2
3020	Reference case	160	1.13935				
3029	Entire Reactor	200	1.13770	-.165	-.0041		
3030	Entire Reactor	100	1.14117	+.182	-.0030		
3023	Reflector Control & Outer Refl.	200	1.13998	+.063	+.0016		
3024	Reflector Control & Outer Refl.	100	1.13827	-.108	+.0018		
3031	Reflector Control	200	1.14016	+.081	+.0020	+.0277	502.0
3032	Reflector Control	100	1.13805	-.130	+.0022		
3025	Fueled Region	200	1.13331	-.604	-.0151	-.3408	307.6
3026	Fueled Region	100	1.14781	+.846	-.0141		
3027	Flux Traps & All Neck	200	1.14141	+.206	+.0052	+.3972	90.9
3028	Flux Traps & All Neck	100	1.13632	-.303	+.0051		

reflector control region was perturbed agrees very well both in sign and magnitude with what was obtained in the one-dimensional studies, while for the core and inner reflector and flux trap regions we get agreement in sign but the magnitudes differ considerably.

In conclusion, we can state that we have agreement in sign in all cases in which we compare the one-dimensional studies with the two-dimensional studies. We would not expect the magnitudes to agree too closely because of geometry, and the general approach that was taken in the two studies. In the one-dimensional studies, quite severe perturbations were introduced; i.e., voids of 10 and 25%, while the two-dimensional studies were involved with temperature changes from 100°F to 200°F. In this temperature range, the water density does not change radically with temperature.

In the study on the components of the temperature coefficient for the ATR core region only, an overall temperature coefficient for the core of $-.824 \times 10^{-4}$ $\Delta k/^{o}F$ was obtained. These two-dimensional studies gave a core temperature coefficient of -1.45×10^{-4} $\Delta k/^{o}F$ which is in good agreement. It was pointed out in that section that the expansion effect is the most important component of the coefficient and it would be increased; i.e., made more negative, if the reflector shim control regions were poisoned. These two-dimensional studies had 5 grams per liter of D_3BO_3 in reflector control regions which is a significant amount of poison. Thus, we would expect the temperature coefficient of the core computed by the component technique to be very close to the PDQ-3 core temperature coefficient.

9.0 XENON INSTABILITY

When the core of a high flux reactor exceeds a certain size xenon instability can cause the power distribution to oscillate. In large power and production reactors this problem has been recognized for some time and a number of references to previous work on xenon instability are listed at the end of this section. In previous test reactors the neutron flux levels and core sizes have been such that xenon instability has not been a problem. However, in the ATR the high thermal flux level in the core, the loosely coupled lobes and the 4 ft core height make it necessary to investigate the possibility of xenon oscillations.

These oscillations can occur under some conditions because of the delay between a change in the thermal neutron flux and the resulting change in the production of xenon-135 with its very high absorption cross section. When an increase in the thermal flux occurs in a region of a core the Xe-135 concentration promptly decreases because of the increased burnup while at the same time the rate of formation of iodine-135, the precursor of Xe-135, is increased. Since nearly all of the xenon is produced by radioactive decay of iodine with a 6.7 hour half life there is a delay between the increase in the flux and the increase in the xenon production. In a reactor with fixed fuel both the prompt change in burnup and the delayed change in production of Xe-135 at any location in the reactor are related to the flux change in the same region.

In a slab reactor sufficiently long that xenon oscillations occur the core can be considered, for purposes of explanation, as divided into two halves, say top and bottom. The total power is held constant but no control is exerted over the power in the individual halves. Assume that a small increase in flux occurs in the top half. This increase has the prompt effect of decreasing the xenon concentration in this part of the reactor while increasing the amount that will appear later. The decreased xenon concentration lowers the neutron absorption and thus increases the flux which in turn further decreases the amount of xenon. The condition of constant total power requires that an increase in flux in the top be accompanied by a decrease in the bottom. The flux continues to increase in the top and decrease in the bottom until the delayed xenon production causes the process to reverse. The result is that the power oscillates between the top and the bottom of the core.

If the power can be measured and controlled in the individual halves then the onset of instability can be detected and the oscillation suppressed before its amplitude becomes objectionable. The time constants are such that the period of the oscillations is a number of hours and a relatively slow acting control is adequate. Since the reactivity change from the shift in the flux distribution can be kept small by a prompt compensation from the control system the required worth to suppress the oscillations is small.

The xenon oscillation causes the same power to be concentrated in a smaller volume then when the reactor is stable and thus increases the

maximum-to-average power ratio and consequently the peak power density. In the ATR the heat removal from the core is limited by the point of maximum power density and only a small increase in the maximum-to-average power ratio can be permitted.

Three types of potential xenon oscillations in the ATR have been considered as follows:

1. Interlobe oscillations in which the power shifts from lobe to lobe.

2. Horizontal oscillations in which the power shifts around an individual lobe.

3. Axial oscillations in which the power shifts between the top and bottom.

The reactor is probably unstable with respect to interlobe oscillations. However, the power in the individual lobes can be measured and controlled and interlobe oscillations can be effectively suppressed. Therefore, this type of oscillation has not been investigated.

The behavior of the second type of oscillation is adequately described by the treatment of Wick[1]. The requirement for stability is that G be greater than G'. Neglecting the stabilizing effect of the temperature coefficient and selecting the most unstable mode G is given by the relation

$$G = CD\left(\frac{2\pi}{L}\right)^2 ,$$

where

C is a correction factor to account for fast coupling.

D is equal to $D_2\left[1 + \frac{\gamma}{L_2^2}\right]$.

D_2 is the thermal diffusion coefficient of the core.

τ is the Fermi age for the core.

L_2 is the thermal diffusion length in the core.

L is equal to $2\pi R$.

R is the mean radius of a core lobe.

The value of C is found to be 0.2 from Figure 6 of Wicks report. The values of the other constants are listed in Appendix 12.7.

For a 4 ft long core and using conditions applying to the start of a cycle the value of G is 0.12. From Figure 2 of the reference the value of G' for an average core flux of 4×10^{14} n/cm^2 sec is 0.065. Thus there is an ample margin of stability. With the inclusion of the correction factor C for fast coupling the stability criterion is essentially that for a two-group model.

The design and operating conditions of the ATR core are such that with respect to axial oscillations it is near the boundary between the stable and unstable regimes, and it is difficult to definitely determine whether or not the reactor is stable. The ATR control system must include provisions for individual measurement and control of the power in the top and bottom halves of the core only if the reactor is axially unstable. These provisions increase the complexity of the control system and, therefore it is desirable to settle the question of axial stability before the final design of the control system.

The axial stability has been investigated by analytic methods and by use of the CANDLE and TURBO depletion programs. The analytic methods determine stability criteria based upon linear system theory for two-neutron-group, single-region, one-dimensional models. Two approximations have been considered; the first assumes a uniform initial xenon distribution, while the second allows for spatial variation of the initial xenon. The detailed derivation of the stability criterion, assuming the initial xenon distribution is uniform as developed by G. E. Putnam and R. J. Neuhold of Internuclear Company, is carried out in Appendix 12.7. The derivation for the case of nonuniform initial xenon follows in essentially the same manner but is considerably longer and more complicated. The essential steps in establishing the conditions for stability are outlined below.

The two-group neutron balance equations and the kinetic equations for I-135 and Xe-135 describing the model to which the results apply are:

$$D_1 \frac{\partial^2 \phi}{\partial x^2} - \Sigma_f \phi_1 + \nu \Sigma_{f2} \phi_2 = 0$$

$$D_2 \frac{\partial^2 \phi}{\partial x^2} - (\Sigma_a + \Sigma_x)\, \phi_2 + \Sigma_s \phi_1 = 0$$

$$\frac{\partial I}{\partial t} = - \lambda_I I + \gamma_I \Sigma_{f2} \phi_2$$

$$\frac{\partial x}{\partial t} = \lambda_I I + \gamma_x \Sigma_{f2} \phi_2 - \lambda_x X - \Sigma_x \phi_2$$

where

D_1 and D_2 are the fast and thermal diffusion coeficients respectively.

$\Sigma_f = D_1 B_1^2 + \Sigma_{a1} + \Sigma_R - \nu\Sigma_{f1}$

$\Sigma_s = \Sigma_R + fD_1 B_1^2$

Σ_{f1} and Σ_{f2} are the fast and thermal fission cross sections.

Σ_x is the thermal absorption cross section of Xe-135.

B_1^2 is the horizontal component of the buckling

$\phi_1 = \phi_1(x,t)$, $\phi_2 = \phi_2(x,t)$ are the fast and thermal neutron fluxes.

t is the time variable.

x is the space variable.

$I = I(x,t)$ is the concentration of I-135 atoms.

$Xe = Xe(x,t)$ is the concentration of Xe-135 atoms.

Σ_R is the cross section for transfer from the fast to the thermal group.

f is the fraction of the neutrons leaving the core in the radial direction by fast leakage that are returned to the core as thermal neutrons.

Σ_{a1} and Σ_{a2} are the fast and thermal absorption cross sections of the core.

ν is the number of neutrons produced per fission.

γ_I and γ_x are the total fission yields of iodine and xenon respectively.

λ_I and λ_x are the decay constants for iodine and xenon.

It is seen that the neutron balance equations apply to a single region one-dimensional reactor. The effect of the reflector in a direction perpendicular to the axis is taken into account by including in the source term for the thermal group a fraction of the fast neutron leakage from the core into the reflector. Boundary conditions are

applied requiring that the flux go to zero at the ends of the core in the axial direction. Thus the length used is that of the actual core height plus the total axial reflector savings.

The neutron balance and the kinetic equations are linearized by expressing each variable as an inital function at time zero plus a small perturbation, subtracting the unperturbed terms whose sum is zero and neglecting second order terms. The equations are then combined to eliminate all variables except the perturbation of the thermal flux. Solutions are assumed with the space and time dependent variables separated and with the space solution expressed as a Fourier series. Then the characteristic equation is obtained and examined for stability. The results are expressed in a form such that the system will be stable if;

$$G > G_C$$

The rather lengthy complete expressions for G and G_C in terms of the reactor constants and dimensions are presented in Appendix 12.7. The value of G_C depends only upon microscopic cross sections and fission yields, which can be assumed to remain constant; and upon the average core thermal flux and the initial macroscopic xenon and fission cross sections. For conditions corresponding to the ATR operating at 250 Mw G_C has a value of 0.0588. The values of G for several modes of oscillation designated by n and core heights L using the assumption of uniform initial xenon are given in Table 9.0A and the data presented graphically in Figure 9.0-1. The fundamental mode, n equal to one, is controlled by the provisions for maintaining constant power and need not be considered. It is evident that the stability is determined by the second harmonic, n equal to two. As previously explained L is for an equivalent bare core and is equal to the active core height plus the total axial reflector savings. From Figure 9.0-1 the maximum value of L for stability after attainment of xenon equilibrium at the start of the cycle is 146 cm. The stability criterion derived so that the spatial variation of the initial xenon is considered gives a critical height of 145 cm for the same conditions. Thus, including the refinement of a space dependent initial xenon distribution does not significantly change the results.

At the start of the cycle the reflector region next to the core is rather heavily poisoned and the total axial reflector savings should be about the same as the MTR value of 17 cm rather than the 30 cm used for D_2O reflected systems as discussed in Section 2.0. Thus the appropriate value of L is 139 cm, 122 cm plus 17 cm, and the condition for stability is met.

In evaluating the effects of changes upon the stability the method requires that the conditions imposed by the neutron balance equations must be satisfied. Thus, any change in a parameter must be compensated so that the system is kept just critical. The conditions near the end of a cycle are determined by assuming that 25% of the fuel and all of the burnable poison is burned up and adjusting the fraction of neutrons returned from the reflector and the fast-to-thermal flux ratio so that the balance equations are satisfied. For the same value of L the reactor

TABLE 9.0-A

STABILITY PARAMETER G FOR THE ATR

(For Stability G $\geq$ 0.059)

n↓ L (cm)→	91.4	122	152	183	213	244	274
2	0.14	0.083	0.055	0.039	0.029	0.022	0.018
3	0.31	0.20	0.14	0.099	0.074	0.058	0.046
4	0.49	0.33	0.23	0.17	0.13	0.10	0.084
5	0.65	0.47	0.34	0.26	0.20	0.16	0.013

NOTE: L = Active core height plus total axial reflector savings.

becomes somewhat more stable with operation. For the second harmonic, n equal to 2, and L equal to 152 cm the value of G increases from 0.046 at the start of the cycle to 0.048 at the end of the cycle while the value of G' does not change significantly. However, the improvement in the reflector because of removal of poison and the axial flux flattening from nonuniform fuel burnup may increase the effective axial reflector savings and hence L. However, only with a D_2O reflector should the total reflector savings be significantly larger than 17 cm. In this case the large thermal diffusion length in the reflector produces a coupling between top and bottom that exerts a stabilizing influence.

The model of the ATR used to study stability by considering small perturbations to a linearized system thus satisfies the criterion for stability. However, in order to keep the calculations tractable it is necessary to use a rather simplified model of the reactor. Although some of the effects neglected such as the negative temperature coefficient would make the system more stable if included, the results are not completely conclusive for the actual reactor.

The neutron depletion codes CANDLE-2 for the IBM-650 and TURBO for the IBM-704 have been used to investigate the stability of more realistic models of the ATR than is feasible by the analytic procedure. These codes take into account the effects of burnup and formation of Xe-135 including the delay between a flux change and the resulting change in xenon production at the flux and power levels existing in the reactor. Thus, the stability of the reactor can be determined by observing the variation with time of the power distribution in the core after the introduction of a perturbation.

The CANDLE-2 program has been used to obtain preliminary estimates for the variables in the TURBO program and to observe the effect of core length upon stability. This program permits the use of only one space dimension and the axial configuration of the reactor is represented in slab geometry through the fueled core. The principal shortcoming of the one-dimensional model is the failure to properly account for the effects of the radial reflector. The radial leakages are represented in the two-group diffusion equations as positive removal terms of magnitudes D_1B^2 and D_2B^2 in the fast and thermal groups respectively. The fast leakage term is fairly representative of the physical process. But in the ATR the thermal leakage is from the reflector into the core and thus has the opposite sign of the one-dimensional model required by the CANDLE-2 program. However, the thermal leakage term is sufficiently small to make the slab representation adequate for the exploratory purposes for which it has been used.

The geometry of the slab model is shown in Figure 9.0-2. The fuel and burnable poison concentrations are chosen to represent the normal core loading of the ATR. The reflector regions at the top and bottom consist of 40% aluminum and 60% water. Criticality is maintained by varying the radial buckling. A power level of 52.5 Mw is used for a 4 ft long core to give approximately the same average power density as for the ATR operating at 250 Mw. The program is used to determine the core composition and the flux distribution after 110 hrs of full power operation so that the reactor conditions after attainment of xenon equilibrium are simulated. The assumption of symmetry about the axial midplane forces the power distribution to also be symmetrical since the computations are idealized in that they do not introduce small perturbations such as are unavoidable in an operating reactor. To reveal any tendency for xenon oscillations to occur, a large perturbation is introduced at this time by adding a 1/v poison to only the lower half of the core. Since the perturbation changes the system the calculations branch at 118 hours to determine the behavior both with the perturbing absorber remaining in the core and with it removed at this time. The variations with time of the powers in end regions of the core are shown in Figure 9.0-3. The power scale is normalized so that the value just before the perturbation is ten and the value in the end to which the poison is added is five just after the perturbation is made. This normalization is made to facilitate comparison with calculations on other models. It is seen that when the absorber is added to the lower end the power in this end immediately drops while the condition of constant total power forces the power in the upper end to rise. The prompt changes in xenon burnup then cause the power to become further unbalanced for a time, the effect becoming a maximum at 118 hours. Continuation with the poison in place causes the powers to approach constant values as equilibrium is attained. The response for this type of excitation is shown only for the CANDLE calculations on a 4 ft core. When the perturbing absorber is removed at 118 hours the properties of the system return to those before the perturbation. This method of excitation is roughly analagous to inserting a resistor into an electrical circuit and then removing it. In this case the power distributions in each end rapidly return towards the value

before the disturbance. However the effects of xenon cause the power density at any point to overshoot beyond the equilibrium value and then return towards it asymptotically. There is no tendency to oscillate either with the perturber retained or removed. If the system is considered analagous to a simple linear system the amount of overshoot is inversely related to the stability and it appears that the system is slightly underdamped.

The power distributions have been determined for a one-dimensional model with a 6 ft core operating at the same average power density as previously. The perturbation is introduced and removed as before but in order to obtain convergence it is necessary to reduce the amount of absorber added. The results are shown in Figure 9.0-4 with the power densities normalized as described previously to remove the effects of the difference in the disturbances. The overshoot is considerably larger than in the 4 ft core but there is still no indication of oscillations.

The TURBO calculations are made for a cylindrical model representing one lobe of the ATR with a 4 ft high core. The geometry of the model is shown in Figure 9.0-5. This two-dimensional representation permits a reasonably correct description of the radial reflector in contrast to the one-dimensional studies in which the descriptions of this region are rather crude. In particular the TURBO studies consider the coupling of top and bottom through the reflector, and control of reactivity by a thermal poison in a water annulus around the core. Also with this model it is not necessary to assume an axial reflector savings and the effect of the radial reflector on end leakage is taken into account. The main deficiency in the representation arises from the overemphasis on the reflector properties because of the larger fractional radial leakage in the single lobe model as compared to the ATR. Thus, the model used is more representative of the fuel regions adjacent to the reflector than the center fuel region.

The procedure is essentially the same as for the CANDLE problems except that criticality is maintained by varying the boron content of the water annulus next to the core. The effects of the perturbation are shown in Figure 9.0-6 which has the same normalization as before. It is evident that the amount of overshoot is considerably less than for the CANDLE case with a 4 ft core which had the same amount of absorber added and removed. This decrease may indicate that reflector effects which only the two-dimensional model adequately considers have a stabilizing effect.

The CANDLE and TURBO codes compute the changes in the isotopic concentrations assuming a constant flux distribution from time step to time step. When the perturbation is introduced and the flux distribution is changing rapidly this assumption underestimates the changes in concentrations and thus may exert a stabilizing influence.

Direct comparison of the various methods is difficult but it appears reasonable to order them so that TURBO calculations, which most accurately

represent the reactor, the CANDLE results and the analytic determinations using linear system theory show decreasing degrees of stability from the former to the latter. The effects of temperature or power coefficients of reactivity are not considered by any of the methods. These effects while probably small should be stabilizing in the ATR. All of the calculations suffer in varying degrees because a three-dimensional model is needed to describe the ATR for this purpose.

The reactor while designated as having a four-lobe core can best be represented by considering it to be made up of five cylindrical fuel regions, one around each of the loops interior to the core. If reflector coupling is important in stabilizing the system it is conceivable that axial oscillations can occur in the center fuel region while the other regions are stable. It may also be necessary to measure and control the radial power distributions in the five individual core regions in order to prevent interlobe oscillations.

The results of the calculations indicate that with a 4 ft high active core the reactor is stable. However, the consequences of uncontrolled oscillations are so great that stability must be established beyond question if the control system is not to include provisions for suppression of oscillations. Thus, further investigations are required. These should include studies on the effects of the reflector with particular respect to the conditions applying to the center fuel region. Also the effects of the numerical procedures used in the depletion codes should be determined.

XENON INSTABILITY REFERENCES

1. R. S. Wick, "Space- and Time-Dependent Flux Oscillations (and Instability) in Thermal Reactors Due to Nonuniform Formation and Depletion of Xenon," WAPD-TM-138, 1958.

2. H. H. Clayton, "Pile Instability Due to Poison," TPI-41, 1946.

3. A. G. Ward, "The Problem of Flux Instability in Large Power Reactors," CRRP-657, 1956.

4. A. Hitchcock and B. E. Roberts, "Axial Stability of the Neutron Flux Distribution," DEG-128 (R).

5. A. Hitchcock, "Nuclear Reactor Stability," Temple Press, 1960.

6. G. J. Tyror, "Controlling Instabilities in Graphite Power Reactors," Nuclear Power, p. 94, June 1959.

7. R. I. Vaughn, "Control Considerations at High Burnup," Nuclear Engineering, p. 20, January 1960.

8. D. Randall and D. S. St. John, "Xenon Spatial Oscillations," Nucleonics, Vol. 16, No. 3, March 1958.

9. A. F. Henry and J. D. Germann, "Oscillations in Power Distribution Within a Reactor," Nuclear Science and Engineering," Vol. 2, No. 4, July 1957.

10. K. Mochizuki and A. Takeda, "An Analysis of Neutron Flux Spacial Oscillation Due to Xenon Buildup in a Large Power Reactor Core," Nuclear Science and Engineering, Vol. 7, No. 4, April 1960.

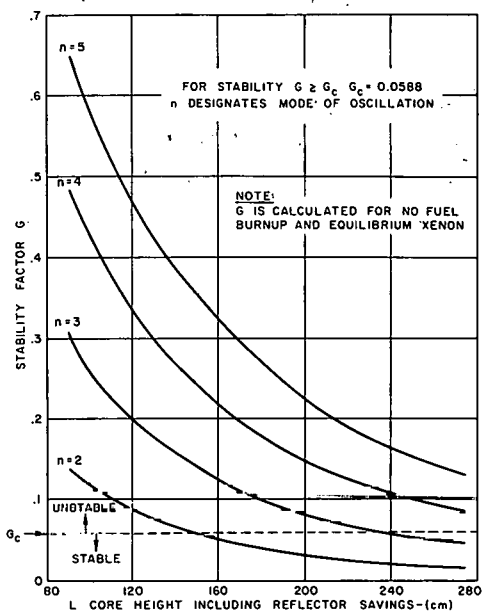

FIG. 9.0-1
STABILITY VERSUS CORE HEIGHT

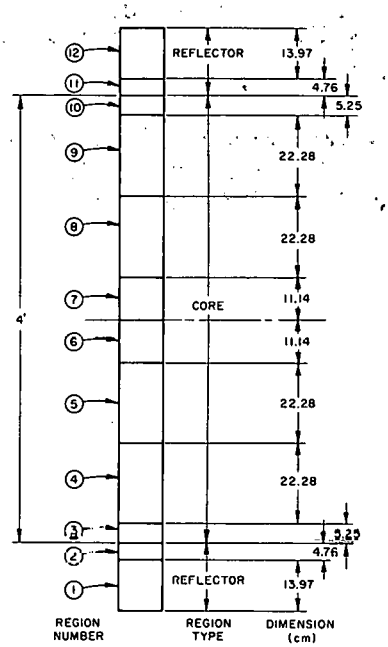

FIG. 9.0-2
ONE-DIMENSIONAL SLAB MODEL WITH FOUR FOOT CORE FOR CANDLE STABILITY CALCULATIONS

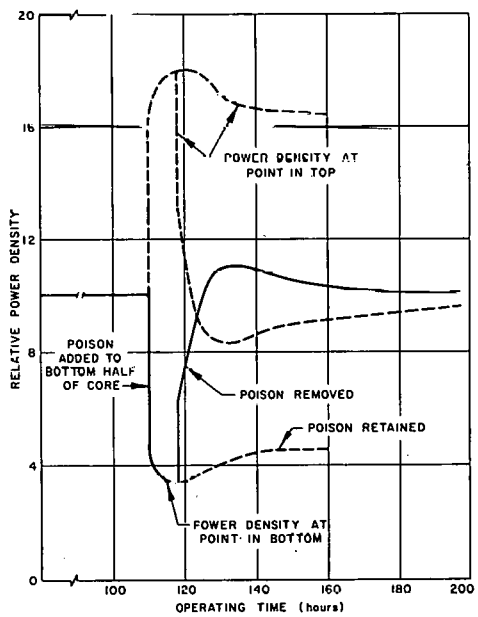

FIG. 9.0-3
RESPONSE TO PERTURBATION OF ONE-DIMENSIONAL MODEL WITH FOUR-FOOT CORE

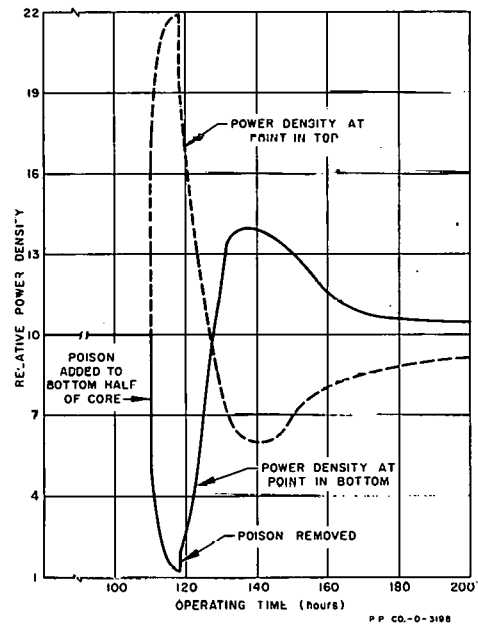

FIG. 9.0-4
RESPONSE TO PERTURBATION OF ONE DIMENSIONAL MODEL WITH SIX FOOT CORE

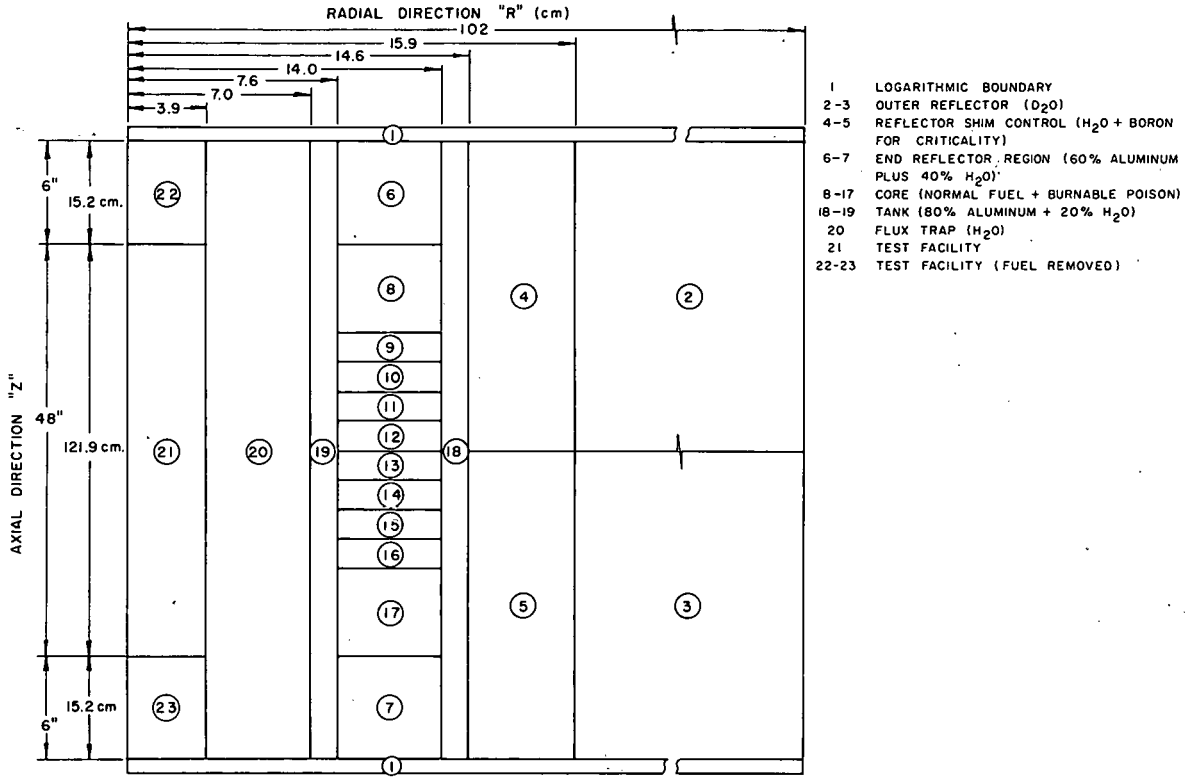

FIG. 9.0-5
TWO-DIMENSIONAL CYLINDRICAL MODEL WITH FOUR FOOT CORE FOR TURBO STABILITY STUDIES

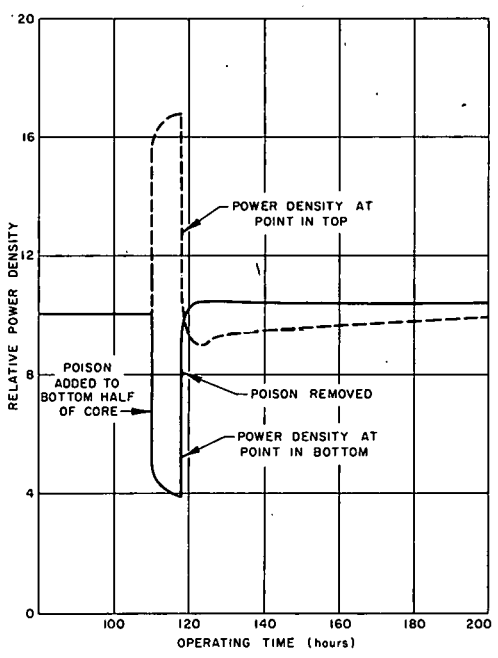

FIG. 9.0-6
RESPONSE TO PERTURBATION OF TWO DIMENSIONAL MODEL WITH FOUR FOOT CORE

10.0 NEUTRON LIFETIME

In the ATR a significant fraction of the neutrons producing fissions spend a major portion of their life in the reflector which contributes what may be considered as an additional group of delayed neutrons. The flux levels required in the ATR experimental facilities can be obtained at reasonable power levels only by designs which have positive void and temperature coefficients in some regions and the delayed neutrons from the reflector are important to the safe operation of the ATR. The effects of several types of reflector shim control and of reflector properties upon the average lifetime of the neutrons and upon the additional delayed group have been calculated for a one-dimensional model of one lobe of the ATR. The influence of the extra group upon the kinetic behaviour has been reported previously.[1]

The average prompt neutron lifetime is obtained by perturbation theory from the change in reactivity produced by addition of a 1/v absorber to all regions of the reactor.[2] This method assumes all neutrons are produced at the instant of fission and give the importance averaged lifetime. That is, the lifetime of a neutron is weighted by the ultimate increase in the total neutron population produced by insertion of one neutron having the same history. Thus, in evaluating the lifetime of a neutron its importance in sustaining the chain reaction is considered. The effects of secondary production such as photo-neutrons are neglected.

The change in reactivity, ρ, as given by two-neutron group diffusion theory using DMM or WANDA is

$$\rho = \frac{k - k_p}{k_p} \quad ,$$

where

k is the effective multiplication factor of the unperturbed reactor,

k_p is the effective multiplication factor after addition of the 1/v poison.

The addition of the poison is represented by adding $\Sigma_{1p} = 0.000002$ and $\Sigma_{2p} = 0.0001$ to the fast and thermal absorption coefficients of the unperturbed system. The average lifetime is then found from the relation

$$L = \frac{\rho}{V_2 \Sigma_{2p}} \quad ,$$

where

$V_2 = 2.75 \times 10^5$ cm per sec is the average neutron velocity of a Maxwellian distribution at 200F.

---

1. D. R. deBoisblanc et al., "Proposal for an Advanced Engineering Test Reactor," IDO-16666 (March 17, 1960).

2. D. G. Ott, "Calculation of Prompt Neutron Generation Time from Reactivity of 1/v Absorber," Internuclear Company Report INT-DGO-56-1 (1956).

The neutrons leaking into the reflector as fast neutrons and returned to the core as fast neutrons constitute a group of delayed neutrons in addition to the six groups delayed in the fission process that are usually considered in kinetic analyses of thermal reactors. The delayed group of neutrons from the reflector can be characterized by the fraction of all fissions that it produces and by its average lifetime. This lifetime is estimated using the following assumptions:

1. All neutrons producing fissions can be considered as having spent almost all of their life in either the reflector (reflector neutrons) or in the core (core neutrons).

2. Any change in reactivity produced by reflector shim control results only from a change in the number of neutrons returned from the reflector.

3. Poisoning the core changes only the thermal utilization and not the relative number of core and reflector neutrons.

4. Changes in one region do not effect the lifetime of neutrons from the other regions.

The fraction of fissions produced by neutrons returned from a clean D_2O reflector in a single lobe model is estimated by a two-group neutron balance and by extrapolating of a plot of k_{eff} versus poison in the reflector to be 35%. The lifetime of the core without burnable poison is estimated to be 35 microseconds from infinite region theory and also from extrapolation of the curve relating average lifetime of all neutrons versus poison in the reflector. The calculation of the lifetime of the reflector group is not greatly effected by the value assumed for the lifetime of the core neutrons.

The results for a number of methods of controlling the reactivity of a single lobe model of the ATR are given in Table 10.0A. The effect on the average neutron lifetime of H_2O contamination of a D_2O reflector is shown in Table 7.0F. The lifetimes listed in Table 10.0-A are quite consistent with the assumptions given above. The variation of the average life of all neutrons in a single-lobe model with poison in a 1/2" water annulus around the core is shown in Figure 10.0-1. The models are similar to those of 7.0-1.

The fraction of reflector neutrons and their lifetime and the average lifetime of all neutrons are shortest when the reflector shim control is producing the largest reduction in reactivity, which corresponds to conditions at the start of the cycle. For reflector control of a given amount of reactivity, blades or poisoning of a narrow annulus produces the smallest decrease in the neutron lifetimes of the reactor and the reflector. Poisoning of the entire reflector reduces the probability of a neutron having many scattering collisions and escaping absorption before returning to the core and thus discriminates against long-lived members in the population returning to the core. On the other hand, poisoning a narrow region of the reflector near the core does not have a severe selective effect on the neutrons returning from

the core and thus produces a much smaller effect on the lifetime of the reflector neutrons than does poisoning the entire reflector.

It is seen that controlling the reactivity by poisoning the core has only a slight effect on the reactor and reflector lifetimes. This result is consistent with the assumptions that this method of control changes only the thermal utilization and that a change in the core has no large effect on the reflector neutrons. Reactors with most of the reflection from heavy water have an inherently longer lifetime than beryllium reflected reactors. It is evident from the effect on the lifetime of poisoning the entire reflector that extraneous absorbers in this region must be limited if the maximum benefit is to be realized from the reflector neutrons.

In the ATR the fraction of reflector neutrons will be considerably smaller than for the one lobe model to which the results of Table 10.0A apply. Consequently, the average lifetime of all neutrons will be appreciably shorter in the ATR than in the single lobe case because this lifetime is largely determined by the reflector neutrons. However the lifetime of the reflector group will be somewhat longer in the ATR because not all of the neutrons return through the control region. From comparison of single lobe and ATR calculations of reflector worth it is estimated that at startup, which is the most unfavorable condition for neutron lifetime, at least 10% of the neutrons will be reflector neutrons with an average lifetime of approximately 800 microseconds for the reactor with a D_2O outer reflector. The average lifetime for the reactor is then about 110 microseconds.

TABLE 10.0-A

EFFECTS OF REACTIVITY CONTROL ON NEUTRON LIFETIMES IN SINGLE-LOBE MODEL OF ATR

Method of Reactivity Control*	Change in k_{eff} produced by control	Average lifetime all neutrons μsec	Average lifetime reflector neutrons μsec	Average lifetime core neutrons μsec	Per cent reflector neutrons	Per cent core neutrons
Clean reference case	0	370	990	35	65	35
Poison in entire refl.	-.03	270	770	35	68	32
Poison in entire refl.	-.13	120	390	35	76	24
Poison in entire refl.	-.24	54	160	35	85	15
Blades in reflector	-.03	340	990	35	68	32
Blades in reflector	-.13	260	970	35	76	24
Blades in reflector	-.24	180	1000	35	85	15
Poison in core	-.03	370	990	32	65	35
Poison in core	-.13	360	960	28	65	35
Poison in core	-.24	350	930	25	65	35
Poison in 1/2" H_2O annulus	-.03	96	230	35	68	32
Poison in 1/2" H_2O annulus	-.13	55	120	35	76	24
Poison in 1/2" H_2O annulus	-.24	34	47	35	85	15
Poison in 6" Be + 10% H_2O reflector	-.03	320	930	35	68	32
Poison in 6" Be + 10% H_2O reflector	-.13	230	850	35	76	24
Poison in 6" Be + 10% H_2O reflector	-.24	130	670	35	85	15

*NOTE: All cases have D_2O outer reflector except cases with reactivity control by poison in Be + 10% H_2O.[2]

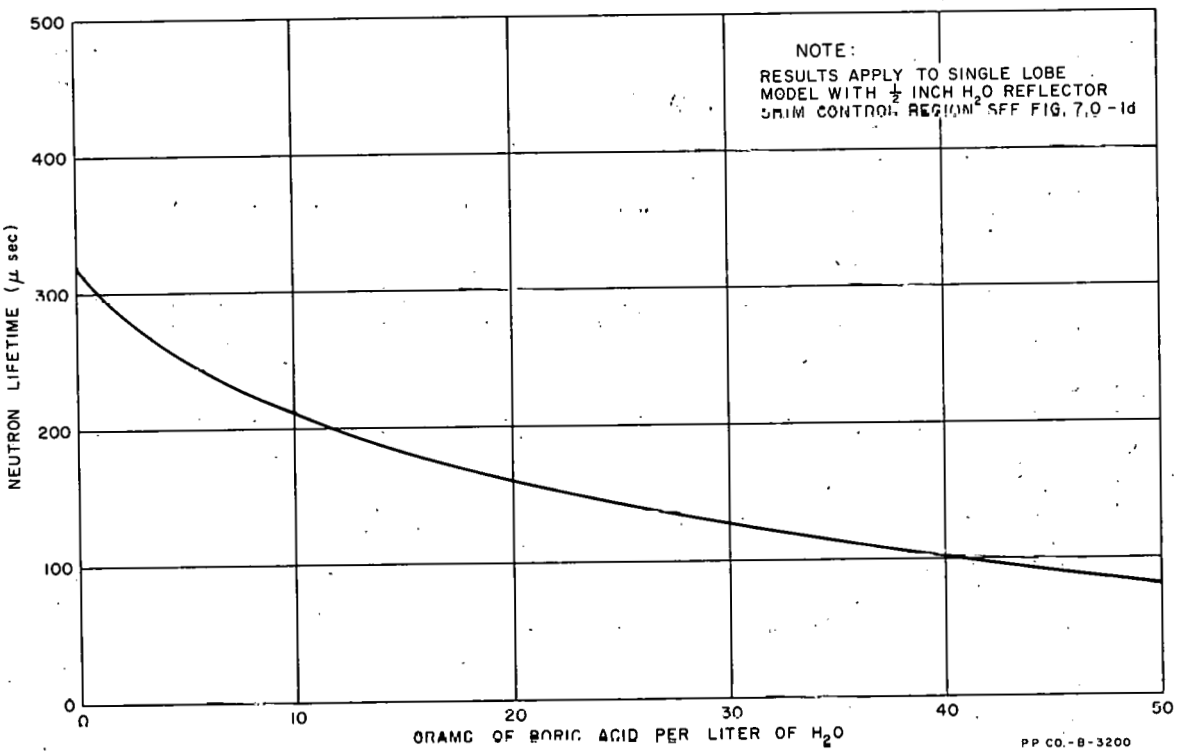

FIG. 10.0 – 1

NEUTRON LIFETIME VERSUS POISON IN REFLECTOR SHIM CONTROL REGION

11.0 GAMMA HEATING IN THE ATR

Gamma heating rates in various regions of the ATR were calculated on the basis of a specific operating power level of 1.0 Mw/liter which corresponds to a reactor power just slightly higher than 250 MW. In order to approximate the system geometry in the calculational model, it was necessary to consider various regions separately and then sum their contributions to the total heating at any given point. Two general geometric source regions were found necessary to describe the system. The outer lobes were described as individual one-lobe models, and the inner lobe was separated into four quarter-lobe sections. These are shown in Figures 11.0-1 and 11.0-2, and the regions of the resulting geometry approximating the ATR configuration is shown in Figure 11.0-3.

The radiation attenuation utilized a program which performs a point to point numerical integration over the source volume. Differential volume sources are treated as point sources and attenuated as:

$$\phi(E) = \frac{S_v(E)}{4\pi R^2}\left[A_1(E)e^{-\left[1+a_1(E)\right]b(E)} + A_2(E)e^{-\left[1+a_2(E)\right]b(E)}\right]$$

where $\phi(E)$ = radiation flux at the detector point arising from source, $S_v(E)$, Mev/cm^2-sec

$S_v(E)$ = radiation source strength of energy group E created in differential volume under consideration, Mev/cc-sec

R = distance between differential volume source and detector, cm

$A_1(E)$, $A_2(E)$, $a_1(E)$ and $a_2(E)$ = curve fitting parameters for the NDA gamma buildup factors for energy

$$b(E) = \sum_{o}^{i} \mu_1(E)\, t_i$$

$\mu_1(E)$ = cross sections of the i^{th} shield material for energy group E, cm^{-1} (absorption coefficient for gammas and removal cross sections for neutrons)

t_i = distance traveled through the i^{th} shield material, cm.

The program allows for a non-uniform source distribution and multi-energy groups.

The core gamma energy spectrum and magnitude was calculated considering prompt fission gammas, fission product decay gammas, fission product decay gammas plus capture gammas in U-235, Al and H_2O.

The energy spectrum of the prompt fission and fission product gammas were obtained from numerical integration of recent Oak Ridge data presented by Peele, et al.[1] Gamma energy spectra for all other system materials were obtained from the work of Deloume[2] and Bartholomew and Higgs.[3]

The relative neutron absorption in the various core materials is shown in Table 11.0-A and the contribution per fission of each core material to the core gamma source is presented in Table 11.0-B.

TABLE 11.0-A

RELATIVE NEUTRON ABSORPTION FOR GAMMA HEATING CALCULATIONS

Material	Relative Absorption
Al	0.028
H_2O	0.16
U-235, Fission Absorption	1.0
U-235, Radiative Capture	0.22

1. R. W. Peele, W. Zobel, T. A. Love, "Measurement of the Spectrum of Short-Lived Fission Product Decay Gamma Rays Emitted from a Rotating Belt," ORNL-2081, 1956.

   R. W. Peele, W. Zobel, T. A. Love, F. C. Maienschein, "Recent Results for the Energy Spectra of Fission Associated Radiation," Oak Ridge National Laboratory, 1958.

2. F. E. Deloume, "Gamma Ray Energy Spectra from Thermal Neutron Capture," General Electric Report GEANP-DC-58-1030, 1958.

3. G. A. Bartholomew, L. A. Higgs, "Compilation of Thermal Neutron Capture Gamma Rays," Chalk River Report No. CRGP-784, 1958.

TABLE 11.0-B

CORE GAMMA SOURCE PER FISSION

Energy Range	Mev per Fission			Prompt	Fission Product	Total
	Al	H_2O	Non-Fiss.U-235			
.6 - 1			0.552	2.82	1.52	4.89
1 - 2			0.444	2.27	1.77	4.48
2 - 3		3.56	0.229	1.17	1.00	2.75
3 - 5	0.072		0.148	0.758	0.495	1.47
5 - 7	0.079		0.033	0.167	0.022	0.30
						13.89

The energy distribution and magnitude of the calculated core gamma sources, evaluated at a specific power of 1 Mw/liter is given in Table 11.0-C.

TABLE 11.0-C

ENERGY DISTRIBUTION OF CORE GAMMA SOURCE

Energy Range Mev	Mev/cc-sec	Watt/cc
.6 - 1	15.1×10^{13}	24.16
1 - 2	13.89×10^{13}	22.22
2 - 3	8.52×10^{13}	13.63
3 - 5	4.56×10^{13}	7.30
5 - 7	0.93×10^{13}	1.49
		68.80

The gamma source from capture in the Be and D_2O reflectors is insignificant and was neglected.

Thermal neutron fluxes through the pressure vessel and thermal shields were not available at the time the program was run and, therefore, the capture gamma source in these components could not be calculated. This source of radiation is expected to contribute to the heating in the components themselves; however, the calculated radiation heating in regions adjacent to the core will not be affected by omitting this radiation component.

As noted in the previous paragraphs, gamma ray buildup is included in the program solution. The buildup factors used[1] are specifically valid only for homogeneous regions. In this particular case, this factor is not troublesome since, with only slight exception, the materials of the system are closely related with regard to atomic number and all exhibit similar buildup characteristics. Therefore, energy absorption buildup factors for water were applied to the entire system.

Gamma absorption coefficients for the elements were taken from the work of Grodstein.[2] The composite linear absorption coefficients for each region of the system were evaluated at the average energy of each of the five energy groups.

A flat power distribution both radially and axially was assumed. The gamma relaxation length for the fuel region ranges between 3 - 5 inches depending on the energy considered. In terms of gamma relaxation lengths, the core is both long and thin. The significance of this with respect to the gamma heating is that the effect of the radial power distribution on the gamma heating is minimized since self-absorption along the radius of the fuel region is relatively low.

The converse is true with regard to the effect of the axial power distribution. Ninety per cent of the gamma heating at a point is due to the fraction of the source which lies within the first two relaxation lengths within the source measured from the detector. This means that for detector points close to the fuel region, axial source points located more than approximately 6 - 10 inches away contribute very little to the heating at the detector under consideration. With a 48-inch core, a cosine power distribution varies essentially linearly over a 12 - 20 inch increment and it is thus sufficiently accurate to use a flat axial power distribution to calculate the average heating and to assume that the axial profile of the gamma heating distribution will coincide with the cosine power distribution. These arguments are of course not valid if the power distribution is not a smoothly varying function.

---

1. H. Goldstein, J. E. Wilkins, Jr., "Calculations of the Penetration of Gamma Rays," NYO-3075, TTS, 1954.

2. Gladys W. Grodstein, "X-Ray Attenuation Coefficients From 10 Kev to 100 Mev," NBS Circular 583, 1957.

Profiles of the gamma heating along sections O-M and O-N of the reactor are presented in Figures 11.0-4 and 11.0-5, respectively. A more detailed breakdown with regard to the location of the important source regions for a given detector point is afforded by Tables 11.0-D and 11.0-E. All values presented are average axial figures. Center line values are obtained by multiplying by the axial maximum-to-average power ratio.

Approximate average gamma heating rates in various components of the reactor system are presented in Table 11.0-F. Also presented in this table is the calculated percentage of the available gamma source absorbed by each component.

The effect of replacing the D_2O reflectors with Be + H_2O is also shown in Figure 11.0-4. From this figure, it is seen that the heating at the exterior of the reflector region is about 25% lower if Be + H_2O is used.

TABLE 11.0-D

GAMMA HEATING ALONG SECTION O-M

Detector Radius, Inches	Contribution from Region, Watts/gram								Total
	A	B	C	D	E	F	G	H	
0	0.5	0.5	0.5	0.5	2.0	2.0	2.0	2.0	10.0
1.75	0.9	0.4	0.2	0.4	1.2	1.2	3.2	3.2	10.7
6.0	0.4	0.4	0.1	0.4	0.28	0.28	5.4	5.4	12.6
9.5	11.0	0.4	0.1	0.4		1.3			13.1
10.25	11.0	0.4	0.1	0.4		0.9			12.7
10.5	9.0	0.2		0.2		0.4			9.8
12.25	10.2	0.18		0.18		0.37			10.9
13.5	9.0					0.3			9.3
13.75	12.5					0.15			12.7
15.0	12.5					0.1			16.0(Core) 12.6(Al)
Center of Fuel	17.0								17.0
17.5	9.5(Al) 12.0(Core)								9.5(Al) 12.0(Core)
17.75	8.3								8.3
20.75	3.0	0.05		0.05					3.1
28.0	0.28	0.03		0.03					0.34
40.5	.035	.009		.009					0.053
42.0	(A, B, D = .015)								0.015

Notes: Average core power density = 1 Mw/liter

See Figure 11.0-3.

TABLE 11.0-E

GAMMA HEATING ALONG SECTION O-N

Detector Radius, Inches	Contribution from Region, Watts/gram								Total
	A	B	C	D	E	F	G	H	
0	0.5	0.5	0.5	0.5	2.0	2.0	2.0	2.0	10.0
1.75	0.7	0.7	0.25	0.25	1.0	2.0	2.0	3.9	10.4
2.75	1.2	1.2	0.2	0.2	0.67	1.6	1.6	6.0	12.67(Al) 16.5(Fuel)
4.5	1.8	1.8	0.16	0.16	0.45	2.0	2.0	13.5	21.8
5.75	2.0	2.0	<0.1	<0.1	0.1	1.3	1.3	10.0	16.7(Al) 21.8(Fuel)
6.75	2.5	2.5	<0.1	<0.1	<0.1	1.0	1.0	8.3	15.3
7.0									9.2
8.5	2.5	2.5				0.7	0.7	2.5	8.9
10.0									8.5
10.25									
11.25									
11.50	2.1	2.1				0.4	0.4	0.25(Lobe) 1.06	6.1
14.0	1.5	1.5				0.2	0.2	0.41	3.8
20.75	0.36	0.36				0.04	0.04	0.15	0.95
40.5	0.021	0.021				0.002	0.002	0.0004	0.046

Notes: Average core power density = 1 Mw/liter

See Figure 11.0-3.

TABLE 11.0-F

GAMMA ABSORPTION

Component	Ave. Gamma Heating Rate			% of γ Source Absorbed	Est. Volume cm^3/cm
	gm/cm^3	$watts/cm^3$	watts/gm		
Experiment (Void)	0	0	0	0	559
SS Press. Vessels	7.86	88.0	11.2	8.8	148
Inner H_2O Refl.	0.96	13.0	13.5	7.2	820
Inner Al Separator Ring	2.7	10.0	3.7	1.0	146
Fuel Region	1.79	30.0	16.7	43.6	2154
Outer Al Separator Ring	2.7	10.0	3.7	1.9	285
Inner D_2O Refl.	1.05	5.8	5.5	15.2	3886
Be & D_2O Refl.	1.588	8.0	5.04	3.1	576
Inner Al & H_2O	2.178	26.4	12.1	6.5	365
Outer D_2O Refl.	1.05	1.0	0.95	11.3	24307
Pressure Vessel	7.86	0.08	0.01	1.4	2007
				~100	35753

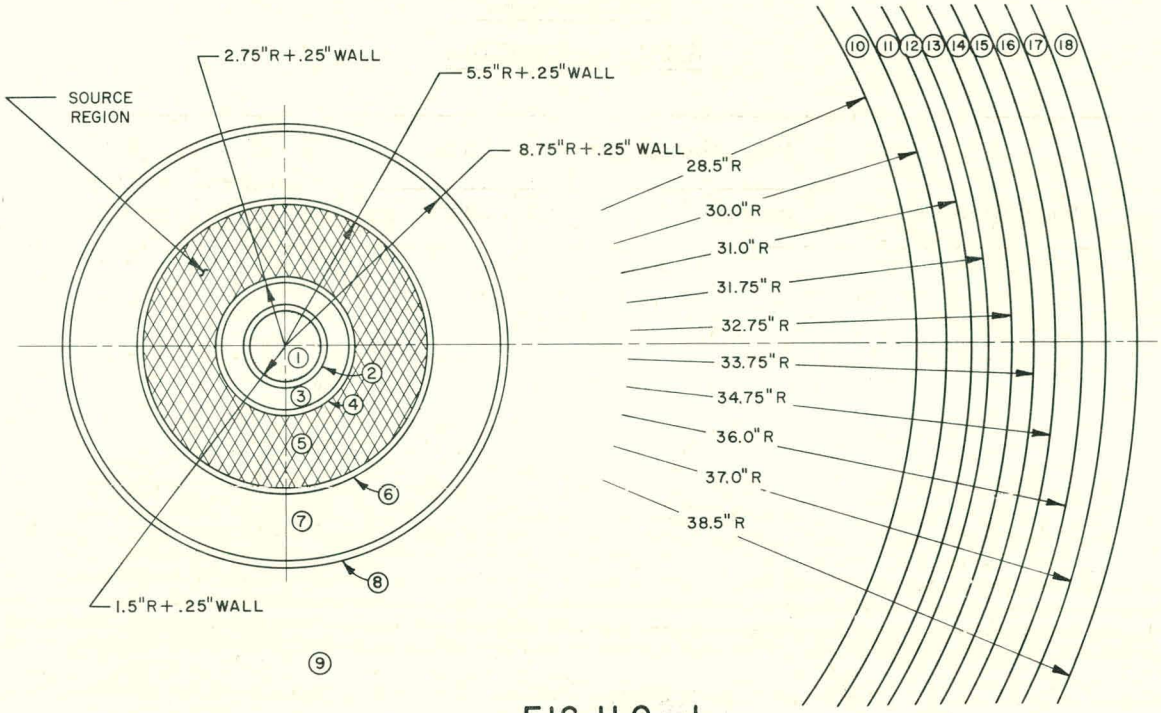

FIG. 11.0 – 1

GAMMA HEATING ANALYTICAL MODEL FOR OUTER LOBE

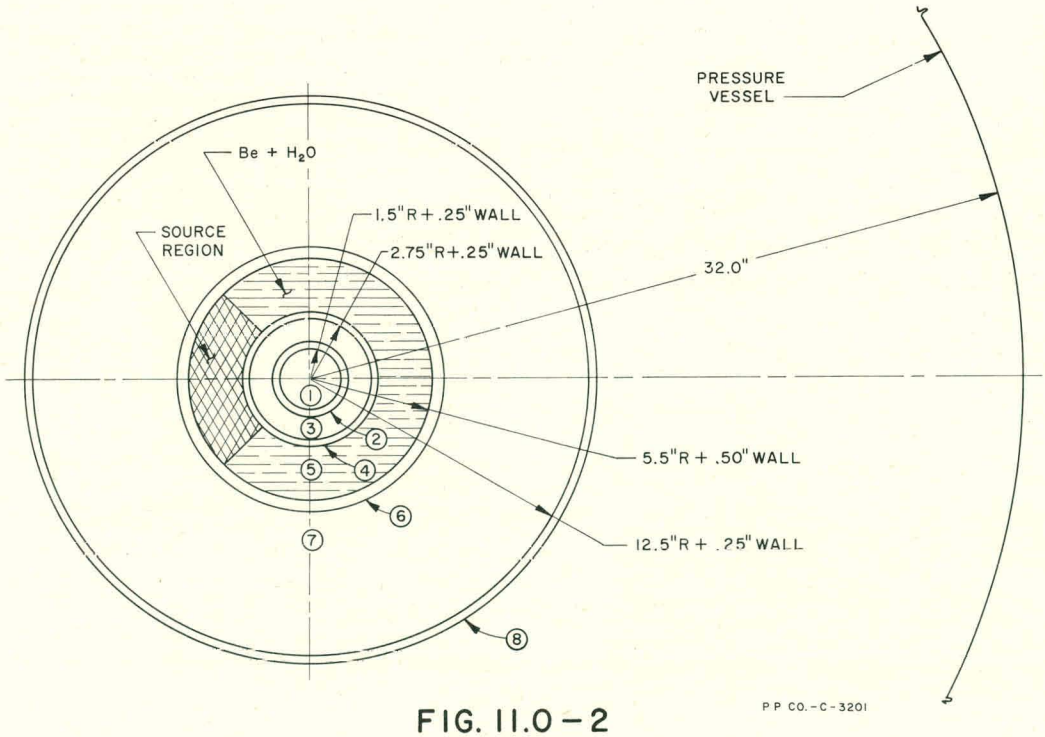

FIG. 11.0 – 2

GAMMA HEATING ANALYTICAL MODEL FOR INNER ONE-QUARTER LOBE

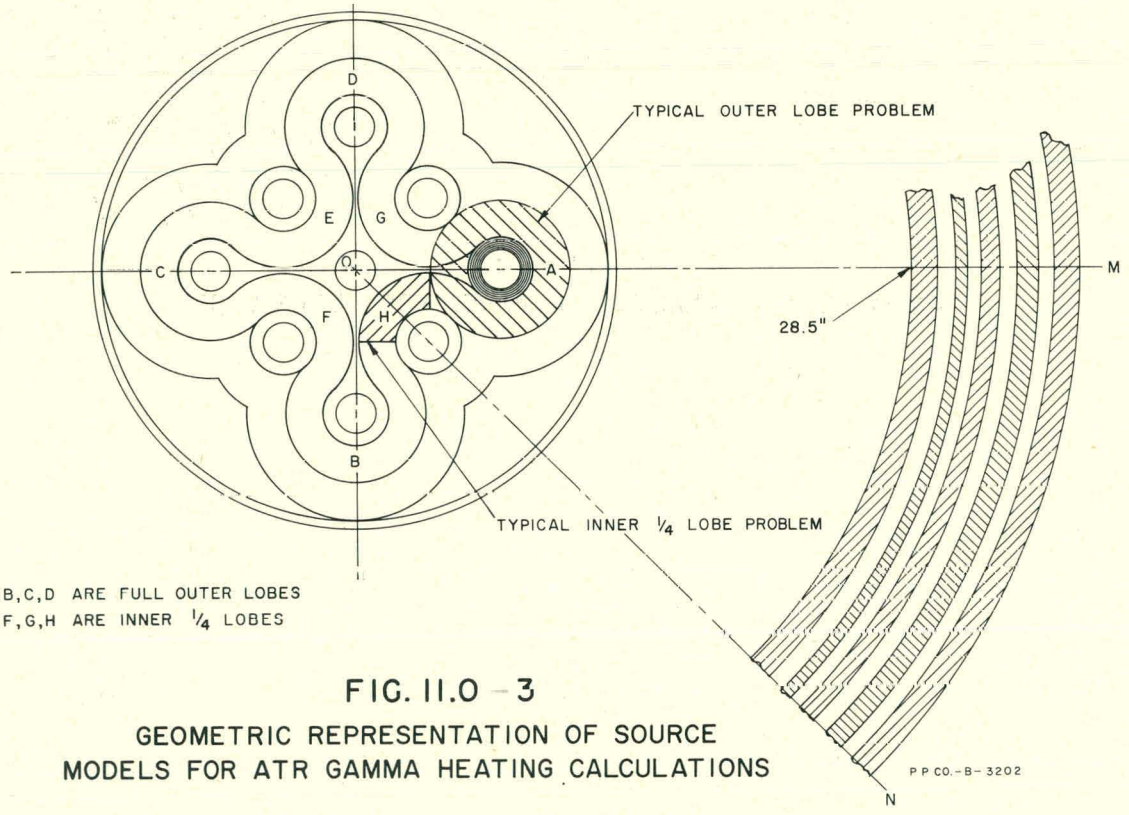

FIG. 11.0 - 3

GEOMETRIC REPRESENTATION OF SOURCE MODELS FOR ATR GAMMA HEATING CALCULATIONS

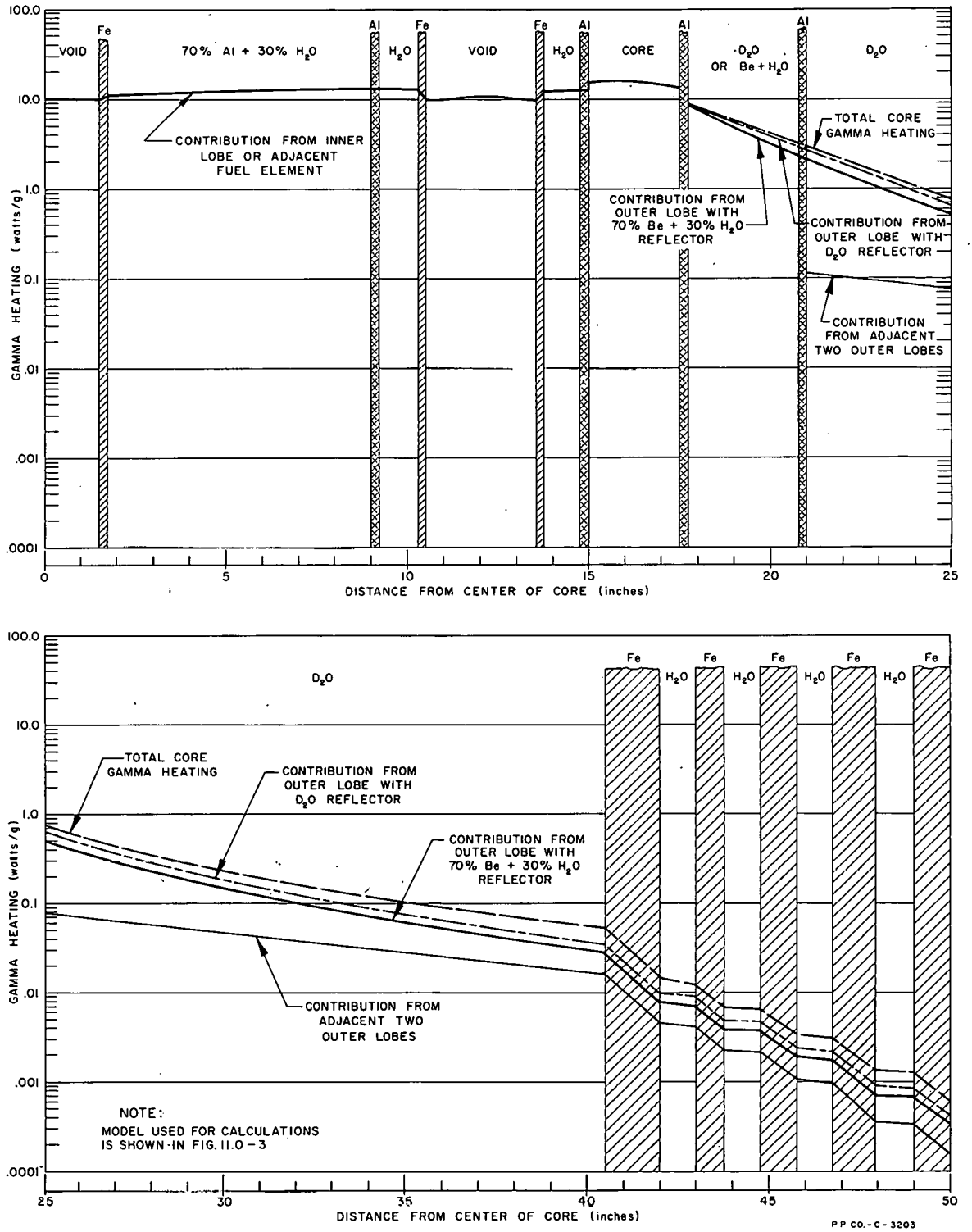

FIG. 11.0-4

AVERAGE GAMMA HEATING ALONG SECTION O-M

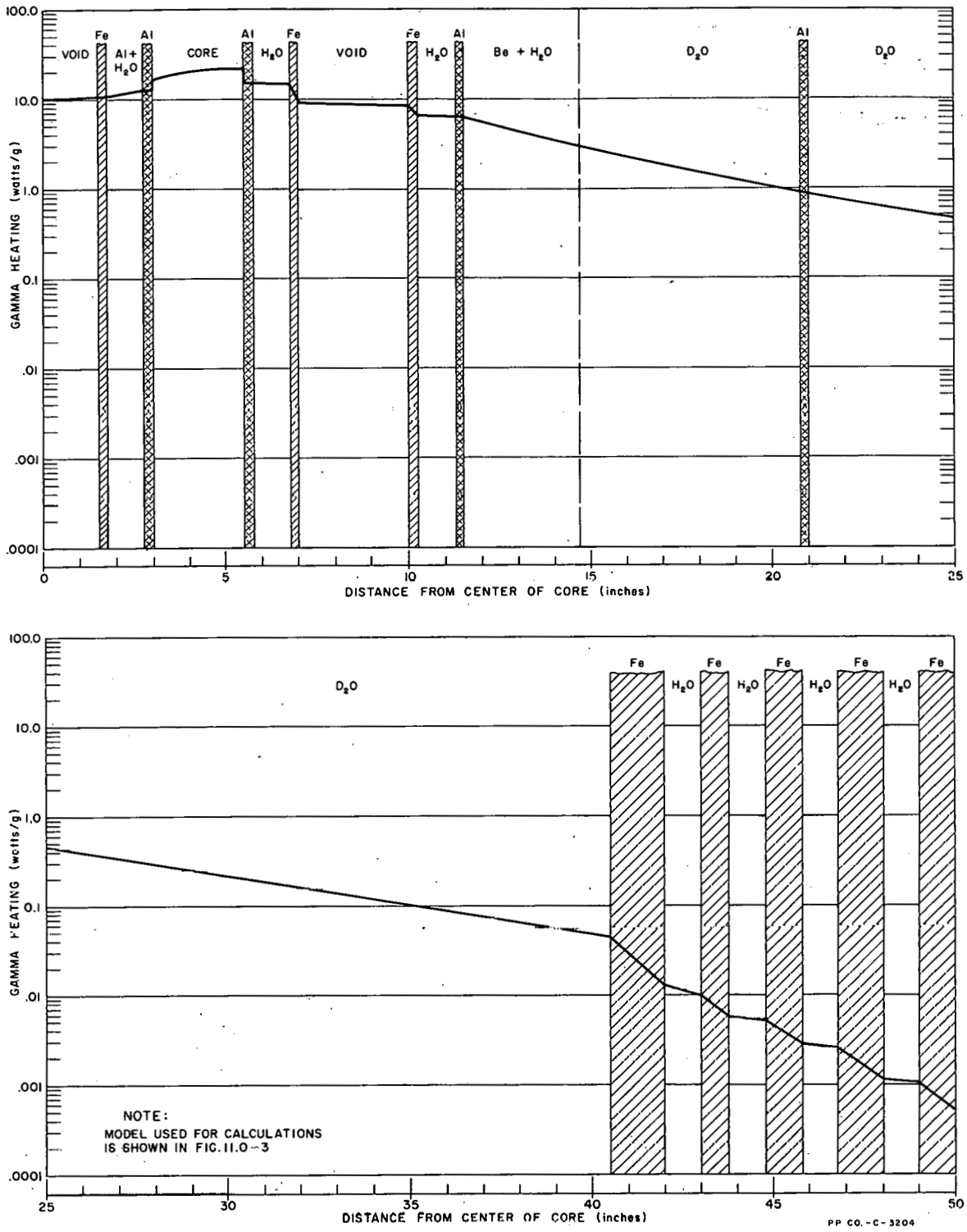

FIG. 11.0 – 5

AVERAGE GAMMA HEATING ALONG SECTION O – N

12.0 APPENDIX

12.1 S_n and Diffusion Theory Comparison

12.11 Introduction

In the reactor physics analysis of the ATR, diffusion theory type calculations were utilized extensively. Because of the general core configuration a valid scheme for homogenization was difficult to achieve. Consequently heterogenity was retained for most of the core structure insofar as was allowable by the limitations on mesh point number of the IBM-704, PDQ-3 code. Many relatively small regions were retained and the question of the validity of diffusion theory type calculations arose. Diffusion theory can be assumed to give good results if one is far from boundaries of dissimilar media and if the absorption cross section is much less than the scattering cross sections. Neither of these conditions are very well satisfied in most of the ATR. Therefore, as a check on the validity of diffusion theory, transport theory in the form of the S_n approximation was used. Carlson's $S_n(n = 4)$ program supplemented by Duane's[1] modification and extension (S-V, n = 4) of this program was used on the IBM-704.

It is concluded, that for the purposes of a conceptual design of the ATR, diffusion theory gives sufficiently accurate results to be relied on for nuclear and engineering design of this core. As expected diffusion theory is deficient in following local peaks and dips for regions with small dimensions compared to a mean free path. Some differences are also noted in the fast fluxes of the four-group scheme. Nevertheless diffusion theory gives adequate results even when applied to a reactor as complex as the ATR.

12.12 Calculation Model

The transport codes used for this study are limited to the three basic geometries: plane, sphere and cylinder. A cylindrical reactor model was chosen as the best representation of one lobe of the ATR. Each different material up to the water gap between the third and fourth fuel plate was taken as a separate region. Thereafter the fuel plates and water gaps were homogenized to the water gap between the sixteenth and seventeenth fuel plates and from there on each different material was a different region until the reactor was terminated after a total radius of 90 cm. The diffusion theory calculations (WANDA code) had the stainless steel pressure tubes homogenized with the void which separates the pressure tube from the gas annulus tube. The total number of mesh points was 224 in every case with the assignment of mesh points the same. The A-1 test was in the center with light water in the moderator flux trap annulus. The initial case had no poison in any region. An axial DB^2 was added only in the D_2O reflector region to take some account of axial leakage.

---

1. B. H. Duane, "Neutron and Photon Transport Plane-Cylinder-Sphere GE-ANPD Program S Variational Optimum Formulation," XDC 59-9-118, January 1959.

12.13 Convergence Difficulties

This first clean case was run using Carlson's S_n code for about 170 power iterations. In studying the flux shape it was clear that the problem would take a few hundred more iterations to converge. The D_2O thermal flux was rising very slowly and almost linearly with each iteration.

This same problem was then run with B. Duane's S-V program with the hope that convergence would be faster by virtue of the acceleration routine, even though each iteration takes about three times longer with this routine. Again the D_2O reflector fluxes continued to rise too slowly to justify running to reasonable convergence. The S-V program provides output in considerable abundance and detail and was used in all later studies after the initial study.

Because of the extremely slow convergence of S-V when converging on the critical number of neutrons per fission K_2, it was decided to run S-V converging on K_6. This type of convergence is known to be more rapid than the K_2 convergence. With K_6 convergence the number of fissions and all isotropic scatterings are divided by a constant K_6. Achieving a solution in this manner adds uniform absorber, in effect, in each region and group in proportion to the total isotopic cross section of the region when K_6 is greater than unity. When K_6 is less than unity, neutron production scatterings are added in the same manner.

12.14 Results

The initial clean case was run with K_6 convergence and converged in about 20 iterations. The fission eigenvalue was 1.2867 and being different than unity the K_6 convergence caused uniform absorber to be added in each region. The WANDA k_{eff} for this case was 1.2867. With K_6 convergence the H_2O absorption cross section became almost twice the actual value while the D_2O absorption cross section was up by a factor of almost seven.

Because the fission eigenvalue of these first cases was far from unity with the resulting adding of absorber with K_6 convergence there is some question as to the validity of the fluxes in comparing them with diffusion theory fluxes. In order to obtain a good case for comparison study with the fission eigenvalue K_2 close to unity, the S-V and WANDA clean case were changed by adding 6.9 g/liter of D_3BO_3 to the 3 in. reflector shim control region. This amount of poison should be fairly representative of what would be required for a typical startup core of the ATR. The WANDA k_{eff} for this case was 1.0005. The equivalent S-V case was run for about 60 power iterations with convergence acceleration on the K_6 eigenvalue. Good convergence was obtained for this case. Thereafter, 24 power iterations with no acceleration were run on the K_2 eigenvalue to obtain flux distributions that could be compared with WANDA results. The K_2 of this S-V problem was 1.029.

The combined WANDA and S-V flux plots from the center of the A-1 experiment well out into the outer reflector are shown in Figures 12.0-1, 12.0-2, and 12.0-3 and 12.0-4, for the four flux groups. The flux plots for the region from about 7 cm to 10 cm, which is through one side of the fuel region where plate, cladding, and moderator were kept separate are shown in Figures 12.0-5, 12.0-6, 12.0-7 and 12.0-8. The calculated fast flux (ϕ_1) peaks at the boundary of the plate and cladding. Physically the fast flux would peak at the center of the plate and the cause of this discrepancy has not been determined.

The average fluxes in the test and other general data are shown in Table 12.0-A.

A study of the flux plots (with regard to core and test region results) shows that the greatest differences occur in the fast neutron fluxes where diffusion theory overestimates the S-V result from 9 to 17% in the test region. Diffusion theory does not show as much of a dip in the first and second group fluxes in the H_2O moderator annulus, and it evidently fails to predict the amount of attenuation fast neutrons suffer in reaching the test region.

Thermal fluxes are well predicted by the diffusion theory result except in the thin, highly absorbing regions such as the stainless steel and the fuel meat. The absorptions in the stainless around the test are 6 to 8% higher in the diffusion theory result.

Besides showing the anomolous peaks in the meat regions in the first and second group fluxes, there is a slight difference in the shape of the fast fluxes in the core. The S_n results show fast fluxes which are relatively greater toward the inside of the core region, and the first group flux is about 30% higher for the S-V case in most of the core region although it almost equals the diffusion theory result at the core edges.

The thermal fluxes in the control region are almost identical, but the fast fluxes show a few percent of difference as the S-V fluxes fall off slightly faster.

In the large D_2O reflector, the S-V fast fluxes attenuate more slowly than the diffusion theory results and finally become equal to the diffusion theory fluxes. The thermal fluxes in this unpoisoned D_2O differ as much as 20% in some places but this is probably due primarily to the fact that in this one region the S-V flux is insufficiently converged to the K_2 eigenvalue. Having converged well on K_6 (with the D_2O poisoned to obtain convergence), 24 iterations is undoubtedly insufficient to obtain good convergence in this D_2O region after the poison is removed for K_2 convergence.

Another significant difference (in addition to the fact that the S_n case predicts a higher K by 2.9% for the given amount of D_3BO_3 in the control region) is that the S-V radial power distribution in the

TABLE 12.0-A

COMPARISON OF DIFFUSION AND TRANSPORT THEORY AVERAGE

FLUX VALUES IN THE A-1 TEST REGION AND POWER PRODUCTION IN THE CORE

	WANDA Case 130	S-V Case 1.130	% Difference (WANDA Value - S-V Value) / S-V Value
K value (K_2)	1.000483	1.0290 ± 0.0001	- 2.77
ϕ_1 (average)	2.64824	2.27217	16.55
ϕ_2 (average)	3.02437	2.77502	9.166
ϕ_3 (average)	3.03374	2.78743	8.836
ϕ_4 (average)	5.33580	5.14721	3.664
($\phi_1 + \phi_2 + \phi_3$ (average)	8.71135	7.83462	11.19
$\frac{\phi_1 + \phi_2 + \phi_3}{\phi_4}$ =	1.63261	1.52211	7.260
Total power of A-1 test	0.029595	0.028494	3.864
Total power of 1st inner fuel plate	0.249783	0.23621733	5.743
Total power of 2nd fuel plate	0.214747	0.20476817	4.873
Total power of 3rd fuel plate	0.189004	0.18249107	3.569
Total power of homogenized center region	1.992697	2.031629	- 1.9163
Total power of 17th fuel plate	0.181629	0.17965728	1.097
Total power of 18th fuel plate	0.1953129	0.19271867	1.346
Total power of 19th fuel plate	0.2122011	0.20894351	1.559

core is flatter. The maximum power in the inside fuel plate is 5.7% less by the S-V result so that the predicted ratio of the radial value of maximum-to-average power will be correspondingly less.

12.15 Conclusions

Insofar as can be determined from this comparison of diffusion theory to S_n transport solutions in flux trap reactors, the only observable failings of the diffusion theory are:

1. Inability to follow the small peaks and dips which occur in the water gaps and fuel plates. (In this instance, the error is small because the diffusion theory solution tends to the mean of the flux in each small region.)

2. Overestimation of the fast fluxes in the H_2O filler, especially near the test region. (The S_n solutions show a dip and a recovery that is not detectable in the WANDA solutions. Here, again, the difference is not serious unless one becomes interested in the fast fluxes in the filler itself.)

3. Overestimation of the thermal flux in the stainless steel or some other strong absorber surrounding the test region. (This fault, though it may represent a small difference reactivity, is evidently due to the familiar lack of ability to follow peaks and valleys. The S_n solution makes the dip in the stainless steel and then quickly recovers in the test region.)

All things considered, diffusion theory is quite adequate for all but the finest detail in studying flux trap reactors as well as reactors composed of large regions.

The S_n fluxes are valid for comparison with diffusion theory only when the S_n fission eigenvalue is near unity with the controlling reactor poisons in their proper position. This is principally due to convergence difficulties connected with the K_2 fission eigenvalue. This study demonstrates the difficulties of using the S_n transport code for thermal reactor systems.

12.2 The Effects of Mesh Description and of Test Region Homogenization

12.21 One-Dimensional Studies

12.211 Introduction

In order to calculate, with two-dimensional codes, the characteristics of the ATR it is highly desirable to homogenize discrete regions of the reactor and specify as few mesh points as possible for the numerical solutions accomplished by codes. In the ATR, the flux levels in the test loop are of the greatest importance, for lobe power level must be adjusted to maintain the specified neutron flux levels in the test.

With one-dimensional diffusion theory the effects of homogenization of the stainless steel pressure tubes and the A-5 test has been studied and further examination has been made of the effects of mesh size on the numerical solution for eigenvalues and fluxes.

12.212 The Effect of Homogenization

The composition of the reactor model used in the homogenization is shown in Table 12.0-B, together with the number of mesh points in each region. The k_{eff} values obtained from the WANDA-4 results, the description of each case run, and the effect of the respective degrees of homogenization are summarized in Table 12.0-C.

In Case 3001*, the void was treated as a discrete region with a diffusion constant of ten and a macroscopic absorption cross section of 1×10^{-5} in all four neutron groups. The perpendicular buckling value used was 0.00043 in all regions except 1, 2, 3, and 4 where it was set equal to zero.

Table 12.0-D shows the effects of homogenization on the neutron group flux levels in each of the four regions which were subjected to homogenization. The most variation is noted in the thermal flux levels, but it must be kept in mind that the real criterion for valid homogenization is that the total absorptions in a material should remain constant.

In accomplishing the homogenization, all macroscopic cross sections including Σ_{tr} (from which D is computed as $\frac{1}{3\Sigma_{tr}}$) were simply weighted by the volumes of the respective regions. For example, $\Sigma_a = \frac{\sum_i V_i \Sigma_{ai}}{\sum_i V_i}$, where Σ_a is the absorption cross section of a

*Case numbers identify WANDA calculations and do not apply to PDQ numbers used elsewhere in this report.

TABLE 12.0-B

REACTOR COMPOSITIONS OF THE HOMOGENIZATION STUDY MODELS

Region No.	Outer Radius of Region (in.)	*Composition of Region	Number of Mesh Intervals in Region
1	1.00	A-5 test	10
2	1.20	Stainless steel	10
3	1.26	Void	2
4	1.34	Stainless steel	4
5	2.75	40% H_2O-60% Aluminum	10
6	3.00	Aluminum	2
7	5.50	Core (nominal fuel loading)	20
8	5.75	Aluminum	2
9	8.75	D_2O + 3 g/liter of D_3BO_3	20
10	9.75	D_2O	4
11	40.50	D_2O	30
12	43.50	Stainless steel	10

*Regions 1, 2, 3, and 4 are the regions subject to homogenization. In WANDA case 3001 there is no homogenization, the stainless steel and the void of region 3 are homogenized in case 3002, and in case 3003 the A-5 test, the stainless steel and the void are homogenized.

TABLE 12.0-C

DESCRIPTION OF CASES AND SUMMARY OF RESULTS

OF HOMOGENIZATION

WANDA Case No.	Regions Combined by Homogenization	k_{eff}	$\frac{\% \Delta k}{k}$	% Error in Total Neutron Absorptions	
				A-5 Test Absorption	Stainless Steel Absorptions
3001	None	0.980060	0	0	0
3002	2, 3, and 4	0.980052	-0.00083	0.1202	0.03761
3003	1, 2, 3 and 4	0.981650	0.1587	-4.816	-5.132

TABLE 12.0-D

EFFECT OF HOMOGENIZATION ON THE AVERAGE GROUP FLUX LEVELS IN THE REGIONS OCCUPIED BY THE A-5 TEST AND STAINLESS STEEL

Neutron-Group Flux	Case No.	Region No. 1	2	3	4
ϕ_1 (0.821 mev $\leq$ E $\leq$ 10 mev)	3001	1.0430	1.0359	1.0353	1.0357
	3002	1.0431	1.0362	1.0354	1.0358
	3003	1.0241	1.0297	1.0316	1.0327
ϕ_2 (5.53 kev $\leq$ E $\leq$ 0.821mev)	3001	1.3443	1.3379	1.3331	1.3304
	3002	1.3439	1.3384	1.3337	1.3300
	3003	1.3468	1.3338	1.3281	1.3246
ϕ_3 (0.625 ev $\leq$ E $\leq$ 5.53 kev)	3001	1.2484	1.2454	1.2451	1.2455
	3002	1.2483	1.2454	1.2451	1.2455
	3003	1.2409	1.2424	1.2431	1.2436
ϕ_4 (thermal) 0 $\leq$ E $\leq$ 0.625 ev	3001	1.0488	1.0302	1.0641	1.0907
	3002	1.0502	1.0261	1.0585	1.0946
	3003	0.9152	1.0523	1.1137	1.1525

NOTE: Flux values are normalized to arbitrary units for each neutron-group and comparisons are valid only within a group.

homogenized set of regions of respective volume, V_i. Hence, even though the thermal flux in region 1 is seen to vary by about 13%, the average flux to which a homogenized material is exposed does not vary nearly so much.

The absorptions in stainless steel and in the A-5 according to each degree of homogenization are shown for each group in Table 12.0-E. It is clear that the only significant variation occurs in the thermal absorption values where there occurs about a 5.5% reduction in absorption due to the homogenization.

It is notable that this reduction takes place in both the A-5 absorptions and the stainless steel absorptions; therefore the error is not due to the fact that the homogenization neglected the fact that the average flux in the stainless steel is different from the average flux in the A-5 test. To correct for the error, one would have to multiply the thermal cross sections by a factor greater than one in order to have the homogenized region absorptions remain the same; and to have the flux in the homogenized regions remain the same one would have to multiply the thermal cross sections by a number less than one.

12.213 The Effect of Mesh Description

The single-lobe model used in the mesh coarseness study was chosen to conform as nearly as possible to the cases which have been run using the PDQ code. The one-dimensional model is described in Table 12.0-F, together with the mesh internal width used in the case with the most coarse mesh.

The coarse mesh size shown in Table 12.0-F was used in WANDA case 3004. In cases 3005, 3006, and 3007 the mesh spacing was reduced in each region by a factor of 2, 4, and 8, respectively; hence, case 3007 has a quite fine mesh spacing.

The results in terms of the flux distributions are shown on Figure 12.0-9 where the neutron group fluxes from case 3007 are plotted and the points from case 3004 are shown. The results in terms of average fluxes in each region and the k_{eff} values obtained are shown in Table 12.0-G.

The largest variation in the value of k_{eff} is 0.033% (between cases 3004 and 3007); that is, the largest variation in mesh spacing has little effect on the neutron balance obtained.

The greatest difference in regional average fluxes occurs in the D_2O reflector where there is over 11% difference in the 1st and 2nd group fluxes. With regard to the test region, the largest variation in the average flux occurs for the thermal neutron group where the coarse mesh results in an average flux about 5% higher than that of the fine mesh case.

Finally, it is noted that the error caused by too coarse a mesh spacing is about the same size and in the opposite direction

TABLE 12.0-E

COMPARISON OF GROUP ABSORPTIONS IN THE A-5 AND THE STAINLESS STEEL (ABSORPTION FOR THE i^{th} GROUP EQUALS VOLUME x FLUX x Σ_{ai} = V ϕ_i Σ_{ai}

Material	Case No.	Absorption Rate				
		Group 1	Group 2	Group 3	Group 4 (thermal)	Total Absorption
A-5	3001	1.0316	0.5640	10.9913	98.4111	110.9980
A-5	3002	1.0317	0.5639	10.9908	98.5450	111.1314
A-5	3003	1.0160	0.5621	10.9332	93.1407	105.6520
Stainless Steel	3001	0.07510	0.07542	15.4638	255.0609	270.6752
Stainless Steel	3002	0.07517	0.07536	15.4638	255.1629	270.7770
Stainless Steel	3003	0.07439	0.0756	15.4180	241.2164	256.7844

TABLE 12.0-F

THE SINGLE-LOBE REACTOR MODEL USED IN THE MESH COARSENESS STUDY

Region No.	Region Composition	Outer Radius or Region (in.)	Interval Width in Most Coarse Mesh (cm)
1	Homogenized A-5 test, stainless steel and void	1.34	1.7018
2	Filler of 40% H_2O and 60% Al	3.00	2.1082
3	Core (nominal fuel loading)	5.50	1.5875
4	Control region, D_2O + 3g/liter of H_3BO_3	8.50	1.9050
5	Reflector, D_2O + 0.25% H_2O	10.50	2.5400
6	Reflector, D_2O + 0.25% H_2O	40.50	12.7000

TABLE 12.0-G

EFFECT OF MESH SPACING ON THE AVERAGE GROUP FLUX AND ON EIGENVALUE

Region No.	Composition	ϕ_1 Case No. 3007	3006	3005	3004	% Error*	ϕ_2 Case No. 3007	3006	3005	3004	% Error*
1	A-5, ss, void homogenized	0.00974	0.00975	0.00979	0.00990	1.6	0.01255	0.01256	0.01258	0.01266	0.9
2	40% H_2O + Al	0.01048	0.01049	0.01054	0.01069	2.0	0.01252	0.01253	0.01258	0.01271	1.5
3	Core (Nominal fuel loading)	0.01067	0.01067	0.01069	0.01076	0.8	0.01251	0.01252	0.01255	0.01264	1.0
4	D_2O + 3 g/liter of D_3BO_3	0.003615	0.003614	0.003612	0.003604	-0.3	0.007712	0.007707	0.007684	0.007605	-1.4
5	2 in. D_2O reflector	0.000839	0.000832	0.000808	0.000747	-11.0	0.003490	0.003468	0.003384	0.003103	-11.1
6	40 in. D_2O reflector	1.35×10^{-5}	1.34×10^{-5}	1.29×10^{-5}	1.19×10^{-5}	-11.9	1.06×10^{-4}	1.05×10^{-4}	1.02×10^{-4}	0.93×10^{-4}	-12.2

Region No.	Composition	ϕ_3 Case No. 3007	3006	3005	3004	% Error*	ϕ_4 (thermal) Case No. 3007	3006	3005	3004	% Error*
1	A-5, ss, void homogenized	0.01181	0.01182	0.01185	0.01195	1.2	0.01047	0.01050	0.01059	0.01097	4.8
2	40% H_2O + Al	0.01183	0.01184	0.01187	0.01195	1.0	0.01354	0.01352	0.01348	0.01337	-1.3
3	Core (Nominal fuel loading)	0.01109	0.01110	0.01111	0.01114	0.4	0.00757	0.00757	0.00757	0.00756	-0.1
4	D_2O + 3 g/liter of D_3BO_3	0.00871	0.00870	0.00866	0.00848	-2.6	0.01218	0.01219	0.01223	0.01229	0.9
5	2 in. D_2O reflector	0.00568	0.00566	0.00558	0.00522	-8.1	0.01642	0.01645	0.01659	0.01695	3.2
6	40 in. D_2O reflector	3.12×10^{-4}	3.11×10^{-4}	3.05×10^{-4}	2.83×10^{-4}	-9.3	0.00594	0.00594	0.00592	0.00581	-2.2

Case No.	k_{eff}
3007	0.99959
3006	0.99964
3005	0.99980
3004	0.99992

to the error caused by homogenization of the stainless steel pressure tube with the A-5 test. The net result is that PDQ cases run with the coarse mesh and homogenized test region and pressure tubes are probably only about a couple of percent in error compared to the more accurate diffusion theory solutions with regard to average neutron flux values in the test region.

The indications are that the k_{eff} value obtained is good to within a small fraction of a percent regardless of the larger mesh spacing and/or homogenization.

12.22 Two-Dimensional Studies

12.221 Introduction

To study the two-dimensional effect of mesh size and homogenization on maximum-to-average power ratios, average experiment fluxes and detailed fluxes along north, east, and diagonal axes from core center line for a typical core of the ATR, three PDQ problems were run. Two of these problems were run on the IBM-704 at NYU. The coarse mesh problem had a mesh of 42 x 42 (1764 internal points) while the fine mesh problem had an 84 x 84 (7056 internal points) mesh. The TRANSAC mesh problem with a mesh of 140 x 140 (19600 internal points) was beyond the capabilities of the IBM-704. This problem was run by Internuclear Company using the PHILCO-2000 machine. There were some slight differences in fueled area and the pressure tubes were homogenized into the experiments in the coarse mesh problem. These differences would account for the change in eigenvalue between the three problems. All three problems used exactly the same two-group reactor constants except for the coarse mesh problem in the regions where pressure tubes were homogenized into the experiments.

12.222 Results

The fine mesh PDQ-3 problem gave essentially the same results as the TRANSAC mesh PDQ-4 problem as can be seen on Table 12.0-H and Figures 4.0-1 through 4.0-8. The coarse mesh problem did give some significant deviations-- in particular the overall core maximum-to-average power density increased by about 18%. The maximum-to-average value quoted in the table does not include the vertical component. Also the average experimental thermal flux dropped significantly for the center experiment and to a lesser extent in the north experiment. In the east and northeast experiment the thermal flux increased somewhat. The east experiment had a zirconium pressure vessel instead of stainless steel. All fluxes have been normalized to a core power of 250 Mw.

The fine mesh was used in most problems for the study of the ATR. When coarse mesh was used for particular studies appropriate corrections were made to obtain effectively fine mesh results.

TABLE 12.0-H

THE EFFECT OF MESH SIZE AND HOMOGENIZATION ON

FLUX AND EIGENVALUE - RESULTS FROM TWO-DIMENSIONAL STUDIES

	Experiment Fluxes n/cm^2 sec x 10^{-15}											
	A-1 (East)			A-3 (Center)			A-5 (North			A-5 (Northeast)		
	Coarse	Fine	TRANSAC	Coarse	Fine	TRANSAC	Coarse	Fine	TRANSAC	Coarse	Fine	TRANSAC
ϕ_f	1.093	1.228	1.251	2.184	2.324	2.315	1.195	1.329	1.308	1.518	1.716	1.688
ϕ_{th}	1.413	1.367	1.308	0.602	0.702	0.685	0.384	0.407	0.397	0.641	0.578	0.561
ϕ_f/ϕ_{th}	0.774	0.898	0.956	3.628	3.310	3.380	3.112	3.265	3.295	2.368	2.969	3.009

	Max/Avg Power Density			Average Core Thermal Fluxes n/cm^2 sec x 10^{-15}		
	Coarse	Fine	TRANSAC	Coarse	Fine	TRANSAC
East Fuel	2.775	2.282	2.320	0.326	0.335	0.334
Center Fuel	1.470	1.482	1.494	0.525	0.525	0.522
North Fuel	2.520	2.492	2.583	0.281	0.291	0.287

Reactor Values			
	Coarse	Fine	TRANSAC
Max/Avg	2.594	2.192	2.213
k_{eff}	1.1325	1.1144	1.1168

12.3 ATR Experiment Specifications and Test Facility Structure

The specifications for the A-1, A-3, and A-5 experiments are given in Table 12.0-J and the structure assumed for the ATR loops is shown in Figure 12.0-10.

TABLE 12.0-J

ATR EXPERIMENT SPECIFICATIONS

	Experiment		
	A-1	A-3	A-5
Kw/foot	200	200	200
Kw/gram	30	15	10
Metal/water ratio	1.0	1.0	1.0
Metal	Zirconium	Zirconium	Zirconium
Atoms U^{235}/cm^3	2.768×10^{19}	5.536×10^{19}	8.304×10^{19}
Neutron flux above .625 ev (n/cm^2-sec)	1.0×10^{15}	1.5×10^{15}	1.0×10^{15}
Thermal neutron flux (n/cm^2-sec)	9.6×10^{14}	4.8×10^{14}	3.2×10^{14}

12.4 Reactor Constants

The constants used in the ATR calculations are given in Tables 12.0-K and 12.0-L. The bulk of the ATR calculations (including the TURBO calculations) used constants given in Table 12.0-K; however, for the temperature coefficient calculations, the constants given in Table 12.0-L were used. Whenever the composition description in these tables is listed in per cent the reference is to volume per cent.

TABLE 12.0-K

NUCLEAR CONSTANTS FOR ATR CALCULATIONS

Composition		3 Fast Group			1 Fast Group	Thermal
		1 of 3	2 of 3	3 of 3	1 of 1	
1.43 Normal Fuel	D	2.4551	1.2376	0.9489	1.5432	0.2704
	Σ_a	0.001384	0.000966	0.017162	0.006286	0.1969
	Σ_r	0.066727	0.081588	0.072758	0.023284	--
	$\upsilon\Sigma_f$	0.001293	0.001672	0.024591	0.008883	0.3804
Normal Fuel	D				1.54355	0.2807
	Σ_a				0.00476	0.142
	Σ_r				0.02442	--
	$\upsilon\Sigma_f$				0.00644	0.267
304 Stainless Steel	D	1.563	0.943	0.390	0.735	0.3188
	Σ_a	0.0003	0.000039	0.00945	0.00404	0.1851
	Σ_r	0.0375	0.005	0.00038	0.0001	--
8.45% 304 SS + 18.55% Void (Homog. Press. Tubes and Void)	D	1.925	1.11	0.463	0.845	0.3914
	Σ_a	0.000045	0.000035	0.0077	0.0033	0.1507
	Σ_r	0.033015	0.003092	0.000174	0.000066	--
87.979% Zircalloy-2 + 12.021% Void (Homog. Press. Tubes and Void)	D				2.099	1.395
	Σ_a				0.000085	0.00476
	Σ_r				0.0	--
Aluminum	D	2.720	1.600	2.250	2.150	3.595
	Σ_a	0.0002	0.000225	0.001775	0.000785	0.01083
	Σ_r	0.016868	0.00202	0.00006	0.000035	--
Beryllium (Pure)	D	1.7262	0.5805	0.4859	0.6828	0.4155
	Σ_a	0.01258	0.000002	0.000054	0.001709	0.0009676
	Σ_r	0.04828	0.92764	0.01690	0.009067	--
	$\upsilon\Sigma_f$	0.016732	0.0	0.0	0.0	0.0
Water (Pure)	D	2.3376	1.1354	0.6110	1.3886	0.1788
	Σ_a	0.001373	0.000012	0.000917	0.000781	0.01674
	Σ_r	0.1012	0.1451	0.1462	0.04709	--
99.75% D_2O + 0.25% H_2O	D	1.9811	1.2514	1.2387	1.3206	0.9052
	Σ_a	0.001802	0.0	0.000002	0.00019	0.00006988
	Σ_r	0.07788	0.03227	0.01931	0.01079	--

(more)

Table 12.0-K (Cont.)

Composition		3 Fast Group			1 Fast Group	
		1 of 3	2 of 3	3 of 3	1 of 1	Thermal
99% D_2O + 1% H_2O	D				1.3138	0.8697
	Σ_a				0.00020	0.0001986
	Σ_r				0.011195	--
97% D_2O + 3% H_2O	D				1.3009	0.8029
	Σ_a				0.000227	0.0005384
	Σ_r				0.012242	--
95% D_2O + 5% H_2O	D				1.2897	0.7460
	Σ_a				0.000253	0.0008782
	Σ_r				0.013257	--
97% Beryllium + 3% H_2O	D	1.7262	0.5907	0.4885	0.7094	0.3959
	Σ_a	0.012564	0.000002	0.00008	0.001928	0.001441
	Σ_r	0.050037	0.031045	0.02075	0.01054	--
	$\upsilon\Sigma_f$	0.016834	0.0	0.0	0.0	0.0
90% Beryllium + 10% H_2O	D	1.7289	0.6153	0.4947	0.7625	0.3587
	Σ_a	0.012465	0.000003	0.000141	0.002338	0.002544
	Σ_r	0.054135	0.039027	0.029776	0.013774	--
	$\upsilon\Sigma_f$	0.016948	0.0	0.0	0.0	0.0
80% Beryllium + 2 % H_2O	D	1.7398	0.6522	0.5040	0.8257	0.3187
	Σ_a	0.012139	0.000004	0.000227	0.002733	0.004121
	Σ_r	0.05995	0.05049	0.04270	0.018056	--
	$\upsilon\Sigma_f$	0.016789	0.0	0.0	0.0	0.0
95% Aluminum + 5% H_2O	D	2.6966	1.8471	3.0985	2.5402	1.795
	Σ_a	0.000262	0.000223	0.00162	0.000867	0.01113
	Σ_r	0.02194	0.01001	0.00683	0.003125	--
80% Aluminum + 20% H_2O	D				1.860	0.740
	Σ_a				0.00077	0.012025
	Σ_r				0.0110	--
70% Aluminum + 30% H_2O	D	2.5816	1.3700	1.4615	1.7379	0.5294
	Σ_a	0.000568	0.000153	0.001528	0.000767	0.0126
	Σ_r	0.04476	0.04552	0.04354	0.01581	--
60% Aluminum + 40% H_2O	D	2.542	1.312	1.200	1.635	0.405
	Σ_a	0.000684	0.000132	0.001445	0.00076	0.0132
	Σ_r	0.0533	0.0600	0.0582	0.0206	--

(more)

Table 12.0-K (Cont.)

Composition		3 Fast Group			1 Fast Group	Thermal
		1 of 3	2 of 3	3 of 3	1 of 1	
97% Beryllium + 3% D_2O	D	1.7238	0.5893	0.4950	0.6901	0.4222
	Σ_a	0.01237	0.000002	0.000052	0.001679	0.0009407
	Σ_r	0.04862	0.02777	0.01698	0.00910	0 --
	$\upsilon\Sigma_f$	0.016508	0.0	0.0	0.0	0.0
95% Beryllium + 5% D_2O	D	1.7217	0.5954	0.5012	0.6948	0.4267
	Σ_a	0.012229	0.000001	0.000051	0.001656	0.0009227
	Σ_r	0.04895	0.02786	0.01702	0.009140	--
	$\upsilon\Sigma_f$	0.016359	0.0	0.0	0.0	0.0
90% Beryllium + 10% D_2O	D	1.7162	0.6111	0.5174	0.7065	0.4387
	Σ_a	0.01186	0.000001	0.000049	0.001591	0.0008779
	Σ_r	0.05000	0.02809	0.01715	0.009222	--
	$\upsilon\Sigma_f$	0.01597	0.0	0.0	0.0	0.0
80% Beryllium + 20% D_2O	D	1.7092	0.6457	0.5532	0.7323	0.4647
	Σ_a	0.01105	0.000001	0.000043	0.001443	0.0007881
	Σ_r	0.05264	0.028535	0.017387	0.009396	--
	$\upsilon\Sigma_f$	0.015049	0.0	0.0	0.0	0.0
Water + 1 g/liter H_3BO_3	D	2.3375	1.1354	0.6109	1.3887	0.1783
	Σ_a	0.001374	0.000017	0.001251	0.000891	0.02249
	Σ_r	0.1012	0.1451	0.1459	0.046994	--
Water + 3 g/liter H_3BO_3	D	2.3374	1.1353	0.6107	1.3889	0.1774
	Σ_a	0.001375	0.000026	0.001918	0.001109	0.03399
	Σ_r	0.10119	0.1451	0.14549	0.04680	--
Water + 10 g/liter H_3BO_3	D	2.3368	1.1350	0.6098	1.3897	0.1742
	Σ_a	0.001381	0.000057	0.004231	0.001861	0.07425
	Σ_r	0.10120	0.14508	0.14392	0.04613	--
Water + 50 g/liter H_3BO_3	D	2.3337	1.1336	0.6053	1.3938	0.1579
	Σ_a	0.001416	0.000236	0.016864	0.005883	0.3043
	Σ_r	0.10122	0.14500	0.13543	0.04258	--
D_2O + 1 g/liter D_3BO_3	D	1.9830	1.2517	1.2374	1.3201	0.8879
	Σ_a	0.001803	0.000006	0.00034	0.00038	0.0059
	Σ_r	0.077875	0.032315	0.019115	0.010686	--
D_2O + 3 g/liter D_3BO_3	D	1.9829	1.2516	1.2344	1.3188	0.8639
	Σ_a	0.001805	0.000017	0.001002	0.000753	0.01756
	Σ_r	0.077876	0.032309	0.018635	0.010374	--

(more)

Table 12.0-K (Cont.)

Composition		3 Fast Group			1 Fast Group	Thermal
		1 of 3	2 of 3	3 of 3	1 of 1	
D_2O + 10 g/liter D_3BO_3	D	1.9825	1.2511	1.2245	1.3147	0.7895
	Σ_a	0.001812	0.000058	0.003189	0.001963	0.05836
	Σ_r	0.077879	0.032288	0.017072	0.009368	--
D_2O + 50 g/liter D_3BO_3	D	1.9802	1.2485	1.1853	1.3012	0.5318
	Σ_a	0.001851	0.000288	0.012763	0.006841	0.2916
	Σ_r	0.077899	0.032168	0.010733	0.005482	--
80% Be + 20% H_2O W/3 g/liter H_3BO_3	D	1.7398	0.6521	0.5039	0.8258	0.3177
	Σ_a	0.012140	0.000007	0.000429	0.002821	0.007572
	Σ_r	0.05995	0.05049	0.04255	0.017981	--
80% Be + 20% H_2O W/10 g/liter H_3BO_3	D	1.7397	0.6521	0.5037	0.8261	0.3155
	Σ_a	0.012141	0.000014	0.000897	0.003025	0.01562
	Σ_r	0.059955	0.050483	0.042217	0.01781	--
80% Be + 20% H_2O W/50 g/liter H_3BO_3	D	1.7383	0.652	0.5024	0.8279	0.3036
	Σ_a	0.012149	0.000053	0.003495	0.004142	0.06163
	Σ_r	0.05996	0.05046	0.04037	0.0185	--
A-1 Experiment 400°F Spectrum	D	2.6172	1.2418	0.9967	1.5459	0.4408
	Σ_a	0.000408	0.000072	0.001807	0.000783	0.02049
	Σ_r	0.05094	0.05335	0.0527	0.01863	--
	$\upsilon\Sigma_f$	0.000099	0.000132	0.002105	0.000822	0.026059
A-3 Experiment 400°F Spectrum	D	2.6134	1.2405	0.9957	1.5461	0.4576
	Σ_a	0.000448	0.000140	0.003091	0.001266	0.0305
	Σ_r	0.050995	0.05333	0.05189	0.01826	--
	$\upsilon\Sigma_f$	0.000198	0.000263	0.00416	0.001616	0.05214
A-5 Experiment 400°F Spectrum	D	2.6096	1.2393	0.9946	1.5462	0.4511
	Σ_a	0.000488	0.000207	0.004345	0.001734	0.04303
	Σ_r	0.05105	0.05331	0.05122	0.01790	--
	$\upsilon\Sigma_f$	0.000297	0.000395	0.006171	0.002385	0.0782
A-1 Loop W/SS Pressure Tube 400°F Spectrum	D	2.4342	1.1781	0.6087	1.2556	0.4120
	Σ_a	0.000227	0.000055	0.004722	0.001838	0.07820
	Σ_r	0.040065	0.03104	0.028082	0.010489	--
	$\upsilon\Sigma_f$	0.000054	0.000072	0.000955	0.000398	0.0145
A-3 Loop W/SS Pressure Tube 400°F Spectrum	D	2.4336	1.1778	0.60853	1.2566	0.4102
	Σ_a	0.000240	0.000077	0.005035	0.001961	0.08234
	Σ_r	0.040064	0.031031	0.027929	0.010397	--
	$\upsilon\Sigma_f$	0.000086	0.000116	0.001519	0.000631	0.02311

(more)

Table 12.0-K (Cont.)

Composition		3 Fast Group			1 Fast Group	Thermal
		1 of 3	2 of 3	3 of 3	1 of 1	
A-5 Loop W/SS	D	2.4328	1.1775	0.6083	1.2580	0.4078
Pressure Tube	Σ_a	0.000258	0.000107	0.005452	0.002123	0.08789
400°F Spectrum	Σ_r	0.040063	0.031018	0.027727	0.010277	--
	$\upsilon\Sigma_f$	0.000129	0.000174	0.002273	0.000942	0.03465

TABLE 12.0-L

NUCLEAR CONSTANTS FOR ATR TEMPERATURE COEFFICIENT CALCULATIONS

Composition		100°F		160°F		200°F*	
		1 Fast Group	Thermal Group	1 Fast Group	Thermal Group	1 Fast Group	Thermal Group
Normal Fuel	D	1.5165	0.2499	1.5322	0.2659	1.5465	0.2773
Burnable Poison	Σ_a	0.005043	0.17467	0.005032	0.16471	0.005023	0.15883
	Σ_r	0.02523	--	0.02480	--	0.02442	--
	$\upsilon\Sigma_f$	0.006449	0.29750	0.006445	0.28051	0.006440	0.27054
D_2O	D	1.2756	0.8419	1.3015	0.8763	1.3207	0.9001
	Σ_a	0.000196	0.0000794	0.000193	0.0000741	0.000190	0.0000708
	Σ_r	0.01117	--	0.01095	--	0.01079	--
90% Be	D	0.7621	0.3492	0.7623	0.3545	0.7625	0.3580
10% Water	Σ_a	0.002359	0.001908	0.002348	0.001785	0.002338	0.001705
	Σ_r	0.01394	--	0.013852	--	0.013773	--
60% Al	D	1.6136	0.3690	1.6271	0.3920	1.635	0.4086
40% Water	Σ_a	0.000768	0.01474	0.000763	0.013898	0.000760	0.01337
	Σ_r	0.02107	--	0.02075	--	0.02050	--
70% Al	D	1.6857	0.4728	1.7128	0.5021	1.7379	0.5234
30% Water	Σ_a	0.000791	0.01430	0.000778	0.01337	0.000767	0.01277
	Σ_r	0.01630	--	0.016043	--	0.01581	--
80% Al	D	1.8745	0.6639	1.8858	0.7015	1.860	0.7282
20% Water	Σ_a	0.00079	0.01333	0.000788	0.01261	0.00077	0.012175
	Σ_r	0.01131	--	0.01115	--	0.0110	--
Pure Water	D	1.3469	0.1583	1.3686	0.1689	1.3886	0.1765
(H_2O)	Σ_a	0.000806	0.01898	0.000793	0.01775	0.000781	0.01696
	Σ_r	0.04855	--	0.04778	--	0.04709	--

12.5 Time Dependent Turbo Constants

The microscopic constants that were used in the TURBO problems to compute the time dependent reactor constants are given in Table 12.0-M and 12-0-N. The fast group constants given in Table 12.0-M were obtained from MUFT-4 calculations and from the TURBO manual.[1] The MUFT-4 program yields three fast group values of D, Σ_a, Σ_R, Σ_f, and $\gamma\Sigma_f$. There are also edits available which will give the portions of the absorption and fission cross sections due to U-235 and U-238. The microscopic values of absorption and fission cross sections of U-235 and U-238 given in Table 12.0-M were calculated from a MUFT-4 problem run for the core of the ATR with no B^{10} in the core. The microscopic transport and removal cross sections were taken from the TURBO manual. Then for the TURBO calculations each of the time dependent compositions was divided into three elements, U-235, U-238, and a special nondepleting element with an atomic density of 0.1×10^{24} atoms/cm^3. The microscopic constants for the special elements were calculated from the previously determined values for U-235 and U-238 and the macroscopic constants from the pertinent MUFT-4 problem.

The thermal constants given in Tables 12.0-M and L2.0-N are Maxwellian averaged constants at the core temperature. Since the experiments were at a higher temperature than the core a self-shielding factor of 0.8696 was used in the TURBO calculation to correct the thermal U-235 absorption and fission cross sections to the temperature of the experiments.

The initial atom densities used in the TURBO calculations are given in Table 12.0-O and the I-135 fission yields are given in Table 12.0-P. Sufficient B^{10} was added to the core composition to give a thermal absorption cross section due to B^{10} of 0.015 cm^{-1}. The initial two-group time dependent reactor constants as calculated by TURBO are given in Table 12.0-Q.

12.6 Power Balancing for TURBO Problems

At each time step in the TURBO problems the power distribution and eigenvalue were adjusted by regulating the thermal neutron poison in the control regions. It was usually necessary to iterate, at each time step, on the poison distribution to obtain the power distribution and eigenvalue within acceptable limits of the desired values. Figure 12.0-11 was constructed as outlined below to aid in the iterations to obtain the correct power balance between center lobe and outer lobes. After the TURBO problems had been run, two other charts (Figure 12.0-12) were constructed to obtain a final adjustment in the neck and reflector poisons so that not only the correct eigenvalue and center power fraction would be obtained but the power distribution between outer lobes would be correct.

12.61 Center Lobe to Outer Lobe (In-Out) Power Balancing

Several symmetrical PDQ problems were run (problems 3002, 3005 through 3009 and 3012) to investigate the effect of neck poison

---

1. J. B. Callaghan et al., "TURBO-A Two-Dimensional Few-Group Depletion Code for the IBM-704," WAPD-TM-95, November 1957.

TABLE 12.0-M

FOUR-GROUP MICROSCOPIC CROSS SECTIONS FOR TURBO PROBLEMS

Element	Type of Cross Section	Cross Section			
		3 Fast Groups			Thermal Group (barns)
		Group 1 (barns)	Group 2 (barns)	Group 3 (barns)	
Fuel	σ_a	0.00868	0.000975	0.01406	0.1433
Regions	σ_R	0.6645	0.8168	0.7502	-
Special Element	σ_{tr}	1.340	2.666	3.446	10.572
A-1 Experiment	σ_a	0.002569	0.000023	0.002875	0.0656
Region	σ_R	0.2278	0.3029	0.2977	-
Special Element	σ_{tr}	0.8155	2.719	3.881	4.524
A-3 Experiment	σ_a	0.002048	0.000169	0.03962	0.7127
Region	σ_R	0.4006	0.3103	0.2793	-
Special Element	σ_{tr}	1.368	2.828	5.472	7.996
A-5 Experiment	σ_a	0.002052	0.000169	0.03843	0.7128
Regions	σ_R	0.4006	0.3102	0.2773	-
Special Element	σ_{tr}	1.368	2.828	5.471	7.979
U-235	σ_{tr}	4.935	7.981	22.62	528.92
	σ_a	1.436	2.447	43.73	518.95
	σ_R	0.1472	0	0	-
	$\nu\sigma_f$	3.599	4.757	69.99	1082.6
	σ_f	1.299	1.918	28.47	438.3
U-238	σ_{tr}	5.805	8.946	8.990	12.127
	σ_a	0.4804	0.3167	23.65	2.155
	σ_R	2.306	0.0400	0	-
	$\nu\sigma_f$	1.159	0	0	0
	σ_f	0.4292	0	0	0

TABLE 12.0-N

THERMAL MICROSCOPIC CROSS SECTIONS FOR TURBO PROBLEMS

Element	σ_{tr} (barns)	σ_a (barns)	σ_f (barns)	$\nu\sigma_f$
U-236	15.54	5.57	0	0
Pu-239	948.1	938.5	657	1960
Pu-240	255	245	0	0
Pu-241	1213.1	1203.5	880	2698
Pm-149	0	0	0	0
I-135	0	0	0	0
Sm-149	60520	60520	0	0
Xe-135	2640000	2640000	0	0
Fsn-Pr*	60	60	0	0
B-10	2950	2950	0	0

*Low cross section fission products.

TABLE 12.0-O

INITIAL ATOM DENSITIES OF TIME DEPENDENT COMPOSITIONS IN TURBO PROBLEMS (Units of 10^{24} atoms/cm^3)

Composition	Special Element	U-235	U-238	B-10
Fuel	0.1	0.00024595	0.00001766	0.000005085
A-1 Experiment	0.1	0.0000154	0	0
A-3 Experiment	0.1	0.00002454	0	0
A-5 Experiment	0.1	0.0000368	0	0

TABLE 12.0-P

FISSION YIELD OF I-135 FOR TURBO PROBLEMS

Element	Fission Yield
U-235	0.061
U-238	0.055
Pu-239	0.070
Pu-241	0.055

TABLE 12.0-Q

INITIAL TWO-GROUP TIME-DEPENDENT REACTOR CONSTANTS AS DETERMINED BY TURBO

Composition	Group	D (cm)	Σ_a (cm^{-1})	$\nu\Sigma_f$ (cm^{-1})	Σ_R (cm^{-1})
Fuel	1	1.5442	0.005007	0.006276	0.02428
	2	0.2772	0.1570	0.2663	-
A-1 Experiment	1	2.0609	0.0004237	0.0003986	0.009819
	2	0.7238	0.01351	0.01450	-
A-3 Experiment	1	1.2565	0.001961	0.0007061	0.01040
	2	0.4102	0.08234	0.02310	-
A-5 Experiment	1	1.2579	0.002123	0.001055	0.01028
	2	0.4078	0.08789	0.03464	-

and reflector poison on the eigenvalue and power distribution between inner lobe and outer lobes. Table 12.0-R lists the results from these problems. These results were plotted to facilitate interpolation between points. Figure 12.0-11 was then constructed from the plots by assuming the effects of the neck and reflector poisons to be independent.

The K values on this chart are the computed differences in eigenvalue from the core with no poison in the controls to the core with poisoned controls, and the P values are quantities determined in a similar manner from the fraction of the total power generated in the center lobe.

The results from one iteration on the poison distribution for a given time step in the TURBO problems were used to obtain the input poison distribution for the next iteration by using Figure 12.0-11. For instance, from the burnout TURBO, for time step 1 (see Table 6.0-B) an eigenvalue of 1.0883 was obtained, and the fraction of the total power generated in the center lobe was 0.2373. Therefore, the eigenvalue should be increased by 0.0017 and the power fraction increased by 0.0027. For this time step the thermal poison in the reflector controls was 0.0180 cm^{-1} and the thermal poison in the neck controls was 0.095 cm^{-1}. Plotting the point determined by these two poison values on Figure 12.0-11, a K value of (-0.1000) and a P value of (+0.0562) is plotted on Figure 12.0-11 and the poison values of 0.0185 for the reflector controls and 0.0830 for the neck controls is read from the plot. These are then the amounts of thermal poison which would be used in the next iteration for time step 1.

12.62 Outer Lobe Power Balancing

Besides the PDQ problems mentioned in Section 12.61, three other PDQ problems (3017 through 3019) were run to investigate the effect of placing a thermal neutron poison in only the east-west reflector regions and leaving the neck control regions and north-south reflector regions clean. The results of these problems are listed in Table 12.0-R. For these problems, A-5 experiments were placed in all four outer lobes. Therefore, it was unimportant whether the east-west reflector regions or the north-south reflector regions were poisoned; hence, the results can be used to estimate the effect of placing poison in either set of reflector regions.

Chart A of Figure 12.0-12 was then constructed from these three PDQ problems and the PDQ problem with no control poison by assuming the effect on eigenvalue and power fraction in each lobe due to poison in either the east-west or north-south reflector control regions to be independent of the poison concentration in the other reflector control regions. The K values on this chart are the computed differences in eigenvalue from the core with no control poison to the core with poisoned controls, the P_{north} and P_{east} values are quantities determined in a similar manner from the fraction of the total power generated in the north lobe and east lobe, respectively.

Chart B of Figure 12.0-12 was constructed from the PDQ problems (Table 12.0-R) where only neck control poison was present.

TABLE 12.0-R

PDQ TWO-DIMENSIONAL PROBLEMS TO INVESTIGATE THE EFFECT OF CONTROL POISON ON EIGENVALUE AND POWER DISTRIBUTION

PDQ Problem No.	Eigenvalue	Poison (cm^{-1})			Power Distribution Fraction of Total Core Power		
		Necks	E-W Reflector System	N-S Reflector System	Center Lobe	East Lobe	North Lobe
3002	1.2249	0	0	0	0.1966	0.2008	0.2008
3005	1.1193	0	0.05829	0.05829	0.3108	0.1723	0.1723
3006	1.1075	0	0.12824	0.12824	0.3291	0.1677	0.1677
3007	1.2082	0.05751	0	0	0.1848	0.2038	0.2038
3008	1.1799	0.28756	0	0	0.1592	0.2102	0.2102
3009	1.1691	1.15024	0	0	0.1438	0.2141	0.2141
3012	1.1505	0	0.01749	0.01749	0.2678	0.1830	0.1830
3017	1.2074	0	0.00493	0	0.2109	0.1805	0.2140
3018	1.1904	0	0.01493	0	0.2256	0.1580	0.2292
3019	1.1756	0	0.03993	0	0.2394	0.1366	0.2438

This chart was constructed on transparent paper since it was to be used on top of Chart A to determine the third variable in the computation. The K values and P_{north} values on Chart B were computed in a manner similar to those for Chart A and the scales are identical to those used on Chart A.

These charts were used, after the TURBO problems had been run, to obtain the final adjustment in the neck and reflector poisons at each time step. For an example, the burnout TURBO problem at time step 1 is again used. The amount of poison (0.018 cm^{-1}) in both reflector systems determines a point on Chart A (marked initial point time step 1). At this point: $K = -0.0758$,

$$P_{north} = -0.0157, \text{ and}$$

$$P_{east} = -0.0157.$$

To achieve the desired values, K must be changed by (+0.0017), P_{north} by (-0.0073), and P_{east} by (+0.0060)(see Tables 6.0-A and 6.0-B), resulting in a K value of (-0.0741), and P_{north} of (-0.0230) and a P_{east} of (-0.0097). These changes are accomplished by changing the poison concentrations in both reflector control systems and in the neck control regions. Now, under the assumption that the effects of a change in one control region are independent of the poison concentrations in the other control regions, any change in the neck control poison will change the fraction of the total power generated in the east lobe and in the north lobe by the same amount.

Thus, some unknown amount of the power fraction change and the eigenvalue change will be made up by a change in the neck control poison. By assuming different amounts of the power fraction change to be made up by the neck control poison, a curve (ΔP curve) can be plotted on Chart A using P_{north} and P_{east} as coordinates. Three points on this curve for time step 1 are as follows:

P_{north}	P_{east}
-0.0230	-0.0097
-0.0227	-0.0094
-0.0223	-0.0090

Values of the reflector poison concentrations determined by points on this curve will then result in the power fraction developed in the east-west reflector system and the north-south reflector system to differ from the required amounts by the same quantity. Now the neck control poison which will take us from this curve to the "Final Value" at K of -0.0741 and a P_{north} of -0.0230 must be found. With Chart B drawn on transparent paper this is done as follows. The point determined by the neck control poison (0.095 cm^{-1}) is plotted on Chart B, this chart is then placed on top of Chart A with the K axes parallel and the point on Chart B lying on top of the ΔP curve previously plotted on Chart A. Chart B is then moved while keeping this orientation until the poison curve of Chart B intersects the "Final Value" previously plotted

on Chart A. The point on the poison curve over the "Final Value" then gives the neck poison, and the point at which the poison curve intersects the curve on Chart A gives the values of the reflector poisons. Thus, for time step 1 of the burnout TURBO problem values of 0.081 cm^{-1} for the neck control poison, 0.0222 cm^{-1} for the north-south reflector control poison, and 0.0156 cm^{-1} for the east-west reflector control poison were obtained.

The charts in Sections 12.61 and 12.62 were constructed for the clean core by assuming the independence of effects from the control regions involved. Although this assumption is not exact, the charts so constructed will still yield good values throughout the charge life when the poison corrections are not too large.

12.7 Derivation of Xenon Instability Criterion

The two-group criterion for axial xenon instability using the assumption of a spacially uniform initial xenon distribution is derived below. The two-group neutron balance equations for the single-region, one-dimensional model investigated are:

(1) $$D_1\nabla^2\Phi_1 - (\Sigma_R + D_1B_1^2 - \nu\Sigma_{f1} + \Sigma_{a1})\,\Phi_1 + \nu\Sigma_{f2}\Phi_2 = 0$$

(2) $$D_2\nabla^2\Phi_2 - (\Sigma_{a2} + \Sigma_x)\,\Phi_2 + (\Sigma_R + f\,D_1B_1^2)\,\Phi_1 = 0$$

Σ_x = Xe cross section

f = fraction of fast group neutron leakage which returns to the core as slow neutrons

Linearize the equations by substituting into (1) and (2) the following:

$$\phi_1(x, t) = \phi_1(x, o) + \psi_1(x, t)$$

$$\phi_2(x, t) = \phi_2(x, o) + \psi_2(x, t)$$

$$\Sigma_x(x, t) = \Sigma_x(x, o) + \delta\Sigma_x(s, t) = \Sigma_{xo} + \delta\Sigma_x$$

$$\Sigma_{a2}(x, t) = \Sigma_a(x, o) + \delta\Sigma_a(x, t) = \Sigma_{ao} + \delta\Sigma_a$$

Perturbations

(3) $$D_1\nabla^2\phi_1 - \Sigma_f\phi_1 + \nu\Sigma_{f2}\phi_2 + D_1\nabla^2\psi_1 - \Sigma_f\psi_1 + \nu\Sigma_{f2}\psi_2 = 0$$

(4) $$D_2\nabla^2\phi_2 + D_2\nabla^2\psi_2 - (\Sigma_{ao} + \Sigma_{xo})\phi_2 - (\delta\Sigma_a + \delta\Sigma_x)\,\phi_2$$

$$- (\Sigma_{ao} + \Sigma_{xo})\,\psi_2 - (\delta\Sigma_a + \delta\Sigma_x)\,\psi_2 + \Sigma_s\phi_1 + \Sigma_s\psi_1 = 0 \text{ , where}$$

$$\Sigma_f = \Sigma_R + D_1B_1^2 - \nu\Sigma_{f1} + \Sigma_{a1}$$

$$\Sigma_s = \Sigma_R + f\,D_1B_1^2$$

$$\phi_1 \equiv \phi_1(x, o) \qquad \text{and} \quad \phi_2 = \phi_2(x, o)$$

If the reactor is critical at $t = 0$ and second ordered terms neglected, since $\frac{\psi(x,t)}{\phi(x,o)} << 1$ (3) and (4) become:

$$(5) \qquad D_1\nabla^2\psi_1 - \Sigma_f\psi_1 + \nu\Sigma_{f2}\psi_2 = 0$$

$$(6) \qquad D_2\nabla^2\psi_2 - (\Sigma_{ao} + \Sigma_{xo})\psi_2 + \Sigma_s\psi_1 - \delta\Sigma_x\phi_2 - \delta\Sigma_a\phi_2 = 0$$

The Laplacian of equation (6) is

$$(7) \qquad D_2\nabla^4\psi_2 - (\Sigma_{ao} + \Sigma_{xo})\nabla^2\psi_2 + \Sigma_s\nabla^2\psi_1 - \phi_2\delta\nabla^2\Sigma_x - \delta\Sigma_x\nabla^2\phi_2 - \delta\Sigma_a\nabla^2\phi_2 = 0$$

where D_2, Σ_{ao}, Σ_{xo}, and $\delta\Sigma_a$ are constant with respect to x.

Rewrite (5) and (6):

$$(8) \qquad \nabla^2\psi_1 = \frac{\Sigma_f}{D_1}\psi_1 - \frac{\nu\Sigma_{f2}}{D_1}\psi_2$$

$$(9) \qquad \psi_1 = -\frac{D_2\nabla^2}{\Sigma_s}\psi_2 + \frac{(\Sigma_{ao} + \Sigma_{xo})}{\Sigma_s}\psi_2 + \frac{\delta\Sigma_x}{\Sigma_s}\phi_2 + \frac{\delta\Sigma_a}{\Sigma_s}\phi_2$$

Substitute (9) into (8):

$$(10) \qquad \nabla^2\psi_1 = -\frac{\Sigma_f D_2}{D_1\Sigma_s}\nabla^2\psi_2 + \frac{\Sigma_f(\Sigma_{ao}+\Sigma_{xo})}{D_1\Sigma_s}\psi_2 + \frac{\Sigma_f\delta\Sigma_x}{D_1\Sigma_s}\phi_2 + \frac{\Sigma_f\delta\Sigma_a}{D_1\Sigma_s}\phi_2 - \frac{\nu\Sigma_{f2}}{D_1}\psi_2$$

Substitute (8) into (7):

$$(11) \qquad D_2\nabla^4\psi_2 - (\Sigma_{ao}+\Sigma_{xo})\nabla^2\psi_2 - \phi_2\delta\nabla^2\Sigma_x - \delta\Sigma_x\nabla^2\phi_2 - \delta\Sigma_a\nabla^2\phi_2 + \frac{\Sigma_s\Sigma_f}{D_1}\psi_1 - \frac{\Sigma_s\nu\Sigma_{f2}}{D_1}\psi_2 = 0$$

Substitute (9) into (11):

$$(12)\quad D_2\nabla^4\psi_2 + (\Sigma_{ao}+\Sigma_{xo})\nabla^2\psi_2 - \phi_2\delta\nabla^2\Sigma_x - \delta\Sigma_x\nabla^2\phi_2 - \delta\Sigma_a\nabla^2\phi_2 - \frac{D_2\Sigma_f}{D_1}\nabla^2\psi_2 + \frac{(\Sigma_{ao}+\Sigma_{xo})\Sigma_f}{D_1}\psi_2 + \frac{\delta\Sigma_x\Sigma_f}{D_1} + \frac{\delta\Sigma_a\Sigma_f}{D_1}\phi_2 - \frac{\Sigma_s\nu\Sigma_{f2}}{D_1}\psi_2 = 0$$

Rewrite (12):

$$(13)\quad \frac{D_1D_2}{\Sigma_f}\nabla^4\psi_2 - \left[\frac{D_1(\Sigma_{ao}+\Sigma_{xo})}{\Sigma_f} + D_2\right]\nabla^2\psi_2 + \left[(\Sigma_{ao}+\Sigma_{xo}) - \frac{\Sigma_s\nu\Sigma_{f2}}{\Sigma_f}\right]\psi_2 + \left[\phi_2 - \frac{D_1}{\Sigma_f}\nabla^2\phi_2\right]\delta\Sigma_x - \frac{D_1\phi_2\delta\nabla^2\Sigma_x}{\Sigma_f} + \left[\phi_2 - \frac{D_1\nabla^2\phi_2}{\Sigma_f}\right]\delta\Sigma_a = 0$$

The equations relating $\delta\Sigma_x$ to ψ_2 are derived as follows:

$$(14)\quad \frac{dI}{dt} = -\lambda_I I + \gamma_I\Sigma_{f2}\phi_2$$

$$(15)\quad \frac{dX}{dt} = \lambda_I I + \gamma_x\Sigma_{f2}\phi_2 - \lambda_x X - \sigma_x X\phi_2$$

γ_I and γ_x are iodine yields and xenon yield each multiplied by total fissions per thermal fission. σ_x = microscopic xenon cross section.

Differentiate (15)

$$(16)\quad \frac{d^2X}{dt^2} = \lambda_I\frac{dI}{dt} + \gamma_x\Sigma_{f2}\frac{d\phi_2}{dt} - \lambda_x\frac{dX}{dt} - \sigma_x\phi_2\frac{dX}{dt} - \sigma_x X\frac{d\phi_2}{dt}$$

Rewrite (15):

$$\lambda_I I = \frac{dX}{dt} = \gamma_x \Sigma_{f2} \phi_2 + \lambda_x X + \sigma_x X \phi_2 \tag{17}$$

Substitute (17) into (14):

$$\frac{dI}{dt} = -\frac{dX}{dt} + \gamma_x \Sigma_{f2} \phi_2 - \lambda_x X - \sigma_x X \phi_2 + \gamma_I \Sigma_{f2} \phi_2 \tag{18}$$

Substitute (18) into (16):

$$\frac{d^2X}{dt^2} = -\lambda_I \frac{dX}{dt} + \lambda_I \gamma_x \Sigma_{f2} \phi_2 - \lambda_I \lambda_x X - \lambda_I \sigma_x X \phi_2 \tag{19}$$

$$+ \lambda_I \gamma_I \Sigma_{f2} \phi_2 + \gamma_x \Sigma_{f2} \frac{d\phi_2}{dt} - \lambda_x \frac{dX}{dt} - \sigma_x \phi_2 \frac{dX}{dt} - \sigma_x X \frac{d\phi_2}{dt}$$

Collect terms:

$$\frac{d^2X}{dt^2} = -(\lambda_I + \lambda_x + \sigma_x \phi_2) \frac{dX}{dt} - (\lambda_I \lambda_x + \lambda_I \sigma_x \phi_2 + \sigma_x \frac{d\phi_2}{dt}) X \tag{20}$$

$$+ \lambda_I (\gamma_I + \gamma_x) \Sigma_{f2} \phi_2 + \gamma_x \Sigma_{f2} \frac{d\phi_2}{dt}$$

Multiply by σ_x:

$$\frac{d^2\Sigma_x}{dt^2} + (\lambda_I + \lambda_x + \sigma_x \phi_2) \frac{d\Sigma_x}{dt} + (\lambda_I \lambda_x + \lambda_I \sigma_x \phi_2 + \sigma_x \frac{d\phi_2}{dt}) \Sigma_x \tag{21}$$

$$= \lambda_I (\gamma_I + \gamma_x) \Sigma_{f2} \phi_2 \sigma_x + \gamma_x \Sigma_{f2} \sigma_x \frac{d\phi_2}{dt}$$

Linearize equation (21) and eliminate second order and unperturbed terms:

$$\Sigma_x = \Sigma(x,o) + \delta\Sigma_x(x,t) = \Sigma_{xo} + \delta\Sigma_x$$

$$\phi_2 = \phi_2(x,o) + \psi(x,t)$$

and neglect second ordered terms.

$$(22)\qquad \frac{d^2\delta\Sigma_x}{dt^2} + (\lambda_I + \lambda_x + \sigma_x\phi_2)\frac{d\delta\Sigma_2}{dt} + (\lambda_I\lambda_x + \lambda_I\sigma_x\phi_2)\,\delta\Sigma_x$$

$$+ \sigma_x\Sigma_{xo}\frac{d\psi_2}{dt} + \lambda_I\sigma_x\Sigma_{xo}\psi_2 = \lambda_I\sigma_x(\gamma_I + \gamma_x)\Sigma_{f2}\psi_2$$

$$+ \gamma_x\sigma_x\Sigma_{f2}\frac{d\psi_2}{dt}$$

The Laplace Transform of (22) is: $\quad L\{f(t)\} \equiv \int_0^\infty e^{-st}f(t)dt$

$$(23)\qquad s^2\,\delta\Sigma_x(x,s) + s(\lambda_I + \lambda_x + \sigma_x\phi_2)\,\delta\Sigma_x(x,s)$$

$$+ (\lambda_I\lambda_x + \lambda_I\sigma_x\phi_2)\,\delta\Sigma_x(x,s) + (s + \lambda_I)\sigma_x\Sigma_{xo}\psi_2(x,s)$$

$$= \{s\,\gamma_x + \lambda_I(\gamma_I + \gamma_x)\}\sigma_x\Sigma_{f2}\psi_2(x,s)$$

$$(24)\qquad \delta\Sigma_x(x,s) = \left\{\frac{s(\gamma_x\Sigma_{f2} - \Sigma_{xo})\sigma_x + \lambda_I\sigma_x\left[(\gamma_I+\gamma_x)\Sigma_{f2}-\Sigma_{xo}\right]}{s^2 + s\left[\lambda_I + \lambda_x + \sigma_x\phi_2(x,o)\right] + \left[\lambda_I\lambda_x\lambda_I\sigma_x\phi_2(x,o)\right]}\right\}\psi(x,s)$$

Define bracket expression as $\Sigma_{f2}\,g\left[\phi_2(x,o),s\right]$ i.e., transfer function then the Laplace transform of equation (13) becomes after elimination of unperturbed term:

$$(25)\qquad \frac{1}{\Sigma_{f2}}\left\{\frac{D_1D_2}{\Sigma_f}\nabla^4\psi_2(x,s) - \left[\frac{D_1(\Sigma_{ao}+\Sigma_{xo})}{\Sigma_f} + D_2\right]\nabla^2\psi_2(x,s)\right.$$

$$\left. + \left[(\Sigma_{ao} + \Sigma_{xo}) - \frac{\Sigma_s\,\nu\Sigma_{f2}}{\Sigma_f}\right]\psi_2(x,s)\right\} +$$

$$\psi_2(x,s)\left[\phi_2(x,o) - \frac{D_1}{\Sigma_f}\nabla^2\phi_2(x,o)\right]\; g\left[\phi_2(x,o),s\right]$$

$$+ \left[\phi_2(x,o) - \frac{D_1\nabla^2}{\Sigma_f}\phi_2(x,o)\right]\frac{\delta\Sigma_a(s)}{\Sigma_{f2}}$$

$$- \frac{D_1\phi_2(x,o)\nabla^2}{\Sigma_f}\left\{g\left[\phi_2(x,o),s\right]\psi(x,s)\right\} = 0$$

(26) $$P \equiv \frac{1}{\Sigma_{f2}}\left\{\frac{D_1 D_2}{\Sigma_f}\nabla^4 - \left[\frac{D_1(\Sigma_{ao}+\Sigma_{xo})}{\Sigma_f} + D_2\right]\nabla^2 + \left[(\Sigma_{ao}+\Sigma_{xo}) - \frac{\Sigma_s \nu \Sigma_{f2}}{f}\right]\right\}$$

$$Q = \left[\phi_2(x,o) - \frac{D_1}{f}\nabla^2\phi_2(s,o)\right] \qquad g\left[\phi(x,o)s\right] = g(x,s)$$

Equation (25) becomes:

(27) $$P\psi_2(x,s) + Q\psi_2(x,s)g(x,s) + \frac{Q\delta\Sigma_a}{\Sigma_{f2}}(s) - \frac{D_1}{\Sigma_f}\phi_2(x,o)\nabla^2\left[g(x,s)\psi(x,s)\right] = 0$$

(28) $$\nabla^2\left[g(x,s)\psi(x,s)\right] = \frac{\partial}{\partial_x}\left[\frac{\partial g(x,s)}{\partial_x}\psi(x,s) + \frac{\partial\psi(x,s)}{\partial_x}g(x,s)\right]$$

$$= \psi(x,s)\nabla^2 g(x,s) + 2\frac{\partial g(x,s)}{\partial_x}\frac{\partial\psi(x,s)}{\partial_x} + g(x,s)\nabla^2\psi(x,s)$$

From (24)

(29) $$g(x,s) = \frac{s(\gamma_x - \Sigma_{xo}/\Sigma_{f2})\sigma_x + \lambda_I\sigma_x\left[(\gamma_I+\gamma_x) - \Sigma_{xo}/\Sigma_{f2}\right]}{s^2 + s\left[\lambda_I+\lambda_x+\sigma_x\phi_2(x,o)\right] + \left[\lambda_I\lambda_x+\lambda_I\sigma_x\phi_2(x,o)\right]}$$

(30) $$\frac{\partial g(x,s)}{\partial_x} = \frac{-\left\{s(\gamma_x-\Sigma_{xo}/\Sigma_{f2})\sigma_x+\lambda_I\sigma_x\left[(\gamma_I+\gamma_x)-\Sigma_{xo}/\Sigma_{f2}\right]\right\}(s\sigma_x+\lambda_I\sigma_x)\frac{\partial\phi_2(x,o)}{\partial x}}{\left\{s^2+s\left[\lambda_I+\lambda_x+\sigma_x\phi_2(x,o)\right]+\left[\lambda_I\lambda_x+\lambda_I\sigma_x\phi_2(x,o)\right]\right\}^2}$$

$$= \frac{-g(x,s)\sigma_x(s+\lambda_i)\frac{\partial\phi_2(x,o)}{\partial x}}{h(s,\phi)}$$

Where

(31) $$h(s,\phi) \equiv s^2 + s\left[\lambda_I+\lambda_x+\sigma_x\phi_2(x,o)\right] + \left[\lambda_I\lambda_x+\lambda_I\sigma_x\phi_2(x,o)\right]$$

$$(32)\qquad \nabla^2 g(x,s) = \frac{-g(x,s)(s\sigma_x+\lambda_I\sigma_x)}{h(s,\phi)} + \frac{2g(x,s)\sigma_x^2(s+\lambda_I)^2\left(\frac{\partial\phi_2(x,o)}{\partial x}\right)^2}{\left[h(s,\phi)\right]^2}$$

Let

$$(33)\qquad l(s) = s(\gamma_x - \Sigma_{xo}/\Sigma_{f2})\sigma_x + \lambda_I\sigma_x\left[(\gamma_I+\gamma_x) - \Sigma_{xo}/\Sigma_{f2}\right]$$

$$l(s) = -as + d$$

$$m(s) = -\sigma_x(s+\lambda_I)$$

Then

$$(34)\qquad g(x,s) = \frac{l(s)}{h(s,\phi)}$$

$$(35)\qquad \frac{\partial g(x,s)}{\partial x} = \frac{-l(s)m(s)}{h(s,\phi)^2}\frac{\partial\phi_2(x,o)}{\partial x}$$

$$(36)\qquad \nabla^2 g(x,s) = \frac{-l(s)m(s)\nabla^2\phi_2(x,o)}{\left[h(s,\phi)\right]^2} + \frac{2\,l(s)m(s)^2\left\{\frac{\partial(\phi_2(x,o))}{\partial x}\right\}^2}{\left[h(s,\phi)\right]^3}$$

$$(37)\qquad \nabla^2\left[g(x,s)\psi(x,s)\right] = \frac{l(s)}{h(s,\phi)}\nabla^2\psi_2(x,s) - \frac{2\,l(s)m(s)}{\left\{h(s,\phi)\right\}^2}$$

$$\frac{\partial\psi(x,s)}{\partial x} - \frac{l(s)m(s)\nabla^2\psi_2(x,o)}{\left\{h(s,\phi)\right\}^2}\psi_2(x,s)$$

$$+ \frac{2\,l(s)m(s)^2\left\{\frac{\partial\phi_2(x,o)}{\partial x}\right\}^2}{\left[h(s,\phi)\right]^3}\psi_2(x,s)$$

From equation (27)

$$(38)\qquad \frac{Q\,\delta\Sigma_a(s)\left[h(s,\phi)\right]^3}{\Sigma_{f2}} = \psi_2(x,s)P\left[h(s,\phi)\right]^3 + \psi_2(x,s)Q\,l(s)\left[h(s,\phi)\right]^2$$

$$- \frac{D_1}{\Sigma_f}\phi_2(x,o)\left\{l(s)\left[h(s,\phi)\right]^2\nabla^2\psi_2(x,s)\right.$$

$$- l(s)m(s)h(s,\phi)\left[\frac{\partial\phi_2(x,o)}{\partial x}\,2\,\frac{\partial\psi_2(x,s)}{\partial x}\right.$$

(38) (Cont.)

$$+ \nabla^2\phi_2(x,o)\psi_2(x,s)\Big] + 2\,l(s)m(s)^2\left\{\frac{\partial\phi_2(s,o)}{\partial x}\right\}^2\psi_2(x,s)\Big\}$$

(39) $$\Big[h(s,\phi)\Big]^2 = s^4+s^2\left[\lambda_I+\lambda_x+\sigma_x\phi_2(x,o)\right]^2+\left[\lambda_I(\lambda_x+\sigma_x\phi_2(x,o)\right]^2$$

$$+ 2s^3\left[\lambda_I+\lambda_x+\sigma_x\phi_2(x,o)\right] + 2s^2\left[\lambda_I(\lambda_x+\sigma_x\phi_2(x,o)\right]$$

$$+ 2s\Big[\lambda_I+\lambda_x+\sigma_x\phi_2(x,o)\Big]\left[\lambda_I(\lambda_x+\sigma_x\phi_2(x,o)\right]$$

(40) Let $b = \lambda_I + \lambda_x + \sigma_x\phi_2(x,o)$

$c = \lambda_I + \sigma_x\phi_2(x,o)$

(41) $$\Big[H(s,\phi)\Big]^2 = s^4 + b^2s^2 + c^2 + 2bs^3 + 2cs^2 + 2bcs$$

$$= s^4 + 2bs^3 + (b^2 + 2c)\,s^2 + 2bcs + c^2$$

(42) $$l(s)\Big[m(s)\Big]^2 = \left[\sigma_x^2s^2 + 2\sigma_x^2\lambda_Is+\sigma_x^2\lambda_I^2\right](-as + d)$$

$$l(s)\Big[m(s)\Big]^2 = -\Big[a\sigma_x^2s^3 + (2a\sigma_x^2\lambda_I - \sigma_x^2d)s^2$$

$$+ (\sigma_x^2\lambda_I^2 - 2\sigma_x^2\lambda_Id)s - \sigma_x^2\lambda_I^2d\Big]$$

We now consider solutions:

(43) $$\psi_2(x,t) = \sum_{n=1}^{\infty} h_n(t)\left[A_n \sin \alpha_n x + B_n \cos \alpha_n x\right]$$

Boundary conditions for any mode: $\square_{x=o}^{x=L}$

$\psi_2 = 0$ for $x = 0$ and $x = L$ $\quad$ L = equivalent bare core height

(44) $$A_n \sin \alpha_n(0) + G_n \cos \alpha_n(0) = 0 \quad \therefore\ B_n = 0$$

$$A_n \sin \alpha_nL + B_n \cos \alpha_nL = 0 \qquad \alpha_n = \frac{n\pi}{L}$$ n is an integral

(45) Let $h_n(t)\, A_n = H_n(t)$

(46) $$\psi_2(x,t) = \sum_{n=1}^{\infty} H_n(t) \sin \frac{n\pi x}{L}$$

(47) $$\nabla^2 \psi_2(x,t) = -\left(\frac{n\pi}{L}\right)^2 \psi_2(x,t)$$

(48) $$\nabla^4 \psi_2(x,t) = \left(\frac{n\pi}{L}\right)^4 \psi_2(x,t)$$

Equation (38) then becomes:

(49) $$P\left[h(s,\phi)\right]^3 + R\,1(s)\left[h(s,\phi)\right]^2 \phi + T1(s)m(s)h(s,\phi)\,\phi^2 - \mu\, 1(s)\left[m(s)\right]^2\phi^3 = 0$$

$$P = \frac{1}{\Sigma_{f2}}\left\{ \frac{D_1 D_2 \pi^4}{\Sigma_f} \frac{n^4}{L^4} + \left[\frac{D_1(\Sigma_{ao}+\Sigma_{xo})}{\Sigma_f} + D_2\right]\frac{\pi^2 n^2}{L^2} + \left[(\Sigma_{ao}+\Sigma_{xo}) - \frac{\Sigma_s \nu\Sigma_{f2}}{\Sigma_f}\right]\right\}$$

$$R = \left[1 + \frac{D_1\pi^2}{\Sigma_f}\frac{1}{L^2} + \frac{D_1\pi^2 n^2}{\Sigma_f L^2}\right] = \left[1 + \frac{D_1\pi^2}{\Sigma_f}\frac{(n^2+1)}{L^2}\right]$$

$$T = \frac{D_1}{\Sigma_f}\left[2\pi^2 \frac{n}{L^2} - \pi^2 \frac{1}{L^2}\right] = \frac{D_1}{\Sigma_f}\pi^2 \frac{(2n-1)}{L^2}$$

$$\mu = \frac{D_1 2\pi^2}{\Sigma_f L^2}$$

(50) $$Ph(s,\phi)\left[s + (\lambda_x + \sigma_x\phi(x,o)\right]^2 + R\left[s + (\lambda_x+\sigma_x\phi(x,o)\right]^2 q(s)\sigma_x\phi(x,o) + T\, q(\varepsilon)\left[\varepsilon + (\lambda_x+\sigma_x\phi(x,o))\right]\left[\sigma_x\phi(x,o)\right]^2 - Mq(s)\left[\sigma_x\phi(x,o)\right]^3 = 0$$

where $q(s) = -(\Sigma_{xo}/\Sigma_f - \gamma_x)s + \lambda_I\left[(\gamma_I+\gamma_x) - \Sigma_{xo}/\Sigma_{f2}\right]$

$$q(s) = -vs - w\lambda_I$$

Let $z = \lambda_x + \sigma_x \phi(x,o)$

$v = \left(\frac{\Sigma_{xo}}{\Sigma_{f2}} - \gamma_x\right)$

$w = \Sigma_{xo}/\Sigma_{f2} - (\gamma_I + \gamma_x)$

$b = \lambda_I + z$

$c = \lambda_I z$

$s + (\lambda_x + \sigma_x \phi(x,o) = s + z$

$\sigma_x \phi(x,o) = F$

(51) $$P\left[s^2 + (\lambda_I + z)s + \lambda_I z\right](s+z)^2 + R\left[-vs - \lambda_I w\right](s+z)^2 F$$
$$+ T(-vs - \lambda_I w)(s+z)F^2 - \mu(-vs - \lambda_I w)F^3 = 0$$

(52) $$(P)s^4 + \left[P(\lambda_I + z3) - RFv\right]s^3 + \left[P3(\lambda_I z + z^2) - RF(2zv + \lambda_I w) - TF^2 v\right]s^2$$
$$+ \left[P(3\lambda_I z^2 + z^3 - RF(z^2 v + 2\lambda_I zw) - TF^2(\lambda_I w + zv) + \mu F^3 v\right]s$$
$$+ \left[P\lambda_I z^3 - RF\lambda_I z^2 w - TF^2 \lambda_I zw + \mu F^3 \lambda_I w\right] = 0$$

which can be put in the form

(53) $$As^4 + Bs^3 + Cs^2 + Ds + E = 0$$

Examination of the numerical values of the coefficients shows that in the characteristic equation (53) all coefficients will be positive if D, the coefficient of S, is positive. Thus, from equation (52) the stability criterion can be written:

(54) $$\frac{P}{R\left(1+2\frac{\lambda_I w}{VZ} + \frac{TF}{RZ}\left(\frac{\lambda_I w}{VZ} + 1\right) - \frac{UF^2}{RZ^2}\right.} - \frac{FV}{3\lambda_I + \lambda_X + \sigma_X \phi(X,0)} \geq 0$$

This can then be put in the form

(55) $G \geq G_C$ where

$$G = \frac{P}{R\left[1 + \frac{2\lambda_I W}{VZ} + \frac{TF}{RZ}\left(\frac{\lambda_I W}{VZ} + 1\right) - \frac{UF^2}{RZ^2}\right]}$$

$$G_C = \frac{FV}{3\lambda_I + \lambda_X + \sigma_X \phi_2}$$

$$P = \frac{1}{\Sigma_{f2}}\left\{\frac{D_1 D_2 \pi^4 n^4}{\Sigma_f L^4} + \left[D_1 \frac{(\Sigma_{ao}+\Sigma_{xo})}{\Sigma_f} + D_2\right]\frac{\pi^2 n^2}{L^2}\right.$$

$$\left. + \left[(\Sigma_{ao}+\Sigma_{xo}) - \frac{\Sigma_s \upsilon \Sigma_{f2}}{\Sigma_f}\right]\right\}$$

$$R = \left[1 + \frac{D_1 \pi^2 (n^2+1)}{\Sigma_f L^2}\right]$$

$$T = D_1 \pi^2 \frac{(2n-1)}{\Sigma_f L^2}$$

$$U = \frac{D_1 2\pi^2}{\Sigma_f L^2}$$

$$F = \sigma_X \phi_2$$

$$W = \left(\frac{\Sigma_{xo}}{\Sigma_{f2}}\right) - (\gamma_I + \gamma_X)$$

$$V = \left(\frac{\Sigma_{xo}}{\Sigma_{f2}}\right) - \gamma_X$$

$$Z = \lambda_X + \sigma_X \phi_2$$

(55) (Cont.)

$$\Sigma_{xo} = \frac{(\gamma_I + \gamma_X)\,\Sigma_{f2}\phi_2}{(\lambda_X + \sigma_X\phi_2)}$$

$$\Sigma_f = \Sigma_R + D_1B_1^2 - \upsilon\Sigma_{f1} + \Sigma_{al}$$

Σ_{f2} = Thermal fission cross section

$$S = \frac{\Sigma_{f1}\bar{\phi}_1 + \Sigma_{f2}\bar{\phi}_2}{\Sigma_{f2}\bar{\phi}_2}$$

f = Fraction of fast neutrons leaking into the reflector that return to the core as thermal neutrons.

TABLE 12.0-S

CONSTANTS FOR XENON STABILITY CALCULATIONS

	Start of Cycle	End of Cycle*
D_1	1.5436 cm	
D_2	0.2807 cm	
Σ_{a1}	0.00476 cm^{-1}	0.00348
$\Sigma_{ao} = \Sigma_{a2}$	0.157 cm^{-1}	0.1109
$\nu\Sigma_{f1}$	0.00644 cm^{-1}	0.00483
$\nu\Sigma_{f2}$	0.267 cm^{-1}	0.2003
$D_1B_1^2$	0.03679 cm^{-1}	
f	0.2547	0.2862
Σ_R	0.02442 cm^{-1}	
σ_X	$2.5 \times 10^{-18} cm^2$	
λ_X	2.1×10^{-5} sec^{-1}	
λ_I	2.9×10^{-5} sec^{-1}	
γ_X	0.003 S	
γ_I	0.064 S	
$\bar{\phi}_2/\bar{\phi}_1$	0.2208	0.3023
$\bar{\phi}_1$	1.16×10^{15} $n\text{-}cm^{-2}\text{-}sec^{-1}$	1.06×10^{15}
$\bar{\phi}_2$	2.56×10^{14} $n\text{-}cm^{-2}\text{-}sec^{-1}$	3.20×10^{14}
Σ_{xo}	0.00778 cm^{-1}	0.0057
S	1.10	1.08

* Values not listed are the same as at start of cycle.

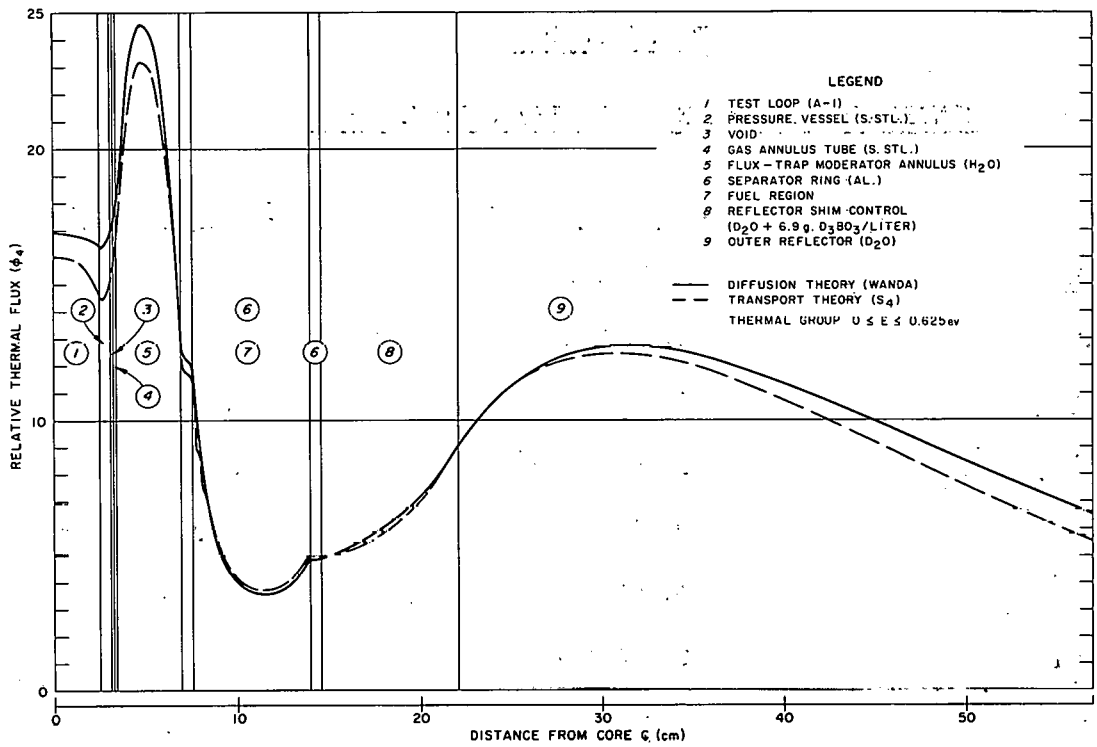

FIG. 12.0-1

THERMAL GROUP DIFFUSION AND TRANSPORT THEORY FLUXES IN A SINGLE-LOBE MODEL OF THE ATR

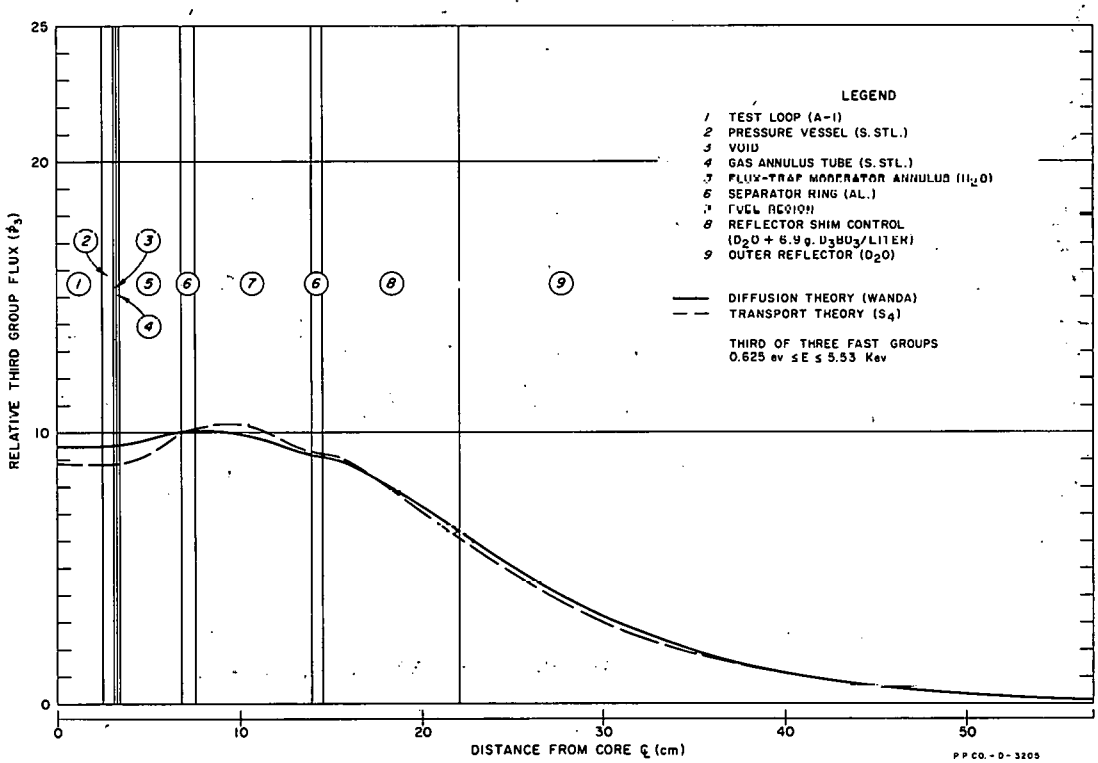

FIG. 12.0-2

THIRD GROUP DIFFUSION AND TRANSPORT THEORY FLUXES IN A SINGLE-LOBE MODEL OF THE ATR

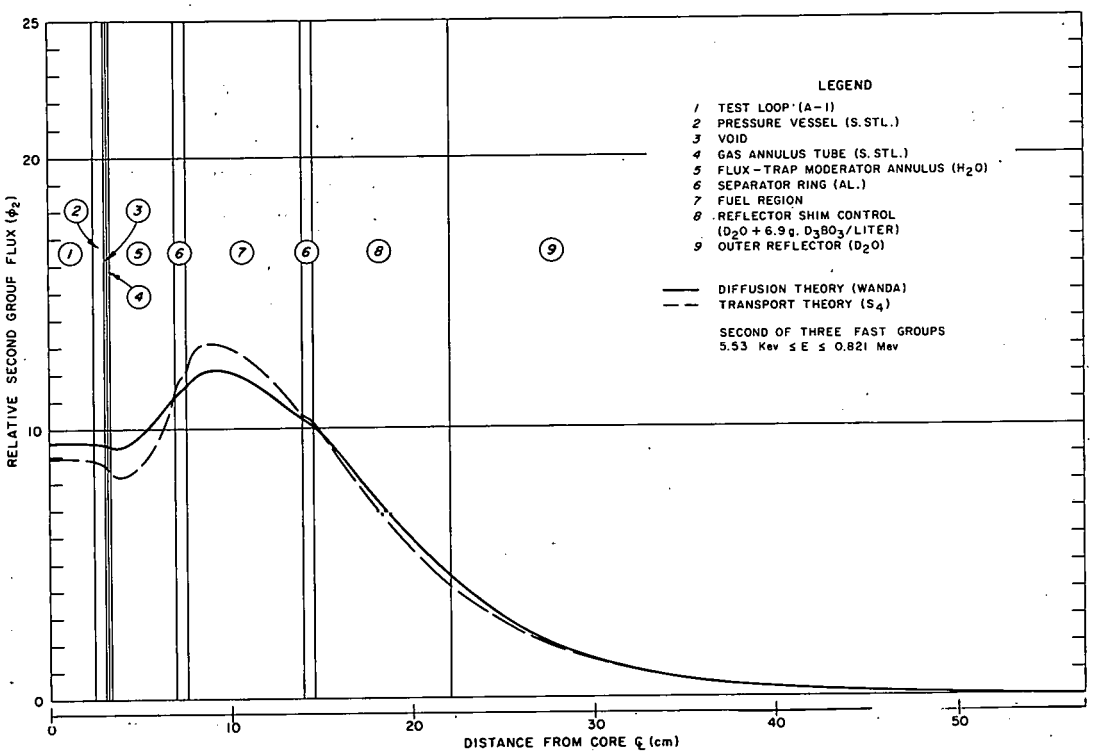

FIG. 12.0-3

SECOND GROUP DIFFUSION AND TRANSPORT THEORY FLUXES IN A SINGLE-LOBE MODEL OF THE ATR

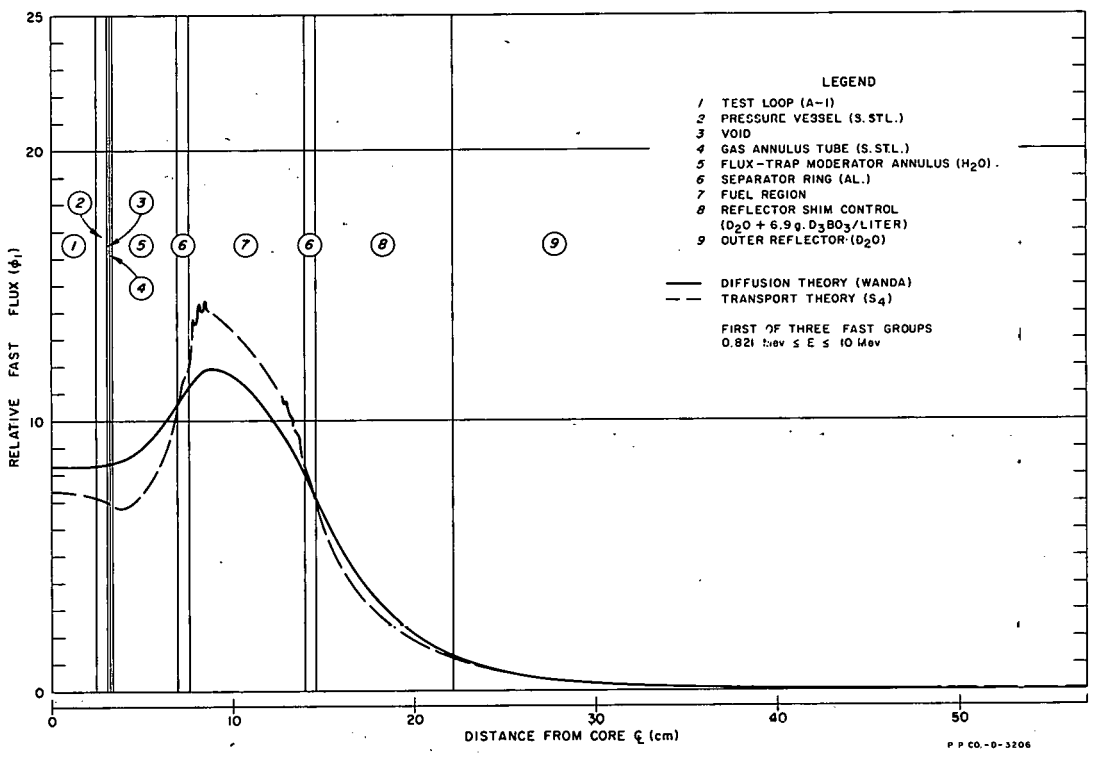

FIG. 12.0-4

FIRST GROUP DIFFUSION AND TRANSPORT THEORY FLUXES IN A SINGLE-LOBE MODEL OF THE ATR

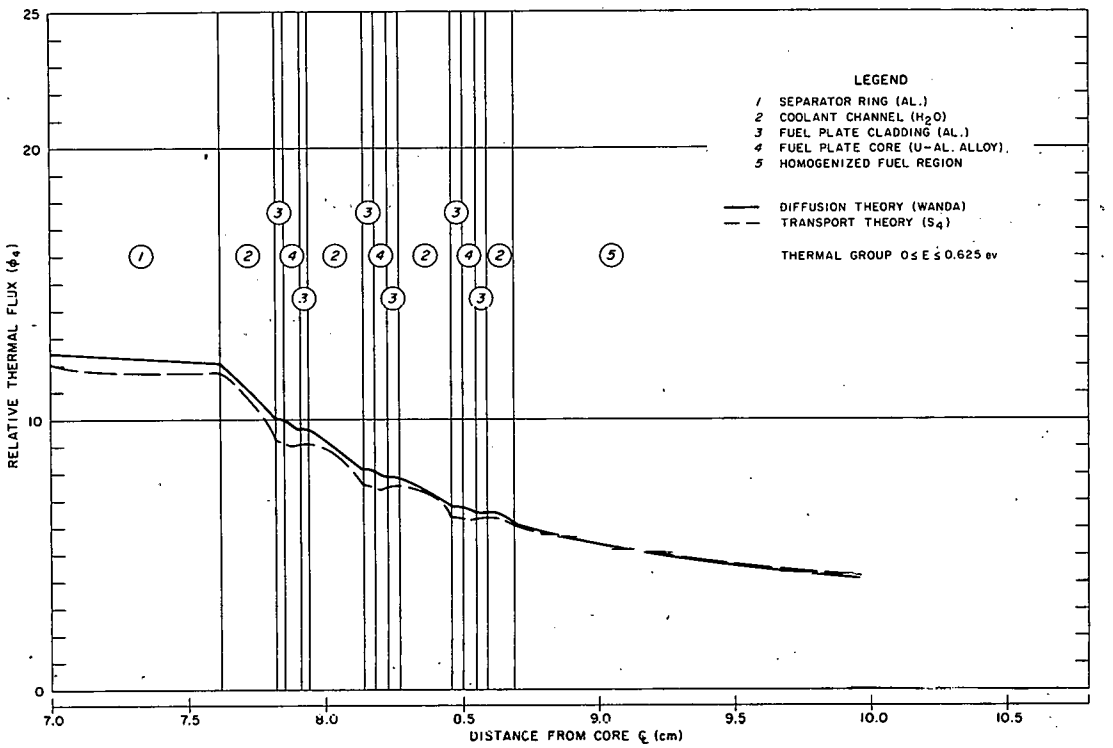

FIG. 12.0-5

THERMAL GROUP DIFFUSION AND TRANSPORT THEORY FLUXES FOR INNER CORE REGION OF A SINGLE-LOBE MODEL OF THE ATR

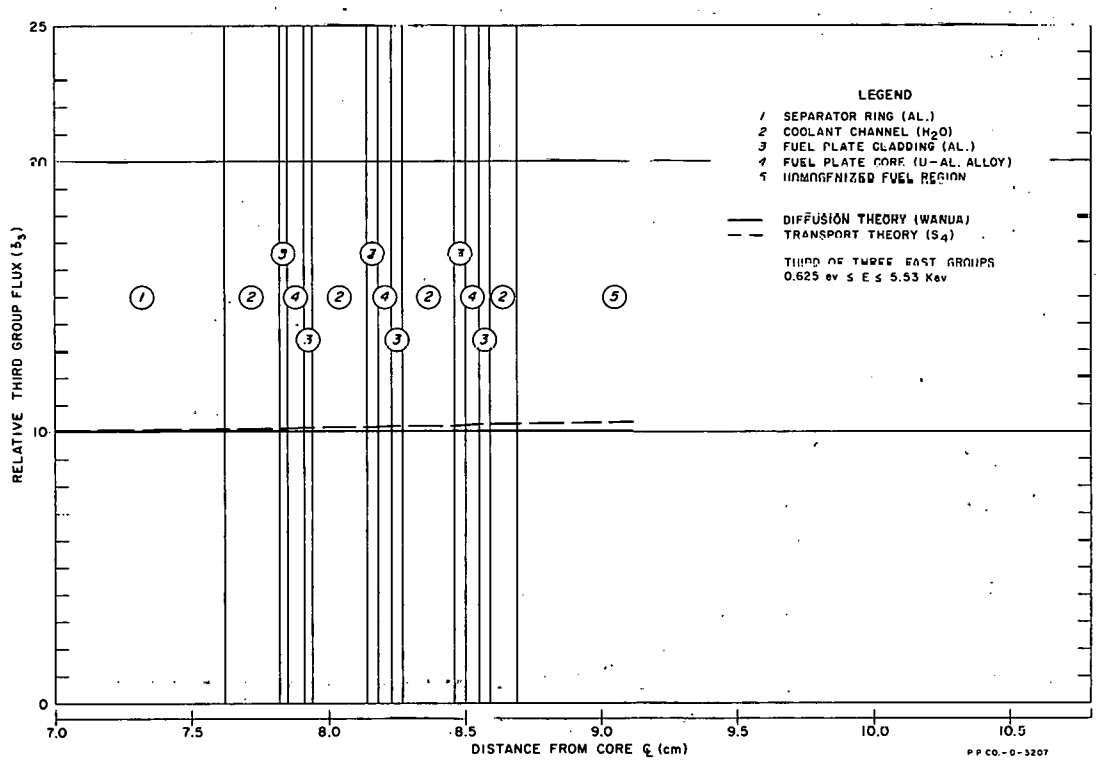

FIG. 12.0-6

THIRD GROUP DIFFUSION AND TRANSPORT THEORY FLUXES FOR INNER CORE REGION OF A SINGLE-LOBE MODEL OF THE ATR

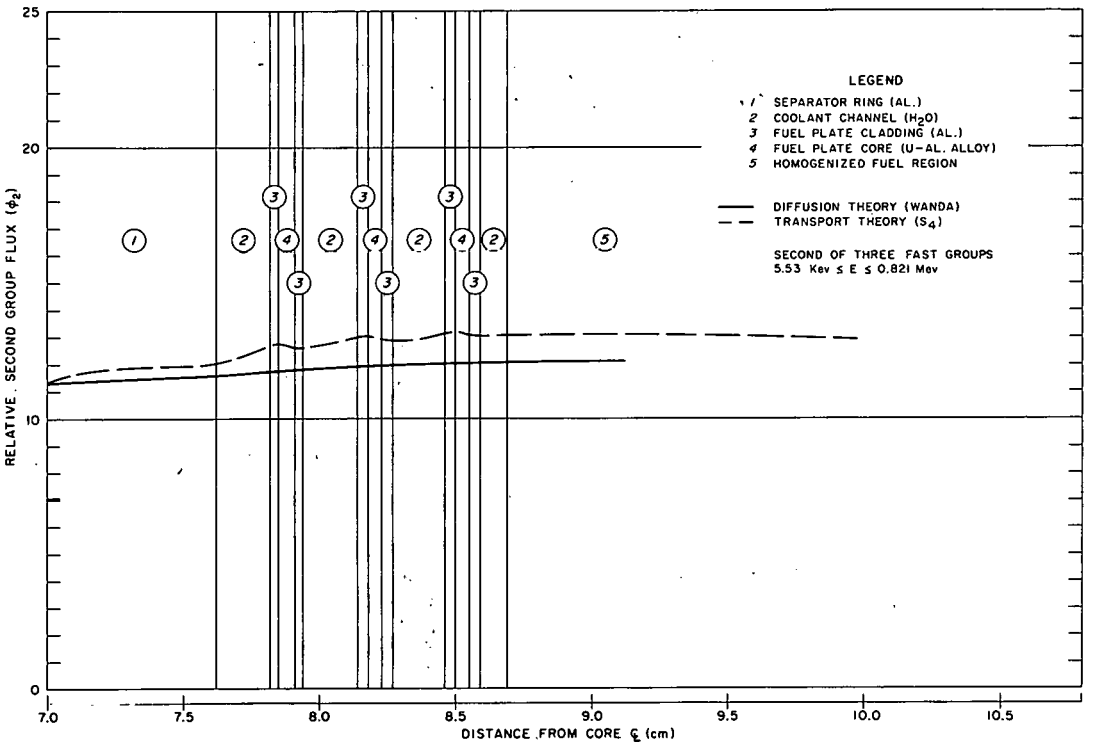

FIG. 12.0-7

SECOND GROUP DIFFUSION AND TRANSPORT THEORY FLUXES FOR INNER CORE REGION OF A SINGLE-LOBE MODEL OF THE ATR

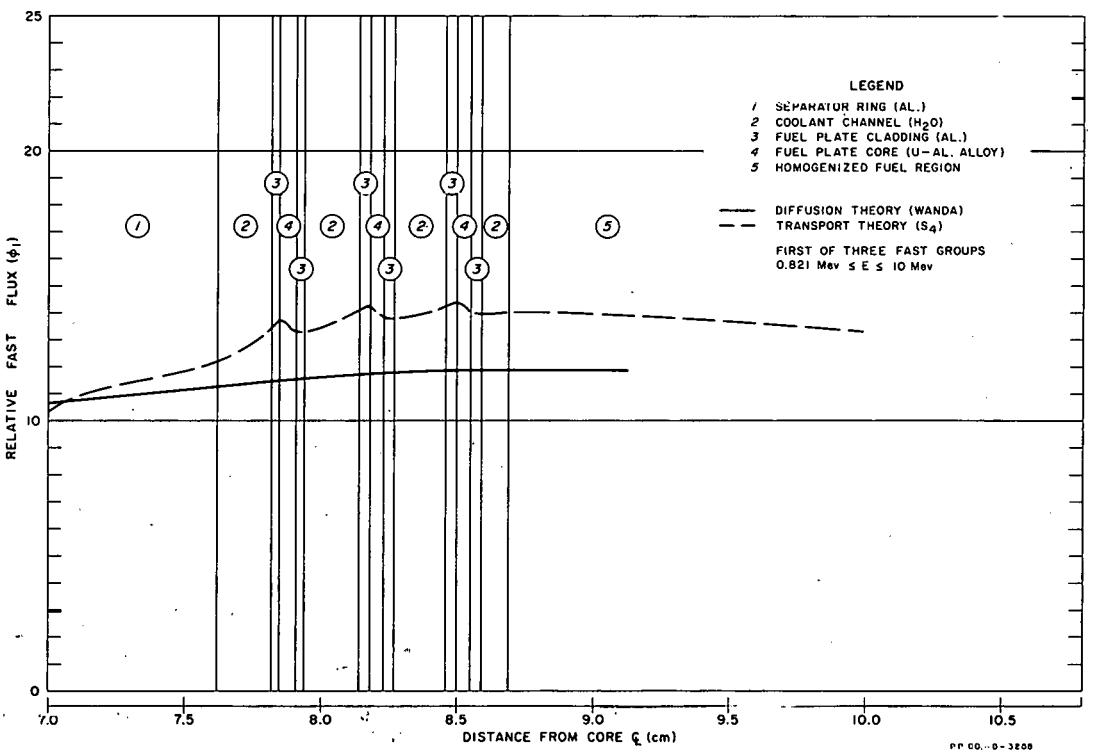

FIG. 12.0-8

FIRST GROUP DIFFUSION AND TRANSPORT THEORY FLUXES FOR INNER CORE REGION OF A SINGLE-LOBE MODEL OF THE ATR

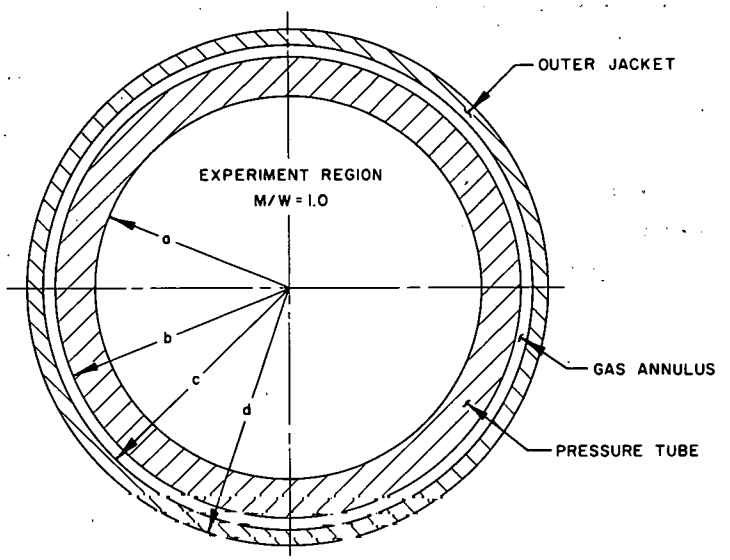

DIMENSION	STAINLESS STEEL LOOP	ZIRCONIUM LOOP
a	1.00"	1.00"
b	1.20"	1.344"
c	1.26"	1.404"
d	1.34"	1.54"

FIG. 12.0-10
ATR TEST FACILITY STRUCTURE

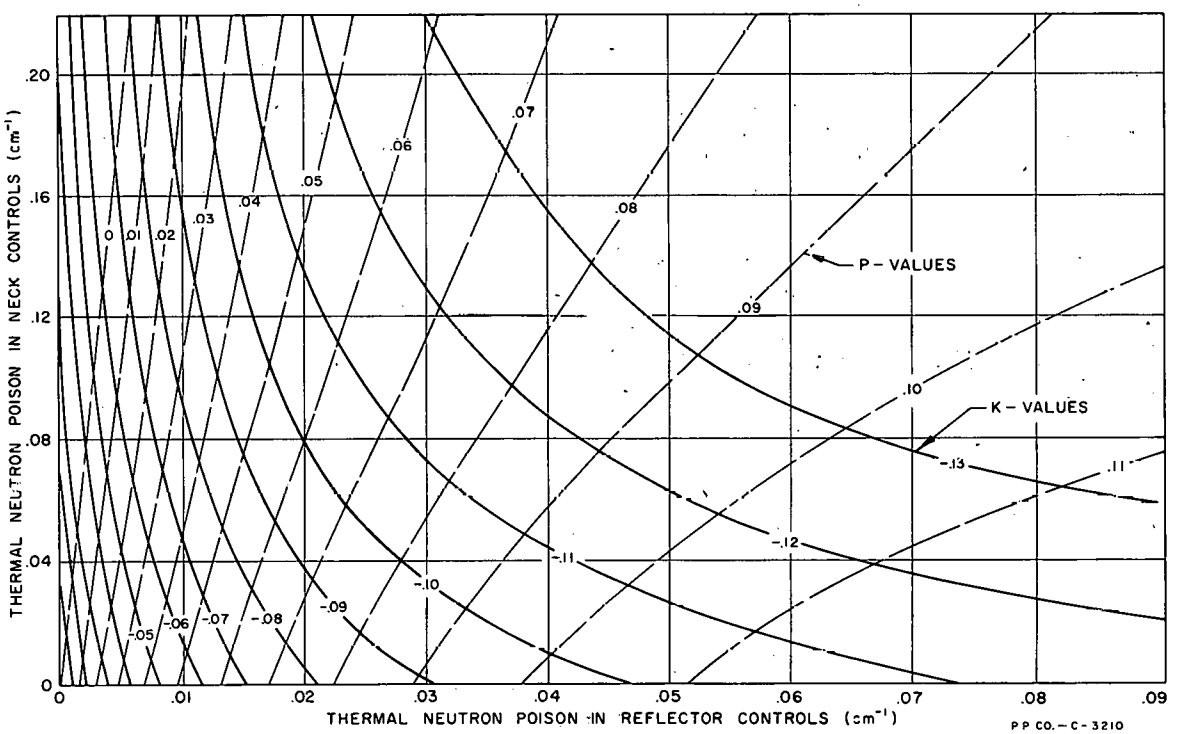

FIG. 12.0-11
CHART TO AID IN THE POWER BALANCING ITERATION AT EACH TIME STEP OF THE TURBO CALCULATIONS

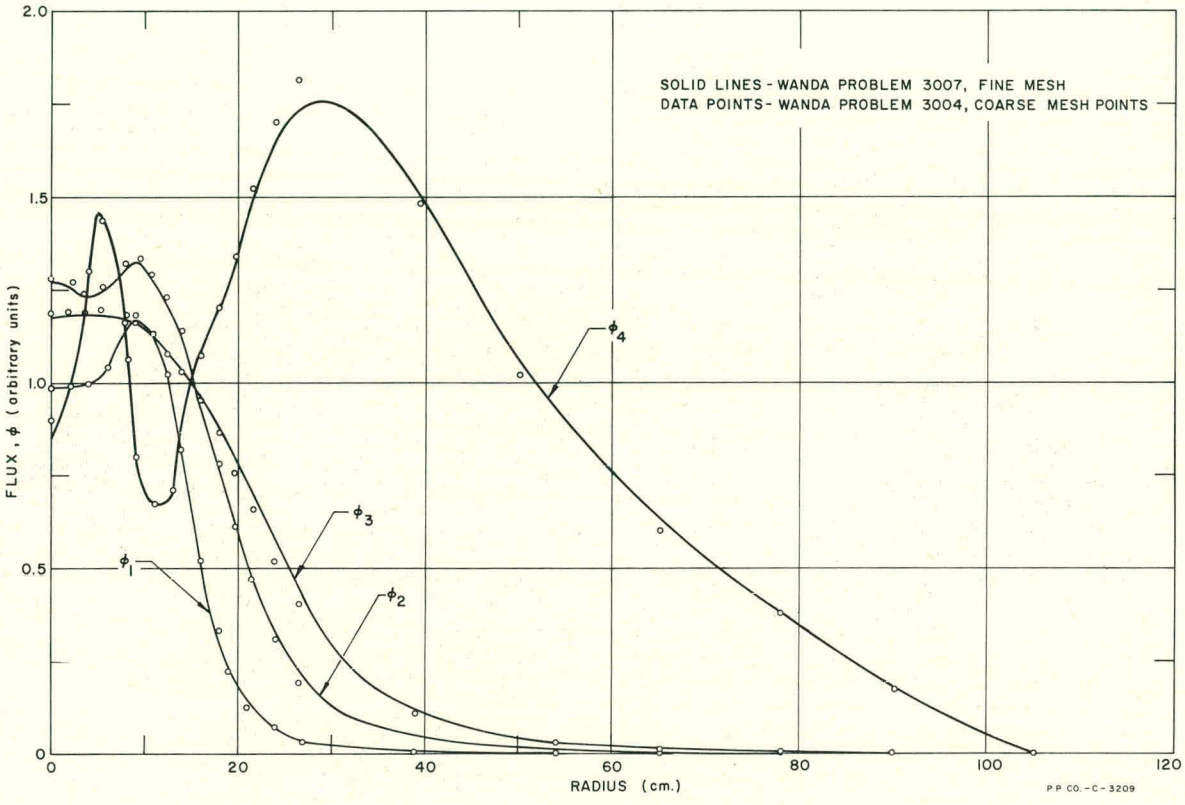

FIG. 12.0-9

EFFECTS OF MESH DESCRIPTION ON NEUTRON FLUX VERSUS RADIUS

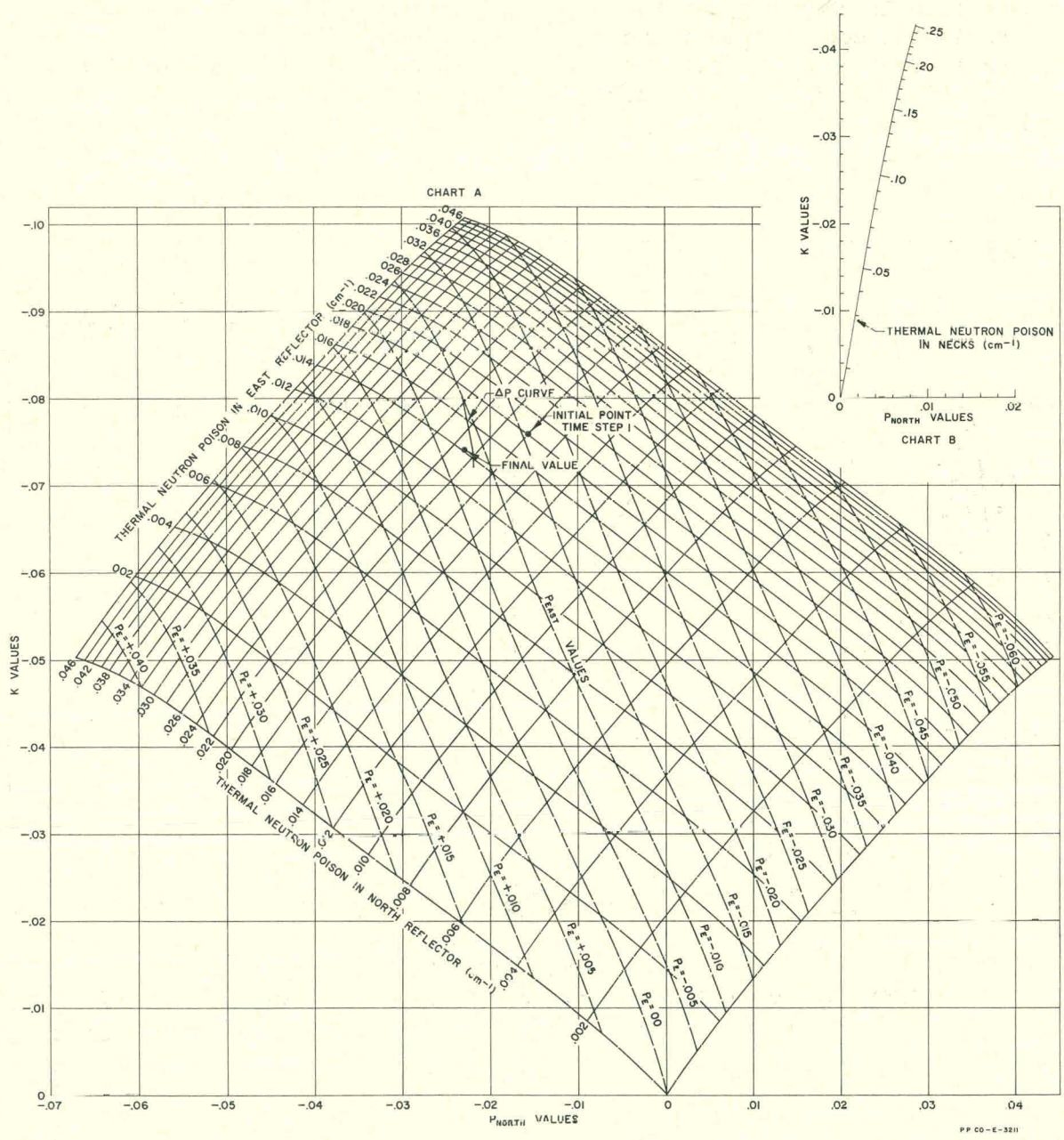

FIG. 12.0-12

CHARTS TO OBTAIN FINAL POISON DISTRIBUTION IN TURBO PROBLEMS

13.0 ACKNOWLEDGMENTS

The Applied Mathematics and Machine Computations Branch of the Atomic Energy Division of Phillips Petroleum Company provided valuable assistance in carrying out the computations for this report and their enthusiastic cooperation is hereby acknowledged. Members of other Branches including Project Engineering, MTR and ETR Operations, Division Engineering and Plant Engineering furnished advice and assistance that substantially facilitated the work described in this report.

PHILLIPS
PETROLEUM
COMPANY

ATOMIC ENERGY DIVISION